Bangor University

DOCTOR OF PHILOSOPHY

A theoretical study of carrier dynamics in semiconductor quantum dots

Cundin, Marta

Award date:
2004

Awarding institution:
Bangor University

Link to publication

A THEORETICAL STUDY
OF
CARRIER DYNAMICS
IN
SEMICONDUCTOR QUANTUM DOTS

BY MARTA CUNDIN

A thesis submitted in candidature for the degree of

DOCTOR OF PHILOSOPHY

School of Informatics

University of Wales, Bangor

June 2004

En memoria de mis abuelos

Jacinto, David y Delfi

Acknowledgments

Firstly I would like to show my appreciation for my supervisor - Dr. Paul Rees - to whom I am enormously grateful for his encouragement and endless patience with me throughout the project and writing this thesis. I wish to thank my group colleagues for making work more enjoyable. Especially, I would like to thank Javier Domínguez for his support, encouragement and crucial help along the thesis. Eskerrik asko Javi emandako laguntzagatik, izugarri garrantzitsua izan da niretzako.

Finally, I would like to thank my family - Ama, Aita and Zuri - for their patience and belief. This wouldn't have been possible without you. Eskerrik asko bihotz-bihotzez!

Abstract

Recent progress in semiconductor growth and fabrication techniques has allowed semiconductor structures of increasing dimensional confinement to be realized. In quantum dot structures carriers are confined in all three dimensions and therefore exhibit a discrete set of energy levels. It is expected that optoelectronic devices incorporating these structures will have improved performance. This study focusses on self-assembled quantum dot structures. In this growth technique, the quantum dots are formed on top of a thin quantum well wetting layer which has been deposited on top of a bulk substrate. The whole structure is finally overgrown by bulk material. The wetting layer plays a crucial role in the operation of quantum dot optoelectronic devices. Initially carriers diffuse into the $2D$ wetting layer before either recombining or being captured by the self-assembled quantum dots. Once captured in the dots, they either relax into lower energy levels or are re-excited back to the wetting layer. Therefore the wetting layer supplies the quantum dots with a carrier reservoir and hence plays a large part in the carrier dynamics.

In this thesis, we calculate the scattering rates for capture from the wetting layer into the quantum dots and the reverse process, the emission of a carrier from the dot into the wetting layer. We also calculate the carrier relaxation rates between quantum confined energy levels in the quantum dots. Using these scattering rates, we construct a rate equation model in order to describe the carrier dynamics of quantum dot structures. The model is used to predict the occupancy of the quantum dots as a function of time, and this allows us to calculate the time-varying optical gain and spontaneous emission rates. This type of model enables us to predict quantum dot laser dynamics including non-linear effects such as gain saturation and spectral hole burning. We also compare the results obtained from our model with time resolved photoluminescence experiments and see good qualitative agreement.

Contents

Chapter 1

Introduction

The research described in this thesis was carried out in the School of Informatics, at the University of Wales, Bangor. The focus of this work was to model the carrier dynamics and optical properties of semiconductor quantum dot structures. The objective of the project was to develop a theoretical model in order to determine the carrier occupation probability in the dots. This involved the construction of a set of rate equations to describe the carrier number in each quantum confined state of each quantum dot. This allows us to describe the optical gain and spontaneous emission rates and therefore the photon dynamics in optoelectronic devices incorporating a quantum dot active medium.

The acronym LASER stands for Light Amplification by Stimulated Emission of Radiation. It refers to a device which produces a source of coherent, monochromatic and directional light. The laser was first developed in 1960 by the physicist Theodore Harold Maiman by using ruby as the active medium [3]. Shortly after the invention of the laser, the possibility of using a semiconductor, such as GaAs as the active medium for a laser was considered. The active medium of a semiconductor laser consists of atoms whose electrons can be excited into higher allowed energy bands by absorbing a photon of light, the energy of the incident photon being equal to the difference in energy between the initial and final states. When an electron in a high energy band interacts with an incident photon, it causes the electron to make a downward transition to a lower energy band. As a result, a photon of the same wavelength as the incident one is emitted. This process, known as stimulated emission, is the amplification process necessary for the lasing. A second requirement for a Laser is an optical resonant cavity which increases the number of stimulated emission events due to multiple passes of the photons through the gain medium. Chapter 2 introduces the relevant theory of semiconductor lasers characteristics which is required for an understanding of the research carried out in this thesis.

It has been demonstrated that reducing the thickness of the active region of the laser to below the de-Broglie wavelength of the carriers significantly improves the operating characteristics of a semiconductor laser. In quantum well lasers [1], the active region thickness is reduced in one direction, so that carriers inside the active region have energies quantized in one direction. This reduction in dimensionality can be extended to 2 directions as in quantum wire lasers, or 3 directions, as in quantum dot lasers. As a result of this confinement of carriers, a quantum dot laser presents the advantages of a gas laser (atomic properties), i.e., a quantized electronic structure and thus discrete optical transitions, but with the flexibility of a semiconductor laser (i.e., it can be electrically pumped).

Early attempts at fabricating quantum dot structures involved complicated growth and lithographic techniques and were largely unsuccessful [2]. However an important breakthrough came with the development of the self-assembled growth technique [4]. A typical growth method known as the Stranski-Krastanov (SK) technique [6] relies on the growth of a highly strained epitaxial layer onto the surface of a semiconductor substrate. The strain between the substrate and the grown film leads to an instability which results in a transition from an uniform layer to clusters of material in order to minimize the energy of the system. These clusters are small enough to confine electrons in three dimensions if surrounded by a material of higher bandgap.

The three dimensional quantum confinement of carriers gives rise to discrete energy level analogous to an atom. The resulting discrete density of states gives rise to high gain in semiconductor devices using these structures. However, in contrast to atoms, quantum dots can be electrically pumped, giving rise to a wide range of applications for optoelectronic devices. Consequently, the use of quantum dots for semiconductor lasers is expected to have superior operational characteristics, in contrast to other less confined structures, such as quantum wells ($1D$ confinement) and quantum wires ($2D$ confinement).

The thin epitaxial layer used to form the quantum dots is called the wetting layer (WL) and itself acts as a quantum well to confine carriers in two dimensions. The process by which a carrier is captured from the wetting layer into the quantum dot is critical for the operation of the optoelectronic device and is the subject of this thesis.

There are several scattering mechanisms which must be considered when studying the carrier dynamics of quantum dot structures. Carriers can be captured from the wetting layer by scattering with other carriers (both in the wetting layer and in the quantum dot) or lattice phonons. The excitation of carriers from individual quantum dots is also possible via the same mechanisms.

In chapter 3 we calculate the scattering rates for typical capture and relaxation processes between the quantum dot and the wetting layer. The approach we take is to extend a semi-analytical analysis given by A. V. Uskov [7] and [8] to calculate these scattering rates for realistic quantum dot structures. We use these calculations to explore the region of validity for the assumptions made in the semi-analytical approach. Our results show that the assumptions are not valid for the high carrier densities present in optoelectronic devices.

The major limitation of the semi-analytical approach is the assumption of a Boltzmann [5] distribution for carriers in the wetting layer, arising from the assumption of low carrier densities (the Boltzmann distribution being a good approximation to the Fermi-Dirac distribution at low carrier densities). In chapter 4 we derive expressions for the capture and relaxation rates including a Fermi-Dirac distribution for carriers within the wetting layer. These expressions take the form of multiple integrals and we outline the method of solving them. Using these expressions we show explicitly the values of carrier density where the semi-analytical approach is valid.

In order to describe the dynamics of carriers in the quantum dot, in chapter 5 we derive a set of rate equations to describe the population of electrons and holes in the quantum confined states. As will be described in chapter 5 this novel approach allows us to correctly determine the occupation-dependent scattering processes. This allows us to investigate quantum dot optoelectronic devices in a non-thermal equilibrium regime. Once the occupancies of the quantum confined electron and hole energy levels are known we are in a position to calculate the optical gain and spontaneous emission rates for the quantum dot structures. Chapter 5 concludes with a simulation of time resolved photoluminescence experiments on quantum dot lasers, where a non-equilibrium treatment is essential.

Finally chapter 6 summarizes the main results of the thesis and alludes to further work which could be instigated as a result of this study.

Bibliography

[1] R. Dingle, W. Wiegmann, and C. H. Henry. *Phys. Rev. Lett.*, Lett. 33:pp. 827, 1974.

[2] I. Jacak, P. Hawrylak, and A. Wojs. *Quantum Dots.* Springer, 1997.

[3] T. H. Maiman. Optical and microwave-optical experiments in ruby. *Phys. Rev. Lett.*, vol. 4:pp. 564, 1960.

[4] P. M. Petroff and S. P. Denbaars. Mbe and mocvd growth and properties of self-assembling quantum dot arrays in iii-v semiconductor structures. *Superlattices and Microstructures*, vol. 15:15, 1994.

[5] W. G. V. Rosser. *An introduction to STATISTICAL PHYSICS.* Ellis Horwood Publishers, 1982.

[6] I. N. Stranski and L. von Krastanov. *Akd. Wiss. Lit. Mainz Abh. Math. Naturwiss. Kl.*, vol. 146:pp. 797, 1939.

[7] A. V. Uskov, F. Adler, H. Schweizer, and M. H. Pilkuhn. *Appl. Phys.*, vol. 81(12), 1997.

[8] A. V. Uskov, J. McInerney, F. Adler, H. Schweizer, and M. H. Pilkuhn. *Appl. Phys. Lett.*, vol. 72(1), 1998.

Chapter 2

Basic Theory

Contents

2.1 Semiconductor Lasers

In this project, we study semiconductor lasers where the active region consists of InGaAs self-assembled quantum dots. A laser requires: (a) a source of pumping energy in order to establish a population inversion between the chosen energy levels (when more carriers are in higher states of excitation than in the lower ones below, making the production of stimulated photons possible, as we will explain later in the chapter), (b) an active medium, where the confinement of carriers can occur and hence electrons and holes can recombine in this region producing photons with energies equal to the band gap of the material, as will be commented in detail in the next section, and finally (c) an optical resonant cavity, in order to obtain optical feedback and hence preserve the gain of the system above the losses. This last requirement ensures that the number of photons created by stimulated emission (we will explain in detail in further sections) exceeds all other mechanisms. It usually consists of two cleaved mirrored facets, with a reflectivity of approximately 30% which ensures that only the correct wavelength of photons will reflect back and forward along the cavity while those photons which are not of the selected frequency remain lost, as the laser wavelength will be in relation with the length of the cavity.

2.2 Transverse confinement of carriers and photons

Since the first semiconductor laser was demonstrated in 1960 [11] huge advances in fabrication have been made, allowing highly efficient low current devices to be produced. In a semiconductor laser stimulated emission of radiation occurred as a consequence of recombination processes of carriers injected across the p-n junction. A p-n junction consists of a semiconductor layer doped with acceptor impurities (p-

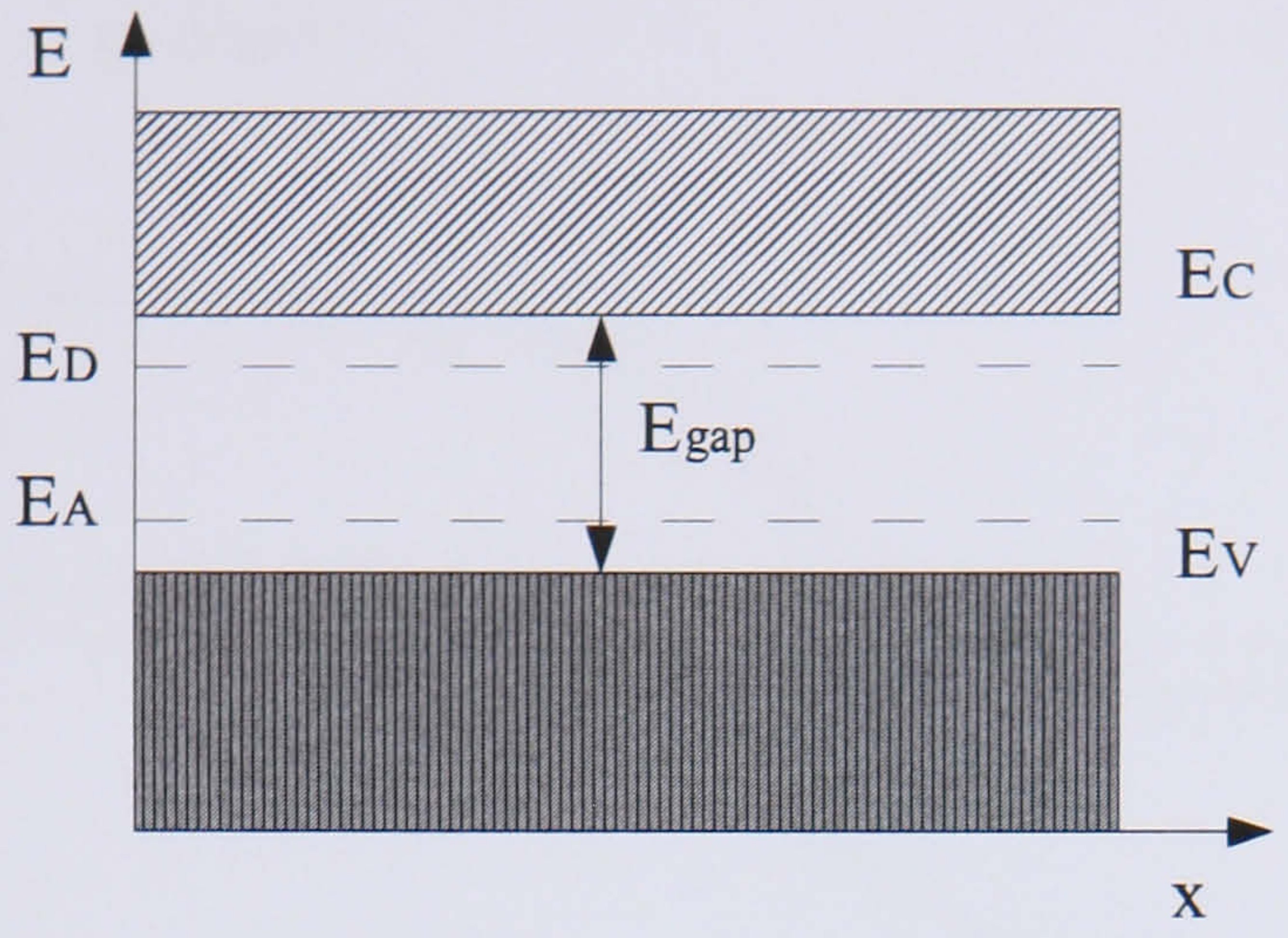

Figure 2.1: When a semiconductor is doped by donor and acceptor atoms, donor and acceptor energy levels, E_D and E_A respectively, appeared inside the energy gap, hence, *donating* an electron (in donor atoms case) or a hole (the acceptor energy level E_A *accepts* an electron creating (donating) a hole in the valence band.

doped semiconductor layer) placed in contact with a n-doped semiconductor layer (a semiconductor layer doped with donor impurities). The impurities introduced incorporate an extra energy level in the bandgap. Donor impurities produce the so-called *donor energy levels* close to the conduction band, whereas acceptor impurities create *acceptor energy levels* near the valence band, as shown in figure 2.1. When n-type and p-type semiconductors are brought into contact, the conduction electrons diffuse across the junction into the p-doped medium in order to populate the holes created by those valence band electrons in the p-doped material that have occupied the acceptor energy level. Holes do the opposite. As a consequence of charged carriers transport, the n-doped material becomes positively charged while the p-doped one becomes negatively charged around the junction. In the vicinity of the junction, a region depleted of electrons and holes appears as an electric field opposing the electrons diffusion from the n-type material to the p-type one arises, illustrated in figure 2.2. The electric field arising from the positively charged donors

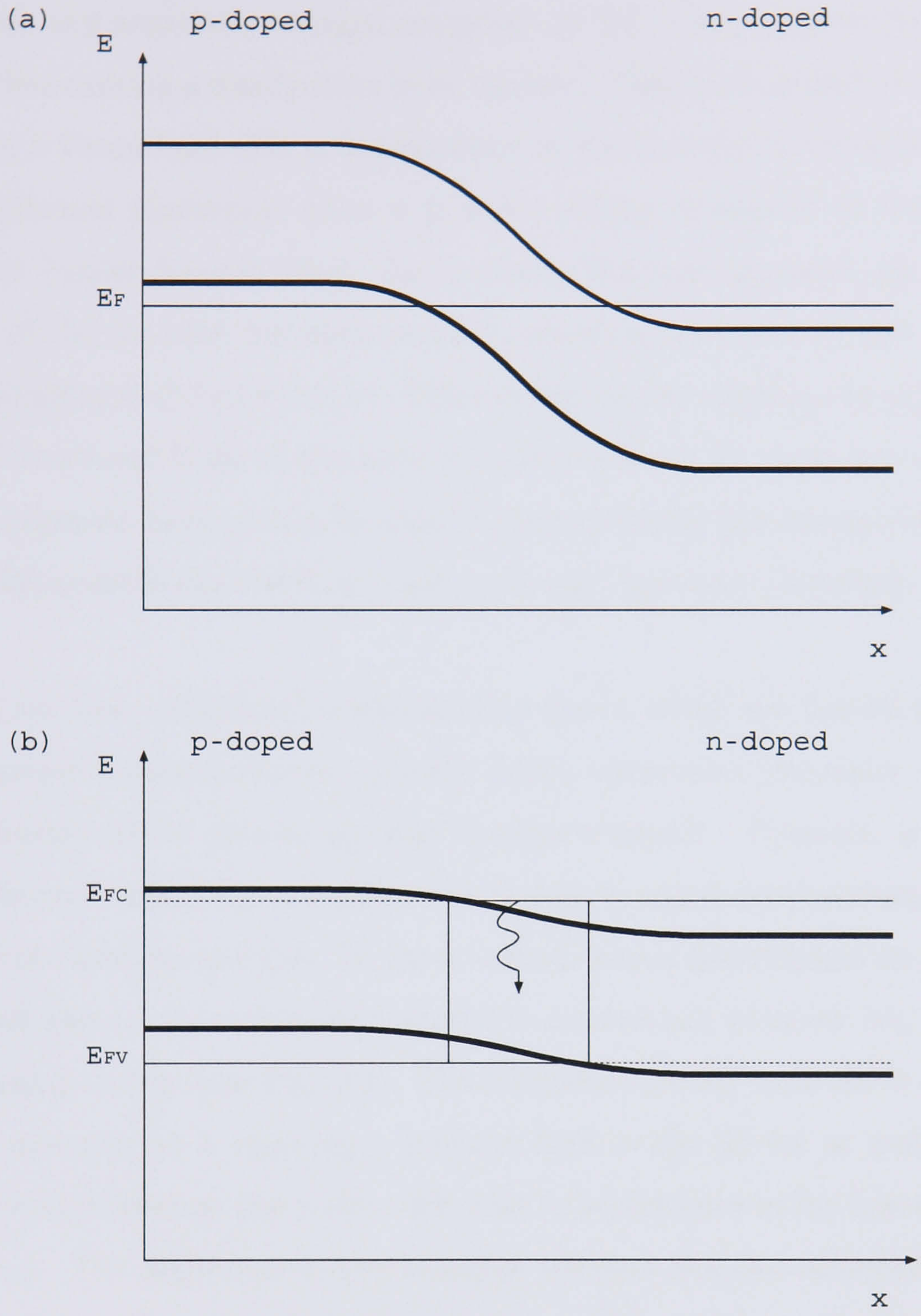

Figure 2.2: Energy band structure for the conduction and valence band edges in a p-n junction (a) when there is no applied voltage in the structure, hence, the Fermi energy is constant. (b) The electron energies are altered when a voltage is applied, confining carriers within the active region in the junction characterized by quasi-Fermi levels E_{FC}, E_{FV} respectively. In both pictures, the uppermost band represents the conduction band while the lowest one features the valence band.

on the n-side and negatively charged acceptors on the p-side, opposes further diffusion of carriers causing a steady state to be reached. Thermal equilibrium is achieved establishing a Fermi level that is independent on the position in the structure.
In nonequilibrium situations, when a positive voltage is applied to the p-side of the junction (under forward bias), the depletion becomes narrower (as the built-in voltage of the junction becomes smaller), allowing a current to flow along the junction, illustrated in figure 2.2(b). This current causes electrons to populate the conduction band and holes to populate the valence band. In these nonequilibrium situations, separate Fermi levels for each of the two bands (conduction and valence bands) called quasi-Fermi levels are used, as it was explained previously.

Until now, we have considered semiconductor lasers which are formed by adjoining same material semiconductor crystals, hence, structures (generally referred as homostructures) where the energy gap remains constant. However, it has been proven to be more useful for optoelectronic devices to adjoin semiconductor crystals with different bandgap energies. In the so-called double heterostructure, a smaller energy band gap ($\sim 0.1 - 0.2\mu m$) material is sandwiched between two regions of higher bandgap energy (see Fig. 2.3). The electrons injected from the n-type semiconductor material by a applying a positive bias to the device as well as holes, injecting the carriers from the p-side, will tend to be confined in the lower band gap active region. The difference in the bandgap between the two materials prevents electrons/holes to diffuse into the p-type/n-type semiconductor material. Therefore the probability of electron-hole recombination processes in this region will increase substantially in this type of semiconductor structures. The lower bandgap active region has a higher refractive index than the outer materials, therefore the light emitted in this region can be guided along the transverse direction (see Fig. 2.3(b) and 2.3(c)). The most important semiconductor lasers are those formed with alloys of elements from the columns *III-V* in the Periodic table of elements. When the center region is made so thin that quantum confinement effects become significant,

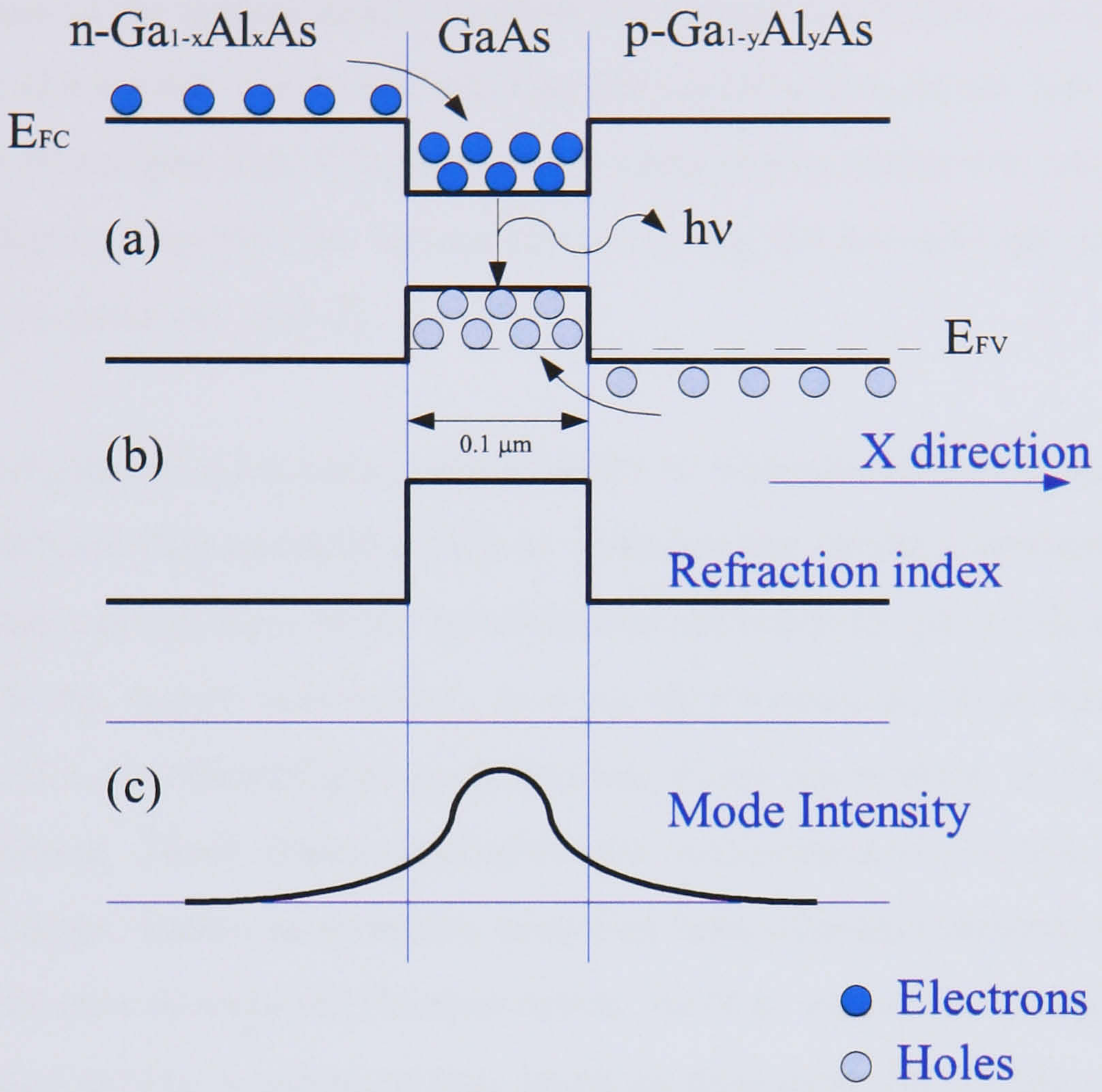

Figure 2.3: (a) Band diagram of forward biased double-heterosturcture GaAs/GaAlAs laser diode. The subscripts x, y refer to the fraction of Ga atoms in GaAs which are replaced by Al ones. The active region, i.e, where carrier recombinations contributing to photon emission into the desired wavelength and hence to gain are confined, is based on GaAs. (b) The refractive index along the cavity making the waveguiding possible through the cavity. (c) The confinement of the optical mode.

we have an extension of the double-heterostructure so-called quantum well laser, which has been demonstrated to have enormous advantages [11] (the confinement of carriers and of the optical mode enhances the interaction between carriers and radiation). In these kind of heterostructures, the center active region has thicknesses below 10 to 20 nm (see Fig. 2.5), so that the carriers are confined in one dimension and their discrete energies can be calculated solving the Schrödinger Equation for a particle in a quantum well [7].

Further developments have been made in order to fabricate optical devices with superior operational characteristics, such as reducing the carrier's environment from a two-dimensional quantum well (*two-dimensional* refers to the number of degrees of freedom in the carrier momentum) to a one-dimensional so-called quantum wire and finally, to a zero-dimensional quantum dot, where the electron is confined in all three-dimensions. Three dimensional quantum confinement of carriers in semiconductor structures, known as quantum dots, has been of major interest due to their promising superior operational characteristics. As in an atom, the lowest part of the electronic structure in a quantum dot, becomes quantized due to the confinement of electrons. The discrete density of states obtained gives rise to high gain in semiconductor devices using these structures. However, in contrast to atoms, quantum dots can be electrically pumped, giving rise to a wide range of applications for optoelectronic devices. Consequently, the use of quantum dots for semiconductor lasers is expected to have superior operational characteristics, in contrast to other less confined structures, such as quantum wells ($1D$ confinement) and quantum wires ($2D$ confinement).

2.3 Electrons in a semiconductor laser

There are significant differences between semiconductor lasers and other classes of lasers, such as, *gas* lasers and *solid-state* lasers. The major advantage of semiconductor lasers is the use of direct electrical pumping. In atomic laser material, electrons surrounding a ion do not interact with neighbouring electrons, whilst electrons in a semiconductor crystal share the whole crystal volume. This is because when two atoms are covalently bonded (as in a semiconductor crystal), the valence electrons of each of the atoms are considerably attracted by the positively charged neighboring nucleus. The electrons position themselves between the atomic cores that compound the bond, organizing (provided they have opposite spin) into the lower energy distribution between the two nuclei. Hence, electrons in semiconductors share the whole crystal occupying allowed bands of states, low-energy valence bands and higher energy ones called conduction bands. In thermal equilibrium and at a temperature of 0 K, conduction bands consist of unoccupied states while valence bands remain occupied by electrons. The energy difference between the two bands is known as the *bandgap* labelled as E_{gap} in figure 2.4. When thermal excitation is included into the system, partial transfer of electrons from the uppermost valence band into the lowest conduction band occur, resulting in the ability of the crystal to conduct electricity.

Each electron within the crystal has a unique spatial wavefunction which defines the motion and properties of the electron and a total energy associated with each allowed state. The electron wavefunctions in the conduction and valence bands of a semiconductor are obtained by solving the Schrödinger equation where the system Hamiltonian, H_0, of the crystal lattice and the energy of the electron E, are related by:

$$H_0\psi = [\frac{\mathbf{p}^2}{2m_0} + V(\mathbf{r})]\psi = E\psi \tag{2.1}$$

where $\mathbf{r}$ is the position vector, $\mathbf{p}$ is the momentum operator ($p = -i\hbar\nabla$ where $\nabla^2 = \frac{d^2}{dx^2} + \frac{d^2}{dy^2} + \frac{d^2}{dz^2}$) [2], m_0 is the free electron mass and $V(\mathbf{r})$ is the potential the electron experiences due to the crystal lattice. The solution of equation 2.1 representing the electron wavefunction can be written as:

$$\psi(\mathbf{r}) = u(\mathbf{r})F(\mathbf{r}) \tag{2.2}$$

where $u(\mathbf{r})$ is a Bloch function which repeats in each unit cell of the crystal due to its periodicity with the crystal lattice (rapidly varying on the scale of the crystal lattice) [2].

$F(\mathbf{r})$, is a slowly varying function known as the *envelope function.* The envelope function can be obtained by solving the Schrödinger equation for the macroscopic potential. This macroscopic potential is due to the spatial dependence of the conduction and valence band edge within the semiconductor heterostructure. This solution of the Schrödinger equation is called the *envelope approximation.* In order to calculate the wavefunctions and energy levels of the electrons in the conduction band and holes in the valence band, we need to solve the Schrödinger equation;

$$-\frac{\hbar^2}{2m^*}\nabla^2\psi = E\psi \tag{2.3}$$

Working in the effective mass approximation, the electrons and holes can be described by a constant effective mass, m^*, depending on the semiconductor material. From Eq. 2.3 we obtain the carrier energy E and the momentum $\mathbf{k}$ in a particular band are related as follows:

$$E(k) = \frac{\hbar^2 k^2}{2m^*} = \frac{\hbar^2}{2m^*}(k_x^2 + k_y^2 + k_z^2) \tag{2.4}$$

where m^* is effective mass of the carrier for a particular band and $\mathbf{k}$ is the momentum of the carrier.

Therefore a parabolic $E - \mathbf{k}$ relationship is associated with the behavior of electrons within a crystal, as illustrated in figure 2.4. Figure 2.4 shows the uppermost valence bands, i.e., ***heavy-hole*** (HH) and ***light-hole*** (LH) as well as the ***spin-orbit/split-off***

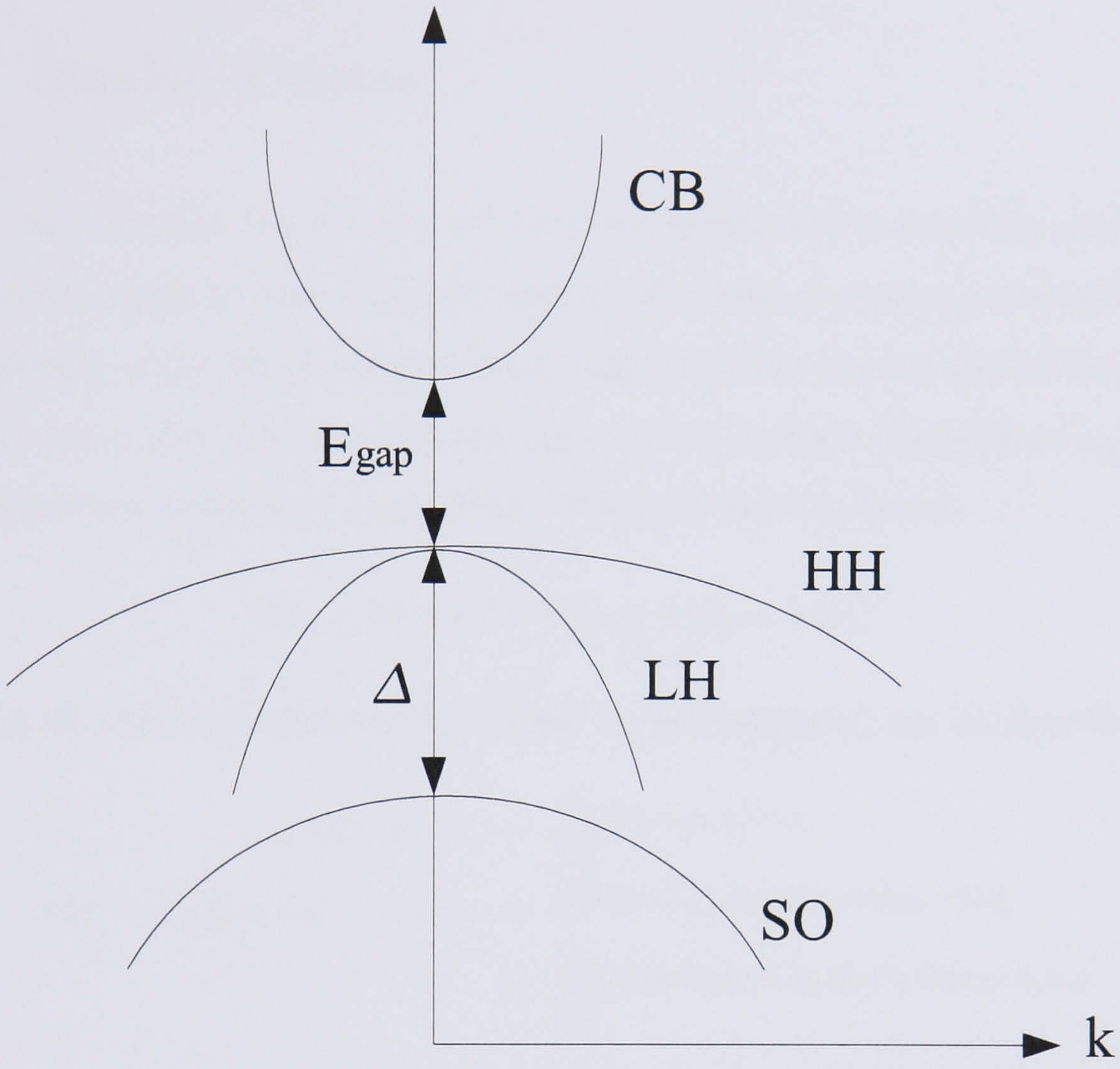

Figure 2.4: A schematic illustration of the heavy-hole (HH), light-hole (LH) and the spin-orbit (SO) valence bands and the lowest conduction band (CB) of a typical semiconductor, as well as their energy separations.

(SO) band. The lowest conduction band (CB) is described too. Hence as equation 2.4 represents, the electron will move much like a free particle in these parabolic bands, but with an effective mass m^*.

2.3.1 Density of states

In order to calculate the number of electrons within the conduction and valence band it is necessary to determine the number of electronic states in the solid. From the properties of the Bloch wavefunction that describes the motion of the electron in a given band (Eq. 2.2) and considering a crystal of finite dimensions L_x, L_y, L_z, the wavefunction must have periodicity within the lattice, hence:

$$\psi(x,y,z) = \psi(x+L_x, y+L_y, z+L_z) \tag{2.5}$$

Following [6], the wavefunction of a carrier in bulk material can be described as

$$\begin{aligned} \psi(x,y,z) &= \frac{1}{\Omega} e^{i[k_x x + k_y y + k_z z]} && (2.6) \\ \psi(x+L_x, y+L_y, z+L_z) &= e^{i[k_x(x+L_x)+k_y(y+L_y)+k_z(z+L_z)]} \\ &= \frac{1}{\Omega} e^{i[k_x x + k_y y + k_z z]} e^{i[k_x L_x + k_y L_y + k_z L_z]} && (2.7) \end{aligned}$$

where Ω is the normalization volume of the semiconductor crystal. Taking into account 2.5, the boundary conditions imposed on the wavefunction $\psi(x,y,z)$ means

$$e^{i[k_x L_x + k_y L_y + k_z L_z]} = 1 \tag{2.8}$$

then

$$|\mathbf{k}_i| = \frac{2\pi}{L_i} \tag{2.9}$$

for $i = x, y, z$. Therefore the discrete values of the $\mathbf{k}$ vector in $\mathbf{k}$-space are given by

$$\mathbf{k} = n_x \mathbf{k}_x + n_y \mathbf{k}_y + n_z \mathbf{k}_z \tag{2.10}$$

for n_x, n_y and n_z in 2.10 integers. Hence the whole crystal volume might be divided into cells each state occupying a volume V_{cell} in **k**-space given by equation 2.11:

$$V_{cell} = \frac{(2\pi)^3}{L_x L_y L_z} \tag{2.11}$$

and consequently we can now associate an electronic state to each differential volume given by Eq. 2.11. Once we have determined the volume occupied by an electronic state, it can provide an expression for the total number of electronic states in the solid per unit energy per unit volume, i.e., the so-called *density of states* (DOS) $\rho(E)$. In order to calculate an expression for the bulk material DOS, we calculate the number of states in **k**-space ($\rho(k)$) within a spherical cell of radius $|\mathbf{k}|$ considering a momentum range k and $k + \mathrm{d}k$, which is obtained dividing the volume of the shell in that momentum range ($(4\pi k^2)\mathrm{d}k$) by the volume occupied by one electronic state (Eq. 2.11), giving:

$$\rho(k)\mathrm{d}k = \frac{(4\pi k^2)\mathrm{d}k}{\frac{(2\pi)^3}{L_x L_y L_z}} \tag{2.12}$$

From equation 2.4 which relates the electron energy in the band with its momentum and taking into account the spin degeneracy factor to allow for the two spin states of each electron, equation 2.12 can be rewritten as follows:

$$\rho(E) = \frac{1}{2\pi^2}\left(\frac{2m^*}{\hbar^2}\right)^{3/2} E^{1/2} \tag{2.13}$$

This density of states function, i.e, the number of electronic states per unit energy interval per unit crystal volume is proportional to the square root of the energy, as can be seen in figure 2.6 (blue line).

However, in quantum well systems where one dimension of the crystal, i.e., L_z decreases to the order of the electron wavelength, i.e., the de Broglie wavelength $\lambda = h/\sqrt{3mk_BT}$ [6] where h [Js] is the Planck's constant [6], T is the temperature of the crystal, m is the particle mass and k_B [J/K] is the Boltzmann's constant [6]. The electronic structure is modified as a result of this reduction in dimensionality.

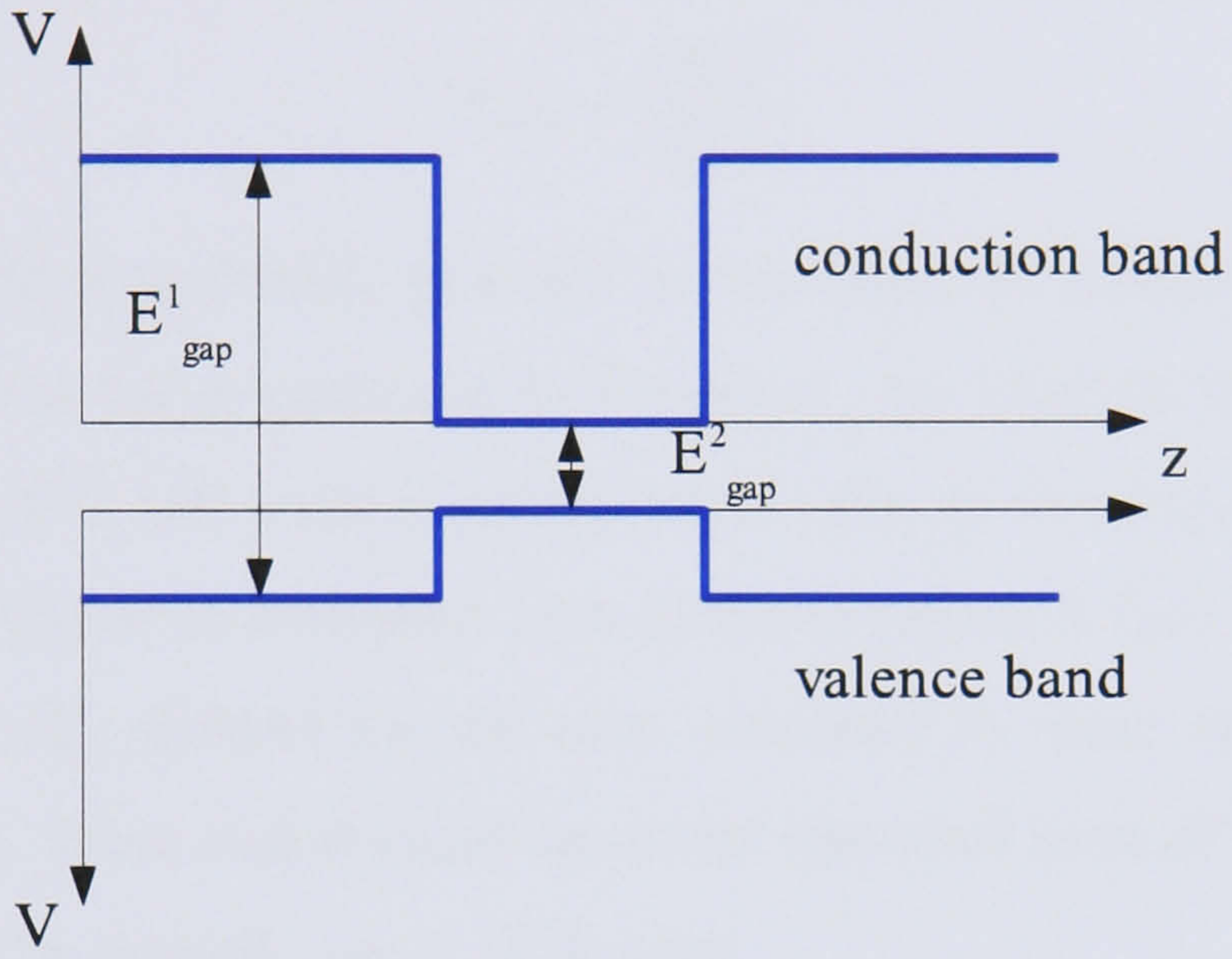

Figure 2.5: The one-dimensional potentials $V(z)$ in the conduction and valence bands which occurs at a heterojunction when two different band-gap materials (E^1_{gap} and E^2_{gap} respectively) are joined together.

In these kind of crystals, the electron can freely move in 2 directions (i.e, in a $2D$ plane), while the component of its momentum in the reduced dimension (normal plane of the layers that constitute the semiconductor structure) acquires discrete (quantified) values. The electron is said to be confined in the region of lower potential as shown in figure 2.5. In this case, the energy bands of the semiconductor are called sub-bands. Hence from equation 2.11, the area occupied in the $k - plane$ by a cell within the crystal will be given by equation 2.14, as follows

$$A_{cell} = \frac{(2\pi)^2}{L_x L_y} \tag{2.14}$$

Following the previous approach, in order to calculate the number of states per unit energy per unit area for a quantum well system, we need to determine the total number of states N^{2D} per unit cross-sectional area in the k-plane. This is given by the product of the area occupied by a circle of radius k (i.e., πk^2) and the spin degeneracy factor (2) divided by the area occupied by each cell (each electronic state, given by Eq. 2.14) and divided again by the total area of the real space (the area occupied by the crystal, i.e., $L_x L_y$), then

$$N^{2D} = 2(\pi k^2)\frac{1}{\frac{(2\pi)^2}{L_x L_y}}\frac{1}{L_x L_y} = \frac{\pi k^2}{(2\pi)^2} \tag{2.15}$$

Making use of equation 2.4, where the electron momentum and the energy of the electron in the sub-band are related, and also equation 2.15, the density of states for a quantum well system, i.e., the number of electronic states per energy (for a single sub-band) per unit volume for a quantum well of width L_z, may be calculated as follows:

$$\rho^{2D}(E) = \frac{\mathrm{d}N^{2D}}{\mathrm{d}E} = \frac{m^*}{L_z \pi \hbar^2} \tag{2.16}$$

In this equation 2.4 the electron momentum and the energy of the electron in the sub-band are related. Figure 2.6 (black color line) shows the density of states for a quantum well active region, per unit volume for 3 sub-bands. In order to calculate the density of states, $\rho^{2D}(E_i)$ at a particular energy E_i, hence, the number of electronic states at that energy per unit volume of *real* space (the crystal dimensions), the contributions from all confined energy levels must be considered, as is shown in figure 2.6.

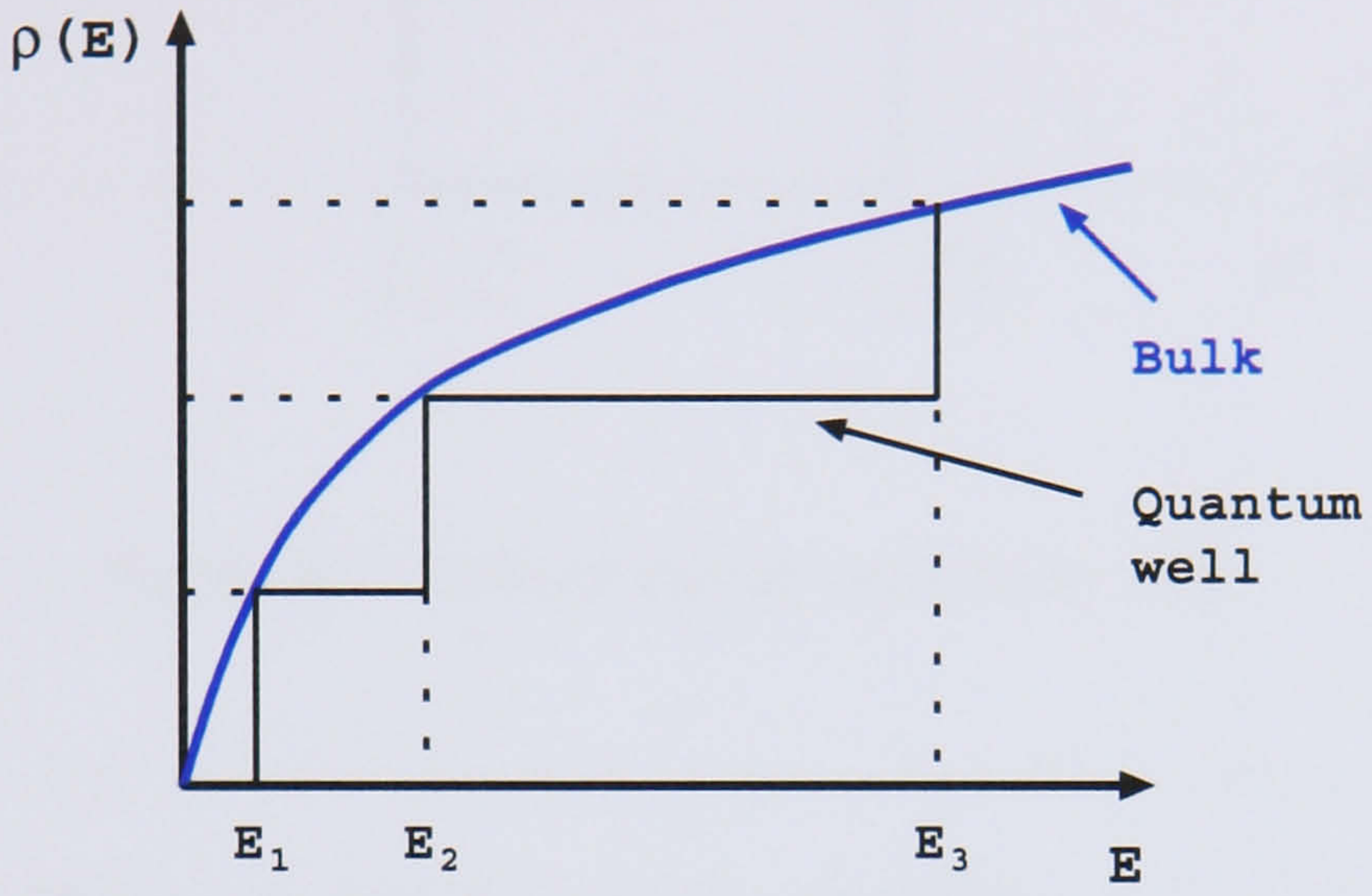

Figure 2.6: Density of states for a bulk material (blue line) and an infinite-barrier quantum well material (black line), showing the first 3 confined states for this last case.

The discrete energy levels E_i shown in figure 2.6, correspond to the solution of the Schrödinger equation given by 2.1 for an infinite-barrier quantum well pictured in figure 2.7. The electron is confined in the z-direction into a potential $V(z) = 0$ region. The envelope function in an infinite-barrier potential, is obtained by solving the differential equation given by Eq. 2.3, hence, the sum of plane waves [2]:

$$\psi(z) = Ae^{ikz} + Be^{-ikz} \tag{2.17}$$

where

$$k^2 = \frac{2m^*}{\hbar^2}E \tag{2.18}$$

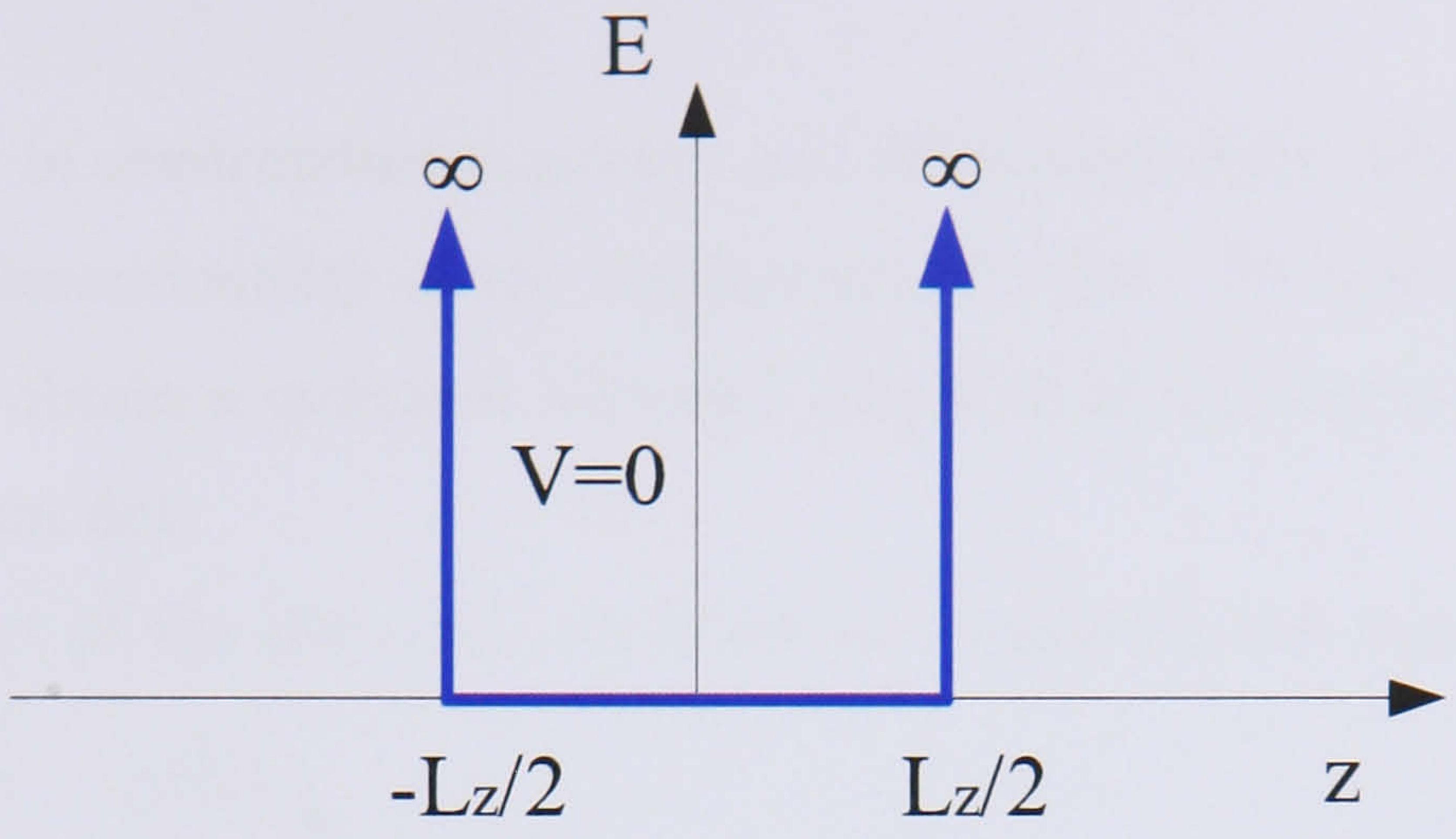

Figure 2.7: Infinite-barrier quantum well.

rewriting the wavefunction given by equation 2.17 [2]

$$\psi = \begin{cases} A\cos kz & \text{(symmetric solutions)} \\ A\sin kz & \text{(antisymmetric solutions)} \end{cases} \tag{2.19}$$

and taking into account that the wavefunction has to be zero at the boundaries, i.e., $\psi(L_z/2) = 0$ (see figure 2.7), for both symmetric and antisymmetric solutions, then

$$\tfrac{kL_z}{2} = n\tfrac{\pi}{2} \quad \text{for } n = 1, 2, 3, ... \tag{2.20}$$

where even quantum numbers correspond to antisymmetric states while odd quantum numbers refer to symmetric ones. Hence, the corresponding discrete energy levels pictured in figure 2.6, i.e., E_i may be obtained by substituting each discrete value of k in equation 2.20 back into equation 2.18, hence

$$E_i = i^2 \frac{\hbar^2 k_i^2}{2m^*} \tag{2.21}$$

for $i = 1, 2, ...$. Therefore, E_1 in figure 2.6, $E_1 = \frac{\hbar^2 k_1^2}{2m^*}$ and $k_1 = \frac{\pi}{L_z}$ (Eq. 2.20 for $n = 1$).

New techniques in semiconductor growth and fabrication have allowed researchers to reduce the dimensionality of the confinement further. By confining carriers in 2 directions we obtain a quantum wire and confining in all 3 spatial directions we obtain a quantum dot.

The lowest part of the electronic structure in a quantum dot becomes quantized due to this confinement of electrons. A three dimensional quantum confinement implies a delta like density of states of the lasing material, hence, the electron can be localized inside the quantum dot in a set of different discrete energy states, or *energy levels* (see figure 2.8).

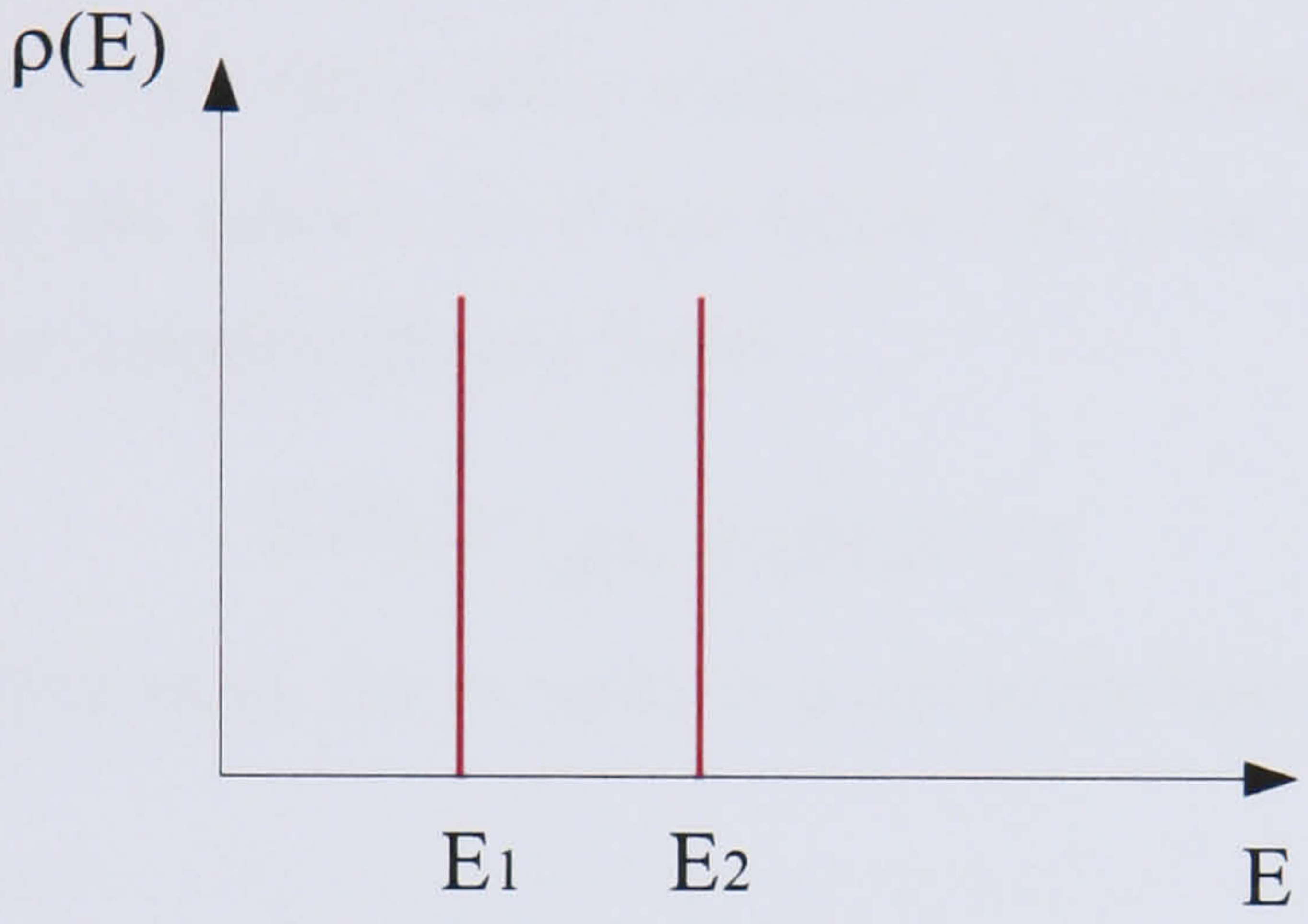

Figure 2.8: Density of states as a function of energy for a quantum dot. The energy levels are quantized in all 3-directions, hence, appearing discrete energy levels.

The use of quantum dots for semiconductor lasers is expected to have superior operational characteristics, in contrast to the continuous DOS of the bulk semiconductor (Eq. 2.13) or to the other less confined structures as quantum wells ($1D$ confinement) or quantum wires ($2D$ confinement). A narrow density of states of a structure with very little variation in quantum dot sizes, may be driven to couple modes of Fabry-Perot cavity, resulting in a narrow gain which improves significantly the performance of optical devices.

2.3.2 Occupancy of the electronic states

In order to calculate the optical/electrical properties of semiconductor structures, it is necessary to determine how electrons occupy the available density of states. Electrons, being fermions, obey Fermi-Dirac statistics. The probability of an electronic state of energy E_b in the valence band (see figure 2.9) to be occupied by a hole is given by Fermi-Dirac statistics [6] as follows:

$$f_v(E_b) = \frac{1}{e^{(E_b - E_{F_v})/k_B T} + 1} \tag{2.22}$$

while in the conduction band, the occupancy probability function for an electron is written as

$$f_c(E_a) = \frac{1}{e^{(E_a - E_{F_c})/k_B T} + 1} \tag{2.23}$$

where E_{F_v} in Eq. 2.22 and E_{F_c} in Eq. 2.23 are the quasi-Fermi levels under conditions in which thermal equilibrium happens to be disturbed, such as, with photoexcitation where a large population of carriers (conduction electrons and holes) is created as pictured in figure 2.9. All energies in equation 2.23 and 2.22 are relative to the band edge and assumed positive into the band. In thermal equilibrium (when no pumping is injected to the semiconductor medium) a single Fermi energy level applies to both valence and conduction bands, located in the middle, $E_{F_v} = E_{F_c} = E_F$ as illustrated in figure 2.10.

2.4 Optical transitions in a semiconductor

Up until now, we have studied how electronic states in a semiconductor may be described by an energy band structure consisting of one conduction band and several

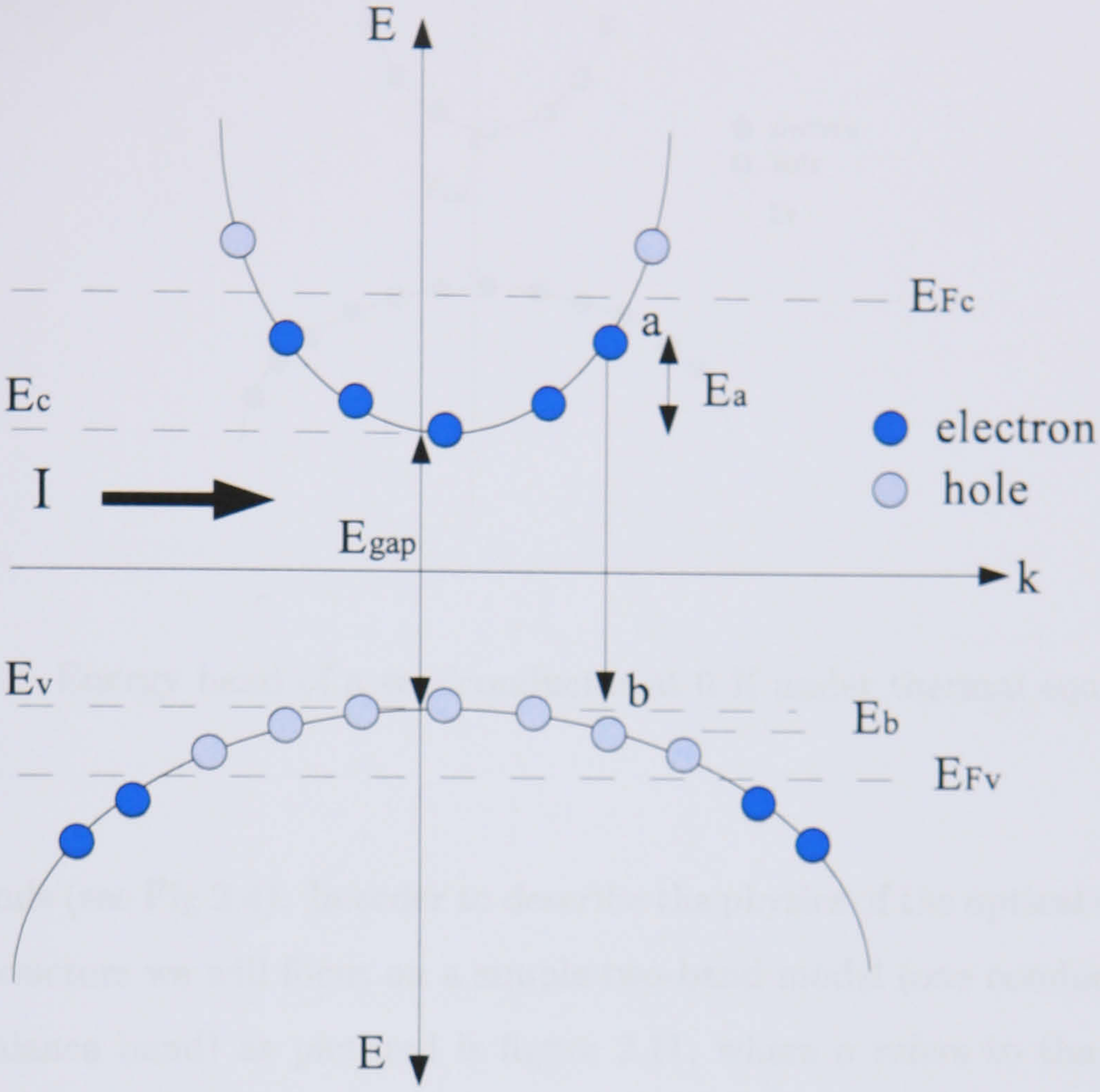

Figure 2.9: A schematic representation of the electronic structure of a pumped semiconductor medium by an external intensity I at 0 K. Quasi-Fermi levels are illustrated for nonequilibrium carrier densities. A transition between two energy states, a and b with the same $\mathbf{k}$ value, i.e., a state in the conduction band at energy $E_a = \frac{\hbar^2 k^2}{2m_c^*}$ and b state in the valence band at energy $E_b = \frac{\hbar^2 k^2}{2m_v^*}$ is highlighted. The lowest energy in the conduction band, i.e, E_c is called the *conduction band edge* whereas the highest energy in the valence band, i.e, E_v is referred as the *valence band edge*.

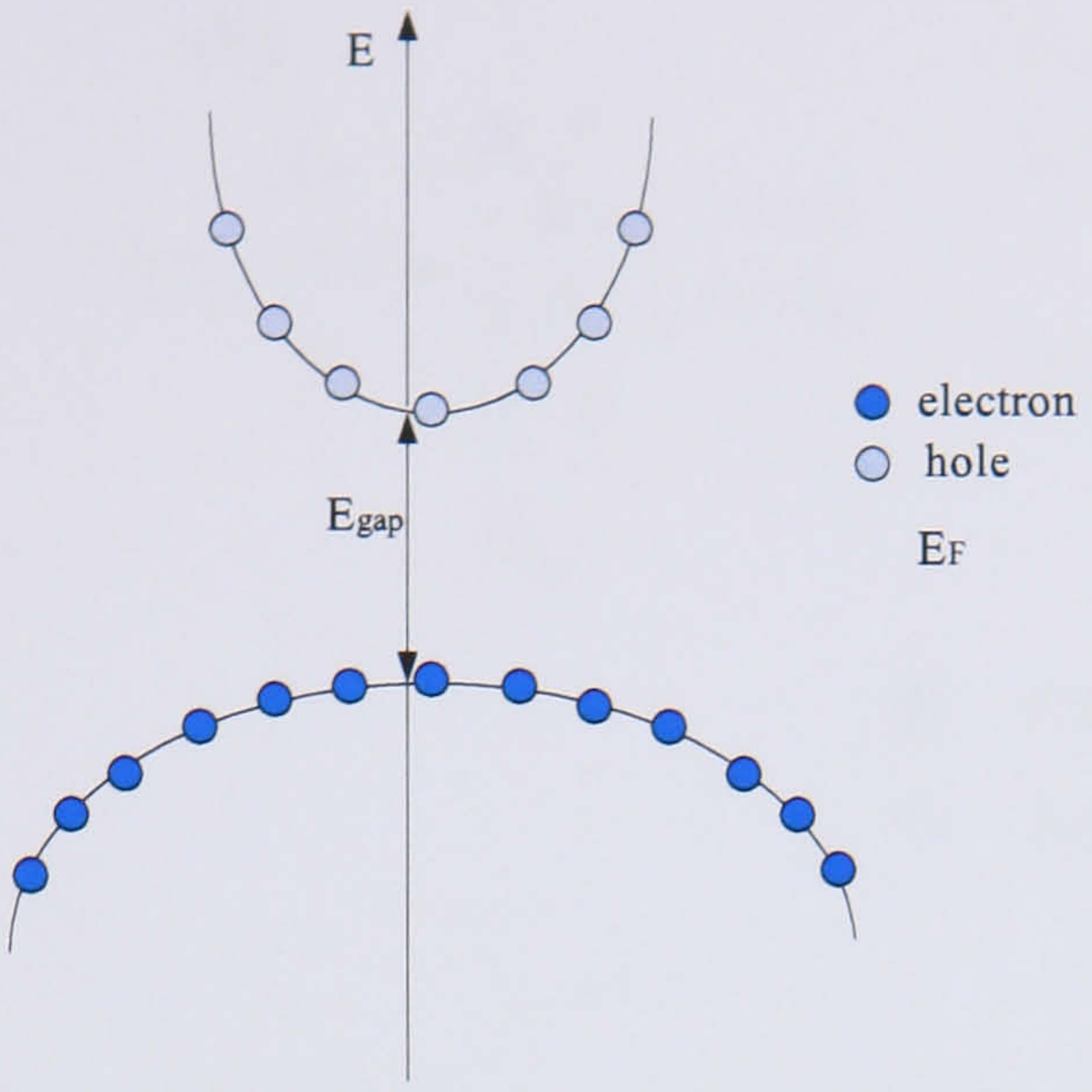

Figure 2.10: Energy band of a semiconductor at 0 K under thermal equilibrium.

valence bands (see Fig 2.4). In order to describe the physics of the optical transitions in semiconductors we will focus on a simple two-band model (one conduction band and one valence band) as pictured is figure 2.11, where a refers to the electronic state in the conduction band at energy E_a previously pictured in figure 2.9, and b represents the electronic state in the valence band at energy E_b. In the absence of thermal or other energy pumping processes, the semiconductor appears to have a completely empty conduction band, while the valence band remains full of electrons.

If an electron in the valence band absorbs light, it is excited into the empty conduction band creating a hole (missing electron) in the valence band (see figure 2.11(a)), hence, a *charge* carrier in the conduction band and a positively *charge* carrier (a hole) in the valence band, allowing electrical conduction. However, only transitions where the momentum ($\equiv \hbar\mathbf{k}$) of the involved initial and final electronic states are equal will be allowed, i.e., the total momentum must be conserved. The difference in the electron momentum (initially in the valence band and in the conduction band

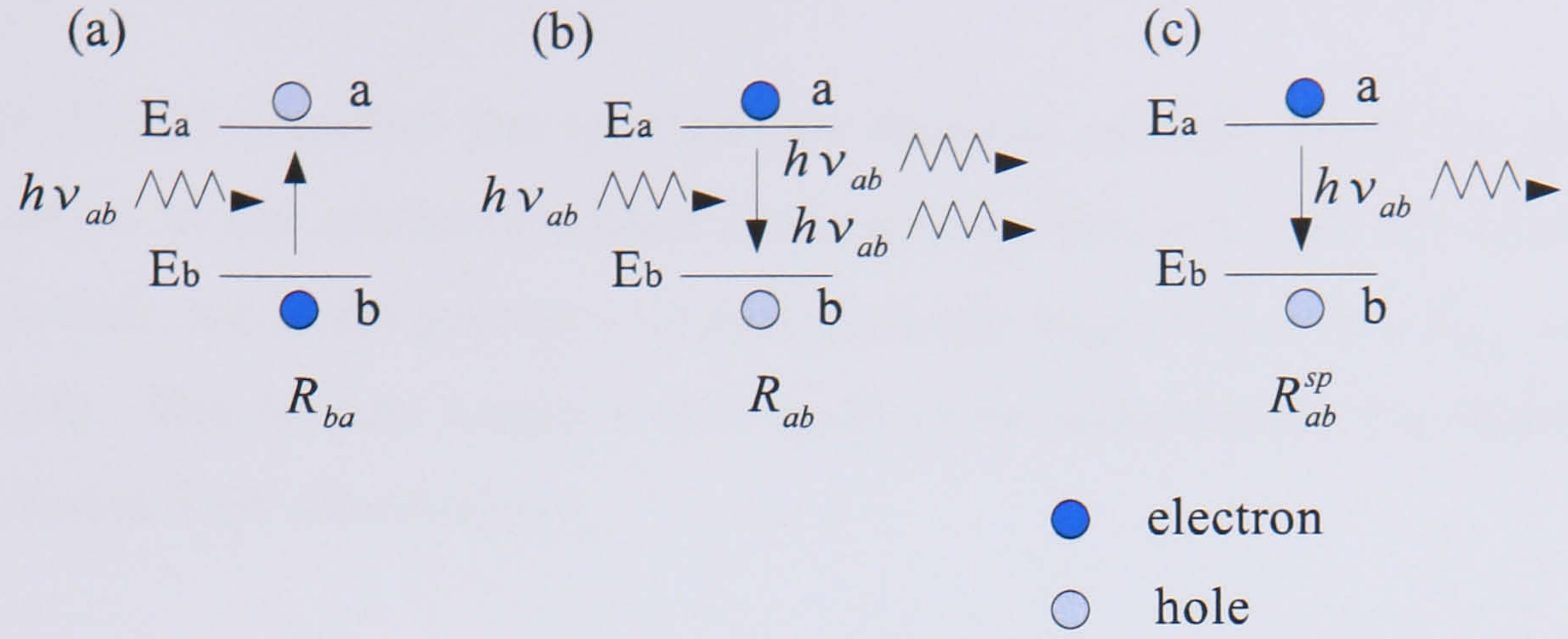

Figure 2.11: A schematic representation of the three types of band to band optical transitions, i.e., spontaneous emission (R^{sp}_{ab}), stimulated emission (R_{ab}) and stimulated absorption (R_{ba}), involving a single level pair *a*-*b* with the same **k** value pictured in figure 2.9.

finally) must be equal to the momentum of the photon involved in the transition (Fig. 2.11(a)). As the momentum of the photon can be neglected comparing to the momentum of the carrier, only vertical transitions (optical transitions) will be allowed (transitions involving electronic states with the same **k** value as pictured in figure 2.9). This is called the **k**-selection rule.

However, when a downward transition is induced by an electromagnetic field, i.e., when an electron in a E_a electronic state undergoes a transition into another electronic state E_b in the valence band as a result of the presence of an electromagnetic field $h\nu_{ab}$ (see Fig. 2.11(b)), another photon identical to the incident is generated. This process is called the stimulated recombination process (or stimulated emission) and in contrast with the previously explained reverse process, i.e., the stimulated absorption process (Fig. 2.11(b)) which creates a hole in the valence band, the stimulated emission process instead generates a hole in the conduction band.

Figure 2.11(c) describes the spontaneous emission process, where an electron in the state a in the conduction band undergoes a transition into the valence band state b, emitting in the process a photon of energy $h\nu_{ab} = E_a + E_b + E_{gap} = E_{ab}$ (see Fig. 2.9). This process happens as a result of *no* inducement of a radiation field (no classical field stimulation).

Both the stimulated emission rate, R_{ab} (described in Fig. 2.11(b)) as well as the spontaneous emission rate, R_{ab}^{sp} (Fig. 2.11(c)) will be proportional to the probability of finding an electron at the energy E_a (Eq. 2.23) and the probability of finding a hole (an unoccupied state) in the energy E_b (Eq. 2.22) in the valence band (see Fig. 2.11(b),(c)), while the stimulated absorption process, R_{ba} (Fig. 2.11(a)) requires the presence of an electron in the valence band state E_b, hence:

$$R_{ab} \propto f_c(E_a) f_v(E_b) \tag{2.24}$$

$$R_{ab}^{sp} \propto f_c(E_a) f_v(E_b) \tag{2.25}$$

$$R_{ba} \propto [1 - f_v(E_b)]\,[1 - f_c(E_a)] \tag{2.26}$$

2.4.1 Reduced density of states

As previously mentioned, only transitions which satisfy both momentum ($\hbar\mathbf{k}$) and energy conservation are allowed, i.e. transitions involving electron and hole states with the same $\mathbf{k}$-vector and where the transition energy E_{ab} is equal to the involved photon energy $h\nu_{ab}$. Consequently, it is more appropriate to consider the number of allowed state *pairs* (transitions) in a semiconductor material, the so-called *reduced* density of states ($\rho_r(E)$). Rather than use the single carrier density of states for electrons and holes, we use the reduced density of states in order to calculate the transition rates previously described.

The density of states referring to the transitions described in figure 2.11, $\rho_r(E_{ab})$ where $E_{ab} = E_a + E_b + E_{gap}$ (see Fig. 2.9) can be obtained for each semiconductor structure (bulk, quantum well, quantum wire and quantum dot) by replacing the effective mass in the previously given formulas (Eq. 2.13 for bulk material, Eq. 2.16 for quantum well structures) by the *reduced* mass m_r^* [2]

$$m_r^* = \frac{m_c^* m_v^*}{m_c^* + m_v^*} \tag{2.27}$$

Therefore taking into account this equation and also the expression for total transition energy E_{ab}, given by

$$E_{ab} = E_a + E_b + E_{gap} \tag{2.28}$$

the energies of the conduction and valence band states, i.e., E_a and E_b, relative to the conduction and valence band-edges respectively, may be described as a function of the energy and the masses as follows;

$$\begin{aligned} E_a &= \frac{\hbar^2 k^2}{2m_c^*} = \frac{m_r^*}{m_c^*}(E_{ab} - E_{gap}) && (2.29) \\ E_b &= \frac{\hbar^2 k^2}{2m_v^*} = \frac{m_r^*}{m_v^*}(E_{ab} - E_{gap}) && (2.30) \end{aligned}$$

For example, taking into account the expression for the density of states for a bulk semiconductor given by equation 2.13 in section 2.3.1, the reduced density of states function for a bulk semiconductor can be given by

$$\rho(E_{ab}) = \frac{1}{4\pi^2}\left(\frac{2m_r^*}{\hbar^2}\right)^{3/2}(E_{ab} - E_{gap})^{1/2} \tag{2.31}$$

2.5 Gain and absorption

In this section we will describe how gain, absorption and spontaneous emission can be calculated for a semiconductor structure. Considering the optical processes described in section 2.4, the transition rates per unit volume per unit time for a single optical mode at the energy $h\nu_{ab}$, for the processes illustrated in figure 2.11 described in equations (2.24), (2.25) and (2.26) can be rewritten as follows [2]:

$$R_{ab} = B_{ab}\rho_r(E_{ab})f_c(E_a)f_v(E_b)\rho_{opt}(h\nu_{ab}) \tag{2.32}$$

$$R_{ba} = B_{ba}\rho_r(E_{ab})\left[1 - f_v(E_b)\right]\left[1 - f_c(E_a)\right]\rho_{opt}(h\nu_{ab}) \tag{2.33}$$

$$R_{ab}^{sp} = A_{ab}\rho_r(E_{ab})f_c(E_a)f_v(E_b) \tag{2.34}$$

where A and B are the Einstein coefficients [3], $\rho_{opt}(h\nu_{ab})$ is the photon density of the optical mode (the number of photons into the optical mode $h\nu_{ab}$), $f_c(E_a)$ and $f_v(E_b)$ are the occupation probabilities given by Eq. 2.23 and Eq. 2.22 respectively, and $\rho_r(E_{ab})$ is the reduced density of states for a transition energy E_{ab}.

It has to be highlighted that R_{ab} and R_{ba} are competing processes as R_{ab} generates a photon while R_{ba} absorbs one, therefore the net decrease rate of photons in a semiconductor (net_{ba}) is given by;

$$net_{ba} = R_{ba} - R_{ab} \tag{2.35}$$

The *absorption* of photons into the mode $h\nu_{ab}$ in a semiconductor material can be described as [2]

$$\alpha(h\nu_{ab}) = \frac{net_{ba}}{\rho_{phot}(h\nu_{ab})} \tag{2.36}$$

where $\rho_{phot}(h\nu_{ab})$ is the density of photons into the optical mode $h\nu_{ab}$ [2]. Therefore the fractional decrease of photons (at energy $\hbar\omega_{ab}$) per unit length of the semiconductor material may be written as follows [2]

$$\alpha(\hbar\omega_{ab}) = \frac{e^2 h}{2\epsilon_0 m_0^2 c\bar{n}(\hbar\omega_{ab})}|M_T|^2\rho_r(\hbar\omega_{ab})\left[1 - f_c(E_a) - f_v(E_b)\right] \tag{2.37}$$

where $|M_T{}^2$ is the momentum matrix element (related to the interaction of the electron with the electromagnetic wave) [2]. The *gain* of the semiconductor material which refers to the net *downward* transitions of an electron producing a photon will be the *negative absorption.* However, when a high carrier density is injected into the system in order to obtain gain, it produces as well an increase in the spontaneous emission rate. The spontaneous emission rate, R^{spon} for the process described in figure 2.11(c) into the mode $\hbar\omega_{ab}$, per unit volume may written as follows [2]

$$R^{spon}(\hbar\omega_{ab}) = \frac{4\pi\bar{n}e^2(\hbar\omega_{ab})}{\epsilon_0 m_0^2 \hbar^2 c^3}|M_T|^2\rho_r(\hbar\omega_{ab})f_c(E_a)f_v(E_b) \tag{2.38}$$

2.6 Threshold gain

A laser requires a gain medium to provide amplification of light. We discussed in the previous section that while stimulated emission increases the number of photons in the cavity, stimulated absorption (Eq. 2.37) decreases them. In order to have light amplification in the cavity, we need to have a surplus of electrons in higher energy levels, i.e., the so-called population inversion achieved by pumping so that more electrons can be stimulated to undergo a downward transition producing photons. However, as we have previously explained, photons will eventually be absorbed resulting in the attenuation of the optical field (absorption losses). Consequently, an optical field which can be amplified propagating through the cavity, is not sufficient to make a laser. It is necessary to have a *resonator*, consisting of two parallel mirrors separated by a distance L and each of them with equal facet reflectivities R in order to enforce the propagating field to traverse repeatedly the amplifying medium (the gain medium). The gain necessary to overcome the material losses, α_0 (optical mode losses of the laser cavity) and the mirror losses is known as the *threshold* material gain, G_{th}, given by [11]

$$G_{th} = \alpha_0 + \frac{1}{L}\ln\left[1/R\right] \tag{2.39}$$

Equation 2.39 actually represents the threshold modal gain of the laser. This can be related to the threshold material (or local) gain [11], g_{th} by the expression;

$$G_{th} = \Gamma g_{th} \tag{2.40}$$

Here Γ is the optical confinement factor, and gives a measure of the overlap of the optical field and the gain producing region of the laser. It should be noted that the gain/absorption calculated using equation 2.37 is the material gain of the semiconductor.

2.7 Self-assembled quantum dot lasers

Since quantum dot structures started to draw the attention of researchers [4], there have been substantial improvements in the fabrication of quantum dot semiconductors for lasers. For device applications, it may be advantageous to place the quantum dots in a quantum well as in self-assembled quantum dot structures (SADs) [9], [1]. Self-assembled In(Ga)As quantum dots are formed on a single-crystal GaAs substrate via Stranski-Krastanov [10] epitaxial growth [5] which is described in the introduction. In this structure, the highly strained quantum well, known as the wetting layer, aids the capture of charge carriers into the dot. Dots are grown on top of the wetting layer while the whole structure is covered by bulk material (Fig. 2.12). The confining potential of the carriers in the wetting layer (of the $2D$ carriers) results from the different band gaps between the wetting layer material and the surrounding bulk material. Initially, carriers diffuse in the lower-band gap $2D$ WL before either recombining or being captured by the SADs, where they can either relax into lower energy levels or re-excite back to the wetting layer. Once in the wetting layer they can diffuse and be captured by other quantum dots within the ensemble. Hence the wetting layer supplies the quantum dots with carriers, appearing as a carrier reservoir.

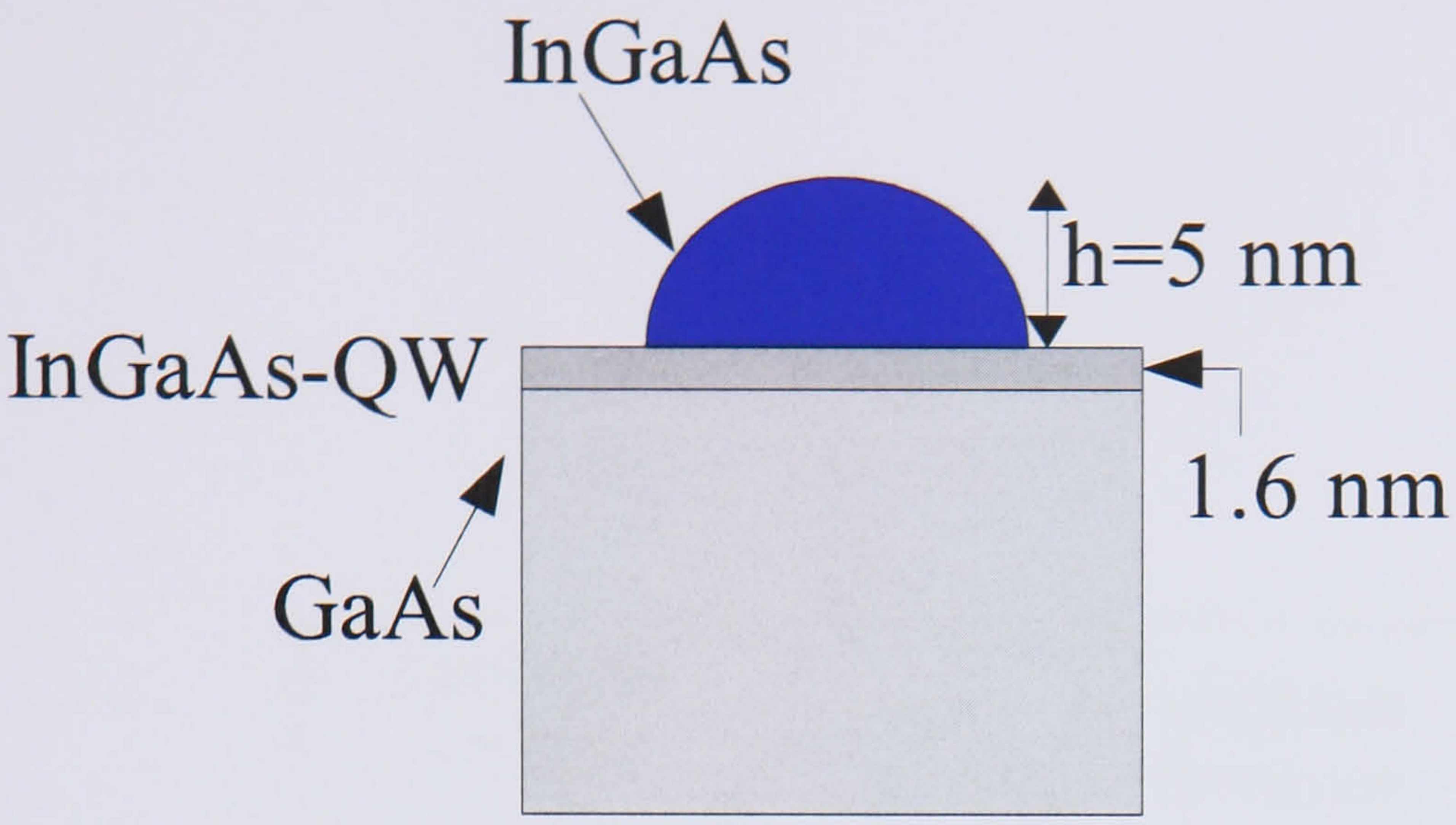

Figure 2.12: Illustration of a self-assembled quantum dot on top of the wetting layer, both embedded in bulk material.

The ensemble of quantum dots formed on the wetting layer usually consists of different sized quantum dots as a result of the difficulties in controlling the growth conditions of these structures. Consequently the energy level structure of each quantum dot will vary from that of a different size quantum dot structure, resulting in a broadening of the delta-like density of states of the quantum dots throughout the ensemble. This kind of broadening is often described by a Gaussian distribution function and it is known as inhomogeneous broadening. However as will be discussed in chapter 5 the model we construct does not use this approximation but considers individual fluctuations in dot sizes.

There is also a broadening of each individual quantum dot state due to carrier scattering mechanisms as a consequence of the Heisenberg uncertainty principle. We will study these different scattering mechanisms responsible for carrier capture and relaxation in the dots and their effect in optical transitions, in detail in fur-

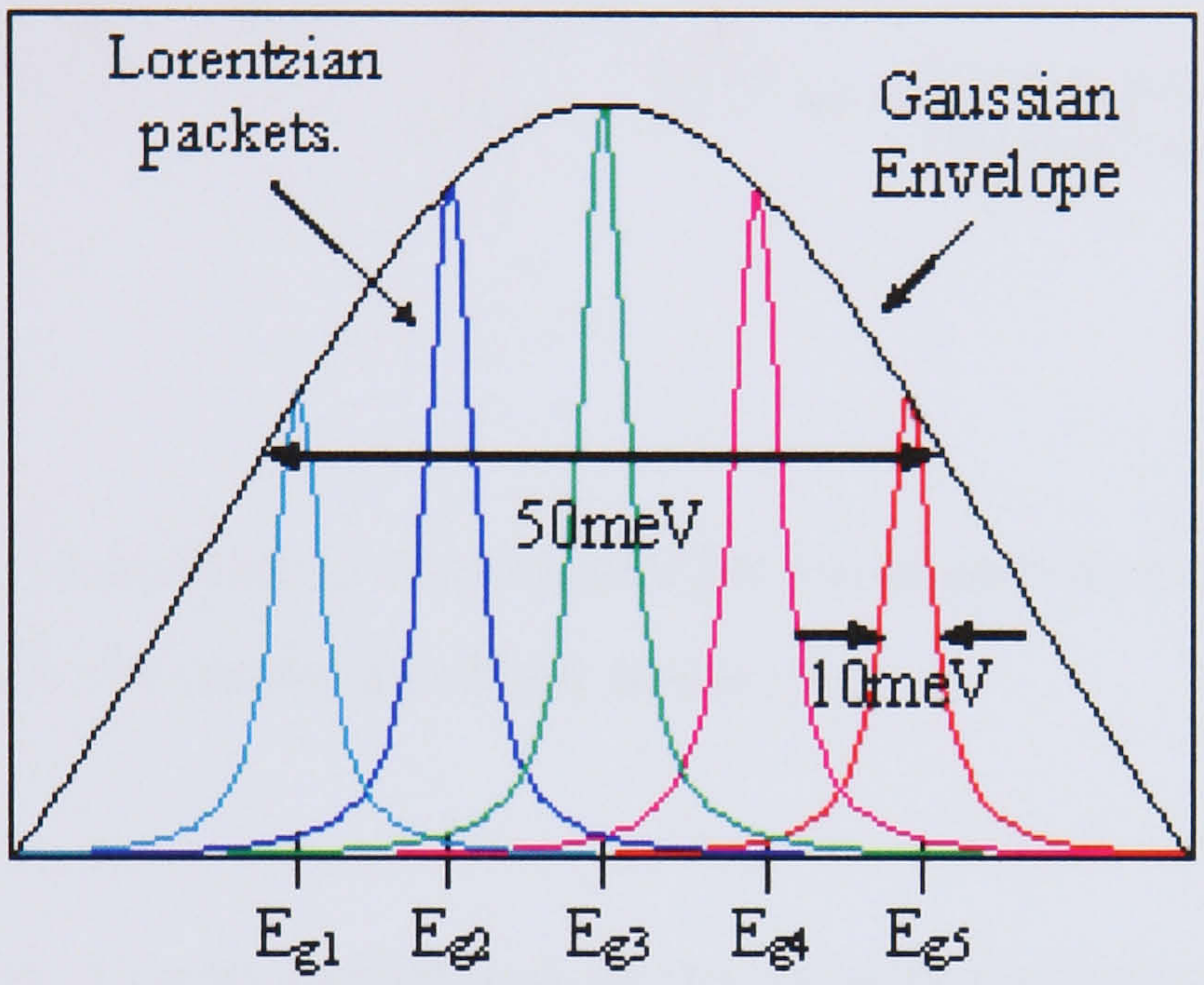

Figure 2.13: Schematic representation of the typical spectral broadening processes in quantum dot lasers, where E_{gi} $i = 1, 2...5$ represents the ground state energy for 5 different sizes of quantum dots [8].

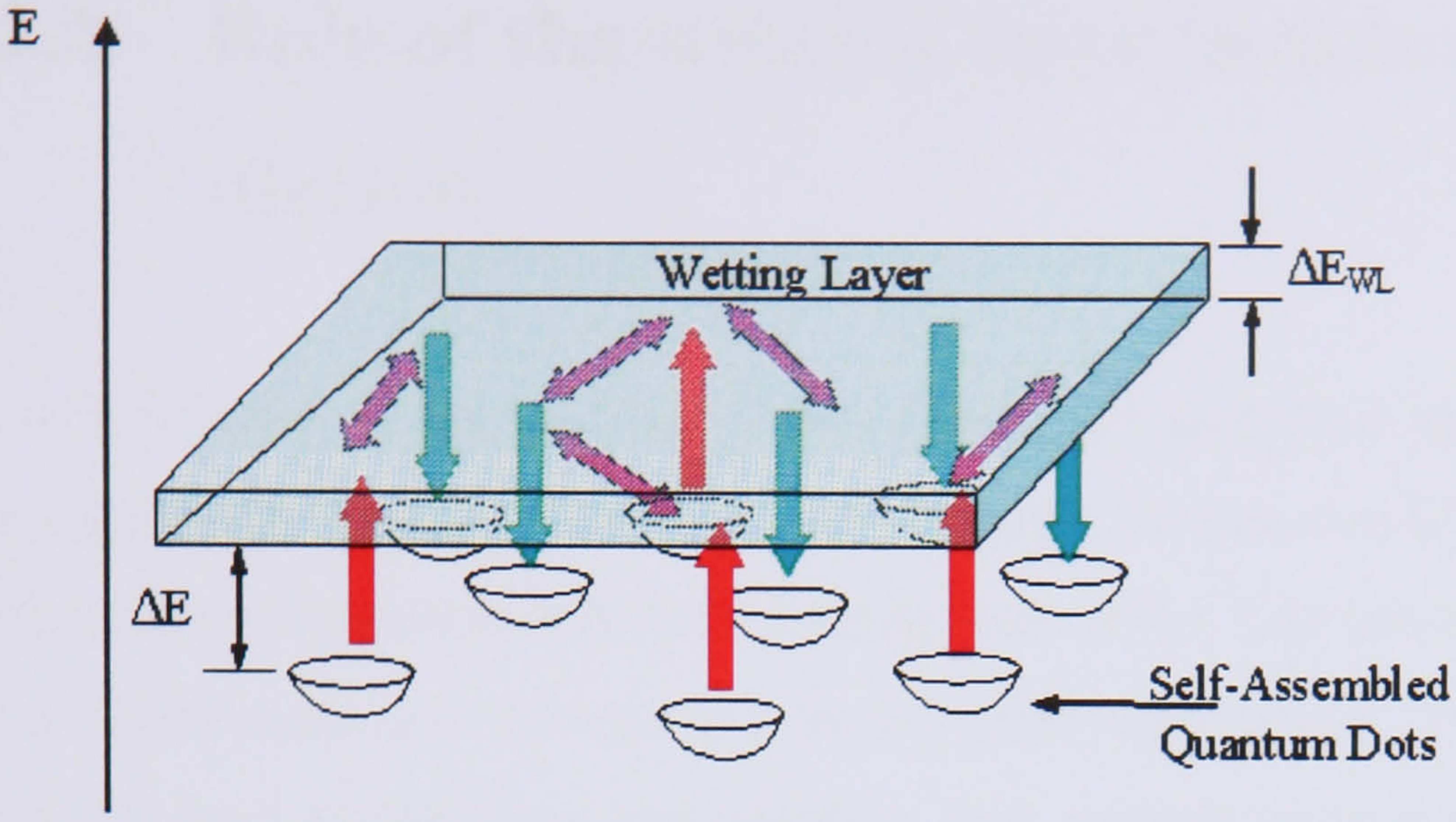

Figure 2.14: Illustration of a self-assembled quantum dot on top of the wetting layer, featuring only the conduction band states [8].

ther chapters. Carrier-carrier and carrier-phonon scattering mechanisms deal to a broadening of the quantum dot discrete energy levels. This so-called homogeneous broadening is described as a Lorentzian function with a width of tens of meV. Both inhomogeneous and homogeneous broadening are represented in figure 2.13. It shows the lowest energy level for five different sizes of quantum dots, all of them being homogenously broadened. Because of the difference in size of the dots within the ensemble, the difference in energy of the plotted ground states, may be described as a gaussian envelope function.

2.8 Role of the wetting layer in quantum dot population

As mentioned in the previous section, when self-assenbled quantum dot structures are grown by Stranski-Krastanov [10] epitaxy, the dots are formed on top of a two-dimensional quantum well ($2D$) wetting layer (WL). Carriers within a QW sub-band are distributed as a $2D$ gas in a Fermi-Dirac distribution. In quantum dot lasers, the injected carriers into the quantum well wetting layer embedding the quantum dots, will eventually be captured into the quantum dots' excited states, and then relax to the fundamental lasing state. The captured carriers within the quantum dot can be re-excited into the wetting layer states, and be captured again by other quantum dots within the ensemble. Hence the wetting layer, has a very important role in the performance of quantum dot based optical devices, as it determines the population statistics of a quantum dot laser.

Figure 2.14 [8] describes the energy representation (for conduction band states only) of the wetting layer and quantum dot system. ΔE in figure 2.14 describes the energy difference between the highest electron energy level within the quantum dot (dependent on the quantum dot size) and the lowest electron energy state in the wetting layer. As a result of the band gap difference between the wetting layer material and the surrounding bulk material (previously pictured in figure 2.12), there is a confining potential for both the $2D$ electrons and the $0D$ electrons, represented by ΔE_{WL} in figure 2.14.

The performance of optical devices based on quantum dot lasers critically depends on the capture of carriers into the quantum dots, as well as the relaxation of carriers through the localized quantum dot states. As we will see in chapters 3 and 4, the population of quantum dots is governed by the efficient scattering mechanisms of carriers between the $2D$ de-localized quantum well states and the discrete localized quantum dot states, as a consequence of the Coulomb interaction.

In chapter 5 rate equations for the carrier occupation probabilities will be derived in order to study the carrier dynamics within the quantum dots.

2.9 Summary

In this chapter a general description of a semiconductor laser has been given. In a semiconductor crystal, electrons occupy allowed states. The total number of states available for occupation by an electron at a particular energy is given by the density of states function. However, in order to calculate the optical/electrical properties of semiconductor structures, it is also necessary to determine the probability of occupation of the allowed states in a crystal. Given that carriers are fermions, the probability of occupation of a state is given by Fermi-Dirac statistics. In this chapter, we have described the density of states for different semiconductor structures, also determining the expressions for the Fermi-Dirac distribution functions of the semiconductor conduction and valence bands. We have emphasized the advantages of a delta like density of states of quantum dot based structures; the electron can be localized in the quantum dot in a discrete set of energy states, therefore this confinement of carriers enhances the chances of recombination processes, improving significantly the performance of devices based on quantum dot structures.

We have also described the different optical transitions in order to determine an expression for the optical gain and spontaneous emission rate. Finally, we focus on self-assembled quantum dot structures formed via Stranski-Krastanov epitaxial growth as explained in 1. We have also described the crucial role of the wetting layer as supplies the quantum dots with a carrier reservoir therefore playing a large part in the carrier dynamics.

Bibliography

[1] F. Adler, M. Geiger, A. Bauknecht, F. Scholz, H. Schweizer, and M. H. Pilkuhn. *Appl. Phys.*, vol. 80:pp. 4019, 1996.

[2] Larry A. Coldren and Scott W. Corzine. *Diode Lasers And Photonic Integrated Circuits.* Wiley-Interscience, 1995.

[3] A. Einstein. On the quantum theory of radiation. *Physicalische Zeitschrift*, (18):pp. 121–128, 1917.

[4] T. Fukui, S. Ando, Y. Tokura, and T. Toriyama. Gaas tetrahedral quantum dot structures fabricated using selective area metalorganic chemical vapor deposition. *Appl. Phys. Lett.*, vol. 58:pp. 2018–2020, 1991.

[5] S. Guha, A. Madukar, and K. C. Rajkumar. *Appl. Phys. Lett.*, Lett. 57:pp. 2110, 1990.

[6] P. Harrison. *Quantum Dots.* Wiley, 1997.

[7] Richard L. Liboff. *Introductory Quantum Mechanics, third edition.* Addison Wesley, 1997.

[8] Dan Mathews. PhD thesis, Cardiff University, 2003.

[9] P. M. Petroff and S. P. DenBaars. *Superlattices Microstruct.*, vol. 15(15), 1994.

[10] I. N. Stranski and L. von Krastanov. *Akd. Wiss. Lit. Mainz Abh. Math. Naturwiss. Kl.*, vol. 146:pp. 797, 1939.

[11] Hans P. Zappe. *Introduction to semiconductor integrated optics.* Artech House, Inc., 1995.

Chapter 3

Semi-analytical approach of Auger scattering rates

Contents

3.1 Introduction

The aim of this work was to develop a model to describe the time dependent occupancy of the quantum states of the QD ensemble. In order to do this, we need to

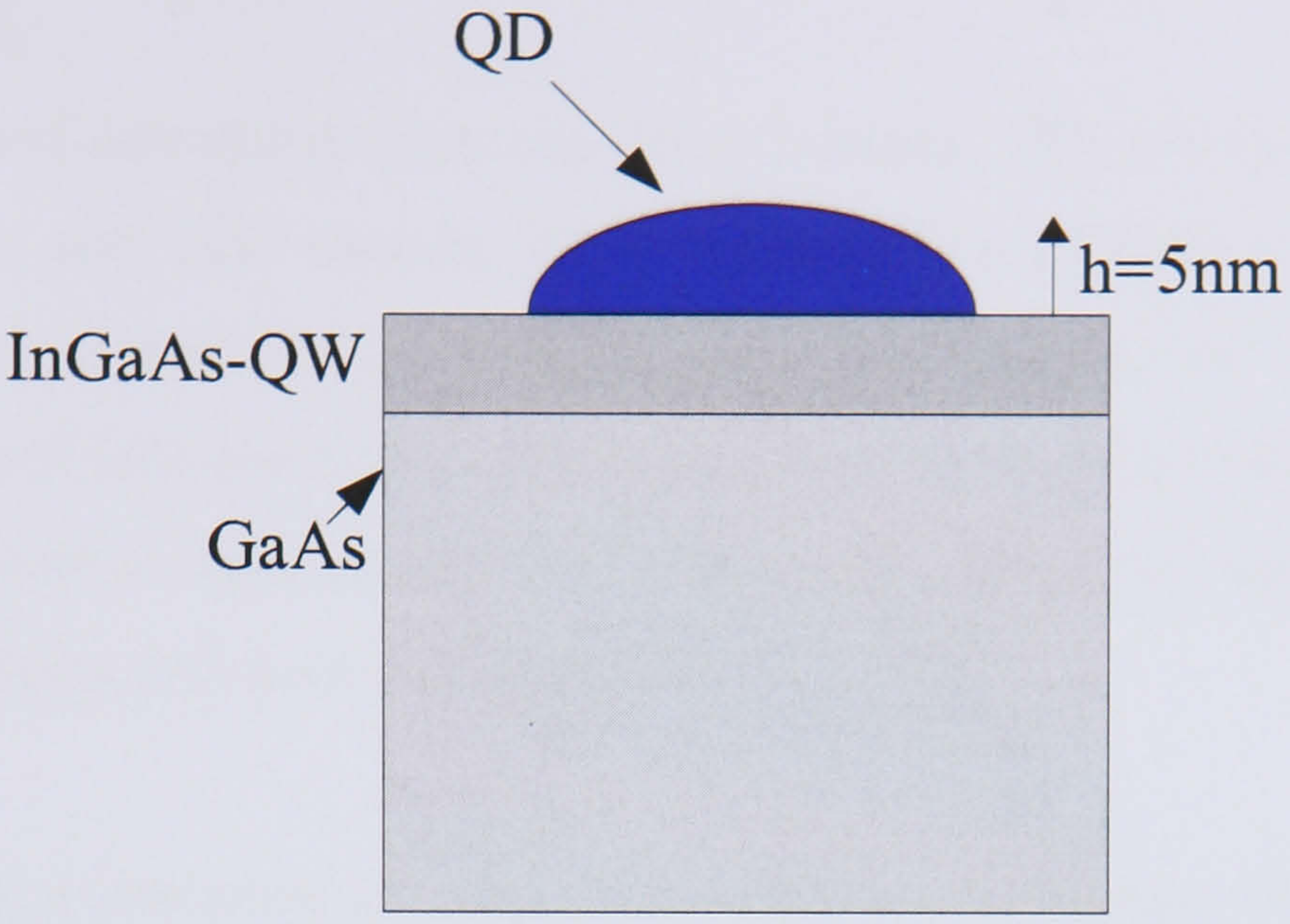

Figure 3.1: Self-Assembled Quantum Dot

calculate the scattering rates between the various energy levels of the dots and the wetting layer. The scattering rates, are determined using Fermi's Golden Rule [2] and require summation over all possible scattering states. This calculation, which is described in full in chapter 4 is highly computer intensive. In order to reduce the computational times, we[1] first investigate the semi-analytical approach to calculating these Auger scattering rates outlined by A. V. Uskov [5], [4]. In these two papers, A. V. Uskov, makes use of the assumption of moderate densities of the carriers in the wetting layer, describing the carriers in the wetting layer by a $2D$ Boltzmann distribution, which significantly simplifies the required mathematical calculations. In the next chapter (chapter 4), the Auger scattering rates have been calculated without making use of the assumption of low carrier densities. Instead a $2D$ Fermi-Dirac distribution is utilized in order to describe carriers in the $2D$ wetting layer. A comparative study between the semi-analytical approach implemented in this chapter, and the results obtained by the formulas derived in chapter 4, will

---

[1] The results given in this chapter have been calculated in conjunction with J. Domínguez.

be accomplished.

In InAs/GaAs self-assembled quantum dot structures, QDs are grown on top of a narrow quantum well ($2D$ wetting layer) while both structures are embedded in bulk material. Carriers in the $3D$ bulk states are first captured by the wetting layer and then scattered into the SADs, where they may recombine either radiatively or non-radiatively before relaxing into $0D$ lower energy states (see figure 3.3). In this chapter, 3 scattering processes are described;

- Figure 3.2(a) describes an Auger like relaxation processes. A $0D$ carrier collides with another carrier in the wetting layer ($2D$ electron). The $0D$ carrier is scattered into a lower state in the dot losing energy while the $2D$ carrier is scattered to a higher energy state in the wetting layer.
- Figure 3.2(b) represents a capture type I process, where $2D$ carriers in the wetting layer collide, one of them is scattered into the quantum dot state while the $2D$ carrier, is scattered into a higher energy state in the wetting layer.
- Figure 3.2(c) describes a capture type II process. In this occasion, a $2D$ carrier is captured into the quantum dot due to scattering with a previously captured $0D$ carrier, which is itself scattered into the wetting layer.

The calculation of the scattering coefficients in [4] and [5] has been followed assuming that SADs have a cylindrical shape of height $H = 4$ nm and diameter $D = 8.0$ nm [1], furthermore, in order to simplify the calculation of the scattering coefficients, relatively low temperatures and densities of the $2D$ and $3D$ carriers (n_2 and n_3 respectively, see figure 3.3) have been considered. Consequently, carriers in the wetting layer are considered to be at the lowest confined $2D$ energy state (z-direction) before the scattering process.

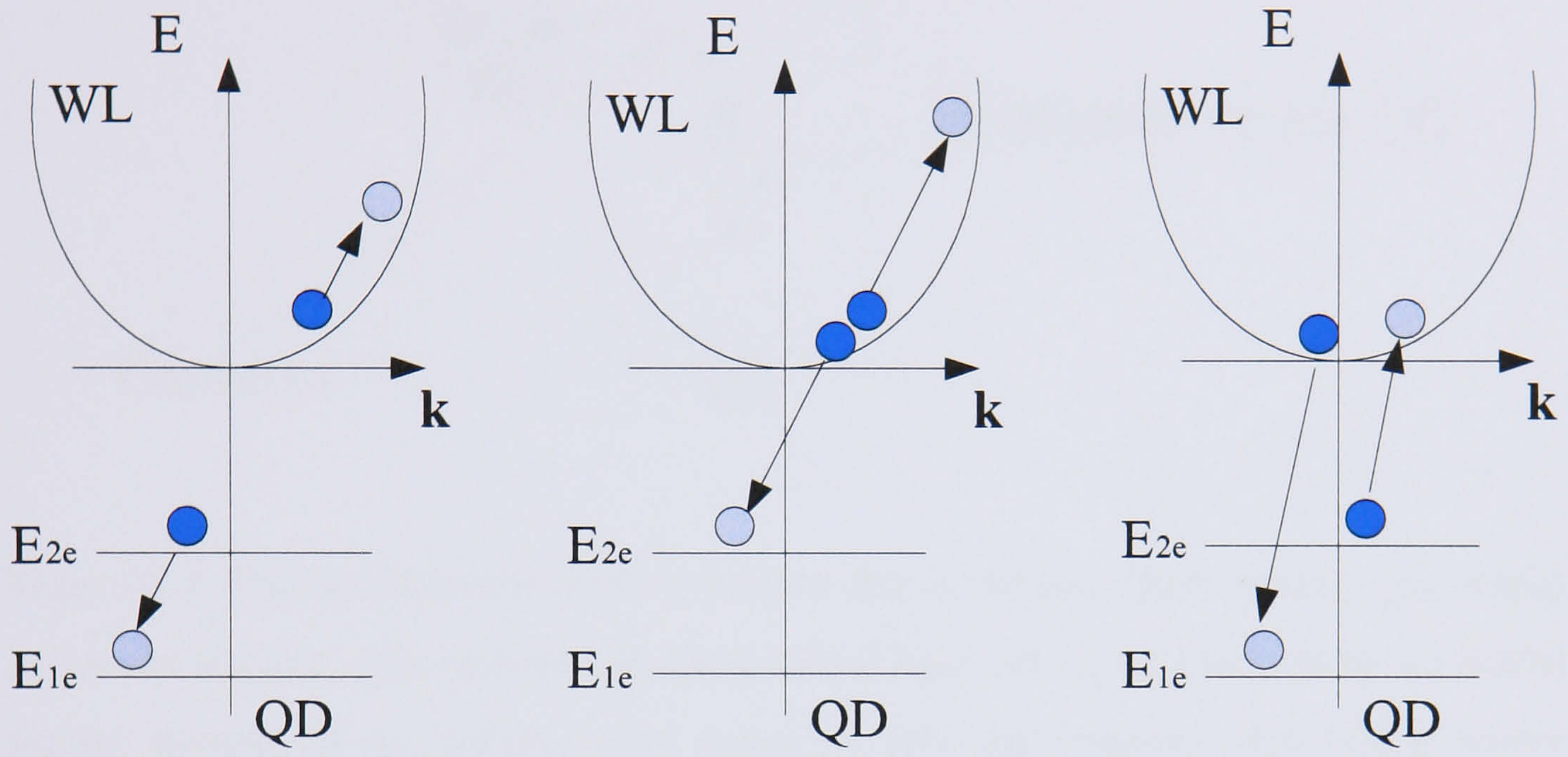

(a) (b) (c)

Figure 3.2: $E - \mathbf{k}$ curve, featuring only the conduction band states. (a) Relaxation of a $0D$ carrier into a lower energy level in the quantum dot via scattering with a $2D$ carrier in the wetting layer. (b) Capture of a carrier into the quantum dot via an Auger type I process. (c) Capture of a carrier into the quantum dot via an Auger type I process.

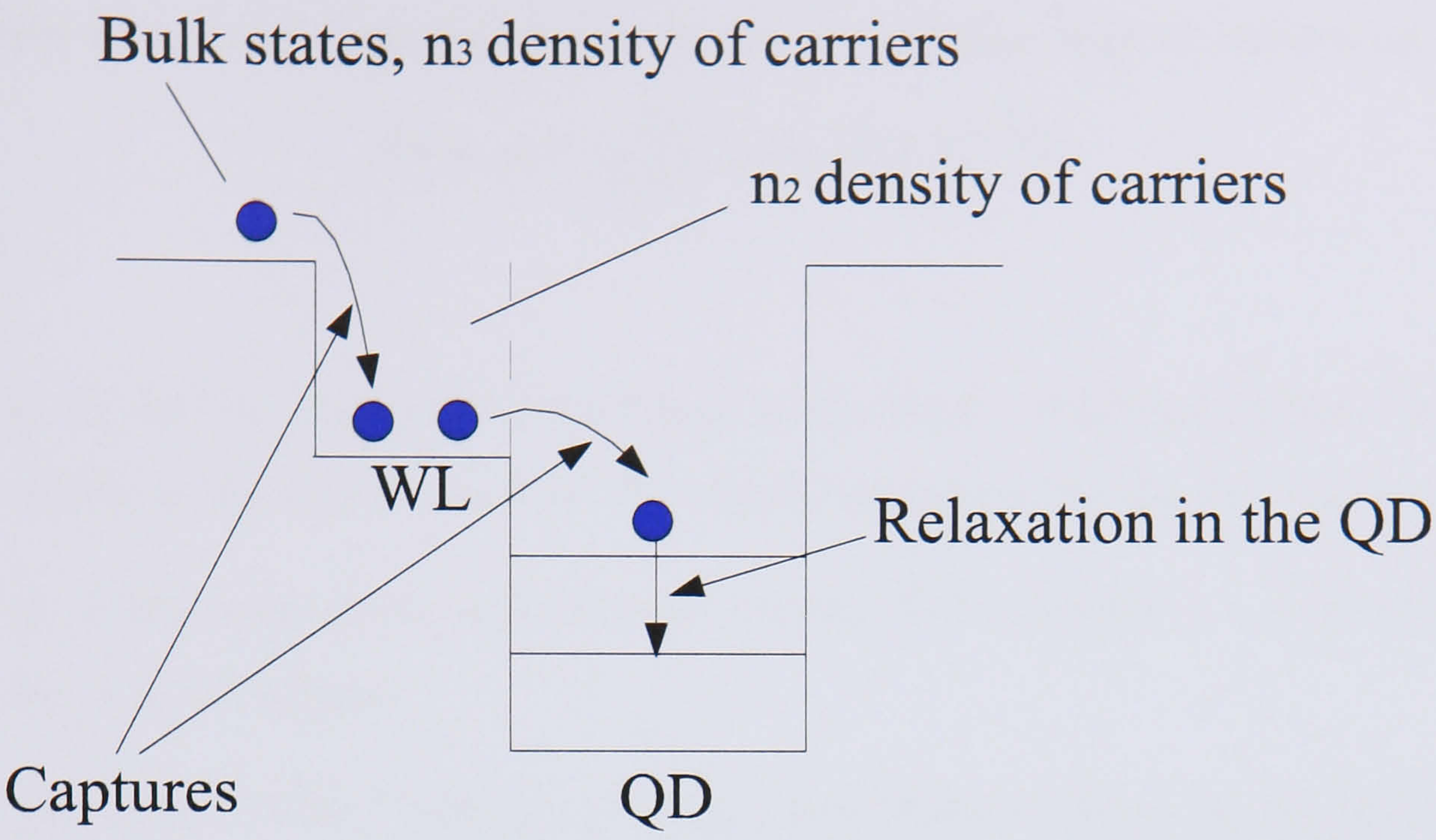

Figure 3.3: Energy diagram of the quantum dot structure. Bulk carriers (an initial n_3 carrier density) are captured by the wetting layer (WL), represented by an initial carrier density of n_2, before being captured into the quantum dot (QD), where relax into a lower energy level. The Coulomb interaction between the QD carriers ($0D$ carriers) and the WL ones ($2D$ carriers) is screened by the bulk carriers ($3D$ carriers).

3.2 Auger relaxation coefficient in SADs

In order to describe the semi-analytical calculation of Auger relaxation rate (Fig. 3.2(a)), we have assumed a carrier has already been captured from the $2D$ wetting layer into an excited $0D$ energy state in the SAD. Once in the quantum dot, it will follow a relaxation process into the $0D$ ground state (see figure 3.3).

Making use of Fermi's Golden Rule [2], the probability of a carrier transition from an initial $0D$ state i scattering to a final energy state f within the quantum dot because of Coulomb interaction between a QD carrier and a $2D$ carrier, which is scattered within the angle θ to $\theta + \mathrm{d}\theta$ in the $x - y$ plane, may be written as in [4]:

$$\mathrm{d}w_{f\mathbf{k}_1,i\mathbf{k}} = \frac{m_c}{2\pi\hbar^3}\left|\langle f,\mathbf{k}_1|U|i,\mathbf{k}\rangle\right|^2\mathrm{d}\theta \tag{3.1}$$

where

- $\mathbf{k}$, $\mathbf{k}_1$ are the in-plane wave vectors in the lowest sub-band of the scattered carrier in the initial and final $2D$ states respectively in the wetting layer.
- m_c is the mass of the $2D$ scattered carrier. The subscript $c = e$ for electrons and $c = h$ for holes.
- The letters i and f refer to initial and final states in the quantum dot respectively. The energy difference between the initial and final state within the quantum dot, is considered to be:
$$\frac{\hbar^2}{2m_c}(k_1^2 - k^2) = E_i - E_f \tag{3.2}$$
- $\left|\langle f,\mathbf{k}_1|U|i,\mathbf{k}\rangle\right|$ is the matrix element of the screened Coulomb interaction. The Screened Coulomb interaction between carriers at $\mathbf{r}_0$ (position vector of the $2D$ carrier) and $\mathbf{r}$ (position vector of the carrier inside the quantum dot) is given by the expression [4]:
$$U = U(|\mathbf{r} - \mathbf{r}_0|) = \frac{e^2\exp(-k_\mathrm{D} \mid \mathbf{r} - \mathbf{r}_0|)}{\epsilon \mid \mathbf{r} - \mathbf{r}_0|} \tag{3.3}$$
where ϵ is the dielectric constant of the material and k_D is the 3D Debye screening wave number
$$k_\mathrm{D} = \sqrt{\frac{4\pi e^2 n_{bulk}}{\epsilon k_\mathrm{B} T_{bulk}}} \tag{3.4}$$
In this last formula, T_{bulk} is the temperature of the $3D$ carriers, k_B is the Boltzmann constant [3] ($k_\mathrm{B} = 1.3807 \times 10^{-23}$ J/K) and n_{bulk} is the $3D$ carrier density. Making use of the dipole approximation, i.e $\mathrm{r} \gg \mathrm{r}_0$ the screened Coulomb interaction (Eq. 3.3) can be rewritten as follows
$$U = U(|\mathbf{r} - \mathbf{r}_0|) \approx U(\mathbf{r}_0) + \frac{e^2\mathbf{r}\cdot\mathbf{r}_0}{\epsilon}\left(\frac{1}{r_0^3} + \frac{k_\mathrm{D}}{r_0^2}\right) \tag{3.5}$$

Including Eq. 3.5 in Eq. 3.1 gives the differential cross section as a function of velocity v for the scattering process of a $2D$ carrier with a $0D$ carrier within the quantum dot which is relaxed from an initial i state to a final f, i.e. [4]

$$\mathrm{d}\sigma^c_{if}(\mathrm{v},\theta) = \frac{2\pi e^4 m_c}{\epsilon^2 \hbar^3}\left[(D^z_{fi})^2 I_1^2 + (D^x_{fi})^2 I_2^2\right]\frac{1}{\mathrm{v}}\mathrm{d}\theta \tag{3.6}$$

where

- D^z_{fi} and D^x_{fi} are the z and x components respectively of the dipole moment. As we have previously mentioned, a cylindrical shape for the SADs has been assumed in [4], i.e., the wave function of a carrier inside an infinite potential quantum dot, characterized by the three quantum numbers n, l, m can be expressed as follows:

  $$\Psi_{nlm}(z,\rho,\psi) = \Psi_n(z)\Psi_l(\rho)\frac{e^{im\psi}}{\sqrt{2\pi}} \tag{3.7}$$

  Taking into account the orthogonality properties of the wave function components in z and ρ directions, i.e.

  $$\int_{-\infty}^{\infty} \mathrm{d}z \Psi^*_{n'}(z)\Psi_n(z) = 0 \qquad n' \neq n$$

  $$\int_{0}^{\infty} \mathrm{d}\rho\rho \Psi^*_{l'}(\rho)\Psi_l(\rho) = 0 \qquad l' \neq l$$

  then the z and x components of the dipole moment in 3.6, i.e., D^z_{fi} and D^x_{fi} may be written in a more accessible way as follows [4]:

  $$D^z_{fi} = D^z_{n'l'm',nlm} = \int \mathrm{dr}\Psi^*_f(\mathrm{r}) z \Psi_i(\mathrm{r}) = d^z_{n'n}\delta_{l'l}\delta_{m'm} \tag{3.8}$$

  where

  $$d^z_{n'n} = \int_{-\infty}^{\infty} \mathrm{d}z z \Psi^*_{n'}(z)\Psi_n(z)$$

  and

  $$D^x_{fi} = D^x_{n'l'm',nlm} = \int \mathrm{dr}\Psi^*_f(\mathrm{r}) x \Psi_i(\mathrm{r}) = d^\rho_{l'l}\delta_{n'n}\frac{1}{2}(\delta_{m'm+1} + \delta_{m',m-1}) \tag{3.9}$$

where

$$d^{\rho}_{l'l} = \int_0^{\infty} \mathrm{d}\rho\rho^2 \Psi^*_{l'}(\rho)\Psi_l(\rho)$$

- I_1 and I_2 [4] are the values of the integrals given by

$$I_l = \int_0^{\infty} \mathrm{d}u \frac{u^l}{(1+u^2)^{\frac{3}{2}}}(1 + k_{\mathrm{D}}h\sqrt{1+u^2})e^{(-k_{\mathrm{D}}h\sqrt{1+u^2})} J_{l-1}(qhu) \tag{3.10}$$

In the last equation, J_l is the Bessel function of order l, h is the distance from the center of the dot to the wetting layer, hence, the height of the dot, H is $H = 2h$. k_{D} is the $3D$ Debye screening wave number given by (3.4), q is the magnitude of the wave vector $\mathbf{q} = \mathbf{k}_1 - \mathbf{k}$. As a consequence of assuming a moderate carrier density and temperature, the initial carrier state energy is assumed to be at the bottom of the quantum well sub-band, hence, $\mathrm{k}_1 \gg \mathrm{k}$. Consequently, and making use of Eq. 3.2, the magnitude of the wave vector q in 3.10 can be rewritten as

$$q_c \approx \mathrm{k}_1 \approx \sqrt{\frac{2m_c}{\hbar}(E_i - E_f)} \tag{3.11}$$

Because of the assumption of moderate carrier densities of the $2D$ carriers in [4], carriers in the wetting layer have been described by a $2D$ Boltzmann distribution $f_c(\mathrm{v})$ as a function of the initial velocity of the scattered $2D$ carrier [4], i.e.,

$$f_c(\mathrm{v}) = \frac{n_2 m_c \mathrm{v}}{k_B T_2} \exp - \frac{m_c \mathrm{v}^2}{2k_B T_2} \tag{3.12}$$

Hence, the carrier relaxation rate from an initial i $0D$ energy state to a final f state in the quantum dot is given in [4] as

$$\gamma^c_{if} = \int_0^{\infty} \mathrm{d}\mathrm{v} f_c(\mathrm{v})\mathrm{v}\, \sigma^c_{if} = \int_0^{\infty} \mathrm{d}\mathrm{v}\, n_2 \frac{m_c \mathrm{v}}{k_B T_2} e^{-\frac{m_c \mathrm{v}^2}{2k_B T_2}}\, \mathrm{v}\, \sigma^c_{if}(\mathrm{v}) = B^c_{if} n_2 \tag{3.13}$$

where $\sigma^c_{if}(\mathrm{v})$ is the integrated cross section of the scattering process given by Eq. 3.6, hence,

$$\sigma^c_{if}(\mathrm{v}) = \int_{-\pi}^{\pi} \mathrm{d}\sigma^c_{if}(\mathrm{v},\theta) = \frac{4\pi^2 e^4 m_c}{\epsilon^2 \hbar^3} \left[(D^z_{fi})^2 I_1^2 + (D^x_{fi})^2 I_2^2\right] \frac{1}{\mathrm{v}} \tag{3.14}$$

Including this last equation into (3.13), we can write the analytical expression for the Auger Relaxation coefficient as in [4]:

$$B^c_{if} = \frac{4\pi^2 e^4 m_c}{\epsilon^2 \hbar^3} \left[(D^z_{fi})^2 I_1^2 + (D^x_{fi})^2 I_2^2 \right] \tag{3.15}$$

where ϵ is the dielectric constant of the material and m_c is the carrier mass.

3.2.1 Numerical Results

We have implemented the equation 3.15 in order to calculate the temperature dependence of the Auger relaxation coefficient on the $3D$ carrier density in the bulk material, as in [4]. To evaluate the integral given by Eq. 3.10, we make use of the trapezoidal rule method with 1000 partitions, constructing the variable u in (3.10) as follows:

$$u_i = 10^{\left(i - \frac{1000}{2}\right)\left(\frac{\log_{10}(1\times 10^{20})}{\frac{1000}{2}}\right)} \tag{3.16}$$

for $i = 1, ..1000$.

The values of the parameters in (3.15) have been taken from [4], i.e.,

- $m_e = 0.1 m_0$ and $m_h = 0.34 m_0$ for the electron and hole masses respectively.
- $\epsilon = 13$ for the dielectric constant.
- $(E_i - E_f) = 0.1 eV$ for the separation between the energy levels E_i and E_f in the quantum dot.
- $H = 4nm$, $D = 8nm$ are the height and diameter of the InAs/GaAs self-assembled quantum dots.
- It has been assumed (as in [4]) that the temperatures of the $3D$ and $2D$ carriers are equal to each other, hence, $T_3 = T_2 = T$.

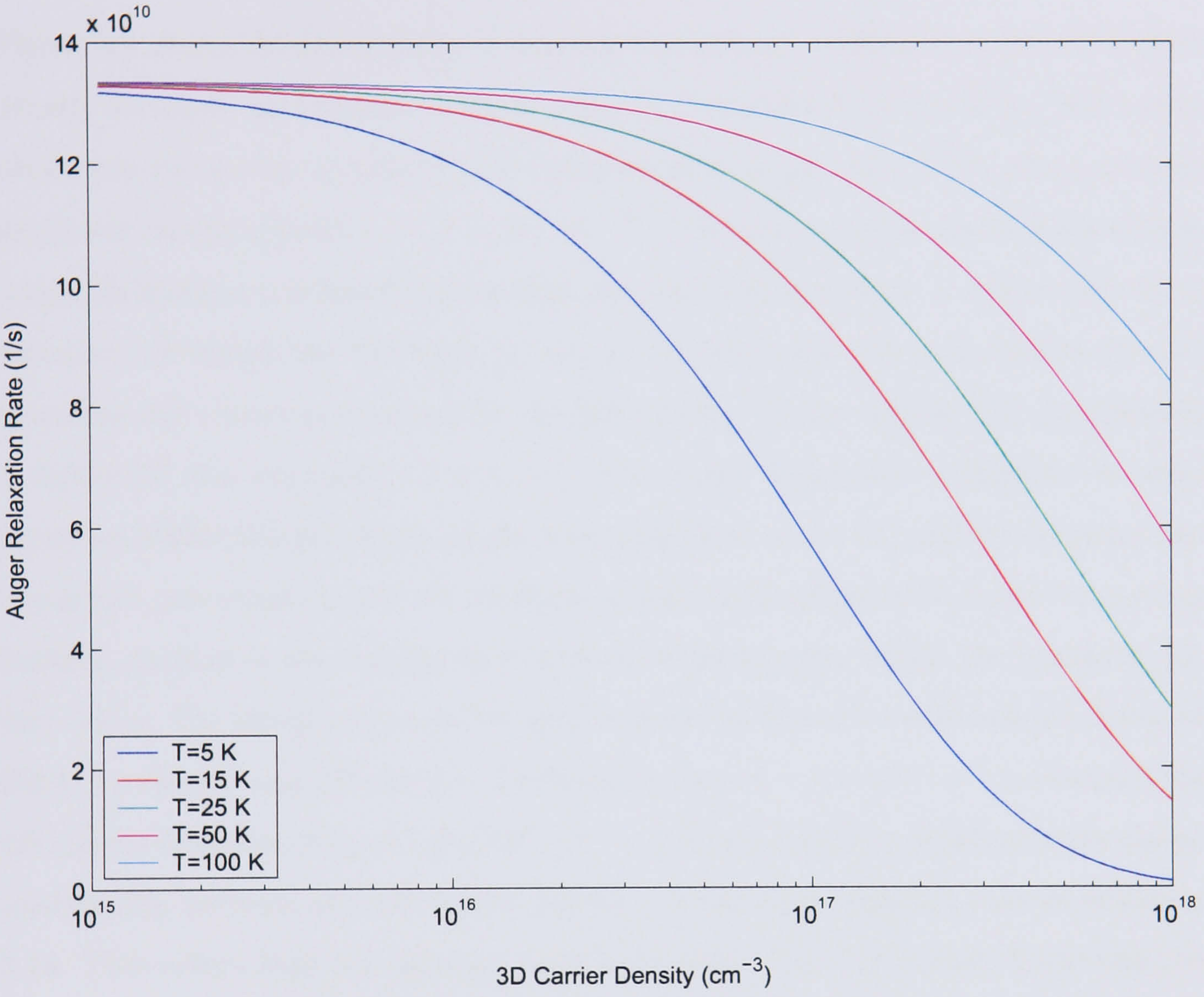

Figure 3.4: Auger Relaxation rate dependence on the $3D$ bulk carrier density for different temperature values.

- In the following numerical result, interband transitions of the form $n' = n \pm 1$ have been considered as in [4], so that the z component of the dipole moment, assuming infinite barriers for the QD, may be estimate as $(d^z_{n'n})^2 \approx \frac{h^2}{6}$ [4].

Figure 3.4 shows the dependence of the Auger relaxation coefficient on the $3D$ carrier density for these parameters. It shows that the dependence of the Auger relaxation coefficient on n_3 may be neglected for temperatures larger than 100 K and relatively moderate carrier densities ($< 5 \times 10^{15}\,\mathrm{cm}^{-3}$). The temperature dependence on the Auger Relaxation coefficient comes from the screening potential as can be seen from equation 3.4 where the Coulomb interaction between the $2D$ carriers and the $0D$ quantum dot carrier is screened by the $3D$ carriers, with a density of n_3 as plotted in figure 3.3 (see equations 3.3 and 3.4). The Auger Relaxation coefficient becomes larger for higher temperatures, as the screening effect of the $3D$ carriers becomes less important (see equation 3.4). In addition, a much more efficient Coulomb interaction between carriers in the wetting layer and the relaxing ones within the quantum dot may occur. For the quantum dot structure shown in figure 3.4 with temperatures of 300 K for the $3D$ and $2D$ carriers, a relaxation rate of $\sim 1.3 \times 10^{11}\,\mathrm{s}^{-1}$ is obtained for $2D$ carrier densities of $n_2 = 1.0 \times 10^{11}\,\mathrm{cm}^{-2}$. It is important to emphasize the linear relationship between the $2D$ carrier density n_2 and the relaxation rate in equation 3.13. This comes from the assumption of low carrier densities, hence, describing the carriers in the $2D$ wetting layer by a Boltzmann distribution (see equation 3.12). In chapter 4, a comparison between the results obtained making use of this assumption, and those achieved by full derivation from Fermi's Golden Rule [2] and Fermi-Dirac statistics, will be accomplished.

In this work we consider n_3 and n_2 to be independent variables as is common in the literature. However, n_3 and n_2 can usually be related by considering a common Fermi level for the semiconductor structure.

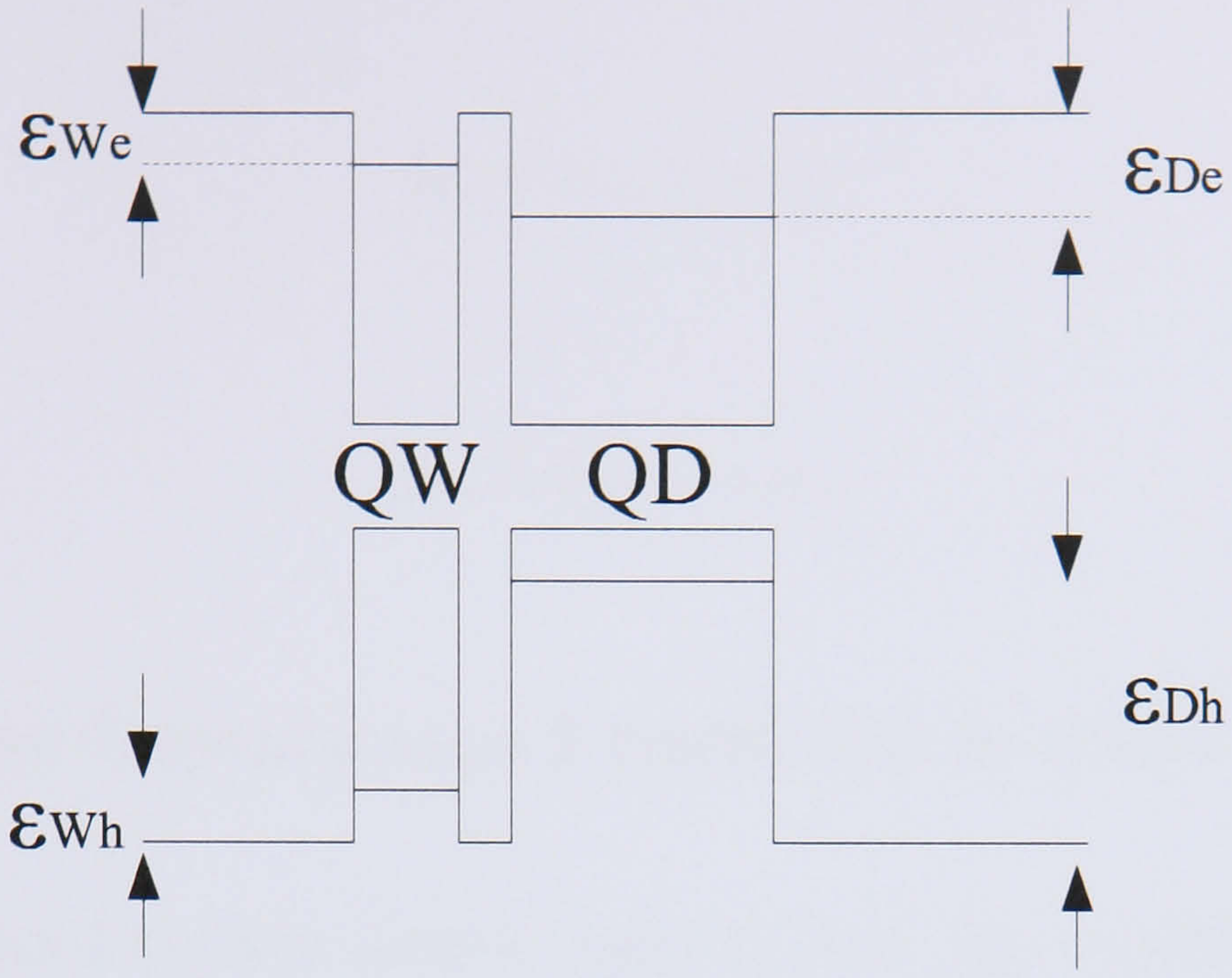

Figure 3.5: The lowest confined energies of a SAD structure.

3.3 Auger Capture type I and type II coefficients in SADs

In this section, we calculate the Auger capture type I and II coefficients as described in [5]. The calculation makes the same approximations as those previously described, i.e., considering relatively moderate carrier densities and temperatures. Again we model the self-assembled quantum dots as cylinders of height $H = 5$ nm and diameters varying from ~ 1 nm to 50 nm. The values for the lowest confined energies for electrons and holes in the quantum dot (ϵ_{De} and ϵ_{Dh} respectively) and quantum well (ϵ_{We} for electrons and ϵ_{Wh} for holes) have been taken from [5] (see Fig. 3.5), taking into account that in the considered InAs/GaAs structures [5] $\epsilon_{Dh} > \epsilon_{De}$ and $\Delta\epsilon_h > \Delta\epsilon_e$ (see Fig. 3.5),

where

$$\Delta\epsilon_e = (\epsilon_{De} - \epsilon_{We}) \tag{3.17}$$

and

$$\Delta\epsilon_h = (\epsilon_{Dh} - \epsilon_{Wh}) \tag{3.18}$$

3.3.1 Auger Capture type I coefficient in SADs

We have calculated the four possible Auger Capture type I coefficients (see Fig. 3.6) making use of the formula derived by A. V. Uskov in [5]. In this kind of processes (capture type I scattering processes) a carrier in the wetting layer (a $2D$ carrier) is captured by the SAD as a consequence of the Coulomb interaction with another $2D$ carrier, which is itself scattered into a higher energy level in the wetting layer. Depending on the carriers taking part in the scattering process, there are four different capture type I scattering coefficients possible, i.e., C_{ee}, C_{eh}, C_{he} and C_{hh} as shown in figure 3.6. Following [5], the Auger capture type I coefficients may be calculated as follows:

$$\begin{aligned} C_{cs} &= \frac{\pi m_s e^4}{4\xi_{01}^2 \hbar^3 {\epsilon_0}^2 \epsilon^2} \frac{D^2}{H} \frac{k_W (k_D + 2k_W + 2q_s)^2}{{q_s}^2 (k_W + q_s)^2 (k_D + k_W + q_s)^2} \\ &\times \frac{{J_0}^2(\frac{q_s D}{2})}{\left[\frac{(q_s D)^2}{(2\xi_{01})^2} - 1\right]^2} \end{aligned} \tag{3.19}$$

where

- $\xi_{01} = 2.4$ is the value of the first root of the zero order Bessel function $J_0(x)$.
- s and c subscripts refer to the scattered and captured carriers respectively, consequently, m_s represents the effective mass of the scattered carrier ($s = e$ when the scattered carrier is the electron, and $s = h$ when the scattered carrier

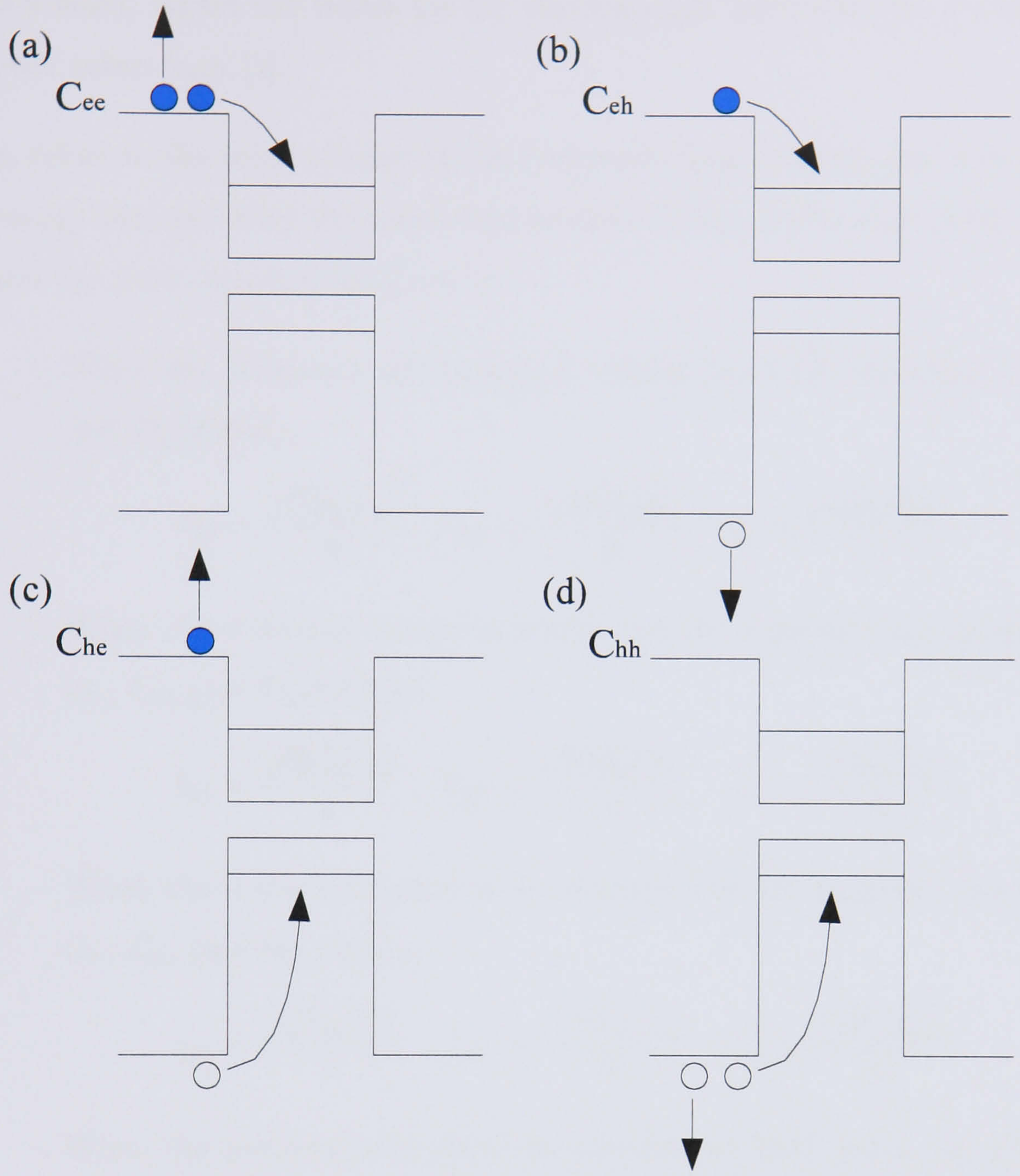

Figure 3.6: Schematic picture of Auger Capture Type I processes. (a) C_{ee}, where a $2D$ electron is captured by the SAD after scattering with another $2D$ electron. (b) C_{eh}, where a $2D$ electron is captured by the SAD after scattering with another $2D$ hole. (c) C_{he}, where a $2D$ hole is captured by the SAD after scattering with another $2D$ electron. (d) C_{hh}, where a $2D$ hole is captured by the SAD after scattering with another $2D$ hole in the wetting layer.

is a hole). Again the values for the electrons and holes effective masses have been taken from [5].

- q_s refers to the wave number of the scattered carrier, taking into account the energy increase after the scattering process. Using (3.17) and (3.18), q_s, k_D and k_W wave numbers are given by:
  - When the scattered and captured carriers are both electrons, i.e., C_{ee} (see Fig.3.6(a)):

    $$k_D = \frac{\sqrt{2m_e\epsilon_{De}}}{\hbar} \quad k_W = \frac{\sqrt{2m_e\epsilon_{We}}}{\hbar} \quad q_s = \frac{\sqrt{2m_e\Delta\epsilon_e}}{\hbar}$$

  - When the scattered carrier is a hole and the captured one an electron, i.e., C_{eh} (see Fig.3.6(b)):

    $$k_D = \frac{\sqrt{2m_e\epsilon_{De}}}{\hbar} \quad k_W = \frac{\sqrt{2m_h\epsilon_{Wh}}}{\hbar} \quad q_s = \frac{\sqrt{2m_h\Delta\epsilon_e}}{\hbar}$$

  - When the scattered carrier is an electron and the captured one a hole, i.e., C_{he} (see Fig.3.6(c)):

    $$k_D = \frac{\sqrt{2m_h\epsilon_{Dh}}}{\hbar} \quad k_W = \frac{\sqrt{2m_e\epsilon_{We}}}{\hbar} \quad q_s = \frac{\sqrt{2m_e\Delta\epsilon_h}}{\hbar}$$

  - When the scattered and captured carriers are both holes, i.e., C_{hh} (see Fig.3.6(d)):

    $$k_D = \frac{\sqrt{2m_h\epsilon_{Dh}}}{\hbar} \quad k_W = \frac{\sqrt{2m_h\epsilon_{Wh}}}{\hbar} \quad q_s = \frac{\sqrt{2m_h\Delta\epsilon_h}}{\hbar}$$

- D and H are the diameter and height of the dot.

Figure 3.7 shows the results of solving equation 3.19 for the calculation of the capture coefficient type I making use of the parameters utilized in [5], i.e., for dot heights of $H = 5$ nm and the lowest confined energies such as, $\epsilon_{De} = 0.2$ eV, $\epsilon_{Dh} = 0.3$ eV, $\epsilon_{We} = 0.03$ eV and $\epsilon_{Wh} = 0.05$ eV, considering moderate carrier densities in the

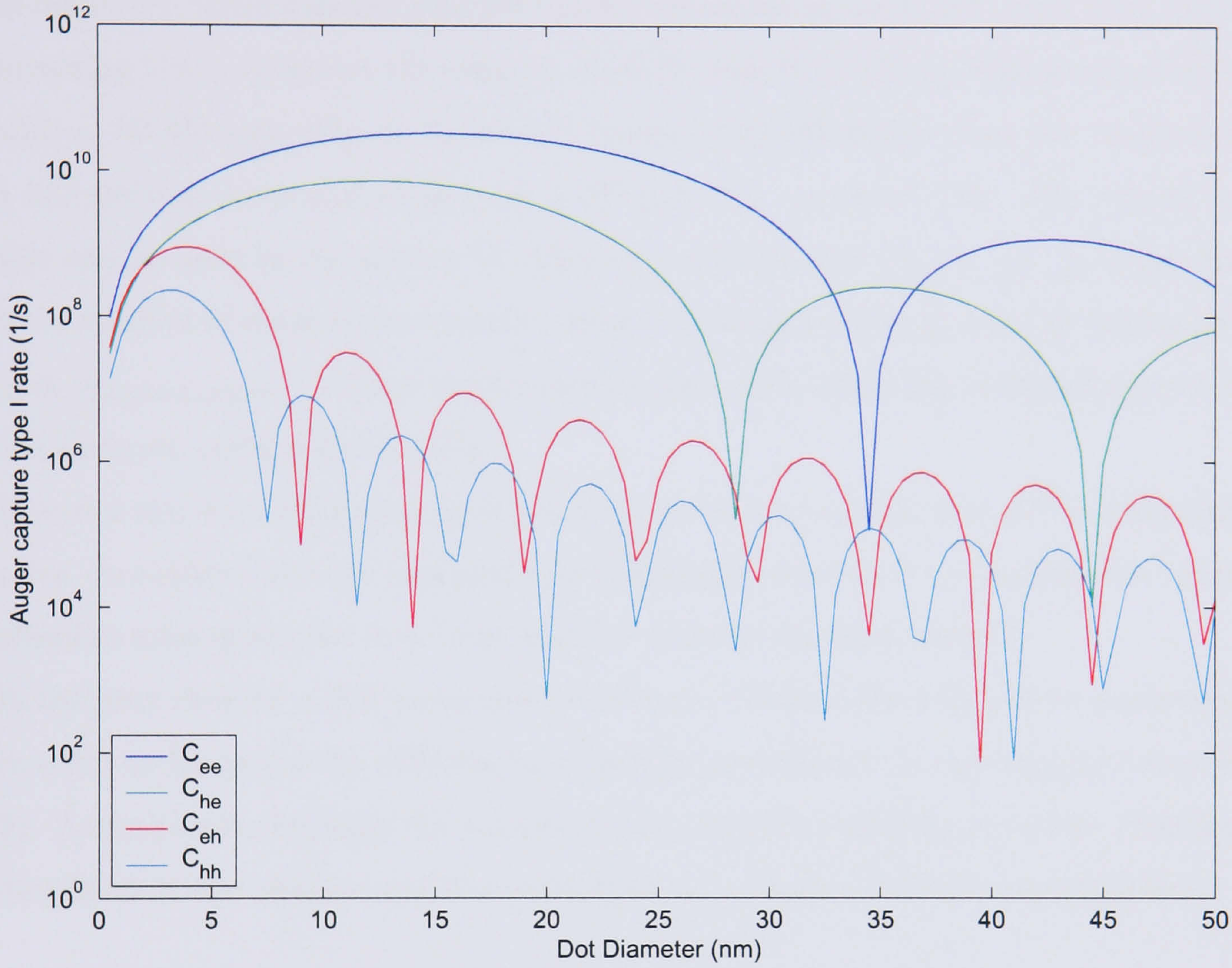

Figure 3.7: The dependence on the quantum dot diameter of the Auger Capture Coefficients C_{ee}, C_{eh}, C_{he} and C_{hh} .

wetting layer (densities of $1 \times 10^{15}\,\mathrm{m}^{-2}$).

There is a strong dependence of the Auger capture type I coefficient on the diameter of the quantum dot and a oscillating nature as a result of the Bessel function of the first kind, i.e., $J_0(x)$ dependence, as can be observed in figure 3.8. As shown in figure 3.7, those capture processes involving electrons are much faster than those involving holes. However, the capture of a hole from the wetting layer after colliding with a $2D$ electron (C_{he} in figure 3.7) occurs more efficiently than the capture of a $2D$ electron after scattering with a $2D$ hole (C_{he} in figure 3.7). The reason for this can be seen in equation 3.19, where we observe that $C_{cs} \propto \frac{1}{{q_s}^4}$. q_s being the wave number of the scattered carrier. Hence, as holes are heavier than electrons and $q_s \propto {m_{\text{scattered carrier}}}^{1/2}$, those carrier capture processes where the scattered carrier is the electron, occur more rapidly.

However this semi-analytical approach does not give a realistic view of the scattering rates. In reality, holes are captured more efficiently than electrons because the heavy effective mass gives rise to a large number of states for scattering [2].

In the next chapter, a full derivation from Fermi's Golden Rule [2] will be performed in order to determine the different scattering rates explained in this chapter (chapter 3). A comparison between the scattering rates obtained making use of the formulas described in this chapter and the ones derived in chapter 4 will be accomplished.

3.3.2 Auger Capture type II coefficient in SADs

In this section we implement the equation given by [5] in order to calculate the Auger capture type II coefficient, B_{he}. This coefficient refers to the Auger capture type II process where a $2D$ hole in the wetting layer is captured by the SAD due to the Coulomb interaction with a previously captured $0D$ electron, which is scattered into a $2D$ state in the wetting layer (see Fig. 3.9). In order to get the results plotted in figure 3.10, we solve the equation for the calculation of the Auger Capture type

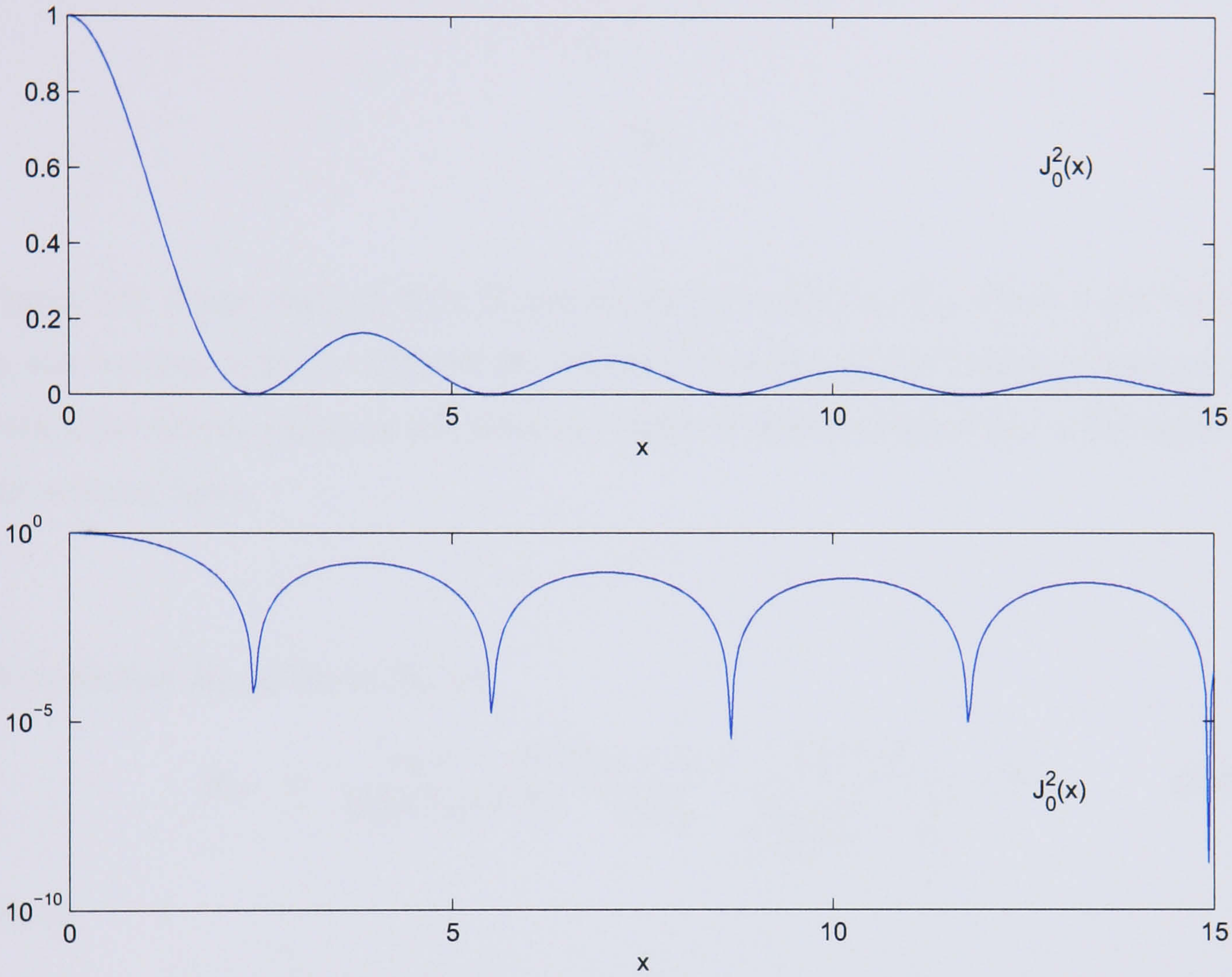

Figure 3.8: The square of the Bessel function of the first kind, i.e., $J_0^2(x)$ plotted on a linear scale (top figure) and on a logarithmic scale (bottom figure).

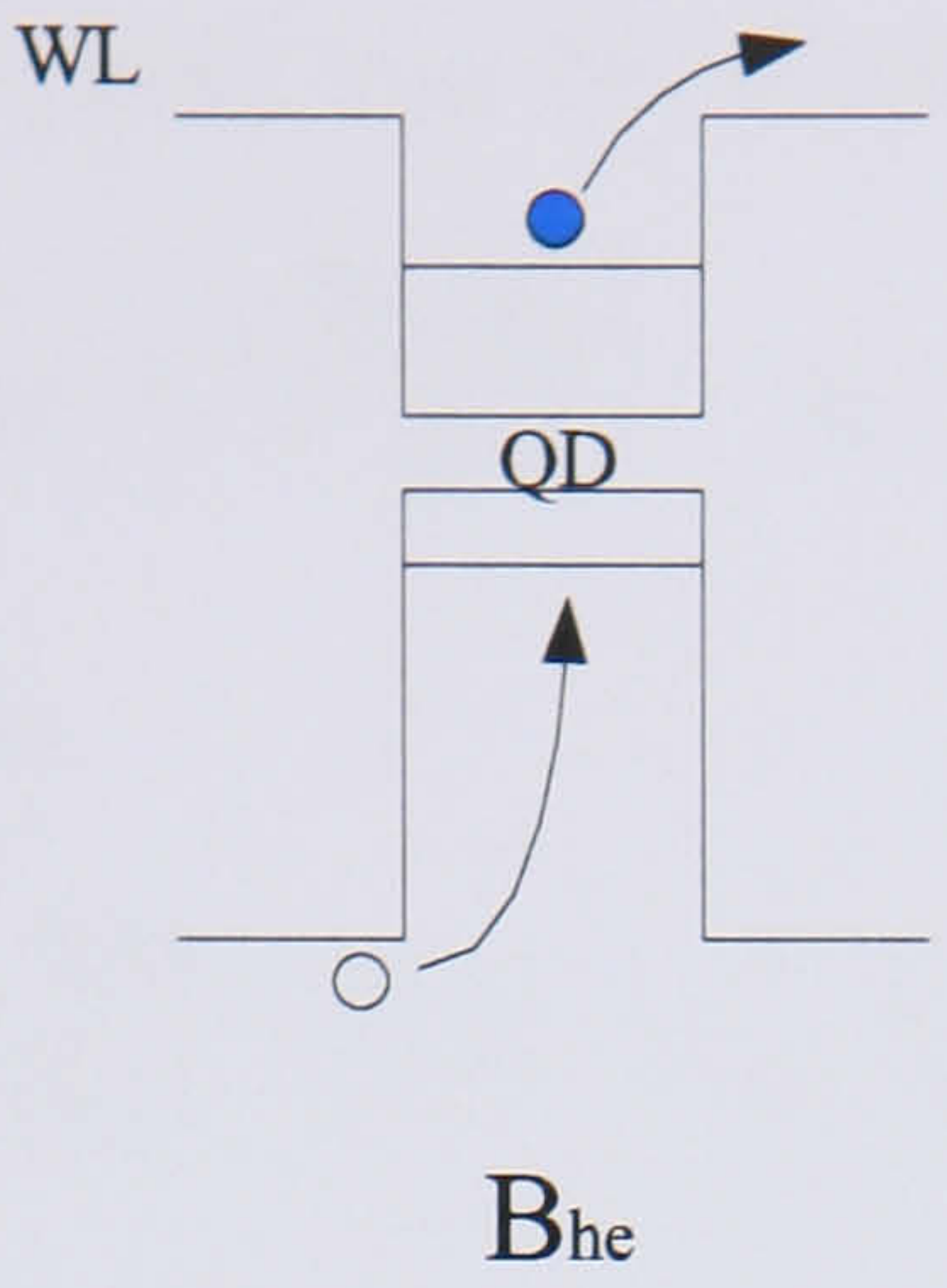

Figure 3.9: Auger capture type II process characterized by B_{he} where a $2D$ carrier in the wetting layer is captured by the SAD because of the Coulomb interaction with a previously captured $0D$ electron, which is itself scattered into a $2D$ state in the wetting layer.

II coefficient B_{he} given in [5], i.e.,

$$B_{he} = \frac{m_e e^4}{4\xi_{01}^4 \hbar^3 {\epsilon_0}^2 \epsilon^2} \frac{D^2}{H^2} \frac{(k_D + k_W)^2}{k_D^2 k_W^2} \frac{{J_0}^2(\frac{q_{he}D}{2})}{\left[\frac{(q_{he}D)^2}{(2\xi_{01})^2} - 1\right]^2} \times F^2 \qquad (3.20)$$

where

- $\xi_{01} = 2.4$ is the value of the first root of the zero order Bessel function $J_0(x)$ as in Eq. 3.19.
- m_e is the mass of the scattered carrier, i.e., the electron effective mass, taken from [5].
- q_{he} refers to the wave number of the scattered carrier, i.e, the electron, which is excited from the quantum dot into the wetting layer, after scattering with a $2D$ hole. Hence, taking into account (3.17) and (3.18), q_{he}, as well as k_D

and k_W wave numbers in (3.20) may be calculated as follows:

$$k_D = \frac{\sqrt{2m_h\epsilon_{Dh}}}{\hbar} \quad k_W = \frac{\sqrt{2m_e\epsilon_{We}}}{\hbar} \quad q_{he} = \frac{\sqrt{2m_e\left(\Delta\epsilon_h - \Delta\epsilon_e\right)}}{\hbar}$$

- The function F is given by

$$F = \int_0^\infty \mathrm{d}u \frac{J_0(u)}{[(u/\xi_{01})^2 - 1]} \frac{1 + [2u/(k_D + k_w)]\, D}{[1 + (2u/(k_D D))]\, [1 + (2u/(k_W D))]} \quad (3.21)$$

- D and H are the diameter and height of the dot as in 3.19.

Figure 3.10 shows the strong dependence on the dot diameter of the Auger capture type II coefficient, B_{he}, as can be observed from equation 3.20. The different in shape comparing to the plot obtained for the capture type I coefficient (figure 3.7) comes from the factor F (see Eq. 3.20 and Eq. 3.21) that appears in equation 3.20 which limits the periodic contribution to the value of B_{he} coming from the bessel function pictured in figure 3.8.

3.4 Summary

In this chapter we have implemented the semi-analytical expressions for the calculation of the scattering capture and relaxation rates in cylindrical self-assembled quantum dot structures. An increase of the Auger relaxation rate for larger temperatures has been observed as the screening effect of the $3D$ carriers on the Coulomb interaction between the wetting layer and quantum dot carriers acquires less importance. Therefore, faster Auger relaxation rates are obtained for larger temperature values.

We have also discussed the strong dependence of both Auger capture type I and II processes on the dot radius, and noted the oscillating nature of the capture type I coefficient, as a result of underlying Bessel function dependence.

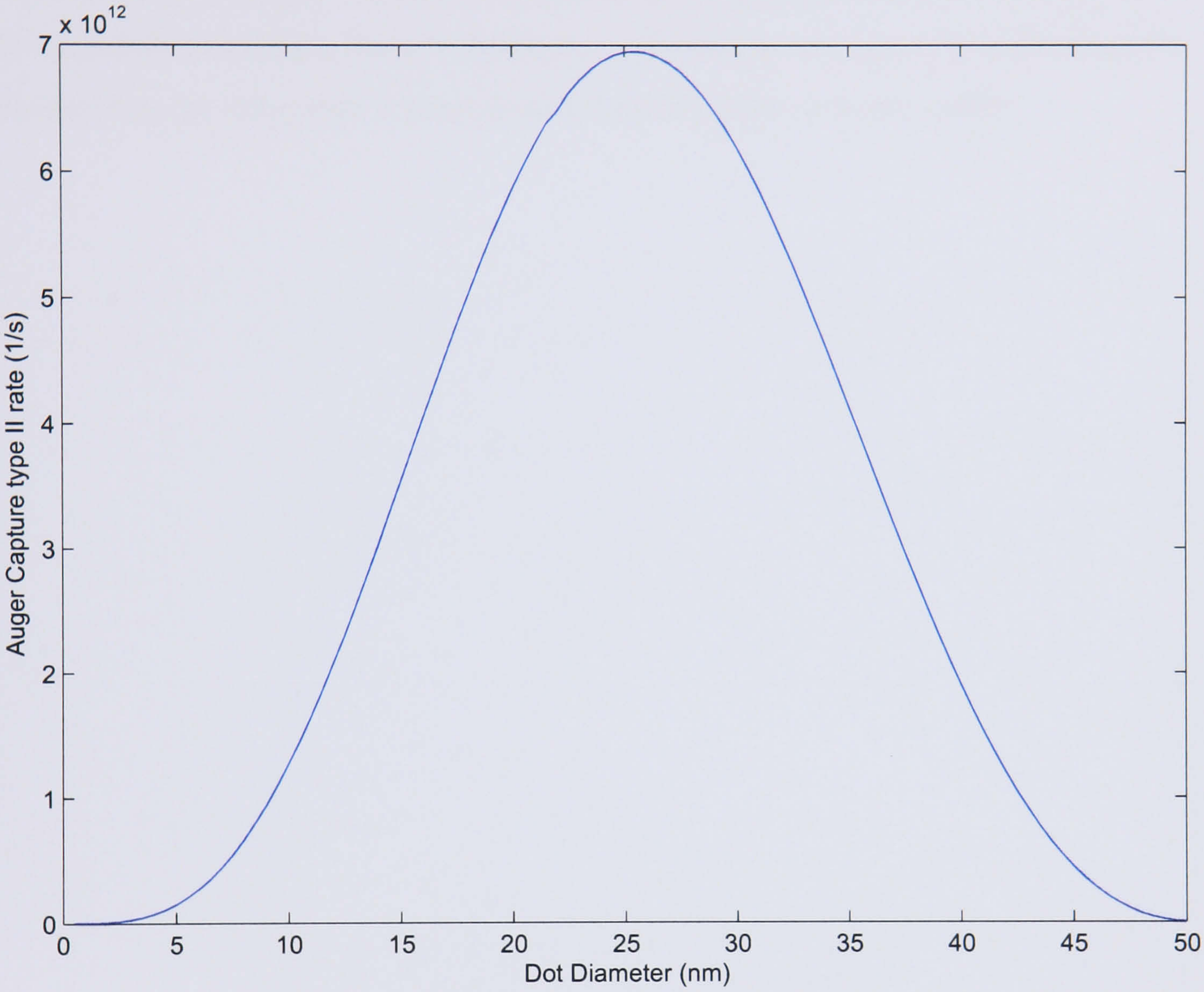

Figure 3.10: The dependence on the quantum dot diameter of the Auger Capture type II Coefficient B_{he}.

However in the next chapter, we will compare the scattering rates obtained by extending the semi-analytical formulas described in this chapter and those given by a full derivation from the Fermi's Golden Rule. Note that in the next chapter, we extend the results of A. V. Uskov in [4] and [5], accounting for intraband transitions by explicitly calculating the wavefunctions and energies and properly evaluating the dipole moment components (equations 3.8 and 3.9) for each dot radius.

Bibliography

[1] F. Adler, M. Geiger, A. Bauknecht, F. Scholz, H. Schweizer, and M. H. Pilkuhn. *Appl. Phys.*, vol. 80(7), 1996.

[2] P. Harrison. *Quantum Dots.* Wiley, 1997.

[3] W. G. V. Rosser. *An introduction to STATISTICAL PHYSICS.* Ellis Horwood Publishers, 1982.

[4] A. V. Uskov, F. Adler, H. Schweizer, and M. H. Pilkuhn. *Appl. Phys.*, vol. 81(12), 1997.

[5] A. V. Uskov, J. McInerney, F. Adler, H. Schweizer, and M. H. Pilkuhn. *Appl. Phys. Lett.*, vol. 72(1), 1998.

Chapter 4

Scattering processes in SADs

Contents

4.1 Introduction

In this chapter we derive equations to calculate the Auger capture and relaxation processes in InAs/GaAs quantum dot structures. The derivation starts from Fermi's Golden rule [3] and includes a Fermi-Dirac distribution for carriers in the wetting layer. We will compare the scattering rates obtained with those achieved by making use of the scattering formulas derived by A. V. Uskov (chapter 3).
We consider the three Auger scattering processes;

- Type I capture process (see Fig. 4.1) involves a 2D carrier (either an electron or a hole in the wetting layer) capture/ejection by the QD structure, after scattering with another $2D$ carrier which is scattered to another higher/lower energy state in the wetting layer.
- Type II capture process instead (see Fig. 4.2), refers to transitions in which a $2D$ carrier is captured inside the quantum dot due to carrier-carrier Coulomb scattering with a previously captured carrier. This carrier is excited from the quantum dot to a $2D$ state within the wetting layer.
- The Auger relaxation between QD energy levels (Fig. 4.3) is due to the Coulomb interaction between carriers in the wetting layer. In this process, a carrier inside the dot, is relaxed/excited to a lower/higher energy state due to the Coulomb-like interaction with a $2D$ carrier in the wetting layer. This $2D$ carrier will go to a higher/lower energy level.

We present a model for the calculation of Auger capture and relaxation rates in self-assembled InAs/GaAs quantum dots, considering a lens-shaped quantum dot with height h (as pictured in figure 4.4) and radius values varying between 5 nm and 40 nm approximately.

The chapter is organized as follows, we first calculate the wavefunction for a car-

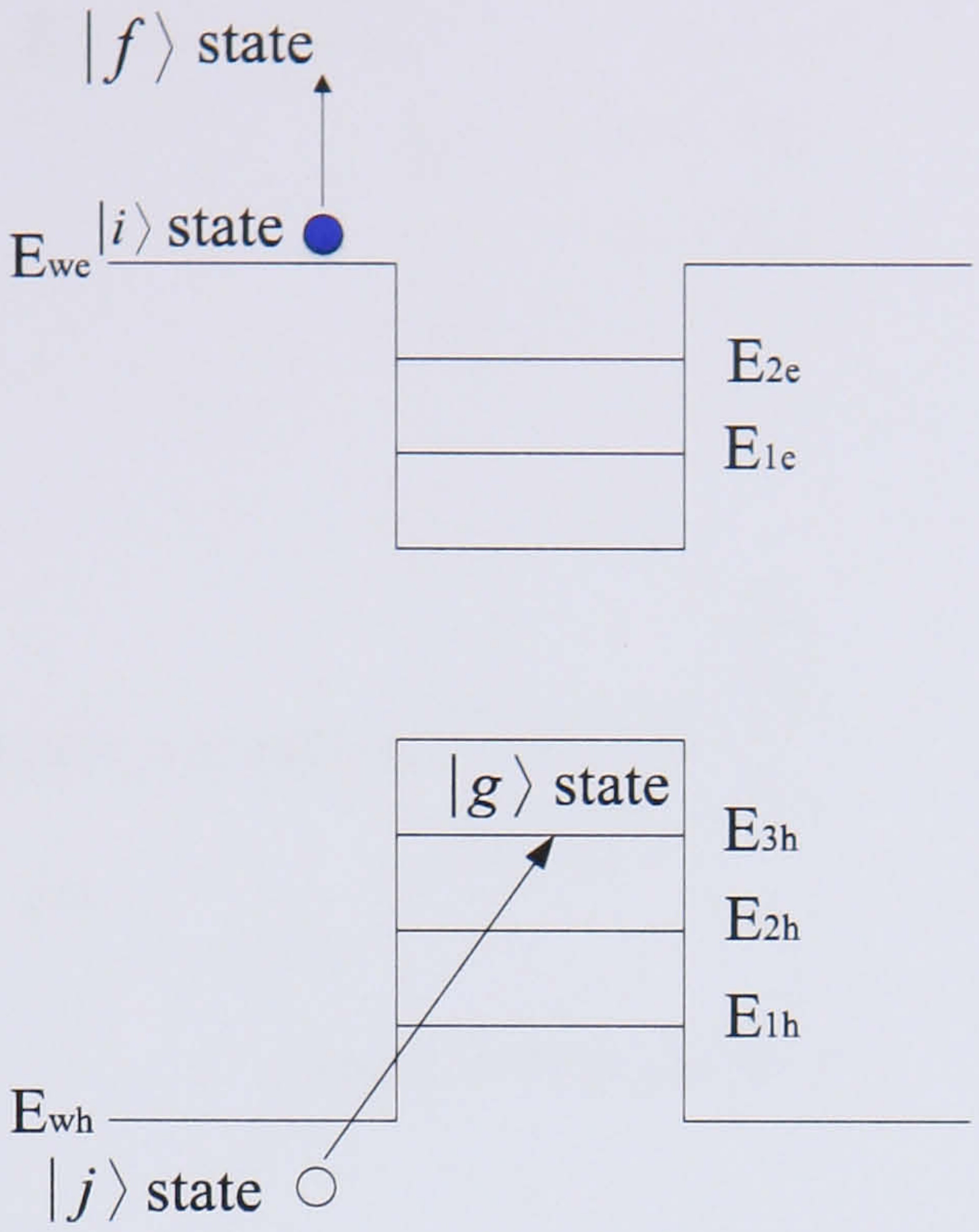

Figure 4.1: Auger Capture Process type I

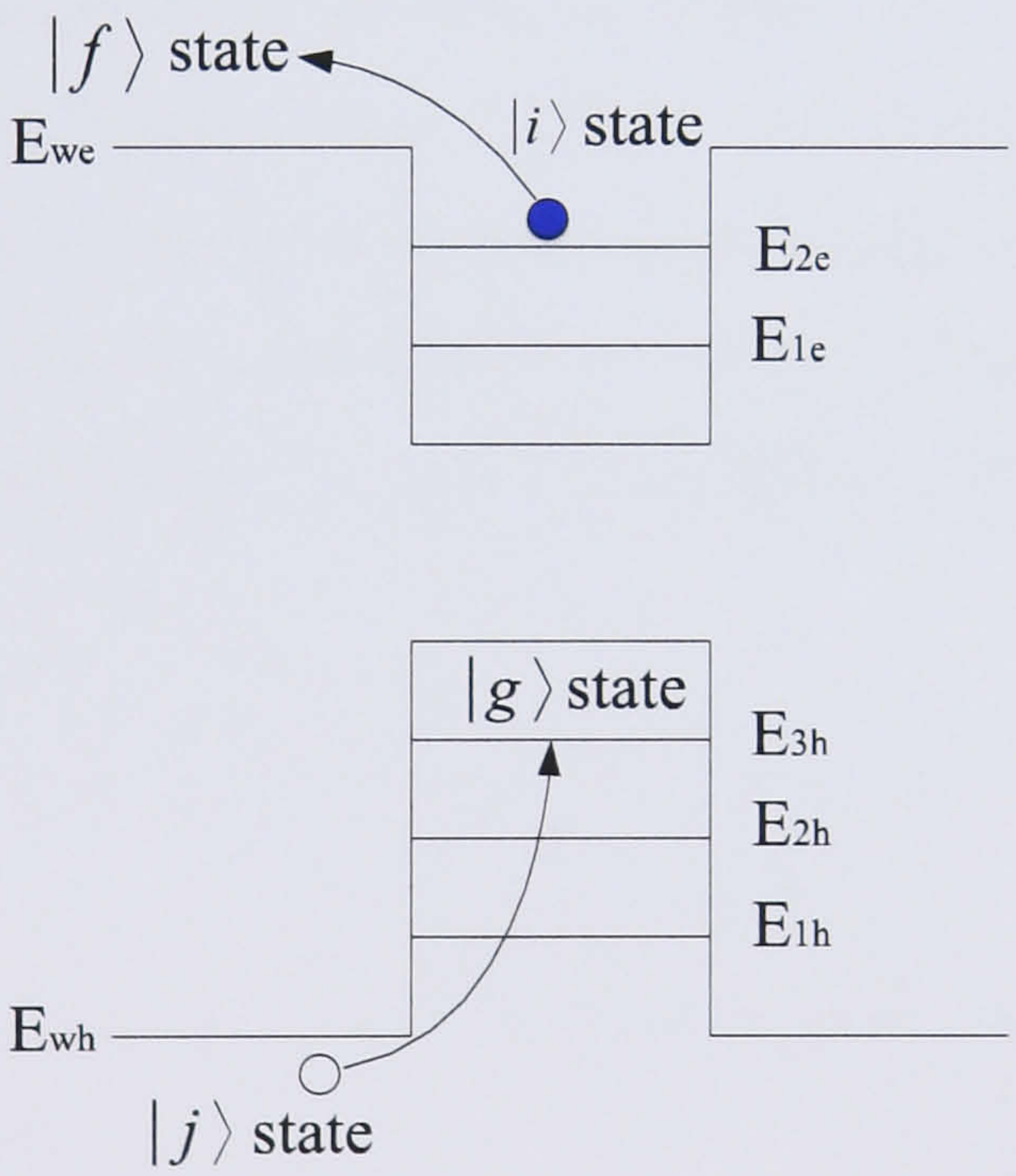

Figure 4.2: Auger Capture process type II

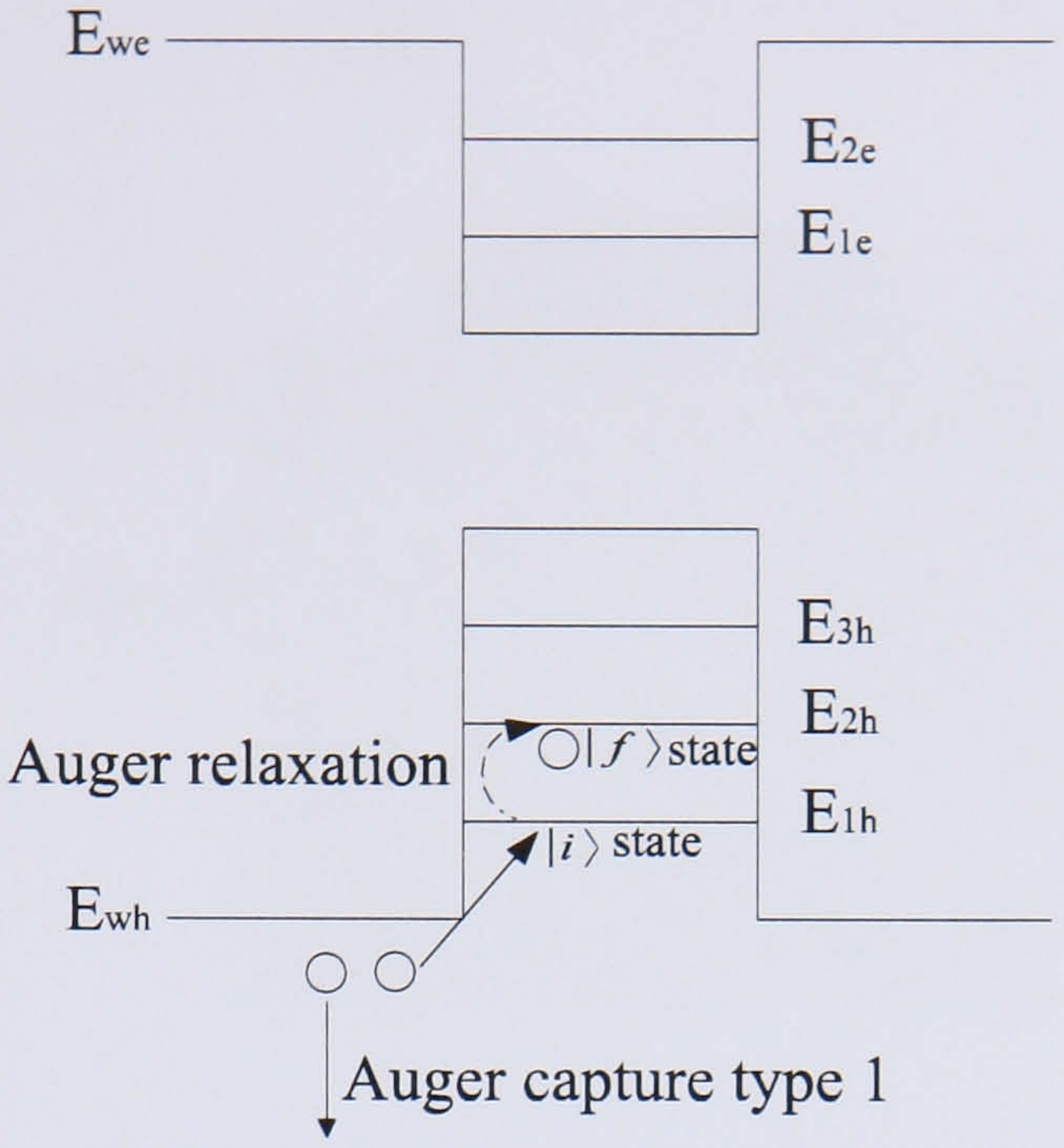

Figure 4.3: Auger Relaxation within the quantum dot.

rier within the SAD and quantum well (wetting layer) structure, for a quantum dot in the shape of spherical lenses shown in figure 4.4, formed on a narrow wetting layer. In the following sections the derivation of the Auger capture type II and type I rates are described. Then we calculate the Auger relaxation rate and finally we compare the results obtained with the semi-analytical expressions used in chapter 3.

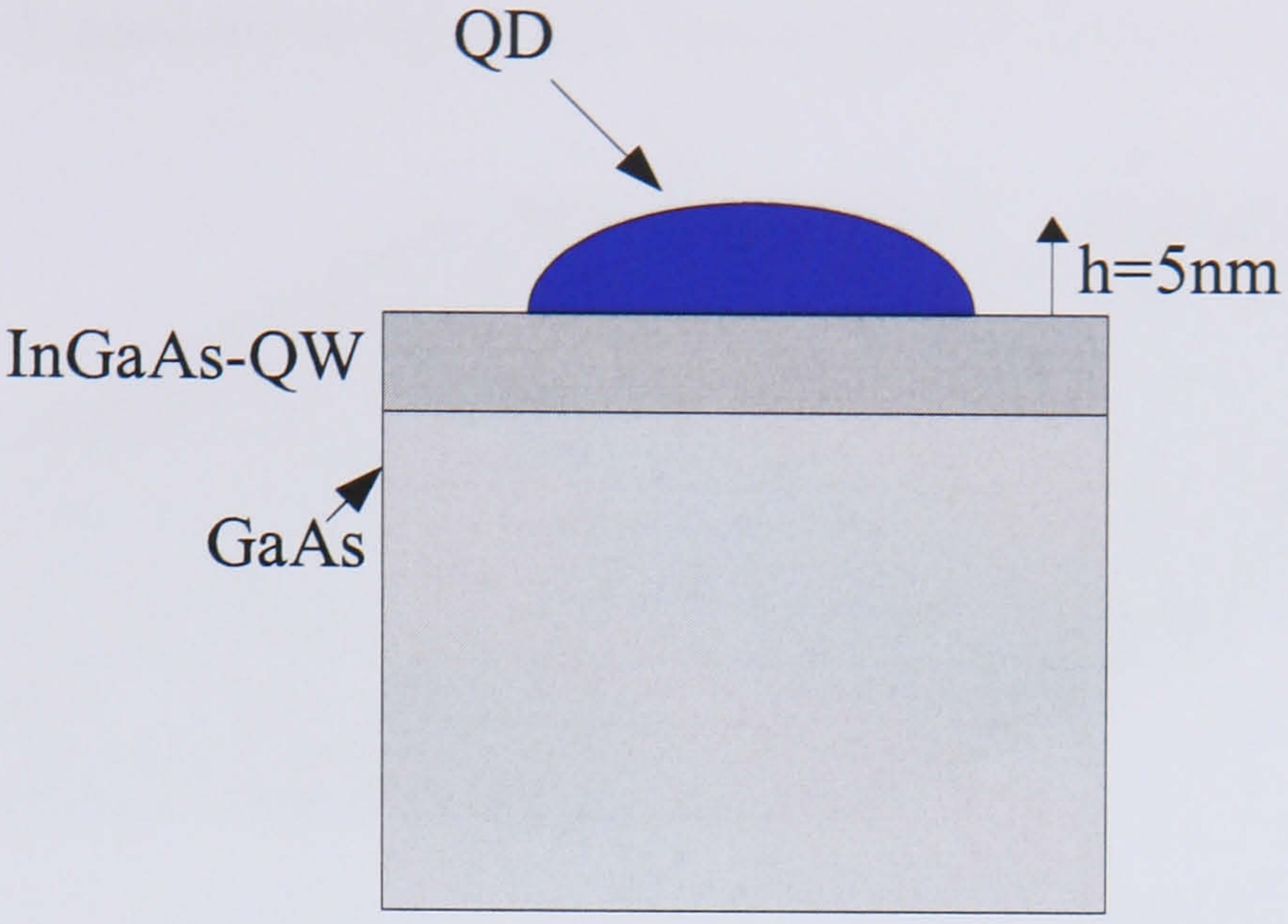

Figure 4.4: Self-Assembled Quantum Dot

4.2 Analysis of the wavefunctions and wave vectors in the QD and QW

4.2.1 Quantum dot wavefunctions and energies

Carriers in a QD are confined in all three directions. We have considered "lens" shaped quantum dot structures, which have much bigger radii than heights (Fig. 4.4) typical of those formed by the self-assembled growth process. The quantum dots are formed at the top of a narrow wetting layer of thickness, t_{wet}, and covered by GaAs bulk material. Consequently, electrons are confined in the quantum well in order to lower their energies, and they are further localized in the area of the quantum dot as the thickness of the the layer increases (Fig. 4.4). Due to the previously mentioned cylindrical symmetry of these quantum dots, a carrier in the quantum dot is confined in 3 directions within a cylindrical symmetry effective potential, $V(\rho, z)$, pictured in figure 4.5. The motion of a carrier of mass m^* inside the quantum dot in a potential field $V(r, z)$ (Fig. 4.5) is described by the Schrödinger Equation in cylindrical coordinates as follows [5]:

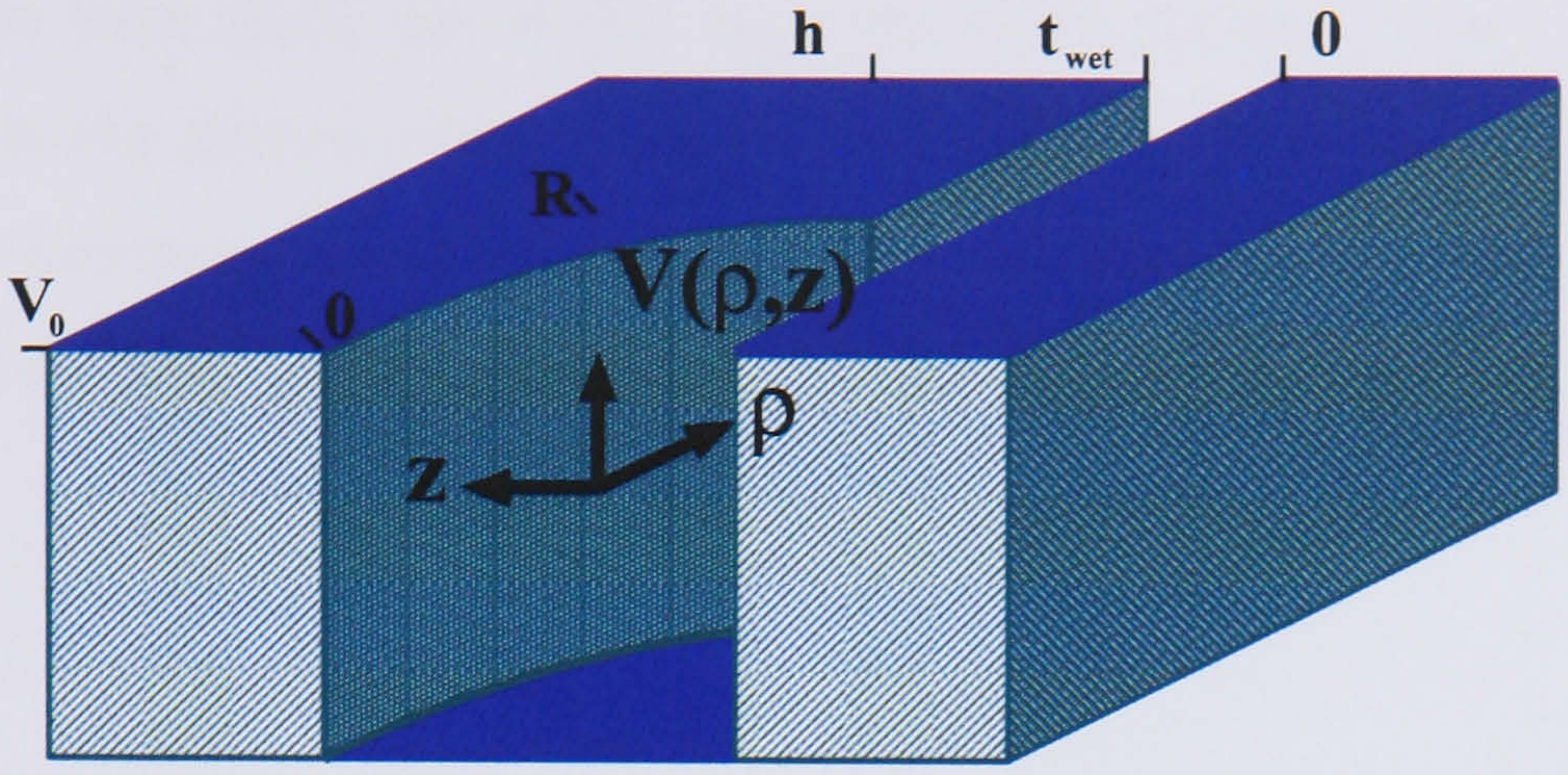

Figure 4.5: Effective $2D$ potential assuming cylindrical symmetry [5].

$$\left[\left(-\frac{1}{r^2}\left(r\frac{\partial}{\partial r}r\frac{\partial}{\partial r}+\frac{\partial^2}{\partial\theta^2}\right)-\frac{\partial^2}{\partial z^2}\right)+V(r,z)\right]\Psi^{\mathrm{D}}(r,\theta,z)$$
$$=E^D\Psi^{\mathrm{D}}(r,\theta,z) \qquad (4.1)$$

As pictured in figure 4.5, the carrier inside the quantum dot is confined in all three directions by the potential $V(r, z)$, schematically represented in figure 4.5, hence

$$V(r,z)=\begin{cases}0 & \text{inside the self-assembled quantum dot}\\ V_0 & \text{outside the self-assembled quantum dot}\end{cases} \qquad (4.2)$$

Note that $V(r, z)$ (figure 4.5) is independent of θ.

Taking account of the fact that each dot within the ensemble has much bigger radius than height, we make use of the adiabatic approximation [5] in order to separate the Hamiltonian for the electrons into a function along the radial direction r and another one perpendicular to the growth plane as in [5], therefore, the wavefunction in equation 4.1 can be written as follows:

$$\Psi^{\mathrm{D}}(z,r,\theta)=\frac{e^{im\theta}}{\sqrt{2\pi}}g_{nr}(z)f_m(r) \qquad (4.3)$$

for an integer momentum m and $g_{nr}(z)$ a slowly varying function of r. As previously mentioned, we have made use of this approximation taking advantage of the fact that carriers in the narrow wetting layer, are strongly confined to the lowest energy level in the z direction, as well as the fact that the potential changes slowly in the r direction (Fig. 4.5) [5]. From equation 4.1 the functions $g_{nr}(z)$ and $f_m(r)$ satisfy:

$$\left[H_z^0 + V(z,r)\right]g_{nr}(z) = E_n(r)g_{nr}(z) \tag{4.4}$$

$$\left[H_r^0 + E_n(r)\right]f_m(r) = E^{\mathrm{D}}f_m(r) \tag{4.5}$$

Introducing the expressions for the Hamiltonian in both z and r directions, equations (4.4) and (4.5) become

$$\left[-\frac{\partial^2}{\partial z^2} + V(r,z)\right]g_{nr}(z) \;=\; E_n(r)g_{nr}(z) \tag{4.6}$$

$$\left[-\frac{1}{r^2}\left(r\frac{\partial}{\partial r}r\frac{\partial}{\partial r} - m^2\right) + E_n(r)\right]f_m(r) \;=\; E^{\mathrm{D}}f_m(r) \tag{4.7}$$

where $E_n(r)$ is the effective lateral confining potential. As previously mentioned, carriers are strongly confined to the lowest sub-band in the narrow wetting layer, hence, we can considerate $E_0(r) = E_{n=1}(r)$ to be the potential energy profile.

In order to calculate the energy states $E_{n=1}(r)$ and the corresponding wavefunction $g_{n=1}r$ (equation 4.6), we divided the *SAD* into a number of segments (see figure 4.7), each of them corresponding to a finite potential well of width $L_z(r)$ and depth V_0, given by the band offset, as pictured in figure 4.6. Because of the symmetry of the potential, the wavefunctions posses even or odd parity. As we are considering strong confinement in the z-direction, we only calculated the ground state energy level (even parity) along the radius r_i. The width of each potential well, $L_z(r)$ was calculated for each radius r making use of the fact that the quantum dot has an elipsoidal shape, hence

$$L_z(r) = t_{wet} + H_{DOT}\sqrt{1-(r/R_{DOT})^2} \tag{4.8}$$

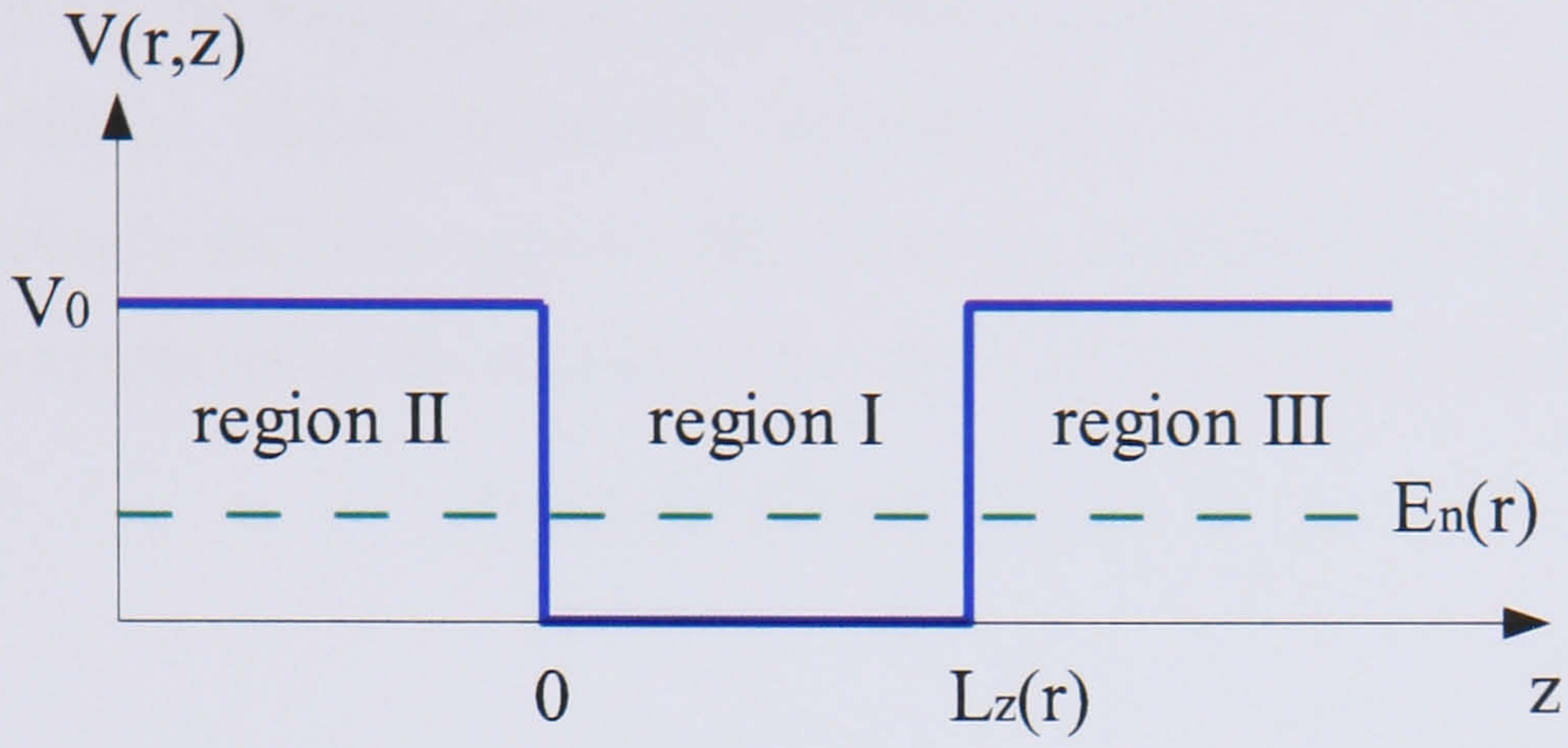

Figure 4.6: Finite potential well

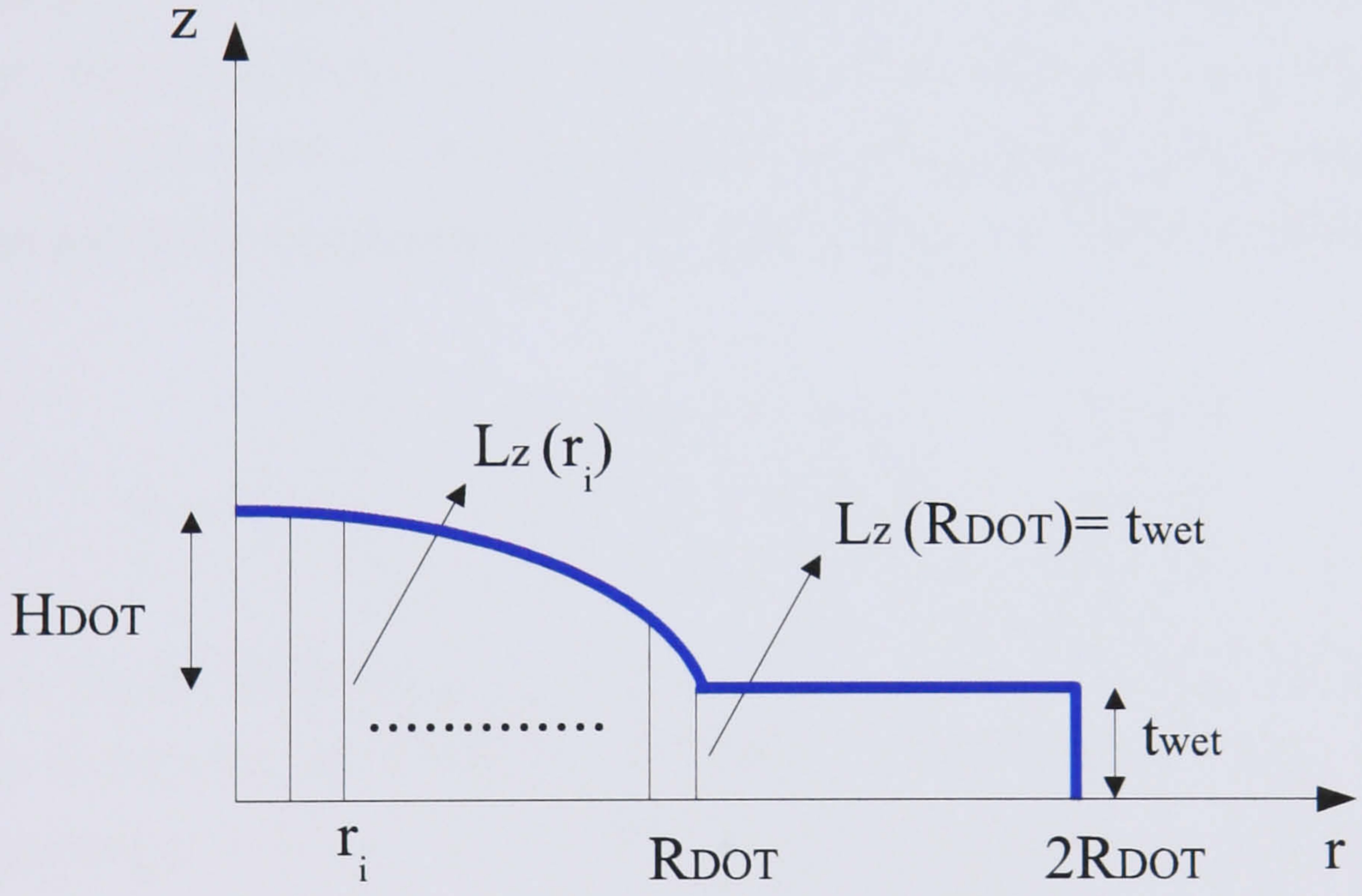

Figure 4.7: Schematic representation of the splitting of the quantum dot into n finite potential wells of width $L_z(r)$, as pictured in figure 4.6

Following [6], we solved the Schrödinger equation 4.6 in each of the 3 regions pictured in figure 4.6, by making use of exponentially decaying solutions for the regions outside the well, i.e., regions II and III, and travelling wave solutions for the region inside the quantum well, i.e., region I. Matching the wavefunctions and their derivatives at the boundaries of the regions, gives (for only the even solution):

$$k_I \tan(k_I L_z(r)/2) = k_{II} \tag{4.9}$$

where

$$\begin{aligned} k_I^2 &= E && (4.10)\\ k_{II}^2 &= V_0 - E && (4.11) \end{aligned}$$

In order to calculate the confined solutions in the wetting layer, i.e. $E_{n=1}(r)$, for each radius r, we numerically solved the equation 4.9. We considered a range of energies, starting from zero to V_0. The corresponding confined ground state energy levels $E_{n=1}(r)$ for each r, were those energy values that satisfied the equation 4.9. The corresponding wavefunction for each radius value r is given by equation 4.12 [6]

$$g_{n=1r}(z) = \begin{cases} A_r \cos(k_I L_z(r)/2) e^{k_{II} z} & \text{region II} \\ A_r \cos(k_I (z - L_z(r)/2)) & \text{region I} \\ A_r \cos(k_I L_z(r)/2) e^{-k_{II}(z - L_z(r))} & \text{region III} \end{cases} \tag{4.12}$$

where A_r can be calculated by the normalization condition $\int_{-\infty}^{\infty} |g_{n=1r}(z)|^2 \, \mathrm{d}z = 1$. In order to calculate the wavefunction along the radial direction, r (Eq. 4.7) and the total energy of the dot, E^{D}, we have followed the method explained in [5]. Approximating the potential $E_n(r)$, to a n-step function, then, the confining potential energy at each radial position r_i will be defined as $E_n(r) = v_i$ (see figure 4.8). As a result, the wavefunction corresponding to a particular energy E^{D} and angular momentum m, at a determined position in the radial direction, r, can be written as [6]:

$$f_m(r_i) = A_i F(k_i r_i) + B_i G(k_i r_i) \tag{4.13}$$

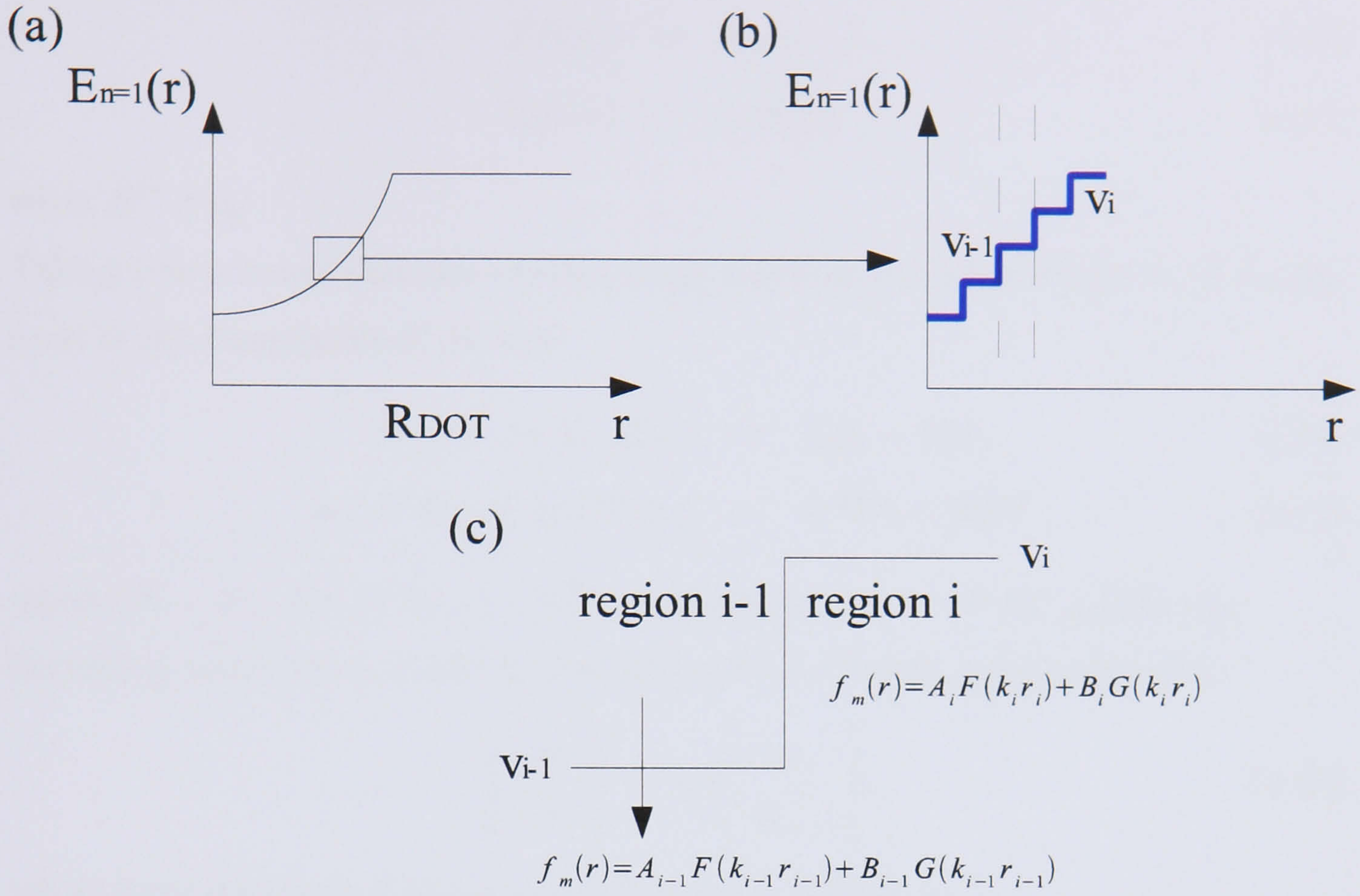

Figure 4.8: (a) Potential energy representation for the solution of the quantum dot wavefunctions in the radial direction. (b) Splitting the potential energy into a n-step potential function. (c) Schematic representation of one of the i-th confined regions.

where $k_i^2 = |E - v_i|$, $(F(k_i r_i), G(k_i r_i))$ are cylindrical Bessel functions, which are defined appropriately depending on which region i of the confined potential plotted in figure 4.8(c) is being considered. Hence,

$$F(k_i r_i) = J_m(k_i r_i) \tag{4.14}$$

$$G(k_i r_i) = Y_m(k_i r_i) \tag{4.15}$$

when $E^{\mathrm{D}} > v_i$ and

$$\begin{aligned} F(k_i r_i) &= K_m(k_i r_i) \quad (4.16)\\ G(k_i r_i) &= I_m(k_i r_i) \quad (4.17) \end{aligned}$$

when $E^{\mathrm{D}} < v_i$.

Taking into account that the wavefunctions and their derivatives have to be continuous at the boundaries of the dot:

$$\begin{aligned} A_{i-1}F_{i-1} + B_{i-1}G_{i-1} &= A_i F_i + B_i G_i \quad (4.18)\\ A_{i-1}\nabla F_{i-1} + B_{i-1}\nabla G_{i-1} &= A_i \nabla F_i + B_i \nabla G_i \quad (4.19) \end{aligned}$$

where $(F_{i-1}, G_{i-1}) = (F(k_{i-1}r_i), G(k_{i-1}r_i))$ and $(F_i, G_i) = (F(k_i r_i), G(k_i r_i))$. Rewriting equations 4.18 and 4.19 making use of a matrix notation, hence

$$\begin{pmatrix} A_i \\ B_i \end{pmatrix} = T_i \begin{pmatrix} A_{i-1} \\ B_{i-1} \end{pmatrix} \quad (4.20)$$

where from equations 4.18 and 4.19, T_i may be written as

$$T_i = \begin{pmatrix} F_i & G_i \\ \nabla F_i & \nabla G_i \end{pmatrix}^{-1} \begin{pmatrix} F_{i-1} & G_{i-1} \\ \nabla F_{i-1} & \nabla G_{i-1} \end{pmatrix} \quad (4.21)$$

In order to obtain the confined dot energies, it is necessary to solve the set of equations 4.18 and 4.19, which is equivalent to finding the total transfer matrix T, defined as:

$$\begin{pmatrix} A_n \\ B_n \end{pmatrix} = \left(\prod_{i=1}^{n} T_i \right) \begin{pmatrix} A_0 \\ B_0 \end{pmatrix} \equiv T \begin{pmatrix} A_0 \\ B_0 \end{pmatrix} \quad (4.22)$$

Taking into account that the wavefunctions need to be finite at the origin, it is necessary to set the coefficient B_0 to zero, hence, $B_0 = 0$. On the other hand, at large values of r, the wavefunction vanish, thus, B_n in equation 4.22 must also be zero, i.e., $B_n = 0$. Under these conditions, equation 4.22 may be written as:

$$\begin{aligned} A_n &= T_{11} A_0 \quad (4.23)\\ 0 &= T_{21} A_0 \quad (4.24) \end{aligned}$$

As $A_0 \neq 0$, the energies of the bound states E_b^D may be obtained from 4.24 as follows,

$$T_{21}(E_b^D) = 0 \tag{4.25}$$

We solve equation 4.25 by first obtaining rough values of the roots by using a set of trial energies, starting from $E_n(r=0)$ to V_0 (the potential well depth, see figure 4.5). The accuracy of these roots is improved using a Newton-Raphson routine [7]. The confined energy states of the dot, E_b^D, were those energy values for which the element of the transfer matrix T_{21} was zero. As expected, it was found that the number of energy levels increases when increasing the dot size.

Taking into account the wavefunction component $g_{n=1r}(z)$ is a slowly varying function of r, we simplify the calculations by assuming $g_{n=1r}(z)$ is independent of r;

$$g_{n=1r}(z) \approx g_{n=1r=0}(z) = \psi_z^{\mathrm{D}} \tag{4.26}$$

Denoting as ψ_{xy}^{D}, the solution of the equation 4.7, hence, making use of this notation, the wavefunction of a carrier within the QD can be expressed as:

$$\Psi^{\mathrm{D}} = \psi_z^{\mathrm{D}} \psi_{xy}^{\mathrm{D}} \tag{4.27}$$

As an example, considering a "lens"-shaped quantum dot of height 5 nm and radius 18 nm as well as a potential barrier $V_0 = 0.244$ eV, the obtained confined electron (of mass $m_e = 0.0445\mathrm{m}_0$ [5]) energy levels are;

$$\begin{aligned} E_0^D &= 0.0974\mathrm{eV} \\ E_1^D &= 0.1234\mathrm{eV} \\ E_2^D &= 0.1531\mathrm{eV} \\ E_3^D &= 0.1921\mathrm{eV} \end{aligned}$$

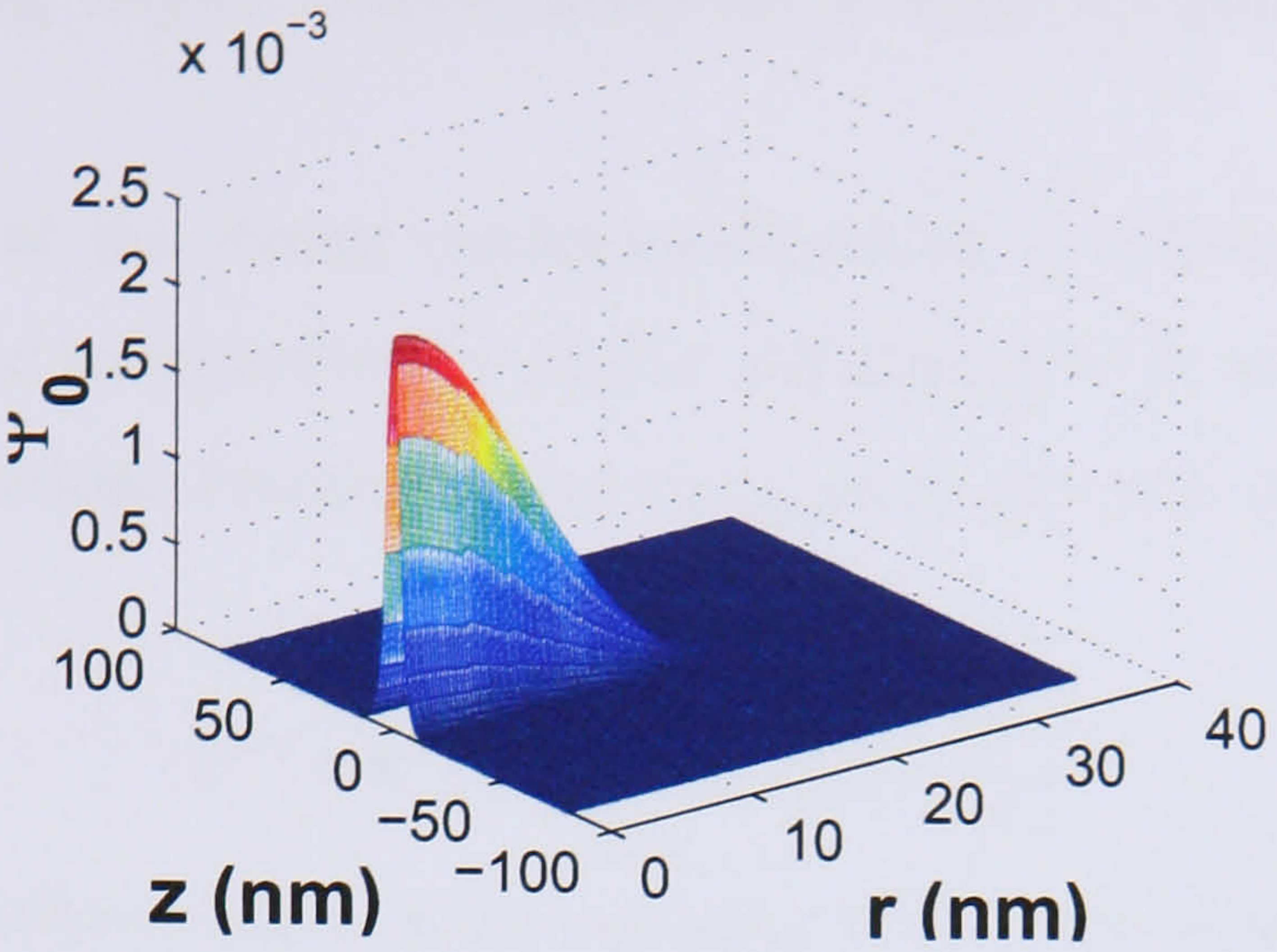

Figure 4.9: SAD ground sate wavefunction

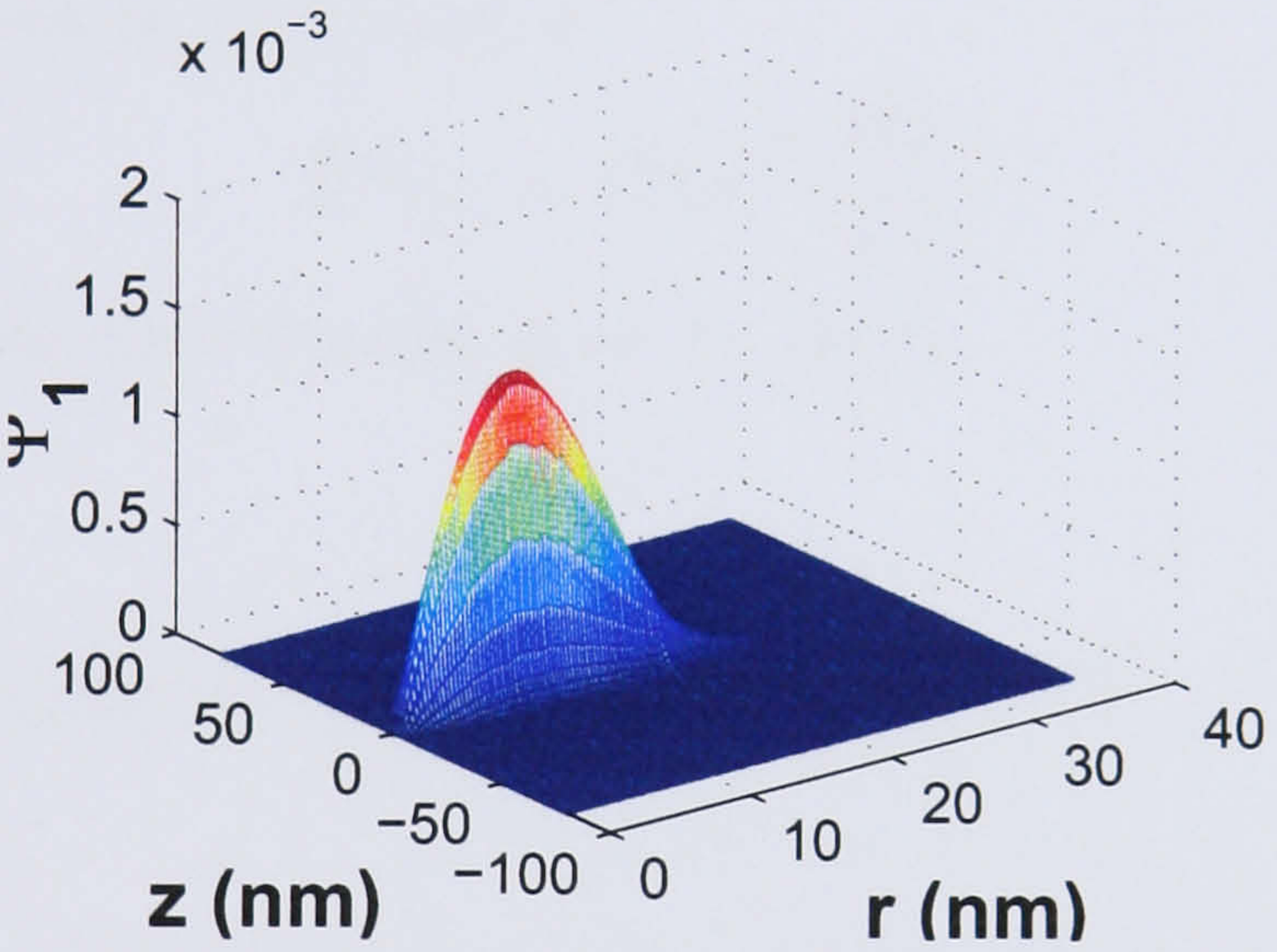

Figure 4.10: SAD excited sate wavefunction

The associated wavefunctions for the ground state Ψ_0 and the excited state Ψ_1 have been plotted in figure 4.9 and figure 4.10 respectively.

4.2.2 Wetting layer wavefunctions and energies

As a consequence of the strong carrier confinement in z-direction in the wetting layer, we are allowed to separate the carrier wavefunctions in the wetting layer, into a product of an envelope function along the growth axis and an in-plane travelling wave, i.e.

$$\Psi^{\mathrm{W}}(\mathbf{r},\mathbf{k}^{\mathrm{W}}) = \psi_z^{\mathrm{W}}(z,k_z^{\mathrm{W}})\frac{e^{-i\mathbf{k}_{xy}^{\mathrm{W}}\mathbf{r}_{xy}}}{\sqrt{A}} \tag{4.28}$$

In order to simplify the notation when referring to the wave functions of the carriers within the quantum dot and quantum well, functions used in further calculations, equations 4.27 and 4.28 are rewritten as follows:

$$\psi^{\mathrm{D}} = (\psi_{xy}^{\mathrm{D}}(\mathbf{r}_{xy}),\psi^{\mathrm{D}}(z)) = (\psi_{m\rho}^{\mathrm{D}}(\rho)\frac{e^{im\theta}}{\sqrt{2\pi}},\psi^{\mathrm{D}}(z)) \tag{4.29}$$

for the equation given by (4.27) and as

$$\Psi^{\mathrm{W}}(\mathbf{r}) = \psi_z^{\mathrm{W}}(z)\frac{e^{-i\mathbf{k}_{xy}^{\mathrm{W}}\mathbf{r}_{xy}}}{\sqrt{A}} \tag{4.30}$$

for the quantum well wave function given by (4.28).

4.3 Auger capture process type II

In this kind of capture process, a hole within the $2D$ wetting layer is captured by the SAD due to the Coulomb interaction with a previously captured $0D$ electron, which is excited from the SAD into the wetting layer (see figure 4.11). The probability of finding a $2D$ carrier which it is initially in state $|j>$ in the wetting layer, captured by the SAD into a discrete state $|g>$ due to Coulomb interaction with a $0D$ carrier in an initial $0D$ state $|i>$, which is excited from the SAD into a $2D$ state $|f>$ within the the wetting layer is given by Fermi's Golden Rule [3]:

$$\frac{1}{\tau_g} = \frac{2\pi}{\hbar}\sum_{\mathbf{k}_f^{xy},\mathbf{k}_j^{xy}} |<f|\tilde{H}|i>|^2\delta(E_F^{total} - E_I^{total}) \tag{4.31}$$

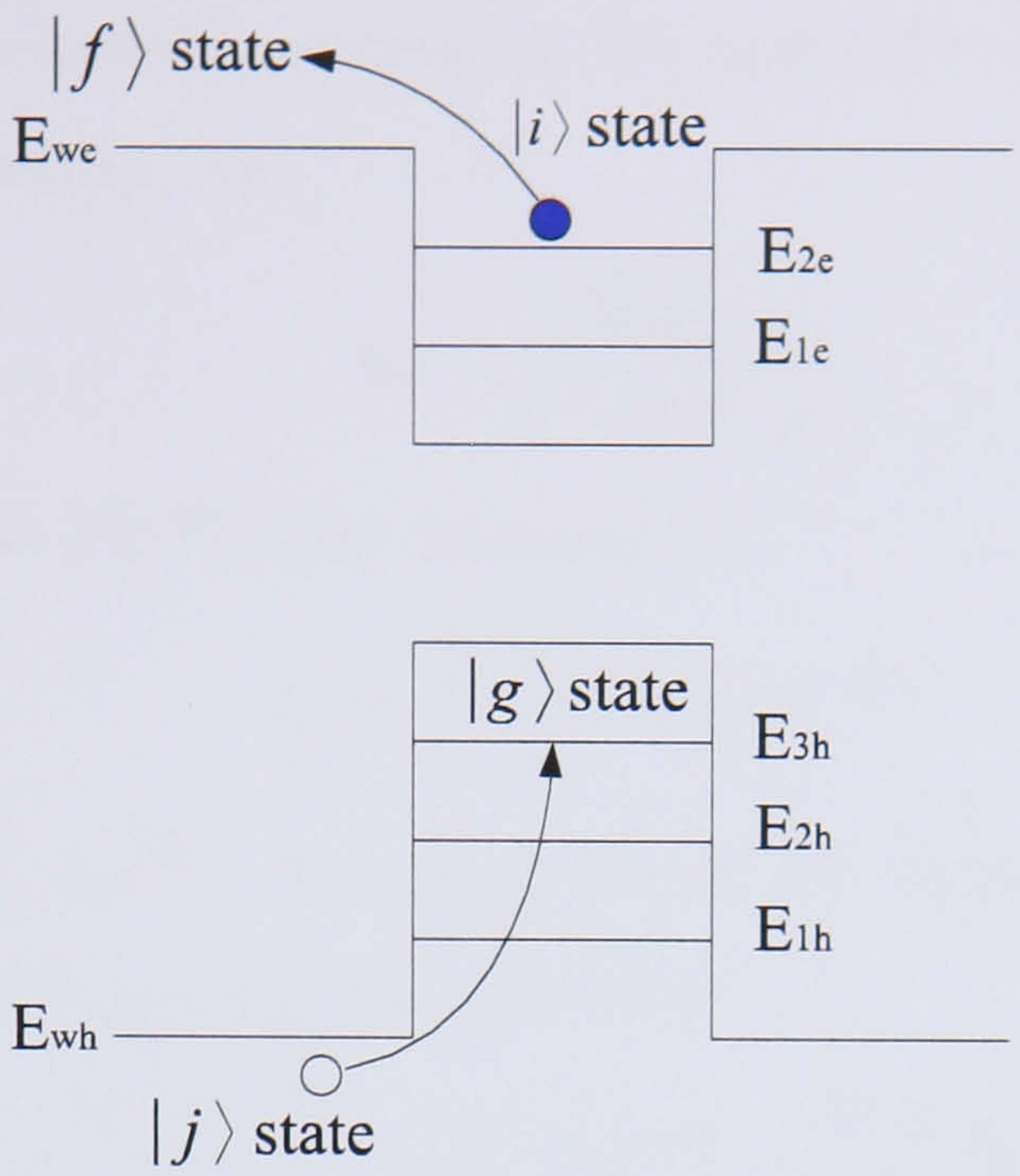

Figure 4.11: Auger Capture process type II

where:

- $|i>$ is the product of the initial state of the scattered carrier in the QD $\longrightarrow\ \psi_i^{\rm D}(z)\psi_i^{\rm D}(\mathbf{r}_{xy})$ and the initial state of the captured carrier in the QW $\longrightarrow\ \psi_j^{\rm W}(z')\frac{e^{-\mathbf{k}_j^{xy}\mathbf{r}'_{xy}}}{\sqrt{A}}$
- $|f>$ is the product of the final state of the scattered carrier in the QW $\longrightarrow\ \psi_f^{\rm W}(z)\frac{e^{-\mathbf{k}_f^{xy}\mathbf{r}_{xy}}}{\sqrt{A}}$ and the final state of the captured carrier in the QD $\longrightarrow$ $\psi_g^{\rm D}(z')\psi_g^{\rm D}(\mathbf{r}'_{xy})$
- $\tilde{H}$ is the $3D$ Screened Coulomb interaction [4]. We consider the $3D$ Screened Coulomb interaction because the carriers in the whole structure contribute to the Coulomb interaction in the scattering process. This interaction between carriers at $\mathbf{r}$ and $\mathbf{r}$' can be written as

$$\tilde{H} = \frac{\mathrm{e}^2 e^{-k_{\rm D}|\mathbf{r}-\mathbf{r}'|}}{\epsilon\,|\,\mathbf{r}-\mathbf{r}'|} \tag{4.32}$$

where ϵ is the dielectric constant of the material and k_{D} is the 3D Debye screening wave number, i.e.,

$$k_{\mathrm{D}} = \sqrt{\frac{4\pi \mathrm{e}^2 n_{bulk}}{\epsilon k_{\mathrm{B}} T_{bulk}}} \tag{4.33}$$

However, using the $3D$ Fourier Transform

$$f_{\mathbf{k}} = \int \frac{1}{L^3} d^3\mathbf{r} f(\mathbf{r}) e^{-i\mathbf{k}\cdot\mathbf{r}}$$

where $f(\mathbf{r}) = \sum_{\mathbf{k}} f_{\mathbf{k}} e^{i\mathbf{k}\cdot\mathbf{r}}$, we make use of the expression for the Screened Coulomb interaction given in [4], therefore

$$\tilde{H} = \frac{\mathrm{e}^2 e^{-k_{\mathrm{D}}|\mathbf{r}-\mathbf{r}'|}}{\epsilon \mid \mathbf{r}-\mathbf{r}'|} = \sum_{\mathbf{k}} V_{\mathbf{k}} e^{i\mathbf{k}\cdot\mathbf{r}} = \frac{4\pi \mathrm{e}^2}{\epsilon V} \sum_{\mathbf{k}} \frac{e^{i\mathbf{k}\cdot(\mathbf{r}-\mathbf{r}')}}{k^2 + k_{\mathrm{D}}^2} \tag{4.34}$$

This will be the expression used for the Screened Coulomb interaction in this study. We will make use of the notation **kr** when referring to the scalar product of $\mathbf{k}\cdot\mathbf{r}$.

Using the Screened Coulomb potential given in (4.34), the matrix element in Fermi's Golden Rule (equation 4.31) may be written as:

$$\begin{aligned} < f|\tilde{H}|i> \;=\; & \Big\langle \Psi_f^{\mathrm{W}}(\mathbf{r},\mathbf{k}_f^{\mathrm{W}}) \Psi_g^{\mathrm{D}}(\mathbf{r}',\mathbf{k}_g^{\mathrm{D}}) \\ & \left| \frac{4\pi \mathrm{e}^2}{\epsilon V} \sum_{\mathbf{k}_{xy},k_z} \frac{e^{i\mathbf{k}_{xy}(\mathbf{r}_{xy}-\mathbf{r}'_{xy})} e^{ik_z(z-z')}}{k_z^2 + k_{xy}^2 + k_{\mathrm{D}}^2} \right| \\ & \Psi_i^{\mathrm{D}}(\mathbf{r},\mathbf{k}_i^{\mathrm{D}}) \Psi_j^{\mathrm{W}}(\mathbf{r}',\mathbf{k}_j^{\mathrm{W}}) \Big\rangle \end{aligned} \tag{4.35}$$

Introducing the expressions for the carriers' wavefunctions within the quantum dot (4.27) and well (4.28), we obtain:

$$\begin{aligned} < f|\tilde{H}|i> \;=\; & \frac{4\pi e^2}{VA\epsilon} \int_{-\infty}^{\infty} \mathrm{d}z\mathrm{d}z' \int_{-\infty}^{\infty} \psi_f^{\mathrm{W}}(z)^* \psi_g^{\mathrm{D}}(z')^* \psi_i^{\mathrm{D}}(z) \psi_j^{\mathrm{W}}(z') \\ \times\; & \iint \mathrm{d}\mathbf{r}_{xy} \mathrm{d}\mathbf{r}'_{xy} \psi_g^{\mathrm{D}}(\mathbf{r}'_{xy})^* e^{-i\mathbf{k}_j^{xy}\mathbf{r}'_{xy}} \psi_i^{\mathrm{D}}(\mathbf{r}_{xy}) e^{i\mathbf{k}_f^{xy}\mathbf{r}_{xy}} \\ \times\; & \sum_{\mathbf{k}_{xy},k_z} \frac{e^{i\mathbf{k}_{xy}(\mathbf{r}_{xy}-\mathbf{r}'_{xy})} e^{ik_z(z-z')}}{k_z^2 + k_{xy}^2 + k_{\mathrm{D}}^2} \end{aligned} \tag{4.36}$$

In order to obtain a more manageable expression, we convert the summation over the wave vectors $\mathbf{k}_{xy}$ and k_z into integrals. Taking into account that the area in $\mathbf{k}$-space occupied by one state in the quantum well is $(\frac{2\pi}{L})^2$. We need to include a factor of $\frac{A}{(2\pi)^2}$ when changing the summation over the wave vector $\mathbf{k}_{xy}$ to an integral, as well as a factor of $\frac{L}{2\pi}$ for the summation over the z component of the wave vector, hence:

$$\begin{aligned} < f|\tilde{H}|i > &= \frac{e^2}{2A\epsilon\pi^2}\int_{-\infty}^{\infty}\mathrm{d}z\int_{-\infty}^{\infty}\mathrm{d}z'\psi_f^{\mathrm{W}}(z)^*\psi_g^{\mathrm{D}}(z')^*\psi_i^{\mathrm{D}}(z)\psi_j^{\mathrm{W}}(z') \\ &\times \iint \mathrm{d}\mathbf{r}_{xy}\mathrm{d}\mathbf{r}'_{xy}\psi_g^{\mathrm{D}}(\mathbf{r}'_{xy})^* e^{-i(\mathbf{k}_j^{xy}+\mathbf{k}_{xy})\mathbf{r}_{xy}}\psi_i^{\mathrm{D}}(\mathbf{r}_{xy})e^{i(\mathbf{k}_f^{xy}+\mathbf{k}_{xy})\mathbf{r}_{xy}} \\ &\times \int_{-\infty}^{\infty}\mathrm{dk}_z e^{i\mathrm{k}_z(z-z')}\int \mathrm{d}\mathbf{k}_{xy}\frac{1}{k_z^2+k_{xy}^2+k_{\mathrm{D}}^2} \end{aligned} \tag{4.37}$$

where A is the normalization area of the 2D gas. Changing the order of the integrations so that we perform first integration over $\mathbf{r}_{xy}$, i.e.

$$\begin{aligned} < f|\tilde{H}|i > &= \frac{\mathrm{e}^2}{2A\epsilon\pi^2}\int_{-\infty}^{\infty}\mathrm{d}z\int_{-\infty}^{\infty}\mathrm{d}z'\psi_f^{\mathrm{W}}(z)^*\psi_g^{\mathrm{D}}(z')^*\psi_i^{\mathrm{D}}(z)\psi_j^{\mathrm{W}}(z') \\ &\times \int_{-\infty}^{\infty}\mathrm{dk}_z e^{i\mathrm{k}_z(z-z')}\int \mathrm{d}\mathbf{k}_{xy}\frac{1}{k_z^2+k_{xy}^2+k_{\mathrm{D}}^2} \\ &\times \int \mathrm{d}\mathbf{r}'_{xy}\psi_g^{\mathrm{D}}(\mathbf{r}'_{xy})^* e^{-i(\mathbf{k}_j^{xy}+\mathbf{k}_{xy})\mathbf{r}'_{xy}} \\ &\times \int \mathrm{d}\mathbf{r}_{xy}\psi_i^{\mathrm{D}}(\mathbf{r}_{xy})e^{i(\mathbf{k}_f^{xy}+\mathbf{k}_{xy})\mathbf{r}_{xy}} \end{aligned} \tag{4.38}$$

so

$$\begin{aligned} < f|\tilde{H}|i > &= \frac{\mathrm{e}^2}{2A\epsilon\pi^2}\int_{-\infty}^{\infty}\mathrm{d}z\int_{-\infty}^{\infty}\mathrm{d}z'\psi_f^{\mathrm{W}}(z)^*\psi_g^{\mathrm{D}}(z')^*\psi_i^{\mathrm{D}}(z)\psi_j^{\mathrm{W}}(z') \\ &\times \int_{-\infty}^{\infty}\mathrm{dk}_z e^{i\mathrm{k}_z(z-z')}\int \mathrm{d}\mathbf{k}_{xy}\left[\frac{G_g(\mathbf{k}_j^{xy},\mathbf{k}_{xy})G_i(\mathbf{k}_f^{xy},\mathbf{k}_{xy})}{k_z^2+k_{xy}^2+k_{\mathrm{D}}^2}\right] \end{aligned} \tag{4.39}$$

where the *form factors* $G_g(\mathbf{k}_j^{xy},\mathbf{k}_{xy})$ and $G_i(\mathbf{k}_f^{xy},\mathbf{k}_{xy})$ are given by:

$$G_g(\mathbf{k}_j^{xy},\mathbf{k}_{xy}) = \int \mathrm{d}\mathbf{r}'_{xy}\psi_g^{\mathrm{D}}(\mathbf{r}'_{xy})^* e^{-i(\mathbf{k}_j^{xy}+\mathbf{k}_{xy})\mathbf{r}'_{xy}} \tag{4.40}$$

$$G_i(\mathbf{k}_f^{xy}, \mathbf{k}_{xy}) = \int \mathrm{d}\mathbf{r}_{xy}\psi_i^{\mathrm{D}}(\mathbf{r}_{xy})e^{i(\mathbf{k}_f^{xy}+\mathbf{k}_{xy})\mathbf{r}_{xy}} \tag{4.41}$$

Changing the order of the integrations, we obtain

$$\begin{aligned} < f|\tilde{H}|i > &= \frac{\mathrm{e}^2}{2A\epsilon\pi^2}\int_{-\infty}^{\infty}\mathrm{dk}_z\int \mathrm{d}\mathbf{k}_{xy}\left[\frac{G_g(\mathbf{k}_j^{xy}, \mathbf{k}_{xy})G_i(\mathbf{k}_f^{xy}, \mathbf{k}_{xy})}{k_z^2 + k_{xy}^2 + k_{\mathrm{D}}^2}\right] \\ &\times \int_{-\infty}^{\infty}\mathrm{d}z\psi_f^{\mathrm{W}}(z)^*\psi_i^{\mathrm{D}}(z)e^{i\mathrm{k}_z z} \\ &\times \int_{-\infty}^{\infty}\mathrm{d}z'\psi_g^{\mathrm{D}}(z')^*\psi_j^{\mathrm{W}}(z')e^{-i\mathrm{k}_{z'}z'} \end{aligned} \tag{4.42}$$

So the matrix element in this Scattering process (Eq. 4.35) may be expressed in a more accessible way as

$$< f|\tilde{H}|i > = \frac{\mathrm{e}^2}{2A\epsilon\pi^2}\int_{-\infty}^{\infty}\mathrm{dk}_z G_z(\mathrm{k}_z)\int \mathrm{d}\mathbf{k}_{xy}\frac{G(\mathbf{k}_j^{xy}, \mathbf{k}_f^{xy}, \mathbf{k}_{xy})}{k_z^2 + k_{xy}^2 + k_{\mathrm{D}}^2} \tag{4.43}$$

where A is the area of normalization of the 2D gas and $G_z(\mathrm{k}_z)$ and $G(\mathbf{k}_j^{xy}, \mathbf{k}_f^{xy}, \mathbf{k}_{xy})$ are the *form factors* given by:

$$\begin{aligned} G_z(\mathrm{k}_z) &= G_{if}(\mathrm{k}_z)G_{jg}(\mathrm{k}_z) \\ &= \int_{-\infty}^{\infty}\mathrm{d}z\psi_f^{\mathrm{W}}(z)^*\psi_i^{\mathrm{D}}(z)e^{i\mathrm{k}_z z}\int_{-\infty}^{\infty}\mathrm{d}z'\psi_g^{\mathrm{D}}(z')^*\psi_j^{\mathrm{W}}(z')e^{-i\mathrm{k}_{z'}z'} \end{aligned} \tag{4.44}$$

$$\begin{aligned} G(\mathbf{k}_j^{xy}, \mathbf{k}_f^{xy}, \mathbf{k}_{xy}) &= G_g(\mathbf{k}_j^{xy}, \mathbf{k}_{xy})G_i(\mathbf{k}_f^{xy}, \mathbf{k}_{xy}) \\ &= \int \mathrm{d}\mathbf{r}'_{xy}\psi_g^{\mathrm{D}}(\mathbf{r}'_{xy})^* e^{-i(\mathbf{k}_j^{xy}+\mathbf{k}_{xy})\mathbf{r}'_{xy}} \\ &\times \int \mathrm{d}\mathbf{r}_{xy}\psi_i^{\mathrm{D}}(\mathbf{r}_{xy})e^{i(\mathbf{k}_f^{xy}+\mathbf{k}_{xy})\mathbf{r}_{xy}} \end{aligned} \tag{4.45}$$

If we now include the matrix element for this type of Scattering process, given by Eq. 4.43, into Eq. 4.31, we obtain an expression to calculate the scattering rate for this type of Coulomb interaction, hence

$$\begin{aligned} \frac{1}{\tau_g} &= \frac{2\pi}{\hbar}\sum_{\mathbf{k}_f^{xy},\mathbf{k}_j^{xy}}\left|\frac{\mathrm{e}^2}{2A\epsilon\pi^2}\int_{-\infty}^{\infty}\mathrm{dk}_z G_z(\mathrm{k}_z)\int \mathrm{d}\mathbf{k}_{xy}\frac{G(\mathbf{k}_j^{xy}, \mathbf{k}_f^{xy}, \mathbf{k}_{xy})}{k_z^2 + k_{xy}^2 + k_{\mathrm{D}}^2}\right|^2 \\ &\times \delta(E_F^{total} - E_I^{total}) \end{aligned} \tag{4.46}$$

where the E_F^{total} and E_I^{total} are the total energy after and before the scattering process respectively

$$\begin{aligned} \delta(E_F^{total} - E_I^{total}) &= \delta\Big(\mathrm{E}_f^z + \frac{\hbar^2}{2m_s}\mathrm{k}_f^{xy2} + \epsilon_g^{DOT} \\ &- \big[\epsilon_i^{DOT} + \mathrm{E}_j^z + \frac{\hbar^2}{2m_c}\mathrm{k}_j^{xy2}\big]\Big) \end{aligned} \tag{4.47}$$

where $\epsilon_g^{DOT} = \mathrm{E}_g^z + \frac{\hbar^2}{2m_c}\mathrm{k}_g^{xy2}$ and $\epsilon_i^{DOT} = \mathrm{E}_i^z + \frac{\hbar^2}{2m_s}\mathrm{k}_i^{xy2}$ are the energies of the final $|g\rangle$ state for the captured carrier inside the quantum dot, and the initial $|i\rangle$ state of the scattered carrier in the dot.

k_f^{xy} and k_j^{xy} are the modulus of the wave vectors in the xy plane, for the scattered and captured carrier respectively, trapped in the wetting layer.

Eq. (4.47) can be simplified rearranging its components in a suitable way by defining a constant Δ as follows:

$$\Delta = \frac{2m_s}{\hbar^2}\big[\epsilon_g^{DOT} - \epsilon_i^{DOT} + \mathrm{E}_f^z - \mathrm{E}_j^z\big] \tag{4.48}$$

then Eq. (4.47) becomes:

$$\begin{aligned} \delta(E_F^{total} - E_I^{total}) &= \delta\big(\frac{\hbar^2}{2m_s}\big[\mathrm{k}_f^{xy2} - \mathrm{k}_j^{xy2} + \Delta\big]\big) \\ &= \frac{2m_s}{\hbar^2}\delta\big(\mathrm{k}_f^{xy2} - \frac{m_s}{m_c}\mathrm{k}_j^{xy2} + \Delta\big) \end{aligned} \tag{4.49}$$

Following the approach of Paul Harrison [3], the argument of the δ-function (Eq. 4.49) may be factorized into:

$$\begin{aligned} \delta(E_F^{total} - E_I^{total}) &= \frac{2m_s}{\hbar^2}\delta\big(\mathrm{k}_f^{xy2} - \frac{m_s}{m_c}\mathrm{k}_j^{xy2} + \Delta\big) \\ &= \frac{2m_s}{\hbar^2}\delta((\mathrm{k}_f^{xy} - \beta(\mathrm{k}_j^{xy}))(\mathrm{k}_f^{xy} + \beta(\mathrm{k}_j^{xy}))) \end{aligned} \tag{4.50}$$

where

$$\beta(\mathrm{k}_j^{xy}) = \sqrt{\frac{m_s}{m_c}\mathrm{k}_j^{xy2} - \Delta} \tag{4.51}$$

has to be real and positive. Returning to equation 4.50 we may emphasize the fact that around the solution $\beta(\mathrm{k}_j^{xy}) = \mathrm{k}_f^{xy}$ the term $(\beta(\mathrm{k}_j^{xy}) + \mathrm{k}_f^{xy})$ is finite and can be extracted from the δ-function. The same applies for the solution around $\beta(\mathrm{k}_j^{xy}) = -\mathrm{k}_f^{xy}$ and the factor $(\beta(\mathrm{k}_j^{xy}) - \mathrm{k}_f^{xy})$ is finite and can also be extracted from the δ-function:

$$\delta(\beta(\mathrm{k}_j^{xy})^2 - \mathrm{k}_f^{xy2}) = \frac{\delta(\beta(\mathrm{k}_j^{xy}) - \mathrm{k}_f^{xy})}{\beta(\mathrm{k}_j^{xy}) + \mathrm{k}_f^{xy}} + \frac{\delta(\beta(\mathrm{k}_j^{xy}) + \mathrm{k}_f^{xy})}{\beta(\mathrm{k}_j^{xy}) - \mathrm{k}_f^{xy}} \tag{4.52}$$

As the modulus of the wave vector $\mathbf{k}_f^{xy}$ has to be a positive value, only the term $\frac{\delta(\mathrm{k}_j^{xy}) - \mathrm{k}_f^{xy})}{\beta(\mathrm{k}_j^{xy}) + \mathrm{k}_f^{xy}}$ of the δ-function will provide a contribution when:

$$\beta(\mathrm{k}_j^{xy}) = \mathrm{k}_f^{xy}$$

then, the expression for the energy conservation within the equation (4.46) can be replaced as follows:

$$\begin{aligned} \delta(E_F^{total} - E_I^{total}) &= \frac{2m_s}{\hbar^2}\delta\left(\mathrm{k}_f^{xy2} - \frac{m_s}{m_c}\mathrm{k}_j^{xy2} + \Delta\right) \\ &= \frac{2m_s}{\hbar^2}\frac{\delta(\beta(\mathrm{k}_j^{xy}) - \mathrm{k}_f^{xy})}{\beta(\mathrm{k}_j^{xy}) + \mathrm{k}_f^{xy}} \end{aligned} \tag{4.53}$$

We will make use of this expression for the δ-function in (4.46) further on in our calculations.

Returning to the Eq. (4.46) and converting the summation over wave vectors $\mathbf{k}_f^{xy}$ and $\mathbf{k}_j^{xy}$ into integrals as we have previously done in Eq. 4.36, thus introducing a factor of $(\frac{L}{2\pi})^4$ we obtain:

$$\begin{aligned} \frac{1}{\tau_g} &= \frac{2\pi}{\hbar}\left(\frac{L}{2\pi}\right)^4 \iint d\mathrm{k}_j^{xy} d\mathrm{k}_f^{xy} \left| \frac{\mathrm{e}^2}{2A\epsilon\pi^2} \int_{-\infty}^{\infty} d\mathrm{k}_z G_z(\mathrm{k}_z) \int d\mathrm{k}_{xy} \frac{G(\mathrm{k}_j^{xy}, \mathrm{k}_f^{xy}, \mathbf{k}_{xy})}{k_z^2 + k_{xy}^2 + k_{\mathrm{D}}^2} \right|^2 \\ &\quad \times \delta(E_F^{total} - E_I^{total}) \end{aligned} \tag{4.54}$$

or

$$\begin{aligned} \frac{1}{\tau_g} &= \Gamma \iint d\mathrm{k}_j^{xy} d\mathrm{k}_f^{xy} \left| \int_{-\infty}^{\infty} d\mathrm{k}_z G_z(\mathrm{k}_z) \int d\mathrm{k}_{xy} \frac{G(\mathrm{k}_j^{xy}, \mathrm{k}_f^{xy}, \mathbf{k}_{xy})}{k_z^2 + k_{xy}^2 + k_{\mathrm{D}}^2} \right|^2 \\ &\quad \times \delta(E_F^{total} - E_I^{total}) \end{aligned} \tag{4.55}$$

where $\Gamma = \frac{e^4}{32\hbar\pi^7\epsilon^2}$

Changing the two-dimensional integrals over the Cartesian in-plane carrier wave vectors $\mathbf{k}_j^{xy}$, $\mathbf{k}_f^{xy}$ and $\mathbf{k}_{xy}$ into polar coordinates, with radii the modulus-es k_j^{xy}, k_f^{xy} and k_{xy} along with angles α_j, α_f, α_{xy} respectively as well as introducing the expression calculated in (4.53) for the conservation of the energy, the previous equation may be written as follows:

$$\begin{aligned}\frac{1}{\tau_g} &= \Gamma\int_0^{2\pi} d\alpha_j \int_0^{2\pi} d\alpha_f \int_0^{\infty} d\mathrm{k}_j^{xy}\mathrm{k}_j^{xy} \int_0^{\infty} d\mathrm{k}_f^{xy}\mathrm{k}_f^{xy} \\ &\times\left|\int_{-\infty}^{\infty} d\mathrm{k}_z G_z(\mathrm{k}_z)\int_0^{2\pi} d\alpha_{xy}\int_0^{\infty} d\mathrm{k}_{xy}\mathrm{k}_{xy}\frac{G(\mathrm{k}_j^{xy},\mathrm{k}_f^{xy},\mathrm{k}_{xy},\alpha_j,\alpha_f,\alpha_{xy})}{k_z^2+k_{xy}^2+k_{\mathrm{D}}^2}\right|^2 \\ &\times\frac{2m_s}{\hbar^2}\frac{\delta(\beta(\mathrm{k}_j^{xy})-\mathrm{k}_f^{xy})}{\beta(\mathrm{k}_j^{xy})+\mathrm{k}_f^{xy}}\end{aligned} \tag{4.56}$$

As we have explained in the scattering captured rate type I, carriers within a QW sub-band are distributed as a 2D gas and hence, they follow a 2D Fermi-Dirac [8] distribution.

$$f_D(\epsilon) = \frac{1}{e^{\frac{\epsilon-\mu}{KT}}+1} \tag{4.57}$$

where (see appendix B)

$$e^{\frac{\mu}{KT}} = e^{\frac{\pi\hbar^2 N}{mKT}} - 1 \tag{4.58}$$

and N is the carrier density within the wetting layer.

Hence, assuming a thermal equilibrium, Fermi-Dirac distribution function can be included in Eq. 4.56 as follows:

$$\begin{aligned}\frac{1}{\tau_g} &= \Gamma\int_0^{2\pi} d\alpha_j \int_0^{2\pi} d\alpha_f \int_0^{\infty} d\mathrm{k}_j^{xy}\mathrm{k}_j^{xy}\mathrm{f}_j^{FD}(\mathrm{k}_j^{xy}) \int_0^{\infty} d\mathrm{k}_f^{xy}\mathrm{k}_f^{xy}(1-\mathrm{f}_f^{FD}(\mathrm{k}_f^{xy})) \\ &\times\left|\int_{-\infty}^{\infty} d\mathrm{k}_z G_z(\mathrm{k}_z)\int_0^{2\pi} d\alpha_{xy}\int_0^{\infty} d\mathrm{k}_{xy}\mathrm{k}_{xy}\frac{G(\mathrm{k}_j^{xy},\mathrm{k}_f^{xy},\mathrm{k}_{xy},\alpha_j,\alpha_f,\alpha_{xy})}{k_z^2+k_{xy}^2+k_{\mathrm{D}}^2}\right|^2 \\ &\times\frac{2m_s}{\hbar^2}\frac{\delta(\beta(\mathrm{k}_j^{xy})-\mathrm{k}_f^{xy})}{\beta(\mathrm{k}_j^{xy})+\mathrm{k}_f^{xy}}\end{aligned} \tag{4.59}$$

Taking into account the δ-function only gives contribution to the integral over the modulus of the in-plane wave vector $\mathbf{k}_f^{xy}$ when:

$$\beta(\mathrm{k}_j^{xy}) = \mathrm{k}_f^{xy} = \sqrt{\frac{m_s}{m_c}\mathrm{k}_j^{xy2} - \Delta} \tag{4.60}$$

with Δ taken from equation 4.48. We can finally give an equation to calculate the probability of finding a 2D carrier captured by the SAD due to Coulomb interaction with a previously captured 0D carrier, which is excited from the SAD into the wetting layer, may be given by:

$$\begin{aligned}\frac{1}{\tau_g} &= \frac{m_s}{\hbar^2}\Gamma\int_0^{2\pi}\mathrm{d}\alpha_j\int_0^{2\pi}\mathrm{d}\alpha_f\int_0^{\infty}\mathrm{dk}_j^{xy}\mathrm{k}_j^{xy}\mathrm{f}_j^{FD}(\mathrm{k}_j^{xy})(1-\mathrm{f}_f^{FD}(\mathrm{k}_j^{xy}))\\ &\times\left|\int_{-\infty}^{\infty}\mathrm{dk}_z G_z(\mathrm{k}_z)\int_0^{2\pi}\mathrm{d}\alpha_{xy}\int_0^{\infty}\mathrm{dk}_{xy}\mathrm{k}_{xy}\frac{G(\mathrm{k}_j^{xy},\mathrm{k}_{xy},\alpha_j,\alpha_f,\alpha_{xy})}{k_z^2+k_{xy}^2+k_{\mathrm{D}}^2}\right|^2\end{aligned} \tag{4.61}$$

4.3.1 Numerical Implementation

In order to resolve numerically the equation above, we rearrange and group the terms in the equation as follows:

$$\begin{aligned}\frac{1}{\tau_g} &= \frac{m_s}{\hbar^2}\Gamma\int_0^{\infty}\mathrm{dk}_j^{xy}\mathrm{k}_j^{xy}\mathrm{f}_j^{FD}(\mathrm{k}_j^{xy})(1-\mathrm{f}_f^{FD}(\mathrm{k}_j^{xy}))\int_0^{2\pi}\mathrm{d}\alpha_j\int_0^{2\pi}\mathrm{d}\alpha_f\\ &\left|\int_0^{2\pi}\mathrm{d}\alpha_{xy}\int_0^{\infty}\mathrm{dk}_{xy}\mathrm{k}_{xy}G(\mathrm{k}_j^{xy},\mathrm{k}_{xy},\alpha_j,\alpha_f,\alpha_{xy})\underbrace{\int_{-\infty}^{\infty}\mathrm{dk}_z\frac{G_z(\mathrm{k}_z)}{k_z^2+k_{xy}^2+k_{\mathrm{D}}^2}}_{f_z(\mathrm{k}_{xy})}\right|^2\end{aligned} \tag{4.62}$$

We first resolve the integral represented by the function $f_z(\mathrm{k}_{xy})$ on the equation above as:

$$f_z(\mathrm{k}_{xy}) = \int_{-\infty}^{\infty}\mathrm{dk}_z\frac{G_z(\mathrm{k}_z)}{k_z^2+k_{xy}^2+k_{\mathrm{D}}^2} \tag{4.63}$$

In order to solve the equation (4.63) and hence, equation 4.62 it is necessary to first calculate the form factors $G_z(\mathrm{k}_z)$ (see Eq. 4.44) which is dependent on the z-component of the wave vector $\mathbf{k} = (\mathbf{k}_{xy}, \mathrm{k}_z)$.

Numerical Implementation of the Form Factor $G_z(\mathrm{k}_z)$

To solve equation 4.44 we consider an integration range, $L = 32 \times h$ where $h = 50\text{Å}$ is the height of the dot. Equation (4.44) may be expressed as

$$\begin{aligned} G_z(\mathrm{k}_z) &= G_{if}(\mathrm{k}_z)G_{jg}(\mathrm{k}_z) \\ &= \int_{-\frac{L}{2}}^{+\frac{L}{2}} \mathrm{d}z\psi_f^{\mathrm{W}}(z)^*\psi_i^{\mathrm{D}}(z)e^{i\mathrm{k}_z z} \\ &\times \int_{-\frac{L}{2}}^{+\frac{L}{2}} \mathrm{d}z'\psi_g^{\mathrm{D}}(z')^*\psi_j^{\mathrm{W}}(z')e^{-i\mathrm{k}_{z'} z'} \end{aligned} \tag{4.64}$$

To perform the integral above, we need to solve two integrals of the form

$$g_z(\mathrm{k}_z) = \textstyle\int_{-\frac{L}{2}}^{+\frac{L}{2}} \mathrm{d}zf(z)e^{-i\mathrm{k}_z z} \tag{4.65}$$

where $f(z) = \psi_f^{\mathrm{W}}(z)^*\psi_i^{\mathrm{D}}(z)$ when solving $G_{if}(\mathrm{k}_z)$ and $f(z) = \psi_g^{\mathrm{D}}(z')^*\psi_j^{\mathrm{W}}(z')$ for $G_{jg}(\mathrm{k}_z)$. In order to implement the code to calculate the equation 4.65, we define a z variable to store the different values (we have considered a set of $n = 2^8$ points) to represent the z-axis within a range $\left[-\frac{z_{max}}{2}, \frac{z_{max}}{2}\right]$ for a separation between the points of $\Delta z = \frac{\frac{z_{max}}{2} + \frac{z_{max}}{2}}{n}$ (see picture 4.12). Hence, each of the points which form the z-axis may be implemented following the equation

$$z_i = -\frac{z_{max}}{2} + \Delta z(i-1) \tag{4.66}$$

for $i = 1, .., n$ and $n = 2^7$ the number of points considered. In order to construct a variable to store a set of values for the implementation of the z-component of the wave vector in equation 4.65, we have followed a similar approach as the one explained above for the z-axis, taking into account that $\mathrm{k}_{z_{max}} \propto \frac{1}{L_z}$. We use an interval of:

$$\left[-\mathrm{k}_{z_{max}}, \mathrm{k}_{z_{max}}\right] = \left[-10^9, 10^9\right] \tag{4.67}$$

taking $n_{k_z} = 2^8$ points, in order to obtain a numerically accurate representation for k_z. Taking into account that $f_z(\mathrm{k}_{xy}) \propto \frac{1}{\mathrm{k}_z^2}$ in (4.63), we calculate each value of k_z

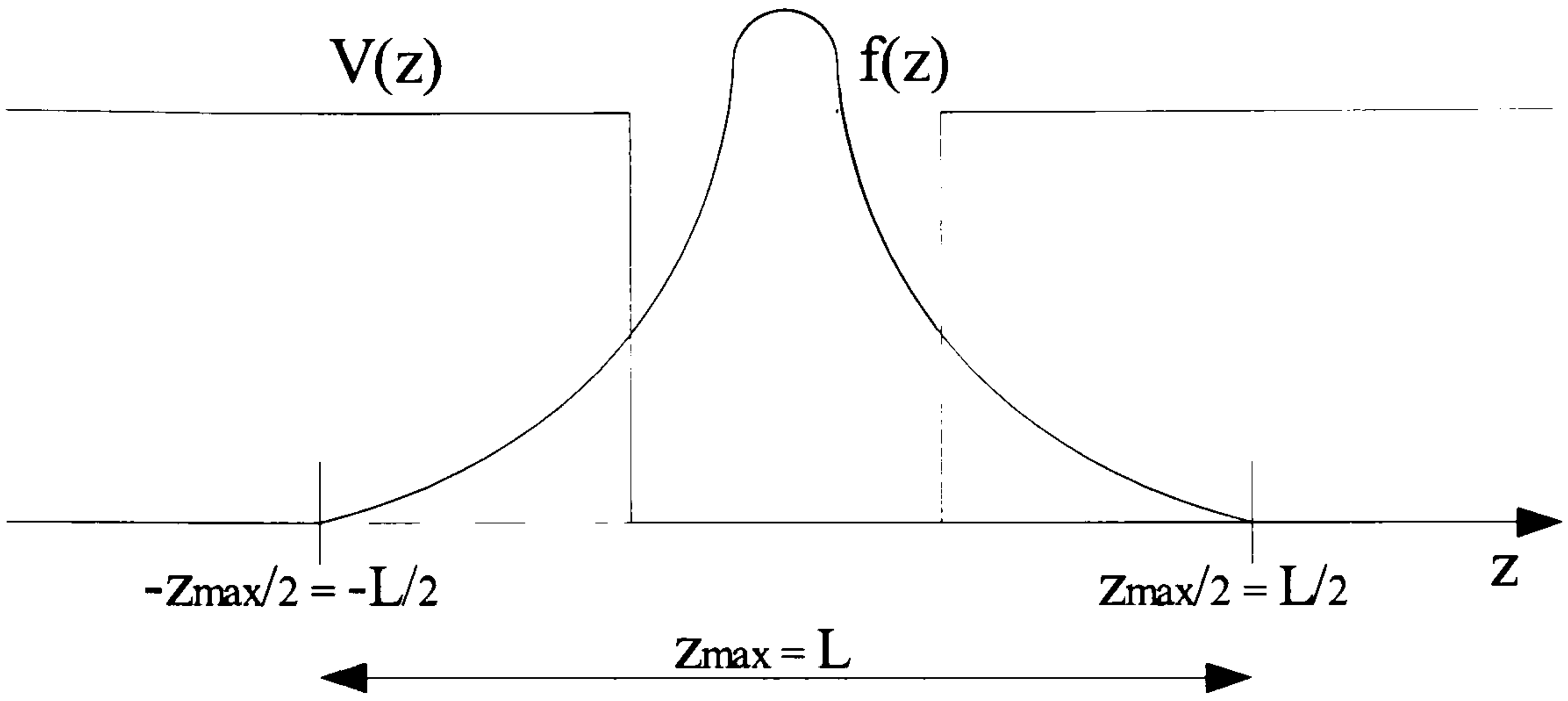

Figure 4.12: A function with a similar shape to the ones included in the calculation of the form factor $g_z(\mathrm{k}_z)$.

parabolically as follows:

$$\mathrm{k}_{zi} = 2\mathrm{k}_{zmax}\frac{2i - n_{k_z} - 1}{2(n_{k_z} - 1)} abs\left[\frac{2i - n_{k_z} - 1}{2(n_{k_z} - 1)}\right] \tag{4.68}$$

Once we have established a set of values to represent k_z and z, we can calculate the integral in Eq. 4.65

$$g_z(\mathrm{k}_{zi}) = \int_{-\frac{L}{2}}^{+\frac{L}{2}} \mathrm{d}z f(z) e^{-i\mathrm{k}_{zi}z} = \int_{-\frac{L}{2}}^{+\frac{L}{2}} \mathrm{d}z f(z)(\cos(\mathrm{k}_{zi}z) - i\sin(\mathrm{k}_{zi}z)) \tag{4.69}$$

for each value k_{zi} from Eq. 4.68. We calculate the integral along the z-axis constructed following (4.66) making use of the trapezoidal rule method [7] considering a number of partitions equal to the total number of points assumed for the representation of the z-axis, hence, 2^8 partitions.

Numerical Implementation of the Form Factor $G(\mathbf{k}_j^{xy}, \mathbf{k}_f^{xy}, \mathbf{k}_{xy})$

In order to calculate the form factor $G(\mathbf{k}_j^{xy}, \mathbf{k}_f^{xy}, \mathbf{k}_{xy})$ in Eq. 4.45, we calculate each of the terms $G_g(\mathbf{k}_j^{xy}, \mathbf{k}_{xy})$ and $G_i(\mathbf{k}_f^{xy}, \mathbf{k}_{xy})$ in (4.45) separately. The same procedure is used to calculate both functions $G_g(\mathbf{k}_j^{xy},\mathbf{k}_{xy})$ and $G_i(\mathbf{k}_f^{xy},\mathbf{k}_{xy})$, so we will only described the procedure to calculate one of them, e.g. $G_i(\mathbf{k}_f^{xy},\mathbf{k}_{xy})$. We can rewrite the form factor $G_i(\mathbf{k}_f^{xy},\mathbf{k}_{xy})$ in (4.45) as follows:

$$G_i(\mathbf{p}) \;=\; \int \mathrm{d}\mathbf{r}_{xy}\psi_i^{\mathrm{D}}(\mathbf{r}_{xy})e^{i\mathbf{p}\mathbf{r}_{xy}} \tag{4.70}$$

where $\mathbf{p} = \mathbf{k}_f^{xy} + \mathbf{k}_{xy}$. Separating the above integral into one along the x-axis and another one along the y-axis, gives:

$$G_i(\mathrm{p}_x,\mathrm{p}_y) \;=\; \int_{-L_x}^{L_x} \mathrm{d}x\, e^{i\mathrm{p}_x x} \int_{-L_y}^{L_y} \mathrm{d}y\, \psi_i^{\mathrm{D}}(x,y)e^{i\mathrm{p}_y y} \tag{4.71}$$

for $\mathbf{p} = (\mathrm{p}_x,\mathrm{p}_y)$, $\mathbf{r}_{xy} = (x,y)$ and $\psi_i^{\mathrm{D}}(x,y)$ represents the radial component of the carrier in the discrete state $|i\rangle$ within the quantum dot (see Eq. 4.29) written in Cartesian coordinates. We have previously calculated the wavefunction associated with the Schrödinger equation in cylindrical coordinates, $\psi^{\mathrm{D}}(\mathrm{r}_{xy})$, so we may calculate the wavefunction of the carrier within the discrete state $|i\rangle$ inside the dot in Cartesian coordinates as follows:

$$\psi_i^{\mathrm{D}}(x,y) = \psi_i^{\mathrm{D}}(\mathrm{r}_{xy})\frac{e^{im\theta}}{\sqrt{2\pi}} \tag{4.72}$$

for $m = 0,1,2...$, $\theta = \arctan\left(\frac{y}{x}\right)$ and r_{xy} the polar variable ρ in (4.29) which satisfies the equation $\mathrm{r}_{xy} = \sqrt{x^2+y^2}$.

In order to solve equation 4.71, and hence the integral along the $\mathbf{k}_{xy}$ vector in (4.62), we need to determine the upper and lower limits for the integrals along the x and y-axis. Taking into account that we have previously implemented the wavefunction of a carrier within the quantum dot along the radial coordinate r_{xy} (see section 4.2) with $n_\rho = 2^8$ number of considered samples and within an interval $[-2R, 2R]$ for $R = 150$ Å the dot radius (see Fig. 4.13). As figure 4.13 shows, for values of the Cartesian coordinates x, y that $\sqrt{x^2+y^2} > 2R$ (pictured in blue color in Fig. 4.13), the wavefunction $\psi_i^{\mathrm{D}}(x,y)$ is assumed to be zero. Once we have set up the intervals to represent the Cartesian coordinates x and y, hence, $[-L_x = -2R, L_x = 2R]$ and $[-L_y = -2R, L_y = 2R]$ respectively, we need to define the wave vector $\mathbf{p}$

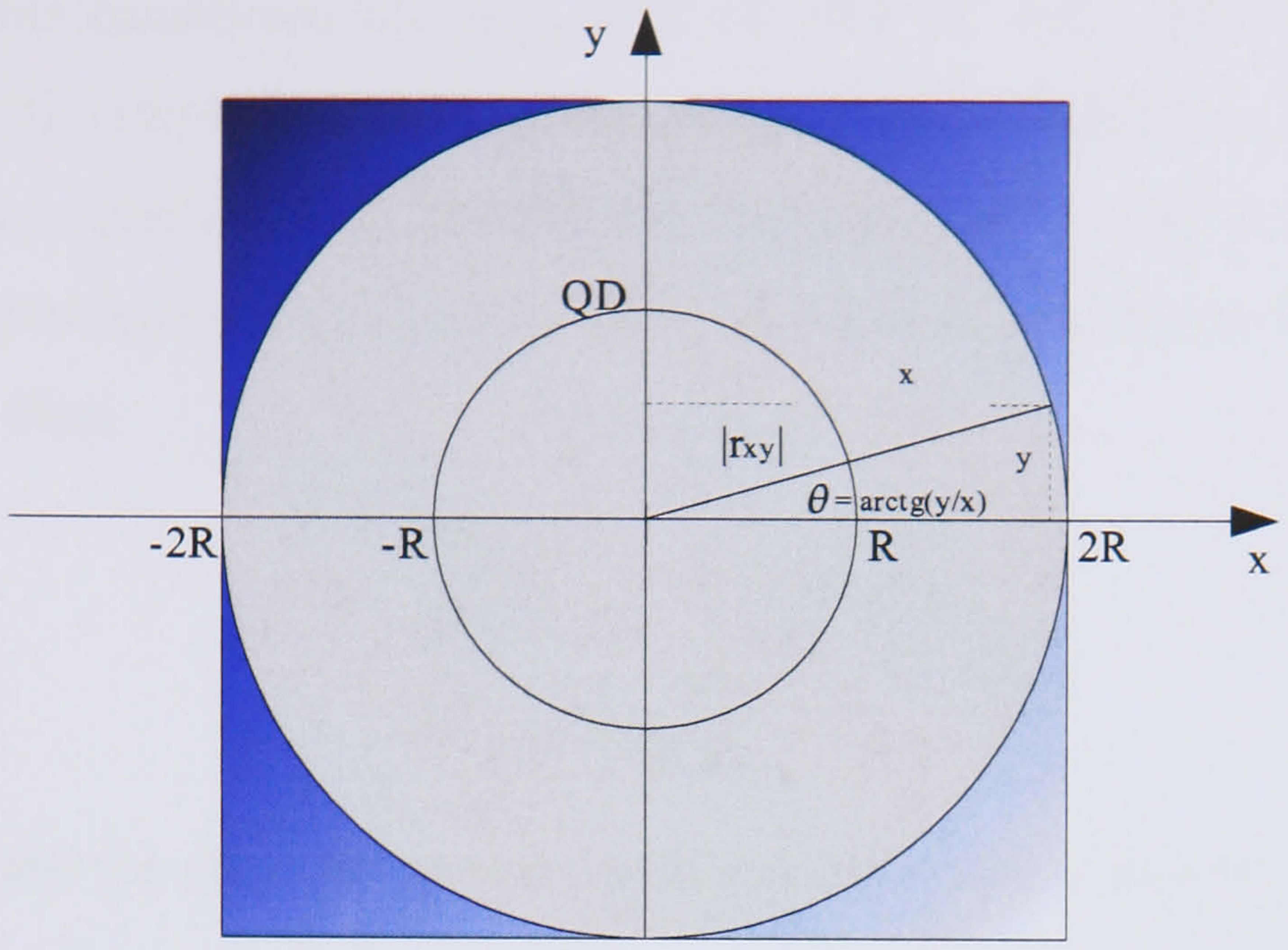

Figure 4.13: Representation of the quantum dot in the Cartesian Plane.

from Eq. 4.70. In order to determine two variables to store a set of values for the implementation of the x and y components of the wave vector $\mathbf{p}$ in 4.70, we have completed a similar approach as the one explained above for the calculation of the form factor $G_z(\mathrm{k}_z)$. To establish the upper and lower limits for the intervals where each of the components of $\mathbf{p}$, i.e., p_x, p_y is going to be defined, we have taken into account that $\mathbf{p} = \mathbf{k}_f^{xy} + \mathbf{k}_{xy}$ (Eq. 4.70) and consider equal maximum and minimum limits for p_x and p_y to be $\mathrm{p}_{x_{max}} = \mathrm{p}_{y_{max}} = 2\mathrm{k}_{j\ max}^{xy}$. In order to estimate a maximum value for the modulus of in-plane wave vector for a carrier in $|j\rangle$ state (see Fig. 4.2) $\mathrm{k}_{j\ max}^{xy}$, we observe that the wetting layer Fermi-Dirac distribution (plotted in figure 4.14) is zero for energy values greater than 0.2 eV. As a consequence, in order to implement the integrals for the calculation of the form factor $G_i(\mathbf{p})$ (Eq. 4.71) as well as for the calculation of equation 4.62, we have considered that:

$$\mathrm{k}_{j\ max}^{xy} = \mathrm{k}_{xy_{max}} = \frac{\sqrt{2m_s E_{max}}}{\hbar} \tag{4.73}$$

where the value considered for E_{max} is 1 eV (0.2 eV ×5). The minimum value considered for the implementation of the wave vector modulus, i.e., ${\rm k}_{j\ min}^{xy}$ has been calculated from equation 4.51. Because the function $\beta({\rm k}_j^{xy}) = {\rm k}_f^{xy}$ has to be positive and real, we determine the minimum value in order to implement the wave vector modulus ${\rm k}_j^{xy}$, then

$$\begin{aligned} \frac{m_s}{m_c}{\rm k}_j^{xy2} - \Delta \geq 0 \\ {\rm k}_{j\ min}^{xy} = \sqrt{\frac{m_c}{m_s}\Delta} \end{aligned} \tag{4.74}$$

where m_c,m_s are the effective masses of the captured and scattered carriers respectively and Δ is given by equation 4.48.

Taking account of the equation 4.73 and of the fact that $\mathbf{p} = \mathbf{k}_f^{xy} + \mathbf{k}_{xy}$ (4.70), we have considered an interval of

$$[-{\rm p}_{x max}, {\rm p}_{x max}] = \left[-2{\rm k}_{j\ max}^{xy}, 2{\rm k}_{j\ max}^{xy}\right] \tag{4.75}$$

in order to determine a set of values (we have considered $n_{{\rm p}_x} = n_{{\rm p}_y} = n_\rho = 2^8$ values) for the implementation of the wave x-component of the vector $\mathbf{p}$ and another interval $[-{\rm p}_{y max} = -2{\rm k}_{j\ max}^{xy}, {\rm p}_{y max} = 2{\rm k}_{j\ max}^{xy}]$ for the implementation of the y-component of the wave vector in order to calculate the integrals in Eq. 4.71. In order to make the calculation of the form factor in (4.71) easier, we have calculated each integral in (4.71) for positive values of the ${\rm p}_x$, ${\rm p}_y$, each value, ${\rm p}_{xi}$, ${\rm p}_{y_i}$ has been calculated as follows:

$${\rm p}_{xi} = \frac{2{\rm p}_{xmax}}{(n_{{\rm p}_x} - 1)}(i-1) \tag{4.76}$$

for $i = 1, ..., n_{{\rm p}_x}$ where $n_{{\rm p}_x} = n_{{\rm p}_y} = 2^8$ as we have previously mentioned.

$${\rm p}_{y_j} = \frac{2{\rm p}_{ymax}}{(n_{{\rm p}_y} - 1)}(j-1) \tag{4.77}$$

for $j = 1, ..., n_{{\rm p}_y}$. Once we have defined the variables to represent the x and y-axis in (4.71), and also each of the components of the wave vector $\mathbf{p}$, i.e., ${\rm p}_x$, ${\rm p}_y$ (see

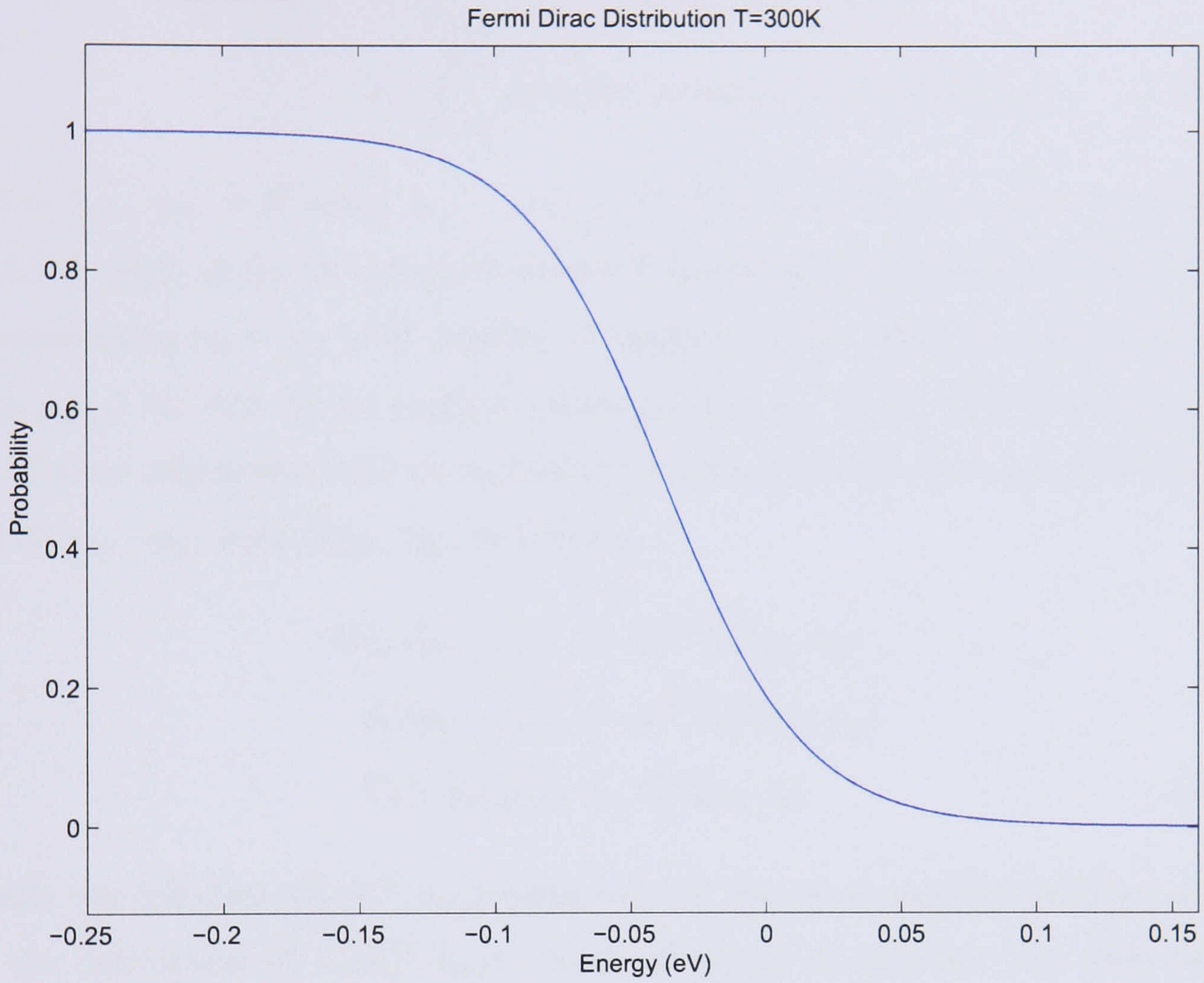

Figure 4.14: Fermi-Dirac distribution for a carrier of mass m_s in the wetting layer at a temperature of 300 K, where $Energy = E - E_F$ eV, for E the electron kinetic energy relative to the conduction band edge.

Eq. 4.76 and Eq. 4.77 above) we can proceed to calculate the form factor in (4.71). The integral in (4.71) may now be solved for each of the positive values p_{x_i} and p_{y_j} given by equations 4.76 and 4.77 as follows:

$$\begin{aligned} G_i(\mathrm{p}_{x_i}, \mathrm{p}_{y_j}) &= \int_{-L_x}^{L_x} \mathrm{d}x\,(\cos(\mathrm{p}_{x_i}x) + i\sin(\mathrm{p}_{x_i}x)) \\ &\times \int_{-L_y}^{L_y} \mathrm{d}y\,\psi_i^{\mathrm{D}}(x,y)(\cos(\mathrm{p}_{y_j}y) + i\sin(\mathrm{p}_{y_j}y)) \end{aligned} \tag{4.78}$$

for $i = 1, ..., n_{\mathrm{p}_x} = 2^8$ and $j = 1, ..., n_{\mathrm{p}_y} = 2^8$. The wave function $\psi_i^{\mathrm{D}}(x,y)$ is given in (4.72). Each of the two integrals is solved following the trapezoidal rule method [7] considering $n_x = n_y = 2^8$ number of sample points. Once we have calculated $G_i(\mathrm{p}_{x_i}, \mathrm{p}_{y_j})$ for each of the positive values p_{x_i} and p_{y_j} (4.76), (4.77) we can make use of some trigonometrical manipulations to calculate $G_i(-\mathrm{p}_x, -\mathrm{p}_y)$, $G_i(-\mathrm{p}_x, \mathrm{p}_y)$ and $G_i(\mathrm{p}_x, -\mathrm{p}_y)$ from $G_i(\mathrm{p}_x, \mathrm{p}_y)$ as follows:

$$\begin{aligned} G_i(-\mathrm{p}_x, -\mathrm{p}_y) &= e^{im\pi} G_i(\mathrm{p}_x, \mathrm{p}_y) \\ G_i(\mathrm{p}_x, -\mathrm{p}_y) &= e^{im\pi} G_i{}^*(\mathrm{p}_x, \mathrm{p}_y) \\ G_i(-\mathrm{p}_x, \mathrm{p}_y) &= G_i{}^*(\mathrm{p}_x, \mathrm{p}_y) \end{aligned} \tag{4.79}$$

Finally we calculate $G_g(\mathbf{k}_j^{xy}, \mathbf{k}_{xy})$ using exactly the same method outlined above for the calculation of $G_i(\mathbf{k}_f^{xy}, \mathbf{k}_{xy})$, which allows us to calculate the form factor $G(\mathbf{k}_j^{xy}, \mathbf{k}_f^{xy}, \mathbf{k}_{xy})$ in (4.62).

Returning to to the calculation of the integral in Eq. 4.63, we proceed with the implementation of the values, $\mathrm{k}^{xy}{}_i$ and $\mathrm{k}_j^{xy}{}_i$ for the modulus of the wave vector $\mathbf{k}_{xy}$ as well as the modulus of the wave vector for the carrier in state $|j\rangle$ (see Fig. 4.2), k_j^{xy} respectively, within an interval $[\mathrm{k}_j^{xy}{}_{min}, \mathrm{k}_j^{xy}{}_{max}]$ (see equations 4.73 and 4.74) as

$$\mathrm{k}_j^{xy}{}_i = \mathrm{k}_j^{xy}{}_{min} + (\mathrm{k}_j^{xy}{}_{max} - \mathrm{k}_j^{xy}{}_{min}) \left[\frac{i-1}{samples-1}\right]^2 \tag{4.80}$$

$$\mathrm{k}_{xy_i} = 0 + \mathrm{k}_{xy_{max}} \left[\frac{i-1}{samples-1}\right]^2 \tag{4.81}$$

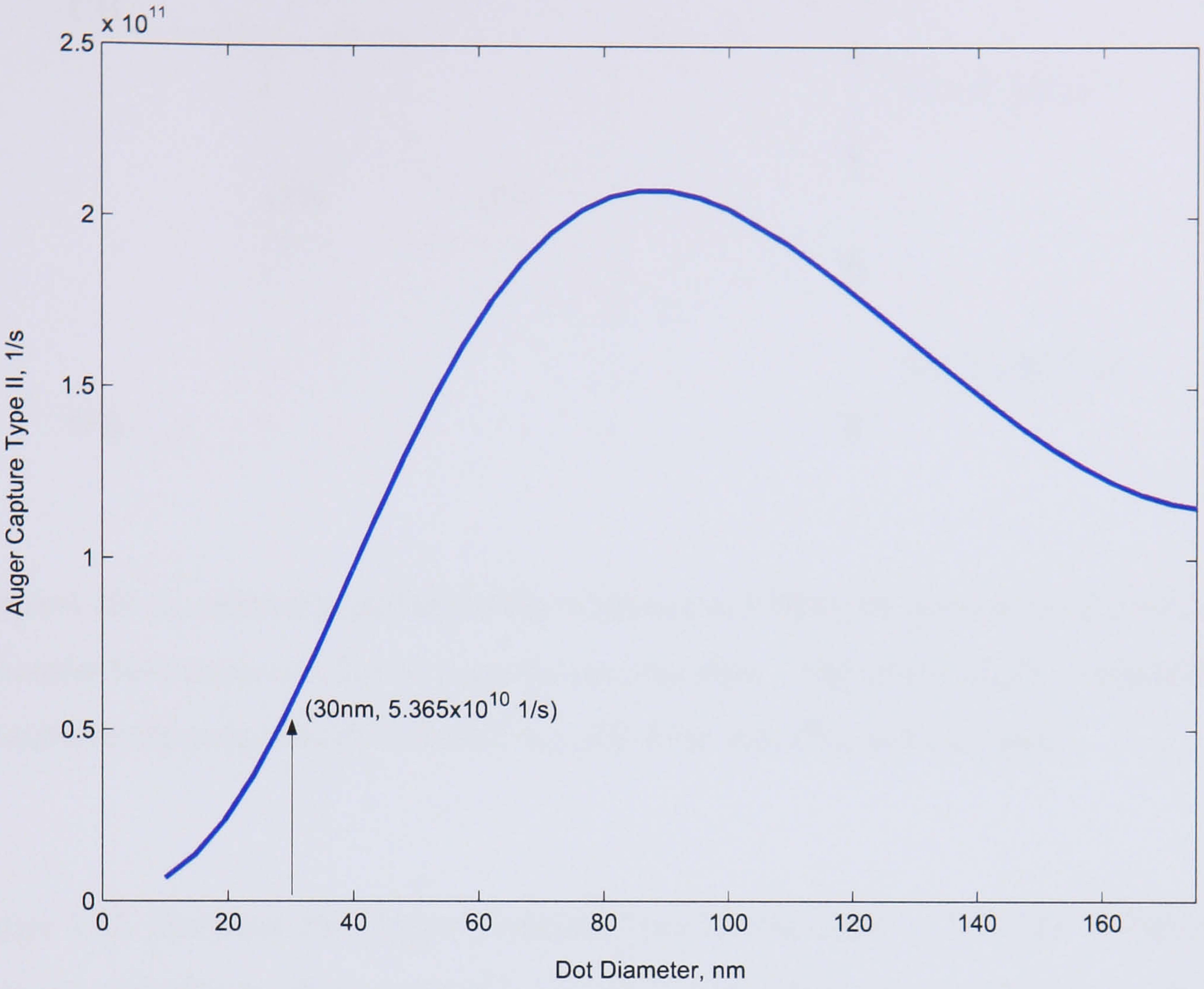

Figure 4.15: Auger Capture Rate type II dependence with dot diameter.

for $i = 1, .., samples = 2^8$. Note that the lower limits for the integration in (4.62) for the modulii k_j^{xy} and k_{xy}, have been taken from zero (the minimum energy value for the subband), and the upper limits for both modulii have calculated from Eq. 4.73. The integrals around the angles α_j, α_f and α_{xy}, have been numerically solved for 2^8 number of partitions. In order to obtain a solution for the capture type II rate (Eq. 4.62), we numerically solve the integrals inside the square modulus in (4.62) for each value of k_j^{xy} (Eq. 4.80), α_j, α_f as previously explained.

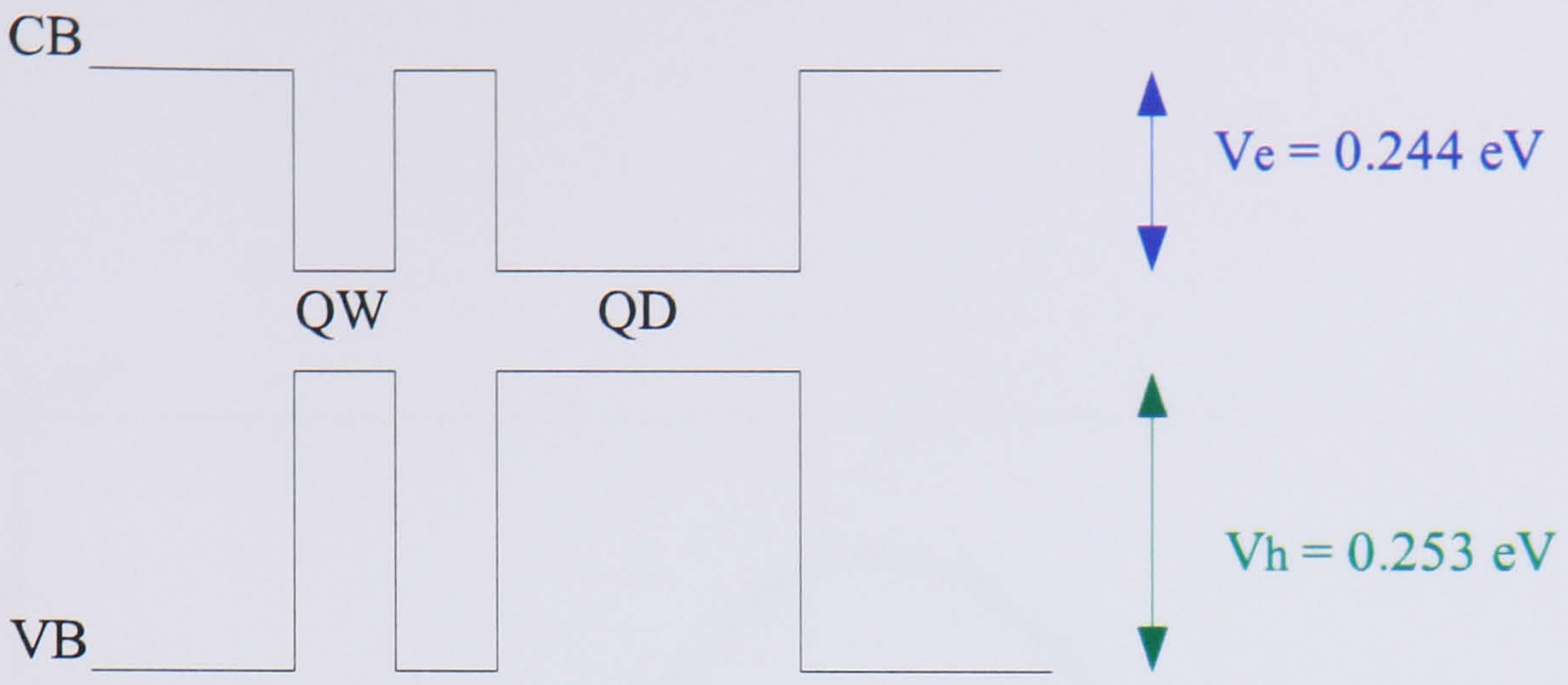

Figure 4.16: A schematic picture of the conduction (CB) and valence band (VB) of a self-assembled quantum dot on top of a wetting layer. The depth of the confinement potential is approximately 244 meV for electrons and 253 meV for holes.

Figure 4.15 describes the Auger Capture type II rate when a $2D$ hole of effective mass $m_h = 0.08 \times m_0$ [5] is captured into the lowest energy level within the quantum dot, due to the Coulomb interaction with a $0D$ electron of effective mass $m_e = 0.0445 \times m_0$ [5], which is itself scattered into the wetting layer. The electron and hole potentials considered for InGaAs quantum dots are shown in figure 4.16.
As a comparison, figure 4.17 shows the results when calculating the Auger Capture type II rate of a $2D$ hole of the same effective mass as previously mentioned, i.e. $m_h = 0.08 \times m_0$ [5], into the lowest energy level of a quantum dot (Fig. 4.16) after scattering with a $0D$ electron of effective mass $m_e = 0.0445 \times m_0$ [5], which is scattered into a $2D$ energy state in the wetting layer, calculated using the formula given by equation 3.20 in chapter 3 for a carrier density of $n_w = 1 \times 10^{15}\text{m}^{-2}$.
For a quantum dot of height $H = 5$ nm and diameter $D = 30$ nm, a much faster scattering rate, i.e., $2.69 \times 10^{13}\text{s}^{-1}$ has been obtained (see Fig. 4.17), comparing to the one given by equation 4.62, i.e. $5.365 \times 10^{10}\text{s}^{-1}$ as can be seen from figure 4.15. In this last figure, the increase of the Auger Capture type II rate with the

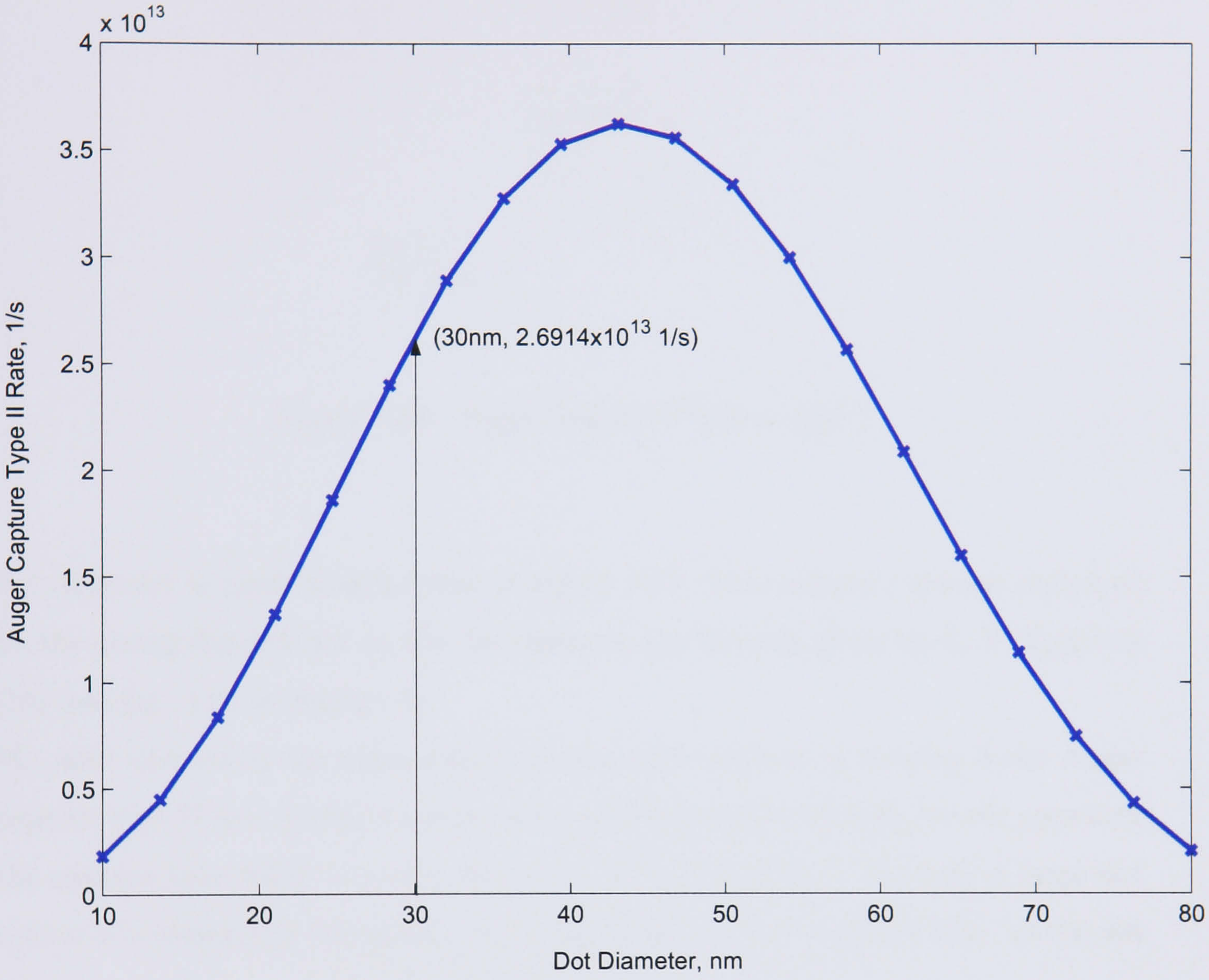

Figure 4.17: Auger Capture Rate type II dependence with dot diameter making use of the formula given by A. V. Uskov in [10].

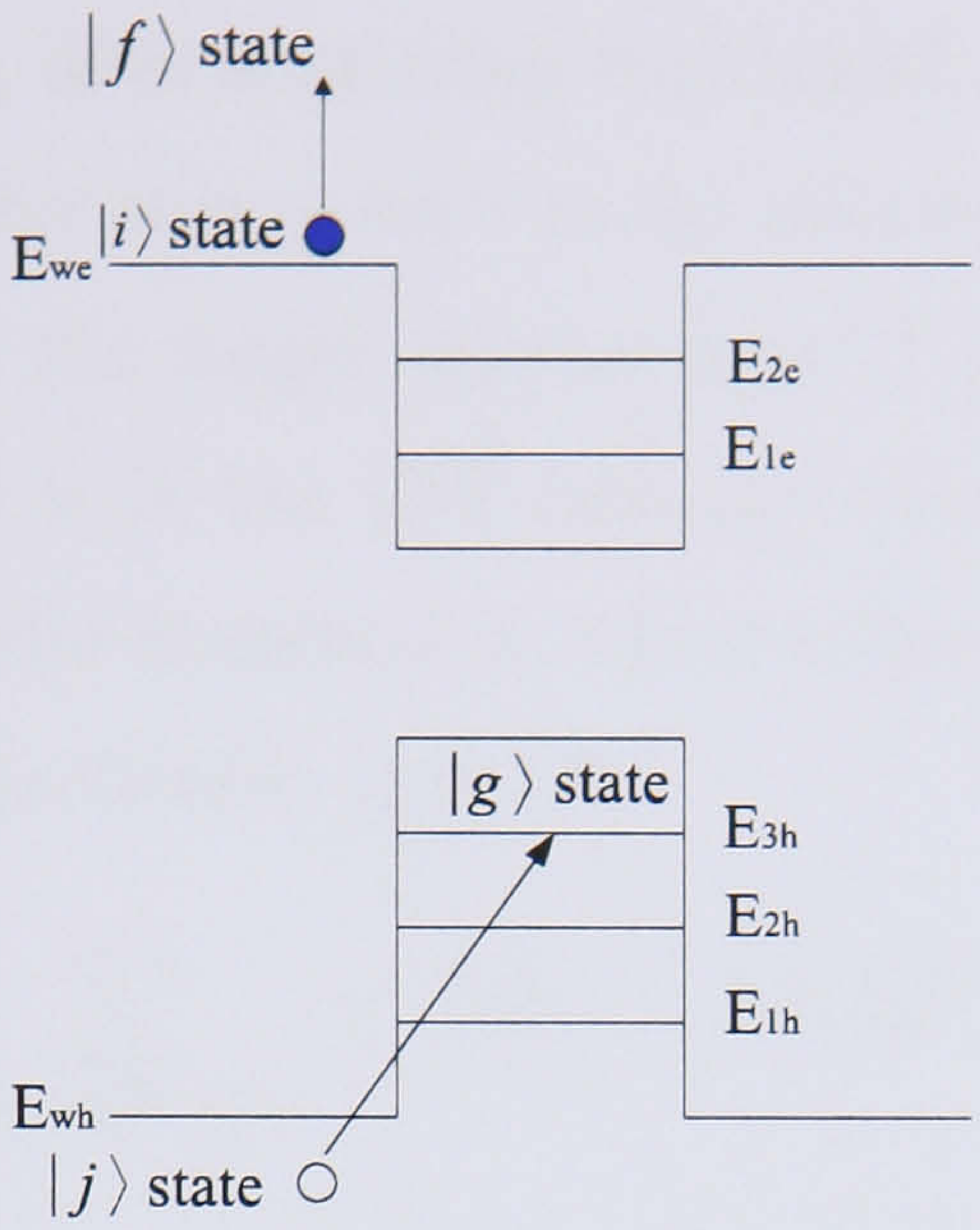

Figure 4.18: Auger Capture Process type I

dot diameter is much slowlier than in figure 4.17. This behavior can be explained by the strong dependence on the dot radius in the formula given by A. V. Uskov in [10] (see Eq. 3.20 in chapter 3).

We note that using the semi-analytical approach outlined in chapter 3 the Auger capture type II rate tends to zero at large values of radius whereas for our approach the capture rate tends to a non-zero value of $1.17 \times 10^{11}\mathrm{s}^{-1}$. For such a large dot radius it is reasonable to expect a non zero tendency of the capture rate, as the dot becomes similar to a quantum well structure.

4.4 Auger capture process type I

In the following section, we describe the procedure to the Auger like capture process, i.e., capture type I. This scattering process (see Fig. 4.18) involves the capture/ejection of a 2D carrier (either an electron or a hole in the wetting layer) by/from the QD structure, after scattering with another 2D carrier which is scattered to another higher/lower energy state in the wetting layer. Following the same procedure as described for the Auger capture type II process, the carrier capture probability from a state $|j>$ in the QW into any other state $|g>$ in the QD by scattering with another carrier in state $|i>$, which is itself scattered into $|f>$ within the QW, is given by Fermi's Golden Rule [3]:

$$\frac{1}{\tau_g} = \frac{2\pi}{\hbar} \sum_{\mathbf{k}_i^{xy},\mathbf{k}_f^{xy},\mathbf{k}_j^{xy}} |< f|\tilde{H}|i >|^2 \delta(E_F^{total} - E_I^{total}) \tag{4.82}$$

where:

- $|i>$ is the product of the initial state of the scattered carrier in the QW $\longrightarrow \psi_i^{\mathrm{W}}(z)\frac{e^{-\mathbf{k}_i^{xy}\mathbf{r}_{xy}}}{\sqrt{A}}$ and the initial state of the captured carrier in the QW $\longrightarrow \psi_j^{\mathrm{W}}(z')\frac{e^{-\mathbf{k}_j^{xy}\mathbf{r}'_{xy}}}{\sqrt{A}}$
- $|f>$ is the product of the final state of the scattered carrier in the QW $\longrightarrow \psi_f^{\mathrm{W}}(z)\frac{e^{-\mathbf{k}_f^{xy}\mathbf{r}_{xy}}}{\sqrt{A}}$ and the final state of the captured carrier in the QD $\longrightarrow$ $\psi_g^{\mathrm{D}}(z')\psi_g^{\mathrm{D}}(\mathbf{r}'_{xy})$
- $\tilde{H}$ is the $3D$ Screened Coulomb interaction given by equation 4.34.

First we will calculate, the matrix element in Fermi's Golden Rule (equation 4.82) introducing the expression calculated for the Screened Coulomb interaction in equation 4.34:

$$\begin{aligned} < f|\tilde{H}|i > \; = \; & \left\langle \Psi_f^{\mathrm{W}}(\mathbf{r},\mathbf{k}_f^{\mathrm{W}})\Psi_g^{\mathrm{D}}(\mathbf{r}',\mathbf{k}_g^{\mathrm{D}}) \left| \frac{4\pi e^2}{\epsilon V} \sum_{\mathbf{k}_{xy},k_z} \frac{e^{i\mathbf{k}_{xy}(\mathbf{r}_{xy}-\mathbf{r}'_{xy})}e^{ik_z(z-z')}}{k_z^2 + k_{xy}^2 + k_{\mathrm{D}}^2} \right| \right. \\ & \left. \Psi_i^{\mathrm{W}}(\mathbf{r},\mathbf{k}_i^{\mathrm{W}})\Psi_j^{\mathrm{W}}(\mathbf{r}',\mathbf{k}_j^{\mathrm{W}}) \right\rangle \end{aligned} \tag{4.83}$$

Introducing the expressions for the carriers' wavefunctions inside the quantum dot (equation 4.27) and well (equation 4.28), we obtain:

$$\begin{aligned} < f|\tilde{H}|i > &= \frac{4\pi e^2}{VA\sqrt{A}\epsilon}\int_{-\infty}^{\infty}\mathrm{d}z\int_{-\infty}^{\infty}\mathrm{d}z'\psi_f^{\mathrm{W}}(z)^*\psi_g^{\mathrm{D}}(z')^*\psi_i^{\mathrm{W}}(z)\psi_j^{\mathrm{W}}(z') \\ &\times \iint \mathrm{d}\mathbf{r}_{xy}\mathrm{d}\mathbf{r}'_{xy}\psi_g^{\mathrm{D}}(\mathbf{r}'_{xy})^* e^{-i\mathbf{k}_j^{xy}\mathbf{r}'_{xy}} e^{i(\mathbf{k}_f^{xy}-\mathbf{k}_i^{xy})\mathbf{r}_{xy}} \\ &\times \sum_{\mathbf{k}_{xy},k_z}\frac{e^{i\mathbf{k}_{xy}(\mathbf{r}_{xy}-\mathbf{r}'_{xy})}e^{ik_z(z-z')}}{k_z^2+k_{xy}^2+k_{\mathrm{D}}^2} \end{aligned} \tag{4.84}$$

The summation over the wave vectors $\mathbf{k}_{xy}$ and k_z can be converted into integrals introducing factors $\frac{A}{(2\pi)^2}$ and $\frac{L}{2\pi}$, respectively, from the density of states, giving:

$$\begin{aligned} < f|\tilde{H}|i > &= \frac{4\pi e^2}{VA\sqrt{A}\epsilon}\frac{A}{(2\pi)^2}\frac{L}{2\pi}\int_{-\infty}^{\infty}\mathrm{d}z\int_{-\infty}^{\infty}\mathrm{d}z'\psi_f^{\mathrm{W}}(z)^*\psi_g^{\mathrm{D}}(z')^*\psi_i^{\mathrm{W}}(z)\psi_j^{\mathrm{W}}(z') \\ &\times \iint \mathrm{d}\mathbf{r}_{xy}\mathrm{d}\mathbf{r}'_{xy}\psi_g^{\mathrm{D}}(\mathbf{r}'_{xy})^* e^{-i\mathbf{k}_j^{xy}\mathbf{r}'_{xy}} e^{i(\mathbf{k}_f^{xy}-\mathbf{k}_i^{xy})\mathbf{r}_{xy}} \\ &\times \int_{-\infty}^{\infty}\mathrm{dk}_z e^{i\mathrm{k}_z(z-z')}\int \mathrm{d}\mathbf{k}_{xy}\frac{e^{i\mathbf{k}_{xy}\mathbf{r}_{xy}}e^{-i\mathbf{k}_{xy}\mathbf{r}'_{xy}}}{k_z^2+k_{xy}^2+k_{\mathrm{D}}^2} \end{aligned} \tag{4.85}$$

Changing the order of the integrals in order to perform the integration over $\mathbf{r}_{xy}$ first, i.e.

$$\begin{aligned} < f|\tilde{H}|i > &= \frac{\mathrm{e}^2}{V\epsilon(2\pi^2)}\int_{-\infty}^{\infty}\mathrm{d}z\int_{-\infty}^{\infty}\mathrm{d}z'\psi_f^{\mathrm{W}}(z)^*\psi_g^{\mathrm{D}}(z')^*\psi_i^{\mathrm{W}}(z)\psi_j^{\mathrm{W}}(z') \\ &\times \int_{-\infty}^{\infty}\mathrm{dk}_z e^{i\mathrm{k}_z(z-z')}\int \mathrm{d}\mathbf{k}_{xy}\frac{1}{k_z^2+k_{xy}^2+k_{\mathrm{D}}^2} \\ &\times \int \mathrm{d}\mathbf{r}'_{xy}\psi_g^{\mathrm{D}}(\mathbf{r}'_{xy})^* e^{-i(\mathbf{k}_j^{xy}+\mathbf{k}_{xy})\mathbf{r}'_{xy}} \\ &\times \int \mathrm{d}\mathbf{r}_{xy} e^{i(\mathbf{k}_{xy}+\mathbf{k}_f^{xy}-\mathbf{k}_i^{xy})\mathbf{r}_{xy}} \end{aligned} \tag{4.86}$$

Converting the integral over the xy plane into a δ-function, thus, introducing a factor of 2π per dimension, then gives:

$$\begin{aligned} < f|\tilde{H}|i > &= \frac{2\mathrm{e}^2}{V\epsilon}\int_{-\infty}^{\infty}\mathrm{d}z\int_{-\infty}^{\infty}\mathrm{d}z'\psi_f^{\mathrm{W}}(z)^*\psi_g^{\mathrm{D}}(z')^*\psi_i^{\mathrm{W}}(z)\psi_j^{\mathrm{W}}(z') \\ &\times \int_{-\infty}^{\infty}\mathrm{dk}_z e^{i\mathrm{k}_z(z-z')}\int \mathrm{d}\mathbf{k}_{xy}\left[\frac{1}{k_z^2+k_{xy}^2+k_{\mathrm{D}}^2}\right. \\ &\times \left.\int \mathrm{d}\mathbf{r}'_{xy}\psi_g^{\mathrm{D}}(\mathbf{r}'_{xy})^* e^{-i(\mathbf{k}_j^{xy}+\mathbf{k}_{xy})\mathbf{r}'_{xy}}\right]\delta(\mathbf{k}_{xy}+\mathbf{k}_f^{xy}-\mathbf{k}_i^{xy}) \end{aligned} \tag{4.87}$$

Performing the integration over $\mathbf{k}_{xy}$, the δ-function then limits the contribution to the point where $\mathbf{k}_{xy}+\mathbf{k}_f^{xy}-\mathbf{k}_i^{xy}=0$, thus, when $\mathbf{k}_{xy}=\mathbf{k}_i^{xy}-\mathbf{k}_f^{xy}$. Making use of this last result:

$$\begin{aligned} <f|\tilde{H}|i> &= \frac{2\mathrm{e}^2}{V\epsilon}\int_{-\infty}^{\infty}\mathrm{d}z\int_{-\infty}^{\infty}\mathrm{d}z'\psi_f^{\mathrm{W}}(z)^*\psi_g^{\mathrm{D}}(z')^*\psi_i^{\mathrm{W}}(z)\psi_j^{\mathrm{W}}(z') \\ &\times \int_{-\infty}^{\infty}\mathrm{dk}_z e^{i\mathrm{k}_z(z-z')}\left[\frac{G_g(\mathbf{k}_j^{xy},\mathbf{k}_i^{xy},\mathbf{k}_f^{xy})}{k_z^2+\left|\mathbf{k}_i^{xy}-\mathbf{k}_f^{xy}\right|^2+k_{\mathrm{D}}^2}\right] \end{aligned} \tag{4.88}$$

where the *form factor* $G_g(\mathbf{k}_j^{xy},\mathbf{k}_i^{xy},\mathbf{k}_f^{xy})$ is given by:

$$\begin{aligned} G_g(\mathbf{k}_j^{xy},\mathbf{k}_i^{xy},\mathbf{k}_f^{xy}) &= G_g(\mathbf{k}_j^{xy}+\mathbf{k}_i^{xy}-\mathbf{k}_f^{xy}) \\ &= \int \mathrm{d}\mathbf{r}'_{xy}\psi_g^{\mathrm{D}}(\mathbf{r}'_{xy})^* e^{-i(\mathbf{k}_j^{xy}+\mathbf{k}_i^{xy}-\mathbf{k}_f^{xy})\mathbf{r}'_{xy}} \end{aligned} \tag{4.89}$$

Changing the order of the integrations, i.e.

$$\begin{aligned} <f|\tilde{H}|i> &= \frac{2\mathrm{e}^2}{V\epsilon}G_g(\mathbf{k}_j^{xy},\mathbf{k}_i^{xy},\mathbf{k}_f^{xy})\int_{-\infty}^{\infty}\mathrm{dk}_z\frac{1}{k_z^2+\left|\mathbf{k}_i^{xy}-\mathbf{k}_f^{xy}\right|^2+k_{\mathrm{D}}^2} \\ &\times \int_{-\infty}^{\infty}\mathrm{d}z'\psi_g^{\mathrm{D}}(z')^*\psi_j^{\mathrm{W}}(z')e^{-i\mathrm{k}_z z'} \\ &\times \int_{-\infty}^{\infty}\mathrm{d}z\psi_i^{\mathrm{W}}(z)\psi_f^{\mathrm{W}}(z)^* e^{i\mathrm{k}_z z} \end{aligned} \tag{4.90}$$

we can finally write an expression for the matrix element in this scattering process, i.e.

$$<f|\tilde{H}|i>=\frac{2\mathrm{e}^2}{V\epsilon}G_g(\mathbf{k}_j^{xy},\mathbf{k}_i^{xy},\mathbf{k}_f^{xy})\int_{-\infty}^{\infty}\mathrm{dk}_z\frac{G_{jg}(\mathrm{k}_z)G_{if}(-\mathrm{k}_z)}{k_z^2+\left|\mathbf{k}_i^{xy}-\mathbf{k}_f^{xy}\right|^2+k_{\mathrm{D}}^2} \tag{4.91}$$

where $G_{jg}(\mathrm{k}_z)$ and $G_{if}(-\mathrm{k}_z)$ are the form factors given by:

$$G_{jg}(\mathrm{k}_z)=\int_{-\infty}^{\infty}\mathrm{d}z'\psi_g^{\mathrm{D}}(z')^*\psi_j^{\mathrm{W}}(z')e^{-i\mathrm{k}_z z'}$$

$$G_{if}(-\mathrm{k}_z)=\int_{-\infty}^{\infty}\mathrm{d}z\psi_i^{\mathrm{W}}(z)\psi_f^{\mathrm{W}}(z)^* e^{i\mathrm{k}_z z}$$

Including the form factors into the calculation of the matrix element, into Fermi's

Golden Rule(equation 4.82), we obtain the probability of having a captured carrier in a particular state(i.e., g state) inside the quantum dot, after scattering with another carrier, in whichever i state in the quantum well; which is itself scattered to any other f state within the same quantum well, gives:

$$\begin{aligned}\frac{1}{\tau_g} &= \frac{2\pi}{\hbar}\sum_{\mathrm{k}_i^{xy},\mathrm{k}_f^{xy},\mathrm{k}_j^{xy}}\left|\frac{2\mathrm{e}^2}{V\epsilon}G_g(\mathrm{k}_j^{xy},\mathrm{k}_i^{xy},\mathrm{k}_f^{xy})\int_{-\infty}^{\infty}\mathrm{dk}_z\frac{G_{jg}(\mathrm{k}_z)G_{if}(-\mathrm{k}_z)}{k_z^2+\left|\mathrm{k}_i^{xy}-\mathrm{k}_f^{xy}\right|^2+k_\mathrm{D}^2}\right|^2 \\ &\times\ \delta(E_F^{total}-E_I^{total}) \qquad (4.92)\end{aligned}$$

where the δ-function represents the conservation of the energy,

$$\begin{aligned}\delta(E_F^{total}-E_I^{total}) &= \delta\Big(\mathrm{E}_f^z+\frac{\hbar^2}{2m_s}\mathrm{k}_f^{xy2}+\epsilon^{DOT}-\big[\mathrm{E}_i^z+\frac{\hbar^2}{2m_s}\mathrm{k}_i^{xy2} \\ &\quad +\mathrm{E}_j^z+\frac{\hbar^2}{2m_c}\mathrm{k}_j^{xy2}\big]\Big) \qquad (4.93)\end{aligned}$$

where $\epsilon^{DOT}=\mathrm{E}_g^z+\frac{\hbar^2}{2m_c}\mathrm{k}_g^{xy2}$.

Rearranging the terms in a suitable way and defining a constant Δ as follows:

$$\Delta=\frac{2m_s}{\hbar^2}\left[\epsilon^{DOT}-\mathrm{E}_j^z\right] \qquad (4.94)$$

then the equation (4.93) becomes:

$$\begin{aligned}\delta(E_F^{total}-E_I^{total}) &= \delta\big(\frac{\hbar^2}{2m_s}\left[\mathrm{k}_f^{xy2}-\mathrm{k}_i^{xy2}-\mathrm{k}_j^{xy2}+\Delta\right]\big) \\ &= \frac{2m_s}{\hbar^2}\delta\big(\mathrm{k}_f^{xy2}-\mathrm{k}_i^{xy2}-\frac{m_s}{m_c}\mathrm{k}_j^{xy2}+\Delta\big) \qquad (4.95)\end{aligned}$$

Again, we will make use of this last result, further in the derivation, in order to reduce the size of the expressions.

Returning to the equation (4.92) and converting the summation over wave vectors k_i^{xy}, k_j^{xy}, k_f^{xy} into integrals, introduces a factor of $\frac{L}{2\pi}$ per dimension, consequently, a factor of $(\frac{L}{2\pi})^6$ needs to be included in this equation, thus:

$$\begin{aligned}\frac{1}{\tau_g} &= \frac{2\pi}{\hbar}(\frac{L}{2\pi})^6\iiint \mathrm{dk}_i^{xy}\mathrm{dk}_j^{xy}\mathrm{dk}_f^{xy} \\ &\times\left|\frac{2\mathrm{e}^2}{V\epsilon}G_g(\mathrm{k}_j^{xy},\mathrm{k}_i^{xy},\mathrm{k}_f^{xy})\int_{-\infty}^{\infty}\mathrm{dk}_z\frac{G_{jg}(\mathrm{k}_z)G_{if}(\mathrm{k}_z)}{k_z^2+\left|\mathrm{k}_i^{xy}-\mathrm{k}_f^{xy}\right|^2+k_\mathrm{D}^2}\right|^2 \\ &\times\delta(E_F^{total}-E_I^{total}) \qquad (4.96)\end{aligned}$$

This last equation may be written as:

$$
\begin{aligned}
\frac{1}{\tau_g} &= \Gamma \iiint \mathrm{d}\mathbf{k}_i^{xy}\mathrm{d}\mathbf{k}_j^{xy}\mathrm{d}\mathbf{k}_f^{xy} \left|G_g(\mathbf{k}_j^{xy}, \mathbf{k}_i^{xy}, \mathbf{k}_f^{xy})\right|^2 \\
&\times \left| \int_{-\infty}^{\infty} \mathrm{dk}_z \frac{G_{jg}(\mathrm{k}_z)G_{if}(\mathrm{k}_z)}{k_z^2 + \left|\mathbf{k}_i^{xy} - \mathbf{k}_f^{xy}\right|^2 + k_{\mathrm{D}}^2} \right|^2 \\
&\times \delta(E_F^{total} - E_I^{total})
\end{aligned}
\tag{4.97}
$$

where $\Gamma = \frac{e^4}{8\hbar\pi^5\epsilon^2}$

Changing the three two-dimensional integrals over the Cartesian in-plane carrier wave vectors $\mathbf{k}_i^{xy}, \mathbf{k}_j^{xy}$ and $\mathbf{k}_f^{xy}$ into polar coordinates, the above equation may be written as follows:

$$
\begin{aligned}
\frac{1}{\tau_g} &= \Gamma \int_0^{2\pi} \mathrm{d}\alpha_j \int_0^{2\pi} \mathrm{d}\alpha_f \int_0^{2\pi} \mathrm{d}\alpha_i \int_0^{\infty} \mathrm{dk}_f^{xy}\mathrm{k}_f^{xy} \\
&\times \int_0^{\infty} \mathrm{dk}_j^{xy}\mathrm{k}_j^{xy} \int_0^{\infty} \mathrm{dk}_i^{xy}\mathrm{k}_i^{xy} \left|G_g(\mathrm{k}_j^{xy}, \mathrm{k}_i^{xy}, \mathrm{k}_f^{xy}, \alpha_i, \alpha_j, \alpha_f)\right|^2 \\
&\times \left| \int_{-\infty}^{\infty} \mathrm{dk}_z \frac{G_{jg}(\mathrm{k}_z)G_{if}(\mathrm{k}_z)}{(\mathrm{k}_z^2 + P(\mathrm{k}_i^{xy}, \mathrm{k}_f^{xy}, \alpha_i, \alpha_f) + k_{\mathrm{D}}^2} \right|^2 \\
&\times \delta(E_F^{total} - E_I^{total})
\end{aligned}
\tag{4.98}
$$

where

$$
P(\mathrm{k}_i^{xy}, \mathrm{k}_f^{xy}, \alpha_i, \alpha_f) = \left|\mathbf{k}_i^{xy} - \mathbf{k}_f^{xy}\right|^2 = \mathrm{k}_i^{xy2} + \mathrm{k}_f^{xy2} - 2\mathrm{k}_i^{xy}\mathrm{k}_f^{xy}\cos(\alpha_f - \alpha_i)
$$

Carriers within a QW sub-band are distributed as a 2D gas and hence, they follow a $2D$ Fermi-Dirac distribution [8].

$$
f_D(\epsilon) = \frac{1}{e^{\frac{\epsilon-\mu}{KT}} + 1} \tag{4.99}
$$

where (see appendix B)

$$
e^{\frac{\mu}{KT}} = e^{\frac{\pi\hbar^2 N}{mKT}} - 1 \tag{4.100}
$$

and N is the carrier density within the wetting layer.

Assuming thermal equilibrium, the Fermi-Dirac distribution function can be included in eq. 4.98 as:

$$
\begin{aligned}
\frac{1}{\tau_g} &= \Gamma \int_0^{2\pi} d\alpha_j \int_0^{2\pi} d\alpha_f \int_0^{2\pi} d\alpha_i \int_0^{\infty} d\mathrm{k}_f^{xy} \mathrm{k}_f^{xy} (1 - \mathrm{f}_f^{FD}(\mathrm{k}_f^{xy})) \\
&\times \int_0^{\infty} d\mathrm{k}_j^{xy} \mathrm{k}_j^{xy} \mathrm{f}_j^{FD}(\mathrm{k}_j^{xy}) \int_0^{\infty} d\mathrm{k}_i^{xy} \mathrm{k}_i^{xy} \mathrm{f}_i^{FD}(\mathrm{k}_i^{xy}) \\
&\times \left|G_g(\mathrm{k}_j^{xy}, \mathrm{k}_i^{xy}, \mathrm{k}_f^{xy}, \alpha_i, \alpha_j, \alpha_f)\right|^2 \left| \int_{-\infty}^{\infty} d\mathrm{k}_z \frac{G_{jg}(\mathrm{k}_z) G_{if}(\mathrm{k}_z)}{\mathrm{k}_z^2 + P(\mathrm{k}_i^{xy}, \mathrm{k}_f^{xy}, \alpha_i, \alpha_f) + k_{\mathrm{D}}^2} \right|^2 \\
&\times \delta(E_F^{total} - E_I^{total}) \qquad (4.101)
\end{aligned}
$$

Following the approach of Paul Harrison [247], the argument of the δ-function, previously calculated (equation 4.95), can be factorized into:

$$
\begin{aligned}
\delta(E_F^{total} - E_I^{total}) &= \frac{2m_s}{\hbar^2} \delta\left(\left[\mathrm{k}_i^{xy2} + \frac{m_s}{m_c} \mathrm{k}_j^{xy2} - \Delta\right] - \mathrm{k}_f^{xy2}\right) \\
&= \frac{2m_s}{\hbar^2} \delta((\beta(\mathrm{k}_i^{xy}, \mathrm{k}_j^{xy}) - \mathrm{k}_f^{xy})(\beta(\mathrm{k}_i^{xy}, \mathrm{k}_j^{xy}) + \mathrm{k}_f^{xy})) \qquad (4.102)
\end{aligned}
$$

where

$$
\beta(\mathrm{k}_i^{xy}, \mathrm{k}_j^{xy}) = \sqrt{\mathrm{k}_i^{xy2} + \frac{m_s}{m_c} \mathrm{k}_j^{xy2} - \Delta} \qquad (4.103)
$$

and has to be real and positive. Around the solution $\beta(\mathrm{k}_i^{xy}, \mathrm{k}_j^{xy}) = \mathrm{k}_f^{xy}$, the other factor in the δ-function in Eq. 4.102, i.e., $(\beta(\mathrm{k}_i^{xy}, \mathrm{k}_j^{xy}) + \mathrm{k}_f^{xy})$ is a constant, and hence, may be taken out from the δ-function, using the δ-function property, i.e., $\delta(ax) = \frac{1}{a}\delta(x)$. Around the solution $\beta(\mathrm{k}_i^{xy}, \mathrm{k}_j^{xy}) = -\mathrm{k}_f^{xy}$ the factor $(\beta(\mathrm{k}_i^{xy}, \mathrm{k}_j^{xy}) - \mathrm{k}_f^{xy})$ is also constant, therefore the same property of the δ-function can be applied. Therefore the δ-function in Eq. 4.102 may be rewritten as follows:

$$
\delta(\beta(\mathrm{k}_i^{xy}, \mathrm{k}_j^{xy})^2 - \mathrm{k}_f^{xy2}) = \frac{\delta(\beta(\mathrm{k}_i^{xy}, \mathrm{k}_j^{xy}) - \mathrm{k}_f^{xy})}{\beta(\mathrm{k}_i^{xy}, \mathrm{k}_j^{xy}) + \mathrm{k}_f^{xy}} + \frac{\delta(\beta(\mathrm{k}_i^{xy}, \mathrm{k}_j^{xy}) + \mathrm{k}_f^{xy})}{\beta(\mathrm{k}_i^{xy}, \mathrm{k}_j^{xy}) - \mathrm{k}_f^{xy}} \qquad (4.104)
$$

As the modulus of the wave number has to be a positive value, only the term $\frac{\delta(\beta(\mathrm{k}_i^{xy}, \mathrm{k}_j^{xy}) - \mathrm{k}_f^{xy})}{\beta(\mathrm{k}_i^{xy}, \mathrm{k}_j^{xy}) + \mathrm{k}_f^{xy}}$ of the δ-function will provide a contribution when:

$$
\beta(\mathrm{k}_i^{xy}, \mathrm{k}_j^{xy}) = \mathrm{k}_f^{xy}
$$

Including eq. (4.104) into equation (4.101), we obtain:

$$\begin{aligned}
\frac{1}{\tau_g} = {} & \Gamma \int_0^{2\pi} \mathrm{d}\alpha_j \int_0^{2\pi} \mathrm{d}\alpha_f \int_0^{2\pi} \mathrm{d}\alpha_i \int_0^{\infty} \mathrm{dk}_i^{xy} \mathrm{k}_i^{xy} \mathrm{f}_i^{FD}(\mathrm{k}_i^{xy}) \\
& \times \int_0^{\infty} \mathrm{dk}_j^{xy} \mathrm{k}_j^{xy} \mathrm{f}_j^{FD}(\mathrm{k}_j^{xy}) \left| G_g(\mathrm{k}_j^{xy}, \mathrm{k}_i^{xy}, \alpha_i, \alpha_j, \alpha_f) \right|^2 \\
& \times \int_0^{\infty} \mathrm{dk}_f^{xy} \mathrm{k}_f^{xy} (1 - \mathrm{f}_f^{FD}(\mathrm{k}_f^{xy})) \left| \int_{-\infty}^{\infty} \mathrm{dk}_z \frac{G_{jg}(\mathrm{k}_z) G_{if}(\mathrm{k}_z)}{\mathrm{k}_z^2 + P(\mathrm{k}_i^{xy}, \mathrm{k}_j^{xy}, \alpha_i, \alpha_f) + k_{\mathrm{D}}^2} \right|^2 \\
& \times \frac{2m_s}{\hbar^2} \frac{\delta(\beta(\mathrm{k}_i^{xy}, \mathrm{k}_j^{xy}) - \mathrm{k}_f^{xy})}{\beta(\mathrm{k}_i^{xy}, \mathrm{k}_j^{xy}) + \mathrm{k}_f^{xy}}
\end{aligned} \tag{4.105}$$

Taking into account the fact that the δ-function only gives contribution to the integral over the modulus of the in-plane wave vector $\mathbf{k}_f^{xy}$ when:

$$\beta(\mathrm{k}_i^{xy}, \mathrm{k}_j^{xy}) = \mathrm{k}_f^{xy}$$

The probability of capturing a carrier in a particular state (i.e., state $|g\rangle$) inside the quantum dot, after scattering with another carrier, in a state $|i\rangle$ in the quantum well; which itself is scattered to any other final state $|f\rangle$ within the quantum well, may be given by:

$$\begin{aligned}
\frac{1}{\tau_g} = {} & \frac{m_s}{\hbar^2} \Gamma \int_0^{2\pi} \mathrm{d}\alpha_j \int_0^{2\pi} \mathrm{d}\alpha_f \int_0^{2\pi} \mathrm{d}\alpha_i \int_0^{\infty} \mathrm{dk}_i^{xy} \mathrm{k}_i^{xy} \mathrm{f}_i^{FD}(\mathrm{k}_i^{xy}) \\
& \times \int_0^{\infty} \mathrm{dk}_j^{xy} \mathrm{k}_j^{xy} \mathrm{f}_j^{FD}(\mathrm{k}_j^{xy}) (1 - \mathrm{f}_f^{FD}(\mathrm{k}_i^{xy}, \mathrm{k}_j^{xy})) \left| G_g(\mathrm{k}_j^{xy}, \mathrm{k}_i^{xy}, \alpha_i, \alpha_j, \alpha_f) \right|^2 \\
& \times \left| \int_{-\infty}^{\infty} \mathrm{dk}_z \frac{G_{jg}(\mathrm{k}_z) G_{if}(\mathrm{k}_z)}{\mathrm{k}_z^2 + P(\mathrm{k}_i^{xy}, \mathrm{k}_j^{xy}, \alpha_i, \alpha_f) + k_{\mathrm{D}}^2} \right|^2
\end{aligned} \tag{4.106}$$

4.4.1 Difficulties with the numerical implementation

There are two major obstacles to the numerical implementation of the equation 4.106.

- The first point to note is that the integral with the respect to k_z is dependent on the variables α_f, α_i, k_i^{xy} and k_j^{xy}. Therefore in the numerical implementation this integral must be calculated each time we calculate an integral with respect to these variables. Previously, when calculating the Auger process type II (equation 4.62), the integral with the respect to k_z was only dependent on the variable k_{xy}, so the calculation of this integral is independent of the integrals over the other variables.

- The second point is more subtle and is due to the fact that the function β is dependent on k_i^{xy} and k_j^{xy}. Therefore using the previous approach for Auger process type II in order to find the maximum and minimum for the limits of the integral with respect to k_j^{xy} by using the function β cannot be used. This is because β varies with the respect to k_i^{xy} and therefore the limits for the integral are also dependent on the variable k_i^{xy}.

These two difficulties unfortunately meant that the time taken to calculate equation 4.106 using the available 2.00 GHz AMD Athlon processor was prohibitively long. Therefore in our model we made the decision to instead use the semi-analytical approach described in chapter 3 to calculate the Auger process type I. This approach does cause some problems for the calculation of the occupancy of an ensemble of quantum dots and these will be alluded to in chapter 5.

4.5 Carrier Auger relaxation in quantum dots

This Coulomb scattering process is characterized by a transition between two different $0D$ states and a further excitation (relaxation) of a $2D$ carrier within the wetting layer (see figure 4.19). We start describing the Coulomb interaction between the $0D$ system and a $2D$ electron (hole) gas. Considering an excitation of wave vector $\mathbf{k}_1 - \mathbf{k}$ (boldface indicates a bidimensional vector, defined in the xy plane) for a carrier in a $2D$ energy state followed by a transition from the $0D$ state $|i\rangle$, to $|f\rangle$ (lateral quantum numbers of the 0D states) within the quantum dot (see Fig. 4.19),

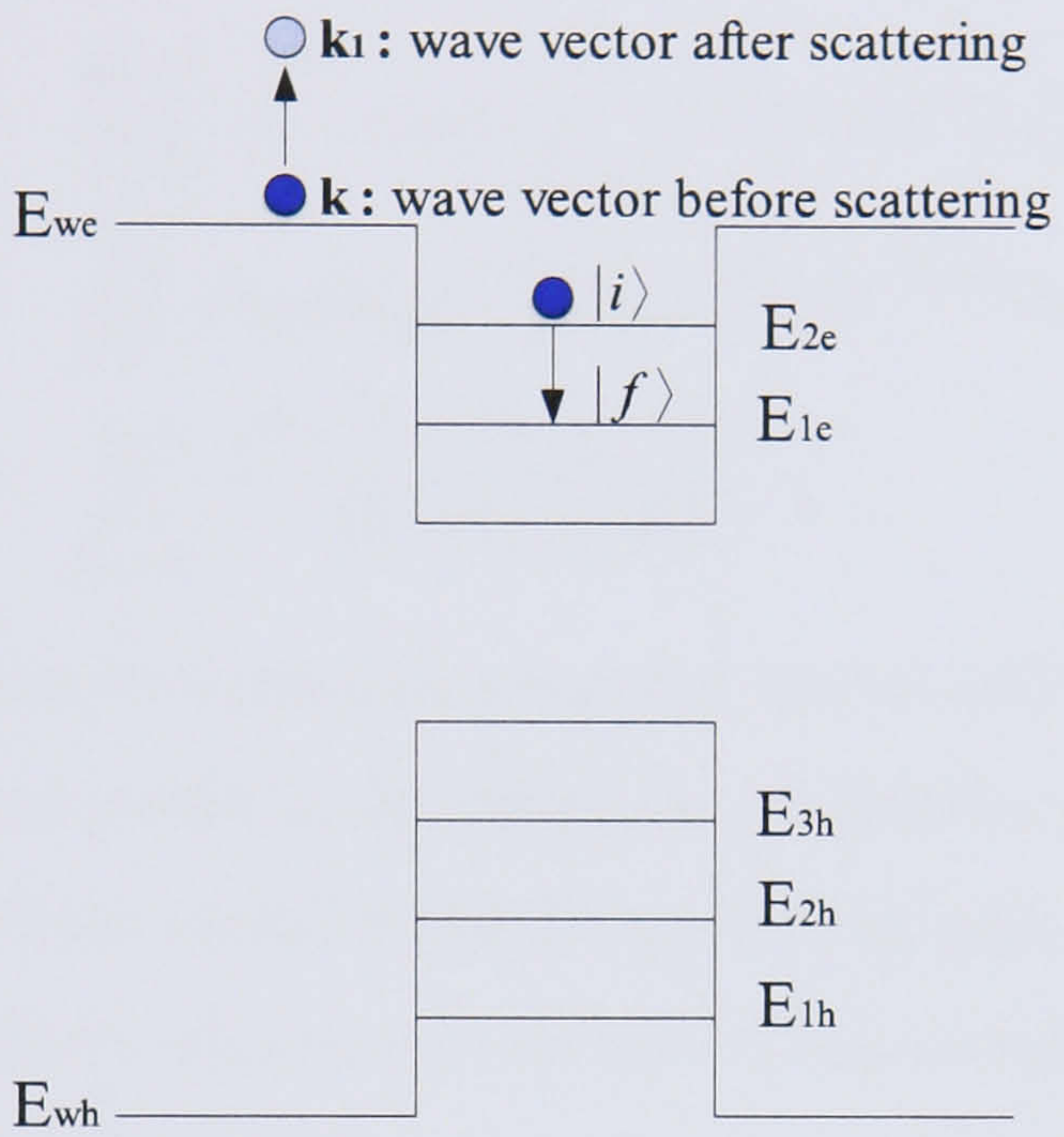

Figure 4.19: Auger relaxation process. A carrier in $|i>$ state in the quantum dot, relaxes into $|f>$ quantum dot state, after scattering with a $2D$ carrier in wetting layer, considering an excitation of wave vector $\mathbf{k}_1 - \mathbf{k}$.

the interaction may be written as follows:

$$
\begin{aligned}
< f|\tilde{H}|i > \;=\;& \left\langle \Psi_1^{\mathrm{W}}(\mathbf{r}',\mathbf{k}_1^{\mathrm{W}})\Psi_f^{\mathrm{D}}(\mathbf{r},\mathbf{k}_f^{\mathrm{D}}) \left| \frac{4\pi \mathrm{e}^2}{\epsilon V} \sum_{\mathbf{k}_{xy},k_z} \frac{e^{i\mathbf{k}_{xy}(\mathbf{r}_{xy}-\mathbf{r}'_{xy})} e^{ik_z(z-z')}}{k_z^2+k_{xy}^2+k_{\mathrm{D}}^2} \right| \right. \\
& \left. \Psi^{\mathrm{W}}(\mathbf{r}',\mathbf{k}^{\mathrm{W}})\Psi_i^{\mathrm{D}}(\mathbf{r},\mathbf{k}_i^{\mathrm{D}}) \right\rangle \qquad (4.107)
\end{aligned}
$$

Introducing the carrier wavefunctions given by Eq. 4.29 for the dot and Eq. 4.30 for the well,

$$
\begin{aligned}
< f|\tilde{H}|i > \;=\;& \frac{4\pi e^2}{VA\epsilon} \int_{-\infty}^{\infty} \mathrm{d}z\mathrm{d}z' \int_{-\infty}^{\infty} \psi^{\mathrm{D}*}{}_f(z)\psi^{\mathrm{W}*}{}_1(z')\psi^{\mathrm{D}}{}_i(z)\psi^{\mathrm{W}}(z') \\
\times\;& \iint \mathrm{d}\mathbf{r}_{xy}\mathrm{d}\mathbf{r}'_{xy}\psi^{\mathrm{D}*}{}_f(\mathbf{r}_{xy}) e^{i\mathbf{k}_1\mathbf{r}'_{xy}} e^{-i\mathbf{k}\mathbf{r}'_{xy}} \psi_i^{\mathrm{D}}(\mathbf{r}_{xy}) \\
\times\;& \sum_{\mathbf{k}_{xy},k_z} \frac{e^{i\mathbf{k}_{xy}(\mathbf{r}_{xy}-\mathbf{r}'_{xy})} e^{ik_z(z-z')}}{k_z^2+k_{xy}^2+k_{\mathrm{D}}^2} \qquad (4.108)
\end{aligned}
$$

Changing the summation over the bidimensional vector defined in the xy plane, $\mathbf{k}_{xy}$ and the one-dimensional vector k_z by integrals, introduces a factor of $\frac{L}{2\pi}$ from the density of states, as we have explained in the previous section for the Auger Capture type II, therefore the above expression can be written as follows:

$$
\begin{aligned}
< f|\tilde{H}|i > \;=\;& \frac{e^2}{2A\epsilon\pi^2} \int_{-\infty}^{\infty} \mathrm{d}z\mathrm{d}z' \int_{-\infty}^{\infty} \psi^{\mathrm{D}*}{}_f(z)\psi^{\mathrm{W}*}{}_1(z')\psi^{\mathrm{D}}{}_i(z)\psi^{\mathrm{W}}(z') \\
\times\;& \iint \mathrm{d}\mathbf{r}_{xy}\mathrm{d}\mathbf{r}'_{xy}\psi^{\mathrm{D}*}{}_f(\mathbf{r}_{xy}) e^{i\mathbf{k}_1\mathbf{r}'_{xy}} e^{-i\mathbf{k}\mathbf{r}'_{xy}} \psi_i^{\mathrm{D}}(\mathbf{r}_{xy}) \\
\times\;& \int_{-\infty}^{\infty} \mathrm{dk}_z e^{i\mathrm{k}_z(z-z')} \int \mathrm{d}\mathbf{k}_{xy} \frac{e^{i\mathbf{k}_{xy}\mathbf{r}_{xy}} e^{-i\mathbf{k}_{xy}\mathbf{r}'_{xy}}}{k_z^2+k_{xy}^2+k_{\mathrm{D}}^2} \qquad (4.109)
\end{aligned}
$$

If we change the order of the integrals in order to calculate the integral over $\mathbf{r}'_{xy}$ first, we obtain:

$$
\begin{aligned}
< f|\tilde{H}|i > \;=\;& \frac{e^2}{2A\epsilon\pi^2} \int_{-\infty}^{\infty} \mathrm{d}z\mathrm{d}z' \int_{-\infty}^{\infty} \psi^{\mathrm{D}*}{}_f(z)\psi^{\mathrm{W}*}{}_1(z')\psi^{\mathrm{D}}{}_i(z)\psi^{\mathrm{W}}(z') \\
\times\;& \int_{-\infty}^{\infty} \mathrm{dk}_z e^{i\mathrm{k}_z(z-z')} \int \mathrm{d}\mathbf{k}_{xy} \frac{1}{k_z^2+k_{xy}^2+k_{\mathrm{D}}^2} \\
\times\;& \int \mathrm{d}\mathbf{r}_{xy}\psi^{\mathrm{D}*}{}_f(\mathbf{r}_{xy})\psi_i^{\mathrm{D}}(\mathbf{r}_{xy}) e^{i\mathbf{k}_{xy}\mathbf{r}_{xy}} \\
\times\;& \int \mathrm{d}\mathbf{r}'_{xy} e^{-i(\mathbf{k}-\mathbf{k}_1+\mathbf{k}_{xy})\mathbf{r}'_{xy}} \qquad (4.110)
\end{aligned}
$$

The integral over the xy plane is a δ-function which introduces a factor of 2π per dimension, gives

$$\begin{aligned} < f|\tilde{H}|i > \; = \; & \frac{2e^2}{A\epsilon}\int_{-\infty}^{\infty}\mathrm{d}z\mathrm{d}z' \int_{-\infty}^{\infty} {\psi^{\mathrm{D}}}^*_f(z){\psi^{\mathrm{W}}}^*_1(z'){\psi^{\mathrm{D}}}_i(z)\psi^{\mathrm{W}}(z') \\ \times \; & \int_{-\infty}^{\infty}\mathrm{dk}_z e^{i\mathrm{k}_z(z-z')}\int \mathrm{d}\mathbf{k}_{xy}\left[\frac{1}{k_z^2+k_{xy}^2+k_{\mathrm{D}}^2}\right. \qquad (4.111) \\ \times \; & \left.\int \mathrm{d}\mathbf{r}_{xy}{\psi^{\mathrm{D}}}^*_f(\mathbf{r}_{xy})\psi_i^{\mathrm{D}}(\mathbf{r}_{xy})e^{i\mathbf{k}_{xy}\mathbf{r}_{xy}}\right]\delta(\mathbf{k}-\mathbf{k}_1+\mathbf{k}_{xy}) \qquad (4.112) \end{aligned}$$

Calculating the integral over $\mathbf{k}_{xy}$, the δ-function limits the contribution to the point where $\mathbf{k}_{xy} = \mathbf{k}_1 - \mathbf{k}$, consequently the above equation becomes:

$$\begin{aligned} < f|\tilde{H}|i > \; = \; & \frac{2e^2}{A\epsilon}\int_{-\infty}^{\infty}\mathrm{d}z\mathrm{d}z' \int_{-\infty}^{\infty} {\psi^{\mathrm{D}}}^*_f(z){\psi^{\mathrm{W}}}^*_1(z'){\psi^{\mathrm{D}}}_i(z)\psi^{\mathrm{W}}(z') \\ \times \; & \int_{-\infty}^{\infty}\mathrm{dk}_z e^{i\mathrm{k}_z(z-z')}\left[\frac{G(\mathbf{k},\mathbf{k}_1)}{k_z^2+|\mathbf{k}_1-\mathbf{k}|^2+k_{\mathrm{D}}^2}\right] \end{aligned} \tag{4.113}$$

where the *form factor* $G(\mathbf{k},\mathbf{k}_1)$ is given by:

$$G(\mathbf{k},\mathbf{k}_1) \; = \; \int \mathrm{d}\mathbf{r}_{xy}{\psi^{\mathrm{D}}}^*_f(\mathbf{r}_{xy})\psi_i^{\mathrm{D}}(\mathbf{r}_{xy})e^{i(\mathbf{k}_1-\mathbf{k})\mathbf{r}_{xy}} \tag{4.114}$$

Changing the order of the integrations as we have done before, we can finally give an expression for the matrix element in this Scattering process, i.e.

$$< f|\tilde{H}|i > \; = \; \frac{2e^2}{A\epsilon}G(\mathbf{k},\mathbf{k}_1)\int_{-\infty}^{\infty}\mathrm{dk}_z\frac{G_{if}(\mathrm{k}_z)G^w(\mathrm{k}_z)}{k_z^2+|\mathbf{k}_1-\mathbf{k}|^2+k_{\mathrm{D}}^2} \tag{4.115}$$

where $G_{if}(\mathrm{k}_z)$ and $G^w(\mathrm{k}_z)$ are the form factors given by:

$$G_{if}(\mathrm{k}_z) = \int_{-\infty}^{\infty}\mathrm{d}z{\psi^{\mathrm{D}}}^*_f(z){\psi^{\mathrm{D}}}_i(z)e^{i\mathrm{k}_z z} \tag{4.116}$$

$$G^w(\mathrm{k}_z) = \int_{-\infty}^{\infty}\mathrm{d}z'{\psi^{\mathrm{W}}}^*_1(z')\psi^{\mathrm{W}}(z')e^{-i\mathrm{k}_z z'} \tag{4.117}$$

Once we have calculated the Coulomb interaction between the $0D$ system and a $2D$ carrier within the wetting layer, we make use of this last expression (Eq. 4.115) in order to calculate the Auger like relaxation rate of a carrier in SAD structures, i.e, the probability of having a carrier relaxed from any possible $|i\rangle$ $0D$ state into any other $|f\rangle$ $0D$ energy state (see Fig. 4.3) as a consequence of an excitation of wave vector $\mathbf{k}_1 - \mathbf{k}$ of the $2D$ electron-hole plasma, is given by Fermi's Golden Rule:

$$\begin{aligned} \frac{1}{\tau_{if}} &= \frac{2\pi}{\hbar} \sum_{\mathbf{k}_1,\mathbf{k}} \left| \frac{2e^2}{A\epsilon} G(\mathbf{k},\mathbf{k}_1) \int_{-\infty}^{\infty} \mathrm{dk}_z \frac{G_{if}(\mathrm{k}_z) G^w(\mathrm{k}_z)}{k_z^2 + \left|\mathbf{k}_1 - \mathbf{k}\right|^2 + k_{\mathrm{D}}^2} \right|^2 \\ &\times \ \delta(E_F^{total} - E_I^{total}) \end{aligned} \tag{4.118}$$

where the total energy exchange during this scattering process, i.e., $\delta(E_F^{total} - E_I^{total})$ may be written as follows,

$$\begin{aligned} \delta(E_F^{total} - E_I^{total}) &= \delta\big(\epsilon_f^{DOT} - \epsilon_i^{DOT} + \frac{\hbar^2}{2m_s}(\mathrm{k}_1{}^2 - \mathrm{k}^2)\big) \\ &= \frac{2m_s}{\hbar^2}\delta\big(\mathrm{k}_1{}^2 - \mathrm{k}^2 + \Delta\big) \end{aligned} \tag{4.119}$$

where $\epsilon_i^{DOT} = \mathrm{E}_i^z + \frac{\hbar^2}{2m_c}\mathrm{k}_i^{xy2}$ and $\epsilon_f^{DOT} = \mathrm{E}_f^z + \frac{\hbar^2}{2m_s}\mathrm{k}_i^{xy2}$ are the total energies of the initial $|i\rangle$ and final $|f\rangle$ $0D$ states respectively for the carrier inside the quantum dot, and Δ is the total energy exchange inside the quantum dot, hence,

$$\Delta = \frac{2m_s}{\hbar^2}(\epsilon_f^{DOT} - \epsilon_i^{DOT}) \tag{4.120}$$

Note that the total energy of the scattered carrier in the wetting layer before and after scattering with a $0D$ carrier, is the result of adding its potential and kinetic components, hence, $E^z + \frac{\hbar^2}{2m_s}\mathrm{k}^2$ before the scattering event, and $E_1^z + \frac{\hbar^2}{2m_s}\mathrm{k}_1{}^2$ after the scattering process. The terms related to the potential energy before and after scattering, do not appear in (4.119) because we are considering that the carrier is strongly confined to the lowest energy level in the z direction, so $E_1^z = E^z$.

Returning to equation 4.115, and following the technique used by P. Harrison in [3] dealing with a similar δ-function as the one given in Eq. 4.119, we can rewrite the equation 4.119 as follows,

$$\begin{aligned}\delta(E_F^{total} - E_I^{total}) &= \frac{2m_s}{\hbar^2}\delta\big(\mathrm{k}_1{}^2 - \mathrm{k}^2 + \Delta\big) \\ &= \frac{2m_s}{\hbar^2}\delta\big((\mathrm{k}_1 - \beta(\mathrm{k})(\mathrm{k}_1 + \beta(\mathrm{k}))\big) \end{aligned} \tag{4.121}$$

where

$$\beta(\mathrm{k}) = \sqrt{\mathrm{k}^2 - \Delta} \tag{4.122}$$

As explained in [3], the equation 4.121 may be approximated to

$$\begin{aligned}\delta(E_F^{total} - E_I^{total}) &= \frac{2m_s}{\hbar^2}\delta\big((\mathrm{k}_1 - \beta(\mathrm{k}))(\mathrm{k}_1 + \beta(\mathrm{k}))\big) \\ &\approx \frac{2m_s}{\hbar^2}\frac{\delta(\mathrm{k}_1 - \beta(\mathrm{k}))}{\beta(\mathrm{k}) + \mathrm{k}_1} \end{aligned} \tag{4.123}$$

Returning to Eq. 4.118 and changing the summation over wave vectors $\mathbf{k}_1$ and $\mathbf{k}$ into integrals, and replacing these vector integrals by the corresponding polar coordinates. We can now write a more manageable expression for the Auger relaxation rate,

$$\begin{aligned}\frac{1}{\tau_{if}} &= \Gamma\int_0^{2\pi} d\alpha \int_0^{2\pi} d\alpha_1 \int_0^{\infty} d\mathrm{k}\mathrm{k} \int_0^{\infty} d\mathrm{k}_1\mathrm{k}_1 \left|G(\mathrm{k}, \mathrm{k}_1, \alpha, \alpha_1)\right|^2 \\ &\times \left|\int_{-\infty}^{\infty} d\mathrm{k}_z \frac{G_{if}(\mathrm{k}_z)G^w(\mathrm{k}_z)}{k_z^2 + P(\mathrm{k}, \mathrm{k}_1, \alpha, \alpha_1) + k_{\mathrm{D}}^2}\right|^2 \frac{2m_s}{\hbar^2}\frac{\delta(\beta(\mathrm{k}) - \mathrm{k}_1)}{\beta(\mathrm{k}) + \mathrm{k}_1} \end{aligned} \tag{4.124}$$

where

$$\Gamma = \frac{e^4}{2\hbar\pi^3\epsilon^2} \tag{4.125}$$

and

$$P(\mathrm{k}, \mathrm{k}_1, \alpha, \alpha_1) = \left|\mathbf{k}_1 - \mathbf{k}\right|^2 = \mathrm{k}_1{}^2 + \mathrm{k}^2 - 2\mathrm{k}_1\mathrm{k}\cos(\alpha - \alpha_1) \tag{4.126}$$

Taking into account the δ-function only gives a contribution to the integral over the modulus of the in-plane wave vector $\mathbf{k}^1$ when:

$$\beta(\mathrm{k}) = \mathrm{k}_1$$

as well as including the Fermi-Dirac distributions for the carriers in the quantum well (Eq. 4.57) assuming thermal equilibrium, we can finally give a mathematical expression to calculate the probability for transition from the $0D$ state $|i\rangle$ to $|f\rangle$ state within the quantum dot after an excitation of wave vector $\mathbf{k}_1 - \mathbf{k}$ for a carrier in a $2D$ energy state has been taken, hence

$$\begin{aligned}\frac{1}{\tau_{if}} &= \frac{m_s}{\hbar^2}\Gamma \int_0^{2\pi} \mathrm{d}\alpha \int_0^{2\pi} \mathrm{d}\alpha_1 \int_0^{\infty} \mathrm{dkk}\, \mathrm{f}^{FD}(\mathrm{k})(1 - \mathrm{f}_1^{FD}(\mathrm{k}))\, |G(\mathrm{k},\alpha,\alpha_1)|^2 \\ &\times \left| \int_{-\infty}^{\infty} \mathrm{dk}_z \frac{G_{if}(\mathrm{k}_z) G^w(\mathrm{k}_z)}{k_z^2 + P(\mathrm{k},\alpha,\alpha_1) + k_{\mathrm{D}}^2} \right|^2 \end{aligned} \tag{4.127}$$

where $G(\mathrm{k},\alpha,\alpha_1)$, $G_{if}(\mathrm{k}_z)$ and $G^w(\mathrm{k}_z)$ are the *form factors* given by equations 4.114, 4.116 and 4.117 respectively, Γ is the constant given by (4.125) and the term $P(\mathrm{k},\alpha,\alpha_1)$ can be calculated following (4.126).

4.5.1 Numerical Implementation

Equation 4.127 has been solved numerically following the same procedures as for the calculation of Auger type II processes (section 4.3). We first calculate the form factors inside the integral with respect to the z-component of the wave vector $\mathbf{k} = (\mathbf{k}_{xy}, \mathrm{k}_z)$ (4.34), i.e., $G_{if}(\mathrm{k}_z)$ and $G^w(\mathrm{k}_z)$. In order to calculate the integral with respect to k_z in (4.127) we use the same limits as those considered in the previous Auger capture type II process, given by Eq. 4.67.

Again in order to determine the limits for the integral with respect to k in 4.127, we make use of the function β given by equation 4.122.

We have also calculated the form factor $G(\mathrm{k},\alpha,\alpha_1)$ in (4.127) given by Eq. 4.114, following the same steps as previously explained for the calculation of the form factor $G(\mathbf{k}_j^{xy}, \mathbf{k}_f^{xy}, \mathbf{k}_{xy})$ in (4.62).

The integrals with respect to the angles α and α_1, have been numerically solved for 2^8 partitions as for the Auger Capture type II rate (Eq. 4.62). In order to give a solution for the relaxation rate (Eq. 4.127), we have numerically solved the integral

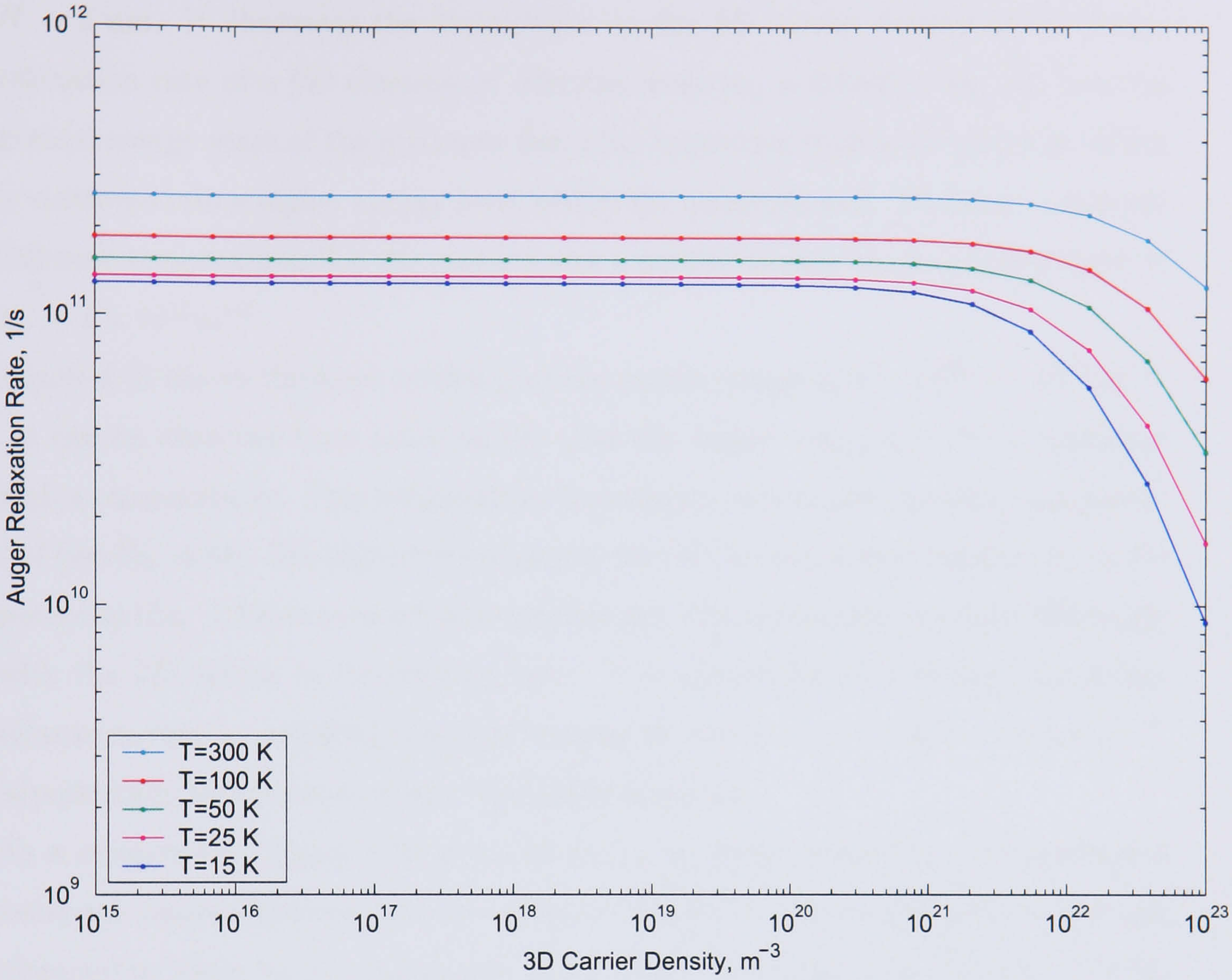

Figure 4.20: Auger Relaxation Rate dependence on the $3D$ carrier density, plotted for different temperatures, numerically solving the analytical formula given by equation 4.127. We have considered a $2D$ carrier density of $1 \times 10^{15} m^{-2}$.

inside the square modulus in (4.127) for each value of k (Eq. 4.80), α and α_1 as previously explained.

Figure 4.20 shows the results of numerically solving equation 4.127 considering the self-assembled quantum dots pictured in figure 4.16 of radii $R = 15$ nm and heights

$H = 5$ nm. It illustrates the dependence on the $3D$ carrier density of the Auger relaxation rate of a $0D$ electron of effective mass $m_e = 0.0445 \times \mathrm{m}_0$ [5], into the ground energy state of the quantum dot, after scattering with a $2D$ electron, which is scattered into a higher energy level within the quantum well. We have considered different temperatures for the carriers and a carrier density in the wetting layer of $n_w = 1 \times 10^{15}\mathrm{m}^{-2}$.

Figure 4.21 shows the same results over the shorter range of $[1 \times 10^{20}, 1 \times 10^{25}]m^{-3}$.

It can be observed from these results that the Auger relaxation rate is larger for higher temperatures. This temperature dependence comes from the screening potential (see Eq. 4.34). For higher temperatures the $3D$ screening wave number k_D in the potential (Eq. 4.33) is reduced and therefore the $0D$ carriers interact more efficiently with the $2D$ carrier in the wetting layer. It is interesting to note that the Auger relaxation rate for relatively small $3D$ carrier densities, i.e., $1 \times 10^{20} - 1 \times 10^{25}m^{-3}$, is practically independent of the $3D$ carrier densities.

As a comparison, figures 4.22 and 4.23 show the Auger relaxation rate calculated using the semi-analytical approach given in chapter 3. All the parameters used are identical to those for the calculation of the Auger relaxation rate illustrated in figures 4.20 and 4.21.

In both graphs the Auger relaxation rate exhibits similar behavior, i.e., the rate remains constant for low values of $3D$ carrier densities but for high $3D$ carrier densities the Auger relaxation rate decreases with the increasing carrier density. It is interesting to note that in figure 4.22 the Auger relaxation rate is independent on the temperature of the carriers for low carrier densities, however our results in figure 4.20 clearly shows that the Auger relaxation rate increases with increasing temperature.

The magnitude of the Auger relaxation rate also differs depending on which calculation is used. For example in figure 4.22 we observe for a $3D$ carrier densities of $n_3 = 1 \times 10^{17}\mathrm{m}^{-3}$ and temperatures of the carriers of 300 K, an Auger relaxation rate of $1.283 \times 10^{12}\mathrm{s}^{-1}$ using the semi-analytical approach given in chapter 3. Whereas

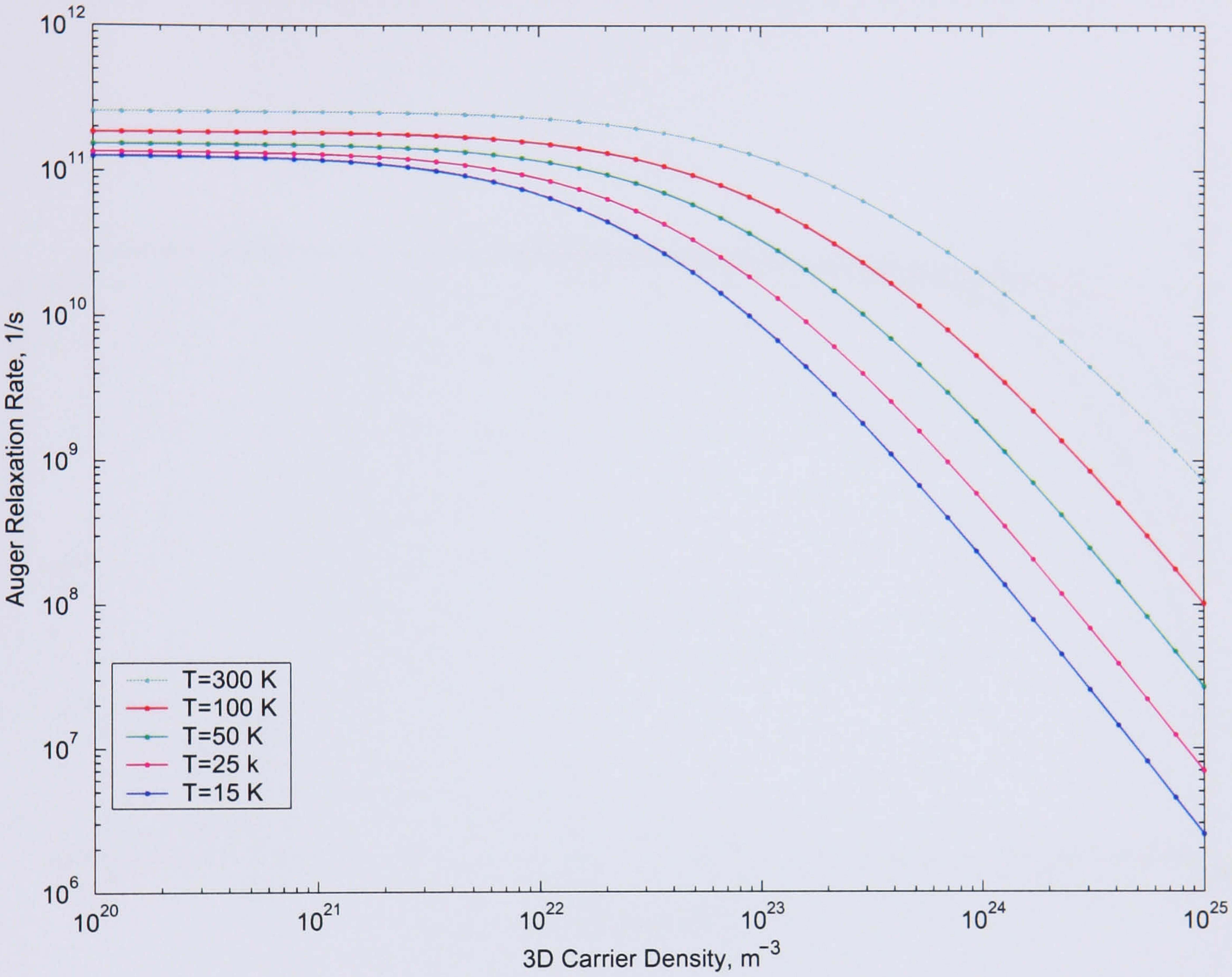

Figure 4.21: Auger Relaxation Rate dependence on the $3D$ carrier density, plotted for different temperatures considering a $2D$ carrier density of $1 \times 10^{15} m^{-2}$.

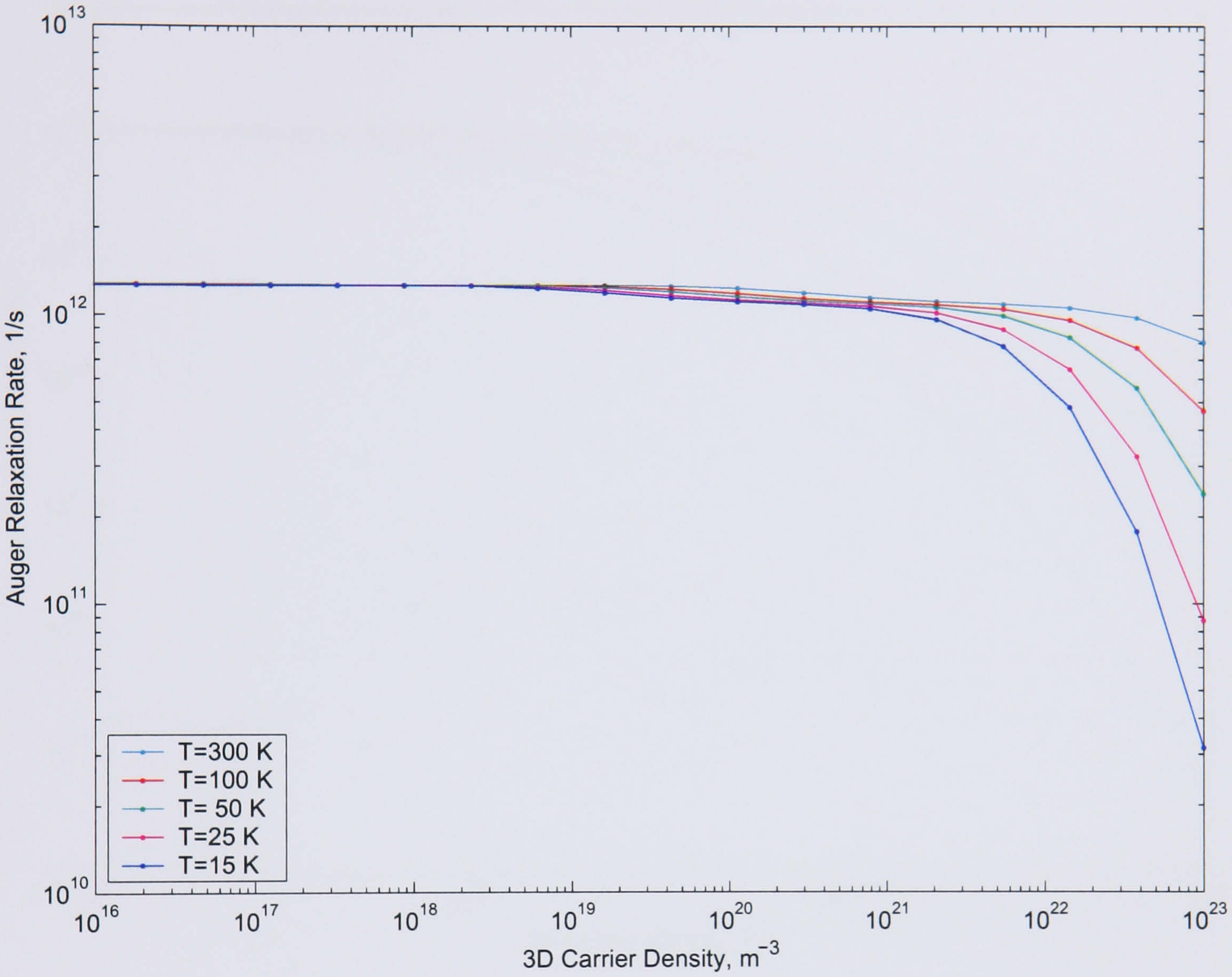

Figure 4.22: Auger Relaxation Rate dependence on the $3D$ carrier density considering A. V. Uskov calculation given in [9], plotted for different temperatures and considering a $2D$ carrier density of $1 \times 10^{15} m^{-2}$.

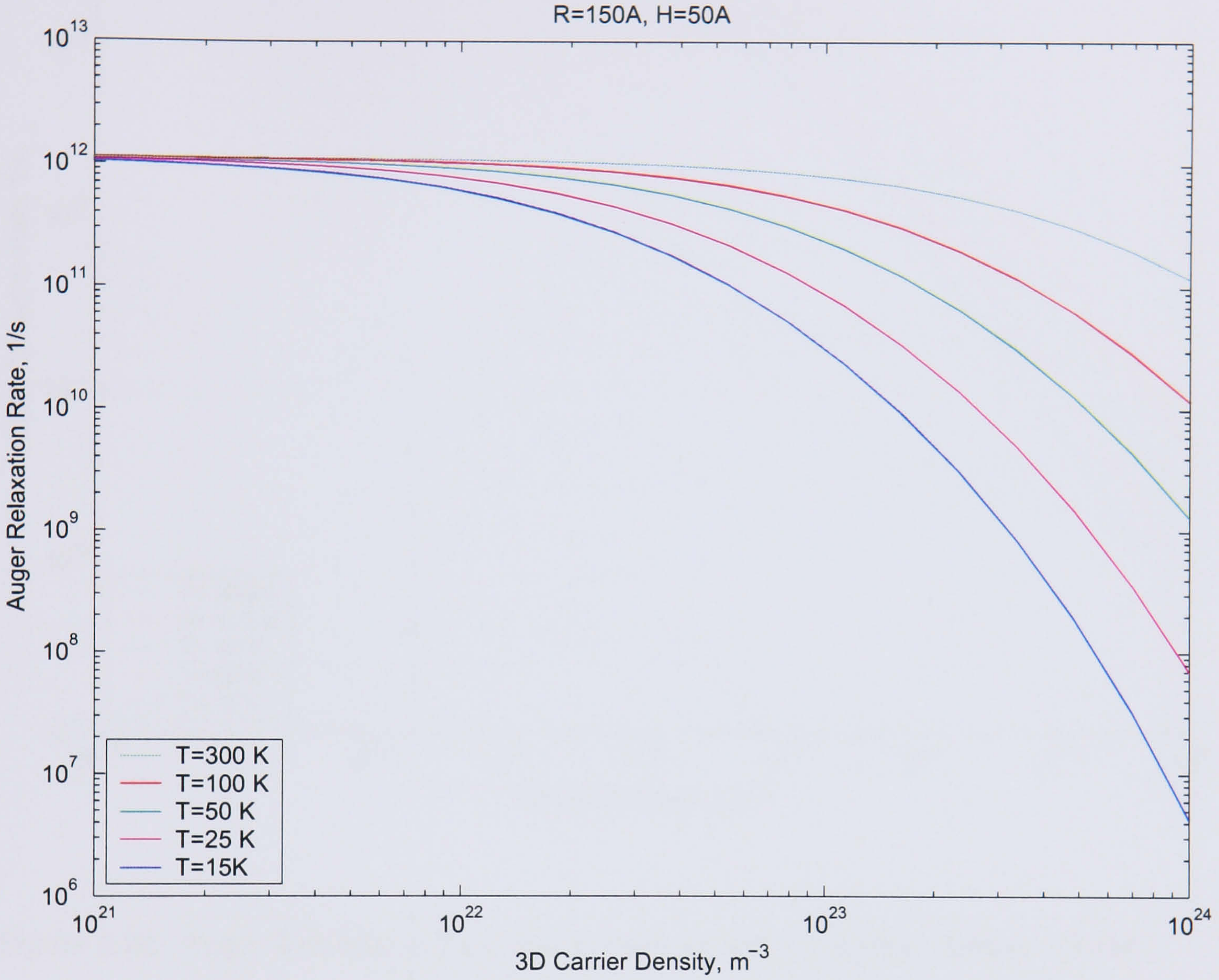

Figure 4.23: Auger Relaxation Rate dependence on the $3D$ carrier density considering A. V. Uskov calculation given in [9], plotted for different temperatures and considering more points in the $3D$ carrier density range $[1 \times 10^{21} - 1 \times 10^{24} m^{-3}]$. We have considered a $2D$ carrier density of $1 \times 10^{15} m^{-2}$

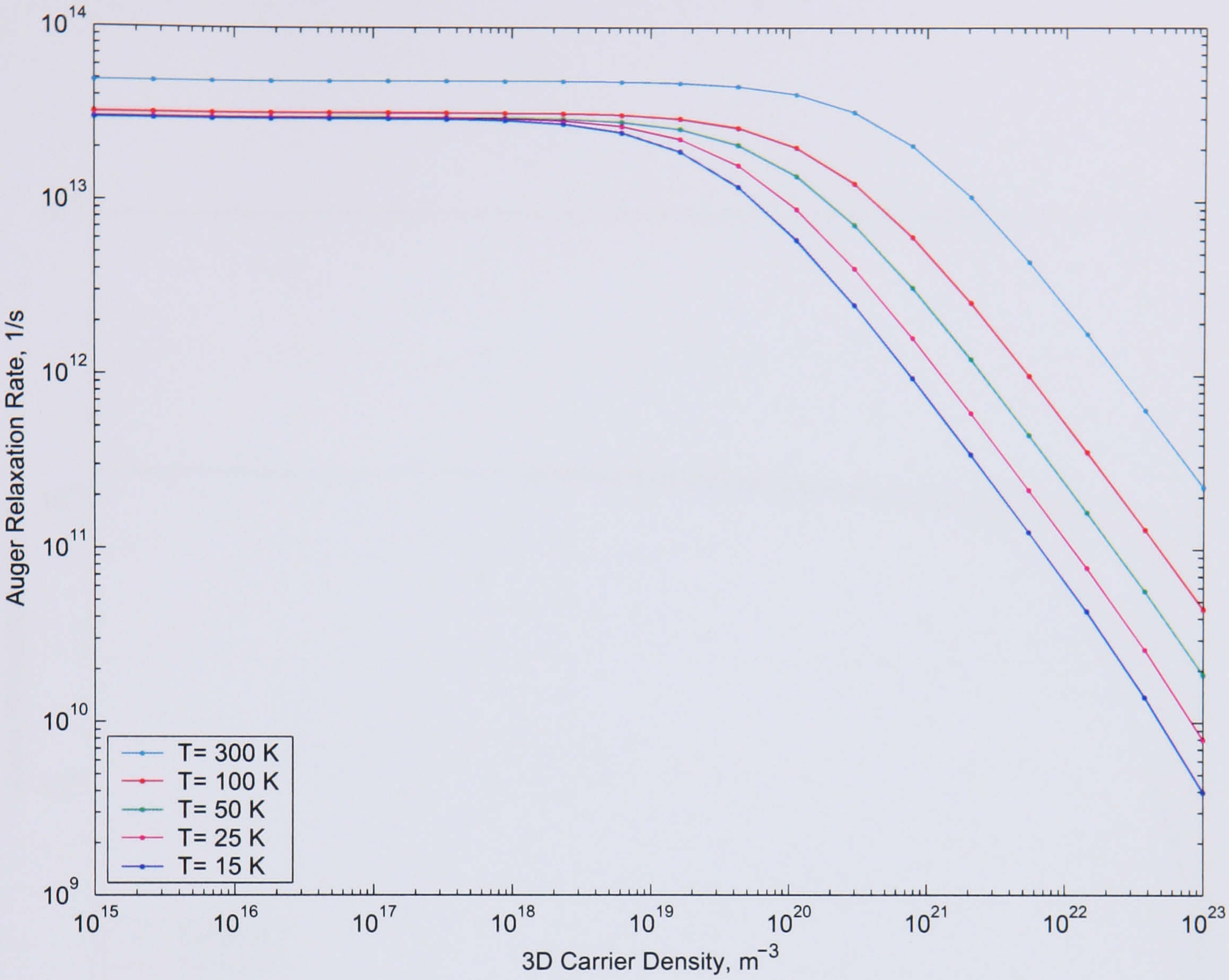

Figure 4.24: Auger Relaxation Rate dependence on the $3D$ carrier density, plotted for different temperatures and considering a $2D$ carrier density of $1 \times 10^{18} m^{-2}$.

from figure 4.20 for the same parameters the lifetime obtained is $2.590 \times 10^{11}\mathrm{s}^{-1}$.

Performing the same calculations at a higher $2D$ carrier density of $10^{18}\mathrm{m}^{-2}$, we obtain the results given in figure 4.24 and figure 4.25 for the semi-analytical approach described in chapter 3. Again as an example, an Auger relaxation rate of $1.14 \times 10^{15}\mathrm{s}^{-1}$ is obtained for a $3D$ carrier density of $1 \times 10^{17}\mathrm{m}^{-3}$ using the semi-analytical approach (figure 4.25). Whereas implementing equation 4.127 we obtain a much

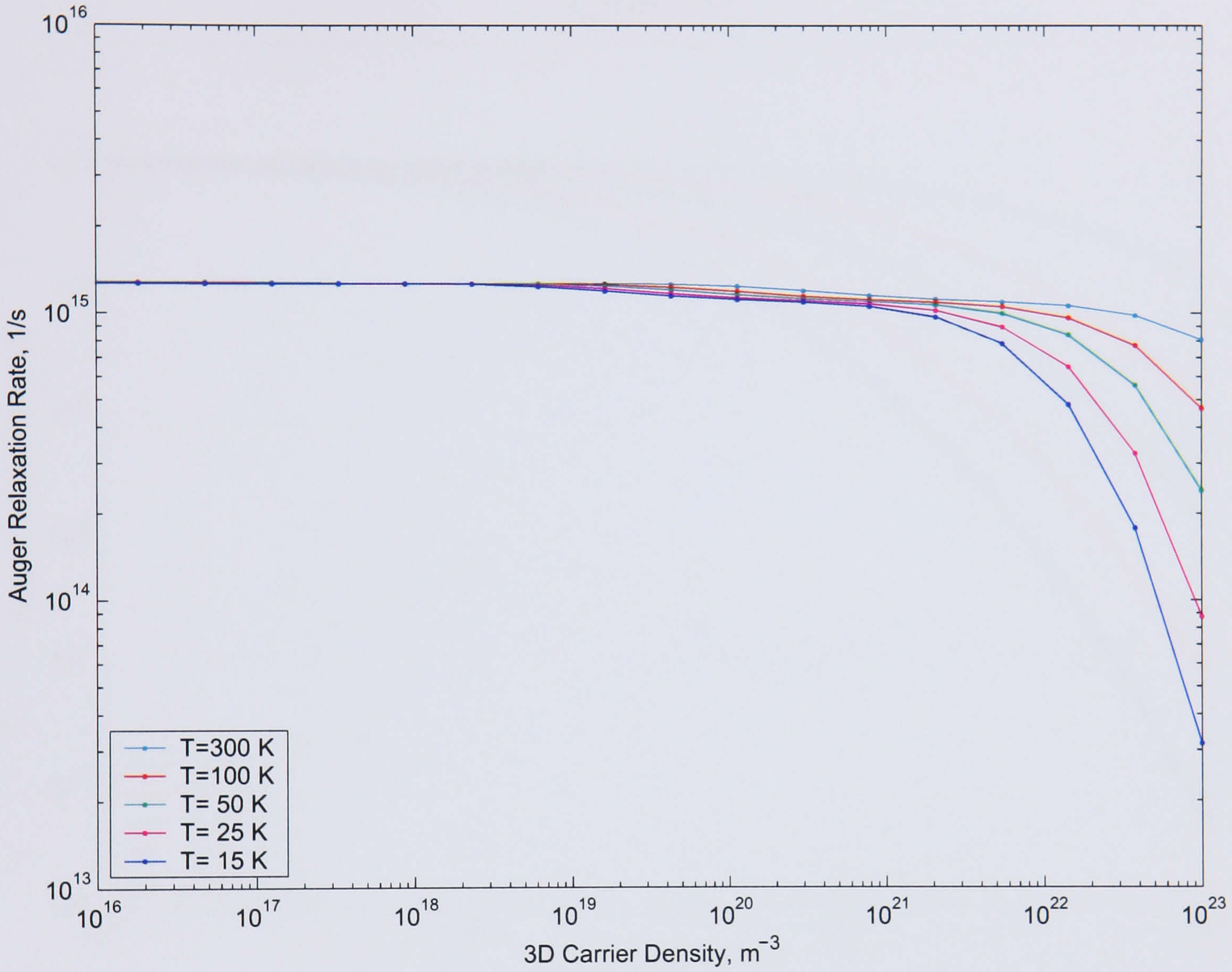

Figure 4.25: Auger Relaxation Rate dependence on the $3D$ carrier density calculated making use of the semi-analytical approach described in chapter 3, plotted for different temperatures and considering a $2D$ carrier density of $1 \times 10^{18} m^{-2}$.

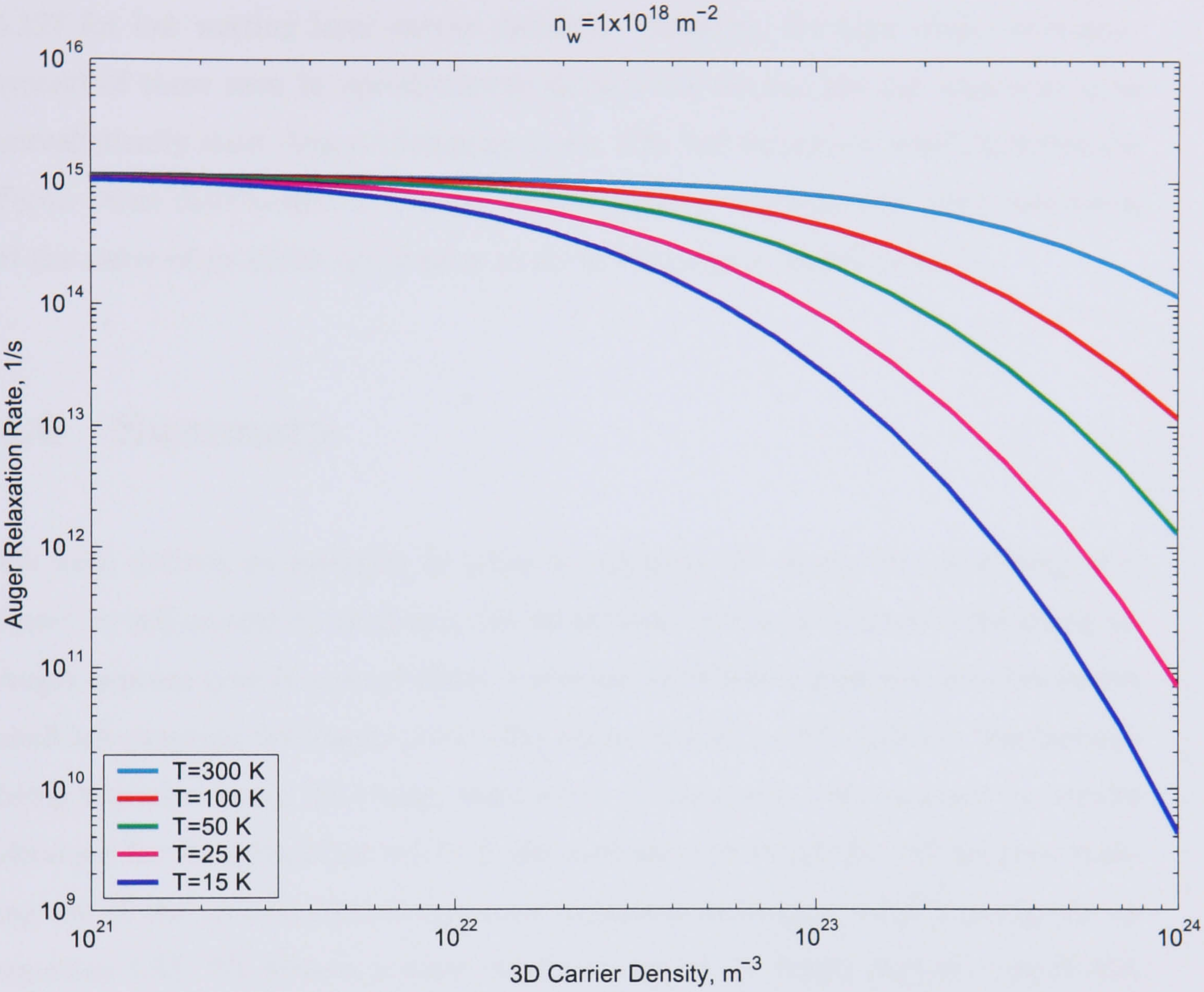

Figure 4.26: Auger Relaxation Rate dependence on the $3D$ carrier density for a $2D$ carrier density of $1 \times 10^{18} m^{-2}$, plotted for different temperatures and considering more points in the $3D$ carrier density range $[1 \times 10^{21} - 1 \times 10^{24} m^{-3}]$.

slower value of $4.89 \times 10^{13}\mathrm{s}^{-1}$ (see Fig. 4.24).

From these graphs it is clear that the results obtained from the semi-analytical calculation are in reasonable agreement with the full derivation given by equation 4.127 for low wetting layer carrier densities. However, for high carrier densities, typical of those seen in optoelectronic devices the semi-analytical approach gives unrealistically short Auger relaxation times. The full derivation which includes the Fermi-Dirac distribution in the $2D$ wetting layer predicts carrier relaxation times of the order of ps which are similar to those obtained in experiments [1].

4.6 Summary

We have derived an equation in order to calculate the Auger like scattering processes in self-assembled quantum dot structures. We have started considering an Auger capture type II process where a wetting layer hole is captured into the lowest confined quantum dot energy level, after scattering with a $0D$ electron, this last one being scattered into a $2D$ energy state in the wetting layer. We compare the results obtained for the calculation of the Auger capture type II rate for this process, making use of the semi-analytical approach explained in chapter 3 and those given by equation 4.62. We observe a more rapid increase of the Auger capture type II rate with the dot diameter when calculating the capture rate using the semi-analytical approach. This behavior is a result of the strong dependence on the dot diameter in the formula given by equation 3.20 in chapter 3. It is also highlighted in this chapter that the Auger capture type II rate obtained making use of the semi-analytical approach tends to zero for large values of dot diameter whereas a non-zero tendency is observed in the results given by equation 4.62. For very large dot radius it is reasonable to expect a non zero tendency of the capture type II rate, as the quantum dot becomes similar to a quantum well structure.

In this chapter, we have also studied an Auger relaxation process where an electron in the first excited confined state in a quantum dot structure relaxes into the ground energy level after scattering with a wetting layer electron, which is scattered into a higher energy level within the quantum well. We compare the results obtained for the calculation of the Auger relaxation rate for the described process, making use of the semi-analytical approach explained in chapter 3 and those given by equation 4.127. We commence comparing the dependence on the $3D$ carrier density of the Auger relaxation rates for an initial carrier density in the wetting layer of $n_w = 1 \times 10^{15}\mathrm{m}^{-2}$ and for different temperature values of the carriers in the structure. The results obtained by making use of the formula 4.127 and those given by the semi-analytical approach illustrate similar behavior. The Auger relaxation rate remains constant for low values of $3D$ carrier densities but for high $3D$ carrier densities the Auger relaxation rate decreases with the increasing carrier density. We observe that the Auger relaxation rate calculated by the semi-analytical approach explained in chapter 3 is independent on the temperature of the carriers for low carrier densities whereas an increase on the rate with increasing temperature is obtained when the Auger relaxation rate is calculated using equation 4.127. A faster relaxation rate is also obtained using the semi-analytical approach given in chapter 3 comparing to the values obtained using equation 4.127. We have performed the same calculations at a higher $2D$ carrier density of $10^{18}\mathrm{m}^{-2}$. As previously, much slower values of the Auger relaxation rate have been obtained when implementing equation 4.127 than those given by the semi-analytical approach.

We can conclude that for low wetting layer carrier densities, the results obtained from the semi-analytical calculation are in reasonable agreement with the full derivation given by equation 4.127 for low wetting layer carrier densities. However, for high carrier densities, typical of those seen in optoelectronic devices the semi-analytical approach gives unrealistically short Auger relaxation times. The full derivation which includes the Fermi-Dirac distribution in the $2D$ wetting layer predicts carrier relaxation times of the order of ps which are similar to those obtained in experiments

[1], [2].

Bibliography

[1] S. Grosse and J. H. H. Sandmann et al. *Physical Review B*, vol. 55:4473–4476, 1997.

[2] M. Grundmann and D. Bimberg. *Physical Review B*, vol. 55:pp. 9740–9745, 1997.

[3] P. Harrison. *Quantum Dots.* Wiley, 1997.

[4] H. Haug and S. W. Koch. *Quantum theory of the optical and electronic properties of semiconductors.* World Scientific, Third edition, 1990.

[5] I. Jacak, P. Hawrylak, and A. Wojs. *Quantum Dots.* Springer, 1997.

[6] Richard L. Liboff. *Introductory Quantum Mechanics, third edition.* Addison Wesley, 1997.

[7] J. H. Mathews. *Numerical Methods For Mathematics, Science, and Engineering, second edition.* Prentice Hall International, Inc., 1992.

[8] W. G. V. Rosser. *An introduction to STATISTICAL PHYSICS.* Ellis Horwood Publishers, 1982.

[9] A. V. Uskov, F. Adler, H. Schweizer, and M. H. Pilkuhn. *Appl. Phys.*, vol. 81(12), 1997.

[10] A. V. Uskov, J. McInerney, F. Adler, H. Schweizer, and M. H. Pilkuhn. *Appl. Phys. Lett.*, vol. 72(1), 1998.

Chapter 5

Energy level population dynamics in SADs

Contents

5.1 Introduction

This chapter focuses on the study of carrier transport in Self-assembled In(Ga)As quantum dot structures, where In(Ga)As quantum dots are formed on a single-crystal GaAs substrate via Stranski-Krastanov [10] epitaxial growth [4]. In this kind of structures, a quantum well, known as the wetting layer, aids the capture of charge carriers into the dots. As explained in previous chapters, these dots are grown on top of the wetting layer while the whole structure is covered by bulk material (Fig. 5.1).

We present a theoretical model to calculate the energy level occupation probability of each dot within a self-assembled ensemble which then allows us to model the gain and spontaneous emission spectra on these quantum dot structures. The ensemble considered consists of a number of different sized dots with randomly varying radii between 18 nm to 20 nm and equal heights of 5 nm. As we have previously mentioned, we consider that the quantum dots (QD) are grown on top of a 1.6 nm-thick quantum well, also known as wetting layer (WL). Initially, carriers diffuse in the lower-band gap $2D$ WL before either being captured by the SADs or recombining either radiatively or non-radiatively.

Dividing the dot ensemble into N different groups depending on their radii, the aim of the model we present is to be able to determine the state (each dot type energy level occupation probability) for all different dot types as a function of time, as well as the gain spectra of the self-assembled quantum-dot structures. Therefore, the carrier occupation of the confined states of each dot type, may be established as a

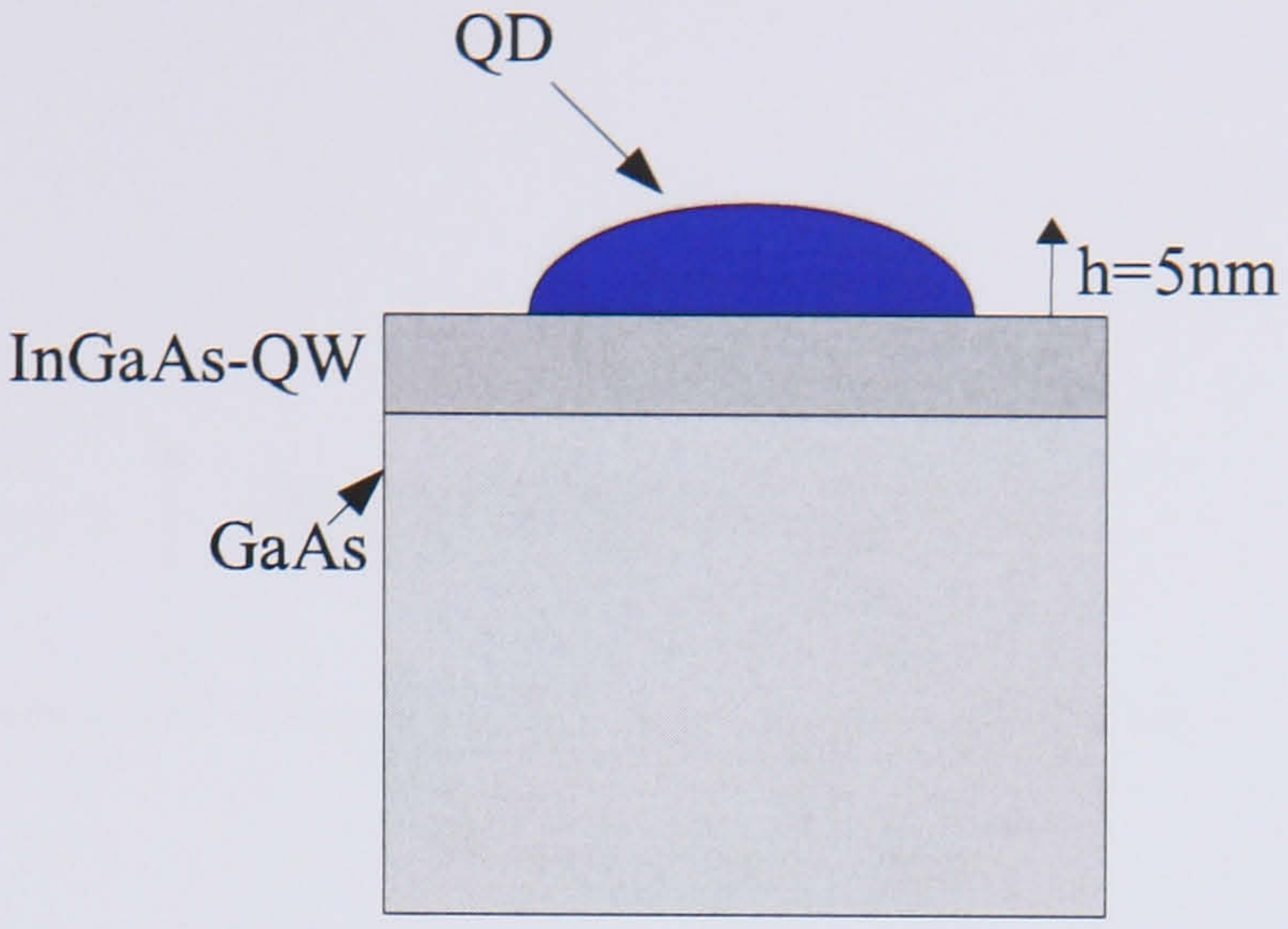

Figure 5.1: Illustration of a self-assembled quantum dot on top of the wetting layer, both embedded in bulk material.

function of time.

5.2 Representation of the dot occupancy

In order to define our model, we will first analyze the different mechanisms involved in the change of carrier populations within the quantum dot. Carriers diffuse through the WL before being captured by the quantum dot due to carrier-carrier Coulomb scattering. Once within the quantum dot these carriers may recombine either radiatively or nonradiatively. Auger-like energy transfer between carriers will describe the intraband relaxation of carriers into different energy levels (see Fig. 5.2).

We consider the Auger capture and relaxation processes in InAs/GaAs quantum dot structures previously described in chapter 4(see Fig. 5.2). We observed that among the Auger capture processes we might distinguish between two types. Type

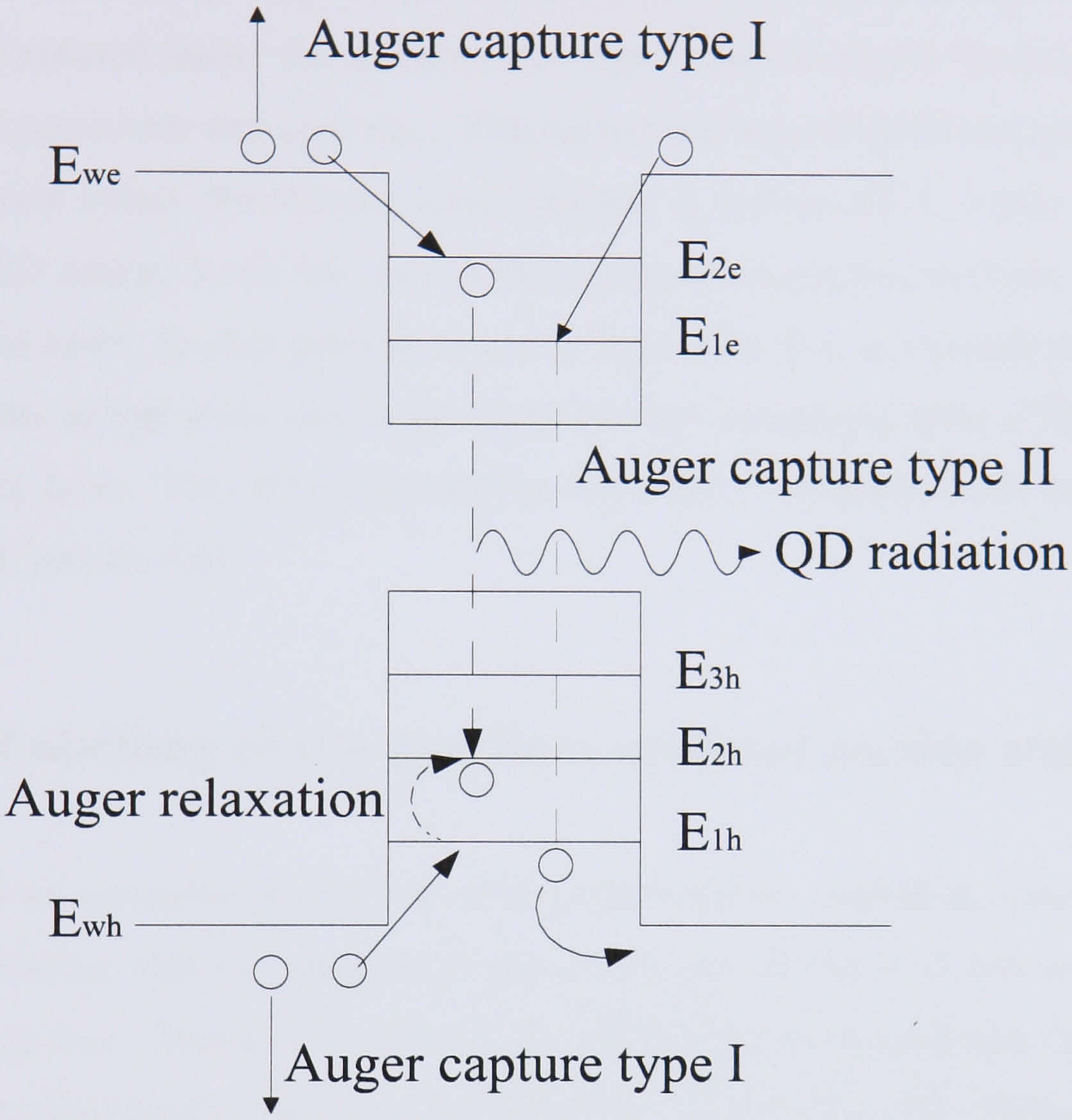

Figure 5.2: A schematic picture of the different scattering mechanisms involved in the carrier dynamics within the SAD structure. E_{we}, E_{wh} are the lowest electron energy levels in the conduction and valence bands respectively.

I capture process involved a $2D$ carrier (either an electron or a hole in the wetting layer) capture/ejection by the QD structure, after colliding with another $2D$ carrier which is scattered to another higher/lower energy state in the wetting layer (see chapter 4, section 4.4). Type II capture processes, refer to transitions where a 2D carrier is captured inside the quantum dot due to carrier-carrier Coulomb scattering with a previously captured one. This carrier was excited from the quantum dot to a 2D state within the wetting layer (chapter 4, section 4.3). Auger relaxation between QD energy levels was due to the Coulomb interaction between carriers in the wetting layer. In this process, a carrier inside the dot, is relaxed/excited to a lower/higher energy state due to the Coulomb-like interaction with a 2D carrier in the wetting layer. This 2D carrier will be scattered to a higher/lower energy level (chapter 4, section 4.5).

5.2.1 Labelling of the quantum confined carrier states

We model an ensemble of quantum dots preserving the individual nature of each dot, considering that the occupation dynamics each of the dots has no effect on neighboring dots. Taking into account the fact that there is quantum confinement in the three dimensions, discrete energy levels for the carriers exist within the structure. The Pauli exclusion principle only allows one electron per state, therefore, we make use of a binary notation to describe the state of each quantum dot (a factor of 2 is included in all calculations to allow for spin up and spin down electrons). While the existence of a carrier in a particular energy state of the dot is represented by a 1, a 0 will symbolize its absence. Consequently, the number of confined energy levels in each dot will determine the number of possible 'binary states' where the dot might be found within the structure. The least significant digits will represent energy levels for the electrons (starting from the lowest energy level), whereas there will be as many binary digits for electrons/holes as electron/hole-energy-levels in each dot. Figure 5.3 shows how a recombination process for a five-energy-level dot (2 energy levels for electrons and 4 for holes) may be described by the use of binary notation. This dot with an initial pair of electron-hole in E_{2e} and E_{2h} energy levels respectively, thus in n_{001010} binary state, remains empty, i.e in n_{000000} state, after a $E_{2e} - E_{2h}$ recombination process. For simplicity, in this chapter we give an example of the calculation of the dynamics of a 3-energy-level quantum dot amid the ensemble as shown in figure 5.4.

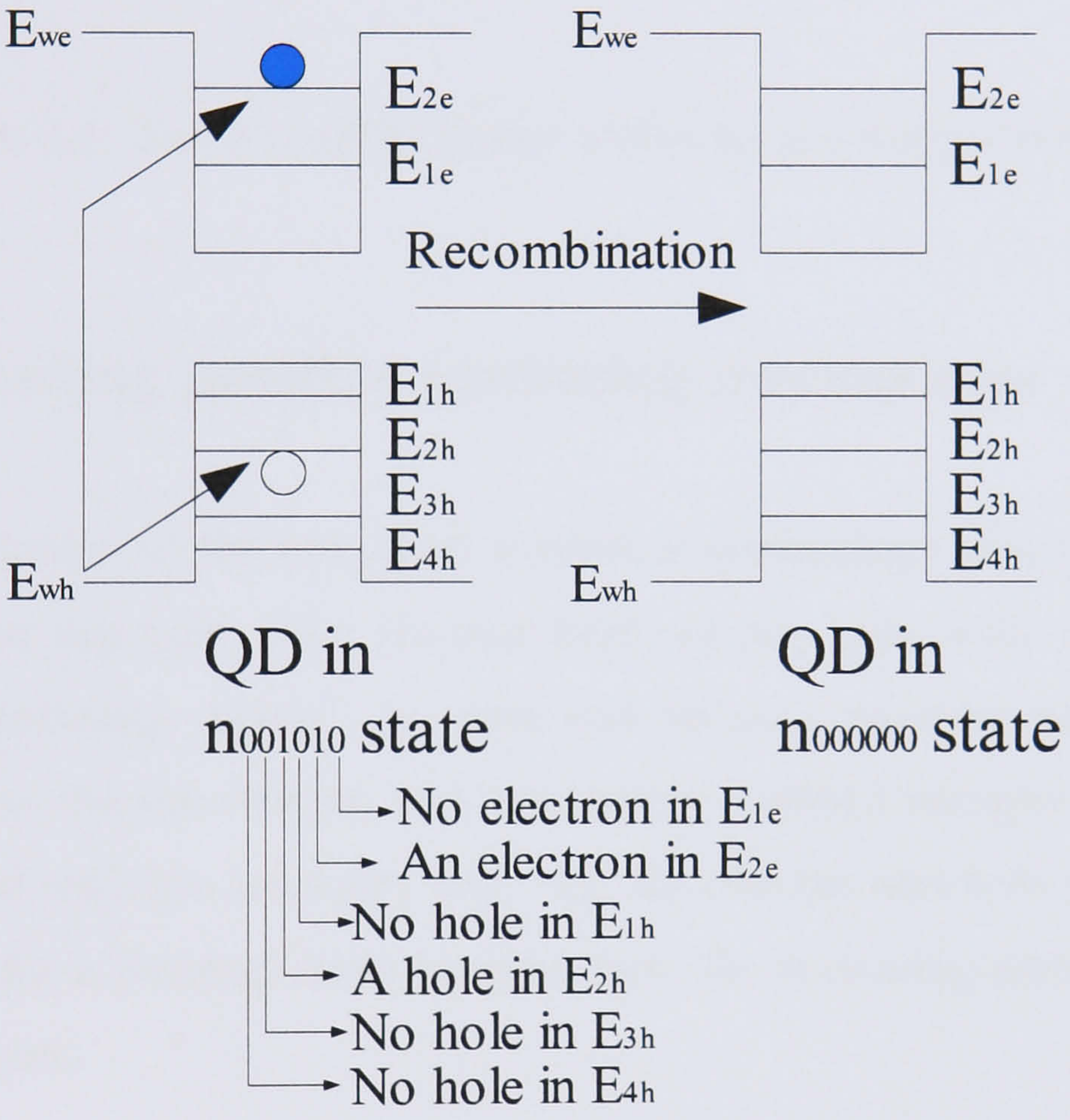

Figure 5.3: Explanation of a recombination process for a six-energy-level quantum dot, making use of binary notation.

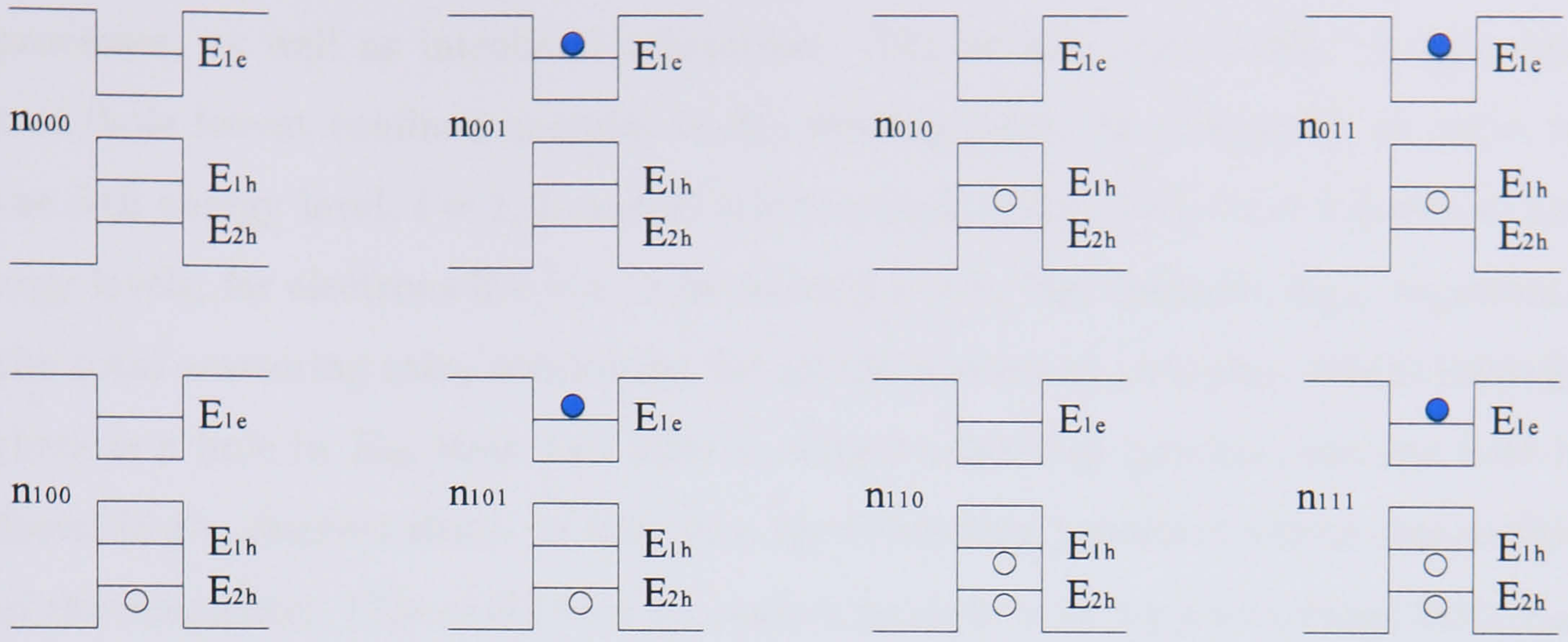

Figure 5.4: The 8 possible binary states for a 3-energy-level QD.

5.2.2 Labelling possible scattering mechanisms

In order to consider all the intraband scattering mechanisms that induce a binary state change for this type of dot (to pass from one particular state to another), we construct a 'scattering matrix', M, rows and columns represent the dot's energy levels as well as the the electron and hole lowest confined energies in the wetting layer, described with the subscript 'we', 'wh' for electron and hole respectively. In this example, for a 3-energy-level quantum dot, the scattering matrix M, may be written as follows:

$$M = \begin{pmatrix} 0 & a_{1ewe} & a_{1e1h} & a_{1e2h} & a_{1ewh} \\ a_{we1e} & 0 & a_{we1h} & a_{we2h} & a_{wewh} \\ a_{1h1e} & a_{1hwe} & 0 & a_{1h2h} & a_{1hwh} \\ a_{2h1e} & a_{2hwe} & a_{2h1h} & 0 & a_{2hwh} \\ a_{wh1e} & a_{whwe} & a_{wh1h} & a_{wh2h} & 0 \end{pmatrix} \tag{5.1}$$

where $a_{E_{FROM}E_{TO}}$ represents the total scattering rate for a carrier transition involving E_{FROM} and E_{TO} energy levels, taking into account both type I and II capture processes, as well as intraband relaxation. The letters we/wh refer to the electron/hole lowest confined energies in the wetting layer. In this study, ic refers to the i-th energy level, $i = 1, 2..numE$ where $numE$ is the dot's total number of energy levels, for electrons if $c = e$ or for holes if $c = h$. For example, a_{2h1h} represents the total scattering rate, accounting for all the scattering processes where initially there is a hole in E_{2h} state and after a certain scattering process, another hole is found in E_{1h} discrete state. In this case, two scattering process could be responsible of this transition. One could be a relaxation process, where a hole relaxes from E_{2h} to E_{1h} energy level. The other could be a capture type II process, where a hole in E_{2h} is scattered into the wetting layer while another hole is captured into E_{1h} energy level.

Taking into account the different binary states for a 3-energy-level quantum dot (Fig. 5.4), the scattering processes involved in the transition from n_{100} state to n_{010} and viceversa are (see Fig.5.5):

1. A relaxation process from E_{2h} to E_{1h} (figure 5.5(a))
2. A capture type II process, where a hole is captured into energy level E_{2h}, due to a scattering process with a previously captured hole in energy level E_{1h} (process described in figure 5.5(b))

It should also be noticed that LO-phonon-carrier capture processes have also been considered in the calculation of all the scattering mechanisms responsible for binary state change of the quantum dot. In a LO-phonon-carrier capture/escape process, a wetting layer carrier is captured/escape by/from the dot by scattering with a bulk LO-phonon (see appendix A). For example, a_{we1e} represents the total scattering rate, accounting for all the scattering processes where initially there is a en electron in the wetting layer which gets captured by the quantum dot into E_{1e} energy level. In this case, two scattering process could be responsible of this transition. One could

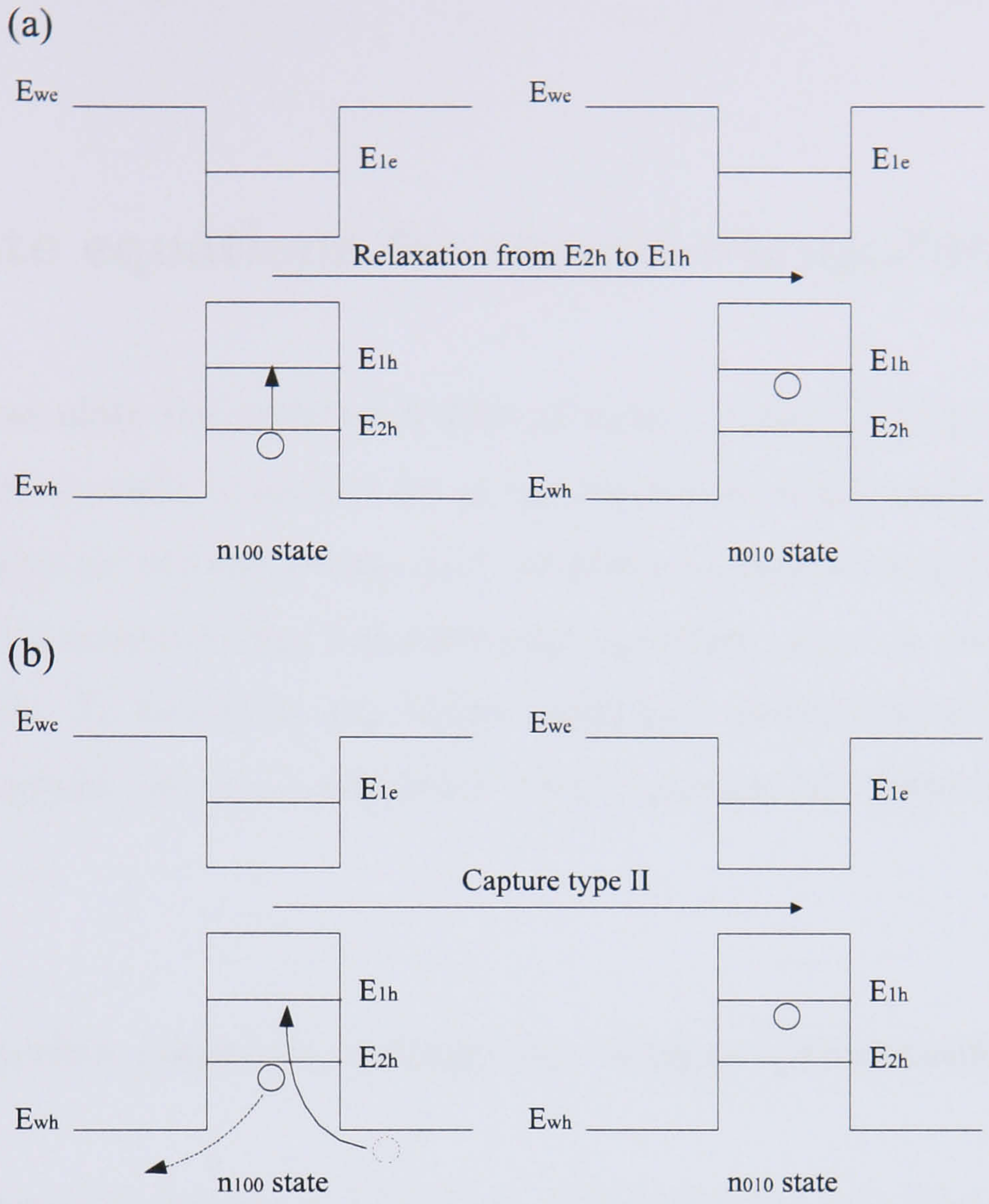

Figure 5.5: (a) Binary state transition after a carrier relaxation process. (b) Binary state transition after a type II capture process. Here a $2D$ hole is captured by the dot, after scattering with a previously captured hole, which is excited from the dot into the wetting layer

be a capture type I process, where a $2D$ electron, after scattering with a $2D$ carrier is captured into E_{1e} $0D$ state. The other could be a LO-phonon-carrier scattering process, where a $2D$ electron is captured into E_{1e} $0D$ state after after scattering with a with a bulk LO-phonon. The calculation for the LO-phonon-carrier capture rates have been carried out by J. Domínguez [8] (see appendix A).

5.3 Rate equations for carrier occupation

In order to calculate the number of dots of radii D (type D dots) in any given binary state s, we need to solve a set of rate equations which need to incorporate terms to account for capture/escape and radiative recombination processes. In this section, we will construct the necessary rate equations, step by step introducing those processes. To determine the carrier occupation probability of each dot type within the ensemble, we have considered a high constant 2D carrier density of $1 \times 10^{15}\mathrm{m}^{-2}$.

5.3.1 Carrier capture/escape by Auger processes

Considering any one particular dot with a radius D within the ensemble, we may calculate the probability of finding this type of dots in a particular s binary state taking into account all the different Auger capture/escape processes responsible for obtaining this considered binary representation s. The rate equation for the number of dots represented by in a binary state represented by s is:

$$\frac{\mathrm{d}N_s^D}{\mathrm{d}t} = -N_s^D \sum_{i,j} a_{ij} + \sum_{i,j,k_{ij}} a_{ij} N_{k_{ij}}^D \tag{5.2}$$

where N_s^D is the number of dots within the ensemble, which have radii equal to D in the s binary state. s refers to the decimal number corresponding to the binary representation. The indices i, j correspond to the different energy levels of the dot type D, so that, for the 3-energy-level dot pictured in figure 5.5, $i, j = 1e, 1h, 2h, we, wh$ (Eq. 5.1). Note $i \neq j$

The second term on the right in Eq. 5.2, symbolizes all different binary states from which the state s could be reached, after a number of scattering processes involving (i,j) energy levels.

5.3.2 Photon interaction

If we now consider only those processes where photons are involved, the number a D radius quantum dots within the ensemble in a particular s binary state, may be given as follows:

$$\begin{aligned}\frac{\mathrm{d}N_s^D}{\mathrm{d}t} &= -\sum_{m\in m^D} R^{spon}_{N_s^D,m} + \sum_{l,m\in m^D} R^{spon}_{N_l^D,m} \\ &\quad -\frac{c\Gamma}{n_r}\sum_{m\in m^D}\left|g_{N_s^D,m}\right| S_m + \frac{c\Gamma}{n_r}\sum_{l,m\in m^D}\left|g_{N_l^d,m}\right| S_m \qquad (5.3)\end{aligned}$$

where Γ is the optical confinement factor and n_r is the refractive index. The terms $g_{N_s^D,m}$ and $R^{spon}_{N_s^D,m}$ represent the contribution to the optical gain and spontaneous emission respectively, that D-type group of dots in binary state s contribute to photons of transition energy m. Note that only recombination processes involving electron and hole energy levels with the same quantum numbers are allowed. The index l in the summations denotes the number of different binary states the dot may be found in. For example, $l = 0, 1, ...2^3$ for the 3-energy-level quantum dot pictured in figure 5.5.

The first term on the right in Eq. 5.3, describes the number of final binary states that could be arrived at from an initial binary state s after spontaneous recombination process. While the second term describes the number of initial states which the final state s might be attained from. In the same way, the last two terms on the right represent the radiative recombinations due to stimulated emission as a result of gain in the semiconductor structure. In the next section we describe how the optical gain and spontaneous emission terms can be calculated.

5.3.3 Optical gain and spontaneous emission

In chapter 2 a derivation of the optical gain and spontaneous emission was described. Following reference [9] and using our binary representation for the quantum confined states in each dot within the ensemble, we calculate the optical gain as follows:

$$\begin{aligned} g(E) &= \frac{2\pi e^2 \hbar}{c n_r \epsilon_0 m_0^2} \sum_{e,h} \frac{|P^{\sigma}{}_{eh}|^2}{E_{eh}} \sum_{s} \left[N_s^{E_{eh}} \left(f_e^{E_{eh},s} + f_h^{E_{eh},s} - 1 \right) \right] \\ &\times \int_{-\infty}^{\infty} B_{eh}(E - E') \mathrm{d}E' \end{aligned} \qquad (5.4)$$

for n_r refractive index. The subscripts e, h refer to the discrete states in the conduction and valence band respectively and E_{eh} represents the energy of the interband transition between the discrete energy levels e and h. P^{σ}_{eh} is the transition matrix element [1]. $f_e^{E_{eh},s}$ and $f_h^{E_{eh},s}$ terms represent the existence (1) or absence (0) of an electron or a hole respectively in the discrete state in the conduction band e and in the valence band h. $N_s^{E_{eh}}$ is the number of dots in binary state s which have an interband transition energy between e and h energy levels of E_{eh}. For example, supposing we consider a dot with an energy structure consisting of 1-energy-level for the holes and 1-energy-level for electrons, then the interband transition energy between the electron/hole ground-energy levels would be $E_{eh} = E_{1e1h}$ (as pictured in figure 5.6). For this 2-energy-level quantum dot in $s = 1$ binary state, i.e., n_{01} state using binary representation, pictured in figure 5.6, $f_e^{E_{1e1h},1} = 1$ and $f_h^{E_{1e1h},1} = 0$. The total optical gain for a given energy E, has been calculated taking into account the contribution of all dots within the ensemble as a Lorentzian homogeneous broadening $B_{eh}(E - E')$ (see Eq. 5.4) around that energy, due to carrier scattering.

The Lorentzian linewidth broadening is given in terms of a convolution as [9]

$$B_{eh}(E-E') = \frac{\frac{\hbar\Gamma_{eh}}{\pi}}{(E-E')^2+(\hbar\Gamma_{eh})^2} \tag{5.5}$$

Here $2\hbar\Gamma_{eh}$ is the lifetime broadening factor, E is the center energy of the optical mode, Γ_{eh} is the scattering rate taking into account all the scattering processes which involved carrier transitions between e and h quantum dot energy levels, so that, using the notation explained in Eq. 5.1, for a 3-energy-level dot(2 for the holes, 1 for the electrons) with an interband transition energy E_{1e1h}, involving E_{1e} and E_{1h} energy levels and a scattering matrix M (Eq. 5.1), Γ_{1e1h} would be calculated as follows:

$$\Gamma_{1e1h} = \left\{\sum_{i=1}^{5} a_{1i} + \sum_{i=1}^{5} a_{i1}\right\} + \left\{\sum_{i=1}^{5} a_{3i} + \sum_{i=1}^{5} a_{i3}\right\} - a_{11} - a_{33}$$

Note that we sum over all the quantum confined states of the quantum dot and the two wetting layer levels (for our 3-energy-level dot the summation is over 5 states). Using the same notation as the one adopted for the calculation of the optical gain, we can determine the spontaneous emission for a given energy E [9] considering the Lorentzian broadening of the optical transitions given by Eq. 5.5, as follows:

$$\begin{aligned} R^{spon}(E) &= \frac{4n_r\pi e^2}{\epsilon_0 c^3 m_0^2 \hbar^2} \sum_{e,h} |P^{\sigma}{}_{eh}|^2 E_{eh} \sum_{s} \left[N_s^{E_{eh}} (f_e^{E_{eh},s} f_h^{E_{eh},s})\right] \\ &\times \int_{-\infty}^{\infty} B_{eh}(E-E')\mathrm{d}E' \end{aligned} \tag{5.6}$$

where n_r, $P^{\sigma}{}_{eh}$, $f_e^{E_{eh},s}$, $f_h^{E_{eh},s}$ and $N_s^{E_{eh}}$ are exactly the same terms as the ones in Eq. 5.4.

5.3.4 Photon Rate Equation

We have now completely described the rate equation for the carriers in the system. Now, we need to take account of the contribution of all the quantum dots within the structure to each of the energy transitions. The photon density in a particular energy transition m, S_m within the structure, may be calculated by solving a rate equation of the form

$$\frac{\mathrm{d}S_m}{\mathrm{d}t} = \beta\sum_{l,d} R^{spon}_{N_l^d,m} + \frac{c\Gamma}{n_r}\sum_{l,d} g_{N_l^d,m} S_m - \frac{S_m}{\tau_p} \tag{5.7}$$

where Γ in equations 5.3 and 5.7, is the optical confinement factor, β is the spontaneous emission coupling efficiency to the lasing mode and τ_p is the photon lifetime in the cavity. In order to calculate the contribution to each energy transition of all the quantum dots within the structure, we may calculate using Eq. 5.4 and Eq. 5.6, each type contribution at a particular energy transition m (i.e. $\sum_{l,d} R^{spon}_{N_l^d,m}$ and $\sum_{l,d} g_{N_l^d,m}$) taking into account all the different binary states l that each dot type d may be found in the ensemble.

5.3.5 Final rate equations

The final set of rate equations for the carrier population within the quantum dot of radius D including both capture/escape processes and radiative recombination processes is given by

$$\begin{aligned}\frac{\mathrm{d}N_s^D}{\mathrm{d}t} = {} & -N_s^D\sum_{i,j} a_{ij} + \sum_{i,j,k_{ij}} a_{ij}N_{k_{ij}}^D - \sum_{m\in m^D} R^{spon}_{N_s^D,m} + \sum_{l,m\in m^D} R^{spon}_{N_l^D,m} \\ & -\frac{c\Gamma}{n_r}\sum_{m\in m^D}\left|g_{N_s^D,m}\right| S_m + \frac{c\Gamma}{n_r}\sum_{l,m\in m^D}\left|g_{N_l^D,m}\right| S_m\end{aligned} \tag{5.8}$$

and the rate equation for the photon density at the energy transition m is given by

$$\frac{\mathrm{d}S_m}{\mathrm{d}t} = \beta\sum_{l,d} R^{spon}_{N_l^d,m} + \frac{c\Gamma}{n_r}\sum_{l,d} g_{N_l^d,m} S_m - \frac{S_m}{\tau_p} \tag{5.9}$$

In order to determine the energy level population probability of each of the dot types within the ensemble, we need to solve a rate equation as the one given by Eq. 5.8 for each type of dot (for all different radii in the ensemble) and for all the different binary states where each type of dot may be found within the ensemble. Hence, for a 8-energy-level quantum dot type, we will need to solve 2^8 different rate equations of the form of Eq. 5.8.

In a laser cavity the Fabry-Perot etalon defines a set of wavelengths which can lase. In this study we have ignored this complication and we simply assume that lasing occurs at the peak of the gain spectrum. Since we are studying the properties of the material gain this has no bearing on the results in this thesis.

5.3.6 Example of the calculation

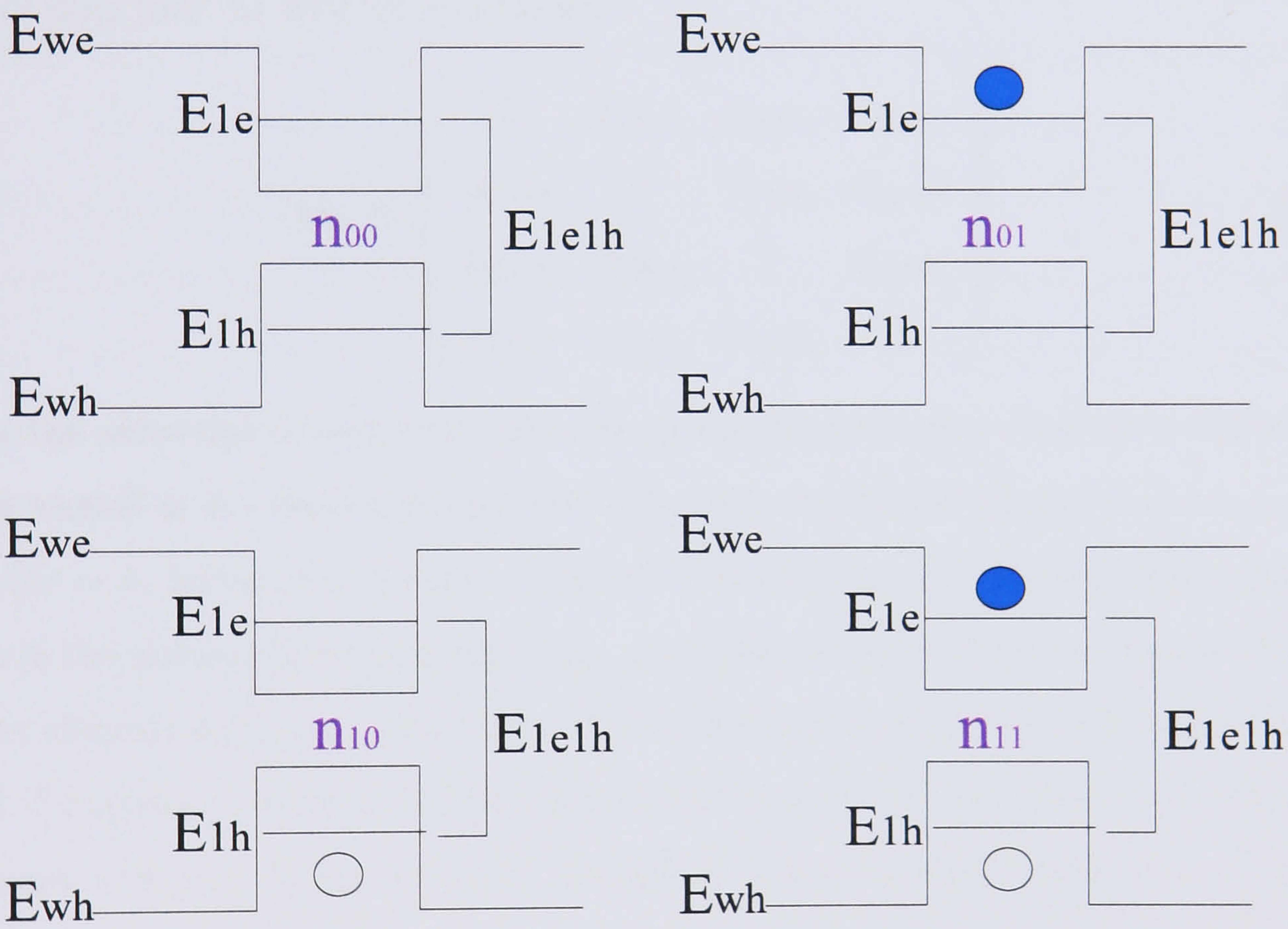

Figure 5.6: Binary state representation of a single electron-hole energy-level quantum dot. We have 2^2 different binary states, i.e., n_{00}, n_{01}, n_{10} and n_{11}.

In order to illustrate the calculation of the rate equations (5.8) and (5.7) for a N^D number of dots with radii equal to D nm within the ensemble, assuming that this type of dots have an energy structure consisting of a single electron/hole-energy-level, with an interband transition energy of E_{11} eV (see figure 5.6). Hence the dots of radius D may be found in 2^2 different binary states depending on the existence or absence of a carrier in their two discrete $0D$ states (see Fig. 5.6). Therefore we can denote n_{ij} for $i, j = 0, 1$ as the number of dots within the ensemble with i electrons in E_{1e} electron-energy-level (see Fig. 5.6) and j holes in E_{1h} hole-energy-level. Figure 5.6 shows the 4 different situations that type D dots may be found within the ensemble. Taking into account Eq. 5.1, the scattering matrix for this type of dots may be written as follows:

$$M_D = \begin{pmatrix} 0 & a_{1ewe} & a_{1e1h} & a_{1ewh} \\ a_{we1e} & 0 & a_{we1h} & a_{wewh} \\ a_{1h1e} & a_{1hwe} & 0 & a_{1hwh} \\ a_{wh1e} & a_{whwe} & a_{wh1h} & 0 \end{pmatrix} \tag{5.10}$$

where the subscript ic represents the i-th quantum dot energy level ($i = 1, 2..numE$ where $numE$ is the dot's total number of energy levels) for electrons if $c = e$ or for holes if $c = h$. Subscripts we and wh are the electron and hole lowest confined energy levels in the wetting layer (see Fig. 5.6). As explained in previous section, each of the matrix element $a_{E_{FROM}E_{TO}}$ represents the total scattering rate considering both type I and II capture processes, LO-phonon-carrier capture [8] and intraband relaxation processes (chapter 4) for a carrier transition where initially there is a carrier in E_{FROM} energy level (either a $0D$ or $2D$ energy level) and after the scattering event, an initially empty energy level E_{TO} is filled with a carrier. The elements in the scattering matrix (Eq. 5.1) which represent transitions involving energy levels for electrons and holes, i.e, a_{1h1e}, a_{1hwe}, a_{1e1h}, a_{1ewh}, a_{we1h}, a_{wewh}, a_{wh1e}, a_{whwe}, refer to Auger capture type II scattering processes. $a_{E_{FROM}E_{TO}}$, when referring to type II capture processes, represents a capture type II process where a $2D$ carrier in the wetting layer is captured by the quantum dot into E_{TO} energy level, after scattering with a previously captured $0D$ carrier in E_{FROM}, this last one being scattered into the wetting layer. Only the coefficients a_{1h1e} and a_{1e1h} in equation 5.10 describe a possible capture type II process. The rest, are set to zero. These coefficients may be calculated either semi-analytically following the equation given for the capture type II scattering process in chapter 3 (Eq. 3.20) or following the equation 4.62 derived in chapter 4.

Using equations 5.8 and 5.9, the set of rate equations required in order to calculate the energy level occupation probability of this type of quantum dots (Fig. 5.6), as well as their contribution at the energy transition $m = E_{1e1h}$, may be written as follows:

$$\begin{aligned}
\frac{\mathrm{d}n_{00}}{\mathrm{d}t} &= a_{1ewe}n_{01} + a_{1hwh}n_{10} - n_{00}\left[a_{1we1e} + a_{wh1h}\right] + R^{spon}_{n_{11},m} \\
&+ \frac{c\Gamma}{n_r}\left[|g_{n_{11},m}| - |g_{n_{00},m}|\right] S_m \\
\frac{\mathrm{d}n_{01}}{\mathrm{d}t} &= a_{1hwh}n_{11} + a_{we1e}n_{00} - n_{01}\left[a_{wh1h} + a_{1ewe}\right] \\
\frac{\mathrm{d}n_{10}}{\mathrm{d}t} &= a_{1ewe}n_{11} + a_{wh1h}n_{00} - n_{10}\left[a_{we1e} + a_{1hwh}\right] \\
\frac{\mathrm{d}n_{11}}{\mathrm{d}t} &= a_{wh1h}n_{01} + a_{we1e}n_{10} - n_{11}\left[a_{1ewe} + a_{1hwh}\right] - R^{spon}_{n_{11},m} \\
&+ \frac{c\Gamma}{n_r}\left[-|g_{n_{11},m}| + |g_{n_{00},m}|\right] S_m
\end{aligned} \tag{5.11}$$

and this type of dots will contribute to the m-th mode as follows:

$$\begin{aligned}
\frac{\mathrm{d}S_m}{\mathrm{d}t} &= \beta\left[\sum_{l,d\neq D} R^{spon}_{N_l^d,m} + R^{spon}_{n_{11},m}\right] + \frac{c\Gamma}{n_r}\left[\sum_{l,d\neq D} g_{N_l^d,m} + \left[|g_{n_{11},m}| - |g_{n_{00},m}|\right]\right] S_m \\
&- \frac{S_m}{\tau_p}
\end{aligned} \tag{5.12}$$

using (5.4) and (5.6) we can calculate the gain and spontaneous emission coefficients in the equations above as follows:

$$\begin{aligned}
g_{n_{00},m} &= \frac{2\pi e^2\hbar}{cn_r\epsilon_0 m_0^2}\frac{\left|{P^\sigma}_{1e1h}\right|^2}{E_{1e1h}}\left[n_{00}(0+0-1)\right] \\
g_{n_{11},m} &= \frac{2\pi e^2\hbar}{cn_r\epsilon_0 m_0^2}\frac{\left|{P^\sigma}_{1e1h}\right|^2}{E_{1e1h}}\left[n_{11}(1+1-1)\right] \\
R^{spon}_{n_{11},m} &= \frac{4n_r\pi e^2}{\epsilon_0 c^3 m_0^2\hbar^2}\left|{P^\sigma}_{1e1h}\right|^2 E_{1e1h}\left[n_{11}(1\times 1)\right]
\end{aligned} \tag{5.13}$$

In order to make computational calculations much faster, we have not included the homogeneous broadening in the calculation of each dot type binary state contribution into each mode ($g_{n_s,m}$), when solving the rate equations for the calculation of the lasing spectra and energy level occupation probability. However, it has been considered to calculate the total optical gain of the structure.

5.3.7 Comparison with other quantum dot models

Several other models describing the carrier dynamics of quantum dot structures have been reported in the literature. One type of model treats the distribution of dot sizes as an inhomogeneous broadening of the discrete density of states (e.g. [9]). This type of model inherently assumes a global thermal equilibrium and that all dots can be described by one Fermi-Dirac distribution. However, calculations of this kind cannot describe non-equilibrium effects, for example the simulation of time resolved photoluminescence.

Rate equation models are often used to describe the dynamics of quantum dot lasers and calculations with different degrees of complexity have been reported in the literature. Simple rate equations for the population of a quantum dot usually ignore the effect that different dot sizes contribute to different optical transition wavelengths. Therefore spectral hole burning can not be accurately predicted (for example [7]).

Another common problem with certain rate equation models is that the occupancy of the levels is calculated using continuous variables rather than discrete occupancy factors of 0 and 1. This can lead to problems with the prediction of dynamics in non-equilibrium regimes.

Our model includes occupancy dependent scattering rates in a rate equation model so that capture and emission processes are calculated correctly (e.g. an electron is more likely to be captured by a dot which has already captured a hole). Even the most complicated models reported to date (for example [5], [3]) neglect this important phenomenon.

5.3.8 Numerical results

The numerical results we present in this chapter have been obtained by integrating the rate equations described in section 5.3 for 1000 ps. As previously mentioned, we have considered an ensemble consisting of 5×10^{22} 'lens'-shaped dots per m^3 where 30 different dot types (depending of their radii) may be found. Therefore, $5 \times 10^{22}/30$ would be the number of dots per m^3 belonging to a particular dot type, although a more realistic Gaussian distribution of radii could have been considered instead. The Scattering rates used have been calculated following the derived formulas for the calculation of the Auger capture type II and Auger relaxation rates, previously formulated in chapter 4 (see Eq. 4.62 and Eq. 4.127). We have considered the semi-analytical formula given in chapter 3 (see Eq. 3.19) for the calculation of the Auger capture type I rates and the LO-phonon-carrier capture rates carried out by J. Domínguez [8].

The parameters we have used are as follows; $m_e = 0.0445\, m_0$ and $m_e = 0.08\, m_0$, the effective masses for electrons and holes respectively [6]. We have estimated equal values of temperatures of the $2D$ wetting layer and $3D$ barrier carriers, i.e., $T_2 = T_3 = 300$ K. For the parameters of the cavity we have considered a confinement

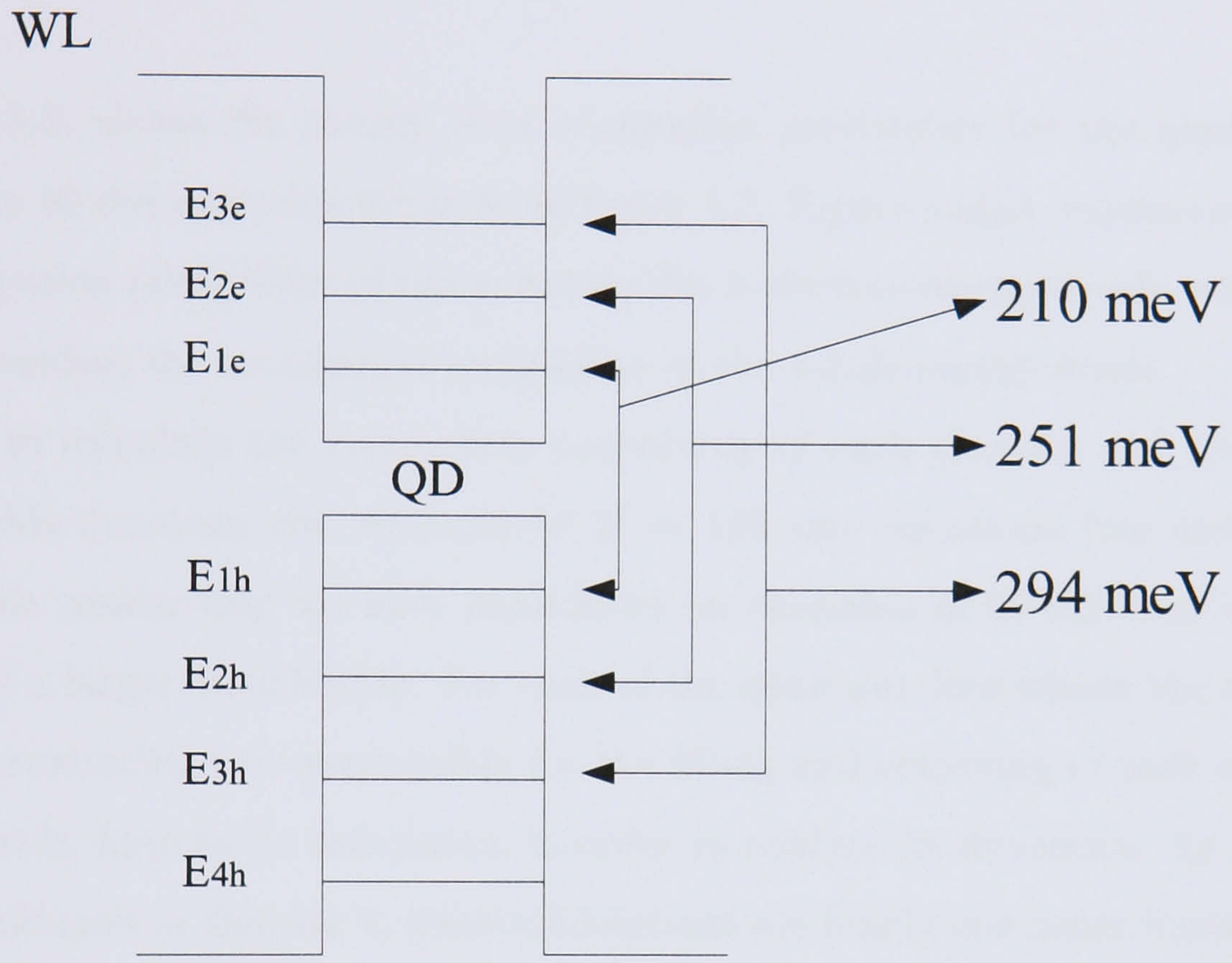

Figure 5.7: Schematic representation of the transition energies of a particular type of dot within the ensemble of radius 19.6 nm and 5 nm height.

factor $\Gamma = 6\%$, the refractive index $n_r = 3.5$, the spontaneous emission coupling efficiency to the lasing mode $\beta = 10^{-4}$ and the photon lifetime $\tau_p = 8.8$ ps [9]. Running our model for a time interval of 1000 ps, we analyze the effect of the carrier dynamics on the optical gain characteristics and allude to the consequences of using quantum dot structures for the active regions of semiconductor laser diodes and optical amplifiers.

Figure 5.8, shows the energy level occupation probability for the quantum dot within the 30-dot ensemble depicted in figure 5.7. Figure 5.8(a), represents the carrier occupation probability of the quantum dot 3-electron-energy-levels, while figure 5.8(b) describes the occupation probability of the 4-hole-energy-levels.

In order to calculate the occupation probability of each electron and hole energy level of this quantum dot we required $2^7 = 128$ rate equations (see section 5.3). This is the reason why we have considered an ensemble of 30 different dot series instead of a larger distribution. For each of the quantum dots within the ensemble, the total scattering rate responsible for the filling and emptying of each of the dot energy levels, have to be calculated, in order to analyze its dynamics. As we previously mentioned in chapter 4, these calculations are highly computer intensive. For example, it took us 10 days on a 2.00 GHz AMD Athlon processor, to obtain the Auger capture type II rates considering each possible carrier transition of each of the quantum dots within the 30 dots ensemble. Running our rate equation model for 1000 ps, required 3 days.

As can be seen in figure 5.8, each energy level of the quantum dot plotted in Fig. 5.7 starts filling with carriers during the first $\sim$ 20 ps.

The highest electron-energy-level, E_{3e}, starts first filling with carriers, as the energy separation between the wetting layer state and the highest confined quantum dot level is smaller, making the capture of carriers more probable than capture to lower energy levels. Then, the discrete state E_{2e} starts to fill with carriers by scattering from E_{3e} and finally E_{1e}.

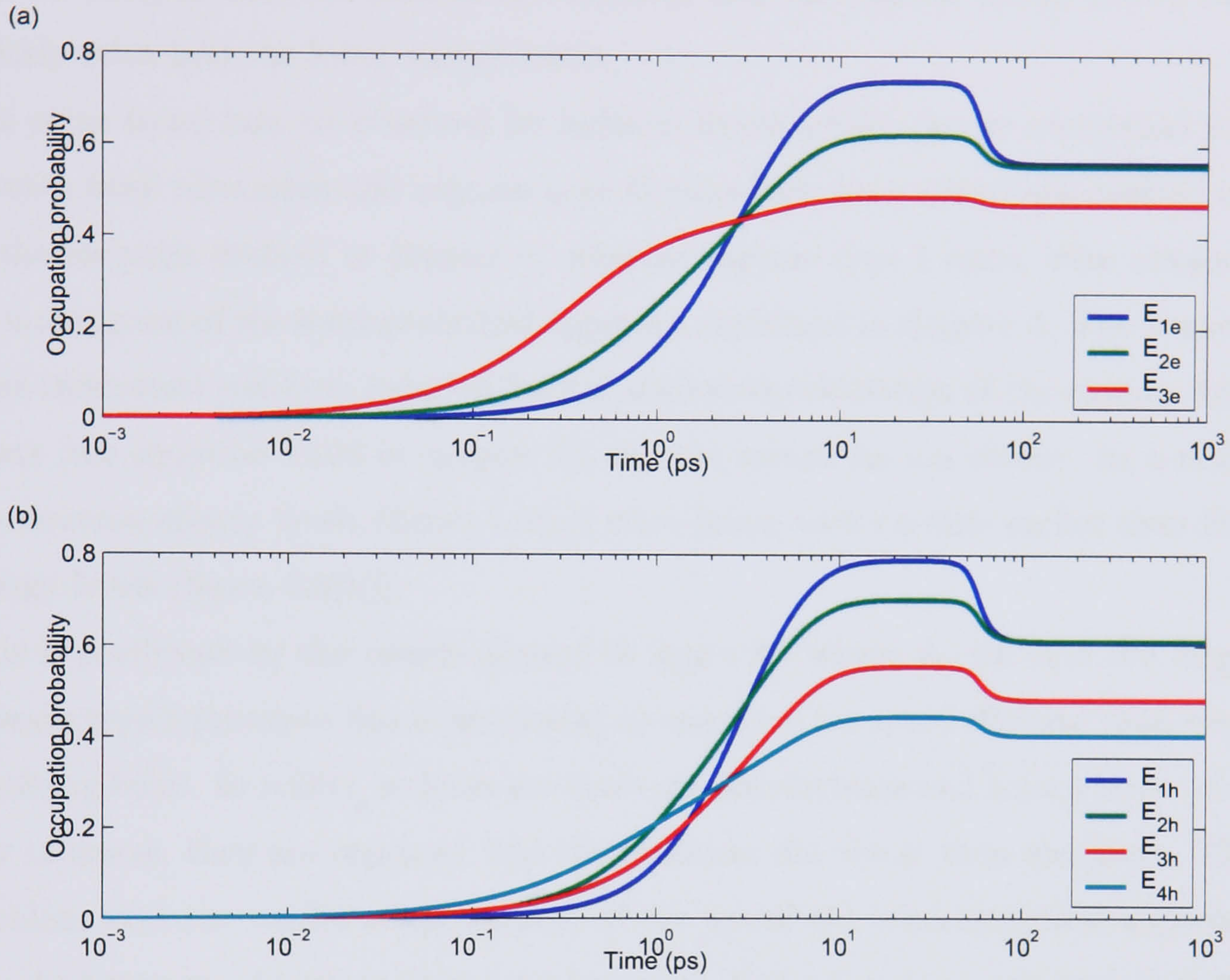

Figure 5.8: (a) Occupation probability of the 3 electron-energy-levels for the dot described in figure 5.7. The radius of the dot is 19.6 nm and its interband transition energy for the electron and holes ground state is 210 meV. (b) Occupation probability of the 4 hole-energy-levels for the dot described in figure 5.7

This phenomenon is due to the fact that carriers relax to lower energy states faster than they are excited to higher energy states. This effect can be observed in figure 5.8(a). The occupation probability is higher for lowest energy levels than for the highest ones, as once the carriers are captured into the highest energy levels, they quickly relax into the lower energy levels.

The same trend may be observed for holes in figure 5.8(b). As we mentioned previously, both relaxation and capture type II rates have been calculated making use of the formulas derived in chapter 4, whereas capture type I rates, were obtained by making use of the semi-analytical approach explained in chapter 3. The tremendous computational time required for the analytical calculation of the capture type I rate (see equation 4.106 in chapter 4), was the reason for our choice. As a result the electron energy levels (figure 5.8(a)) start filling with carriers earlier than hole energy levels (figure 5.8(b)).

This is confirmed by the results plotted in figure 3.7 where we see that the Auger capture type I processes due to scattering by electrons are more effective than those involving holes. In reality, as holes are heavier than electrons and have a larger density of states, they are captured into the quantum dot faster than electrons. This problem with our model arises because of the use of the semi-analytical approach to calculating the Auger capture type I process. Using this approach we ignore the Fermi-Dirac distribution for the carriers in the wetting layer, so the influence of the mass of the carriers is less important. As explained earlier a full calculation of this capture process requires a prohibitively high level of computing and it is left for future work.

After 40 ps, the occupancy of the lowest energy levels is sufficient to give enough gain to overcome the cavity losses. At this point, photons build up (see figure 5.9(a)) in the laser cavity due to stimulated emission. The transition energies of this quantum dot (19.6 nm radius and 5 nm height), i.e., $E_{1e}E_{1h} = 210$ meV, $E_{2e}E_{2h} = 251$ meV and $E_{3e}E_{3h} = 294$ meV, have been represented in figure 5.7. Note that all the energy values in this chapter, are relative to the 1.074 eV bandgap. Consequently, this quantum dot will contribute to the photon densities at those transition energies, as pictured in figure 5.9. E_{1e}, E_{1h} energy levels, have occupancy high enough for gain to overcome cavity losses, hence as seen from the high photon density value at $E_{1e}E_{1h} = 210$ meV (figure 5.9(a)), stimulated emission occurs at 210 meV (radiative recombination processes involving E_{1e} and E_{1h} energy-levels), while the much lower photon densities obtained in figure 5.9(b) and figure 5.9(c), represent photon densities obtained as a result of spontaneous emission processes involving E_{2e} and E_{2h} energy levels (figure 5.9(b)) and E_{3e} and E_{3h} (figure 5.9(c)). The large increase of photons for $E_{1e}E_{1h} = 210$ meV transition energy due to stimulated emission (figure 5.9(a)), coincides with the depletion of carriers in E_{1e} and E_{1h} energy levels in figure 5.8 (spectral hole burning). Stimulated emission, is a very fast process (~ 1 ps) and this depletes carriers in the energy levels efficiently. The remaining empty states are rapidly filled by carriers captured from E_{2e}, E_{3e} and E_{2h}, E_{3h} etc. This can be observed by the reduction of the spontaneous emission of the transitions at $E_{2e}E_{2h} = 251$ meV (figure 5.9(b)) and $E_{3e}E_{3h} = 294$ meV (figure 5.9(c)).

Figure 5.10 shows the absorption spectra obtained for the previously described quantum dot ensemble. Because of the high computational times needed to calculate all the Auger scattering rates responsible of carrier dynamics within the dots, as well as to implement the rate equations describing these dots dynamics, we have only considered an ensemble consisting of 30 different dot types. Hence the optical gain at each transition energy, has been calculated by collecting the individual contributions of all dots within the ensemble, a rather spiky absorption spectra plot is obtained, as pictured in figure 5.10.

As seen in figure 5.9, a maximum photon density is obtained at a transition energy value of 210 meV (figure 5.9(a)). This coincides with the transition energy at which the maximum value for the gain is obtained, i.e., 1.447×10^5 m^{-3} (Fig. 5.10(a)). Figure 5.10(a) describes the absorption spectra until the gain reaches its maximum

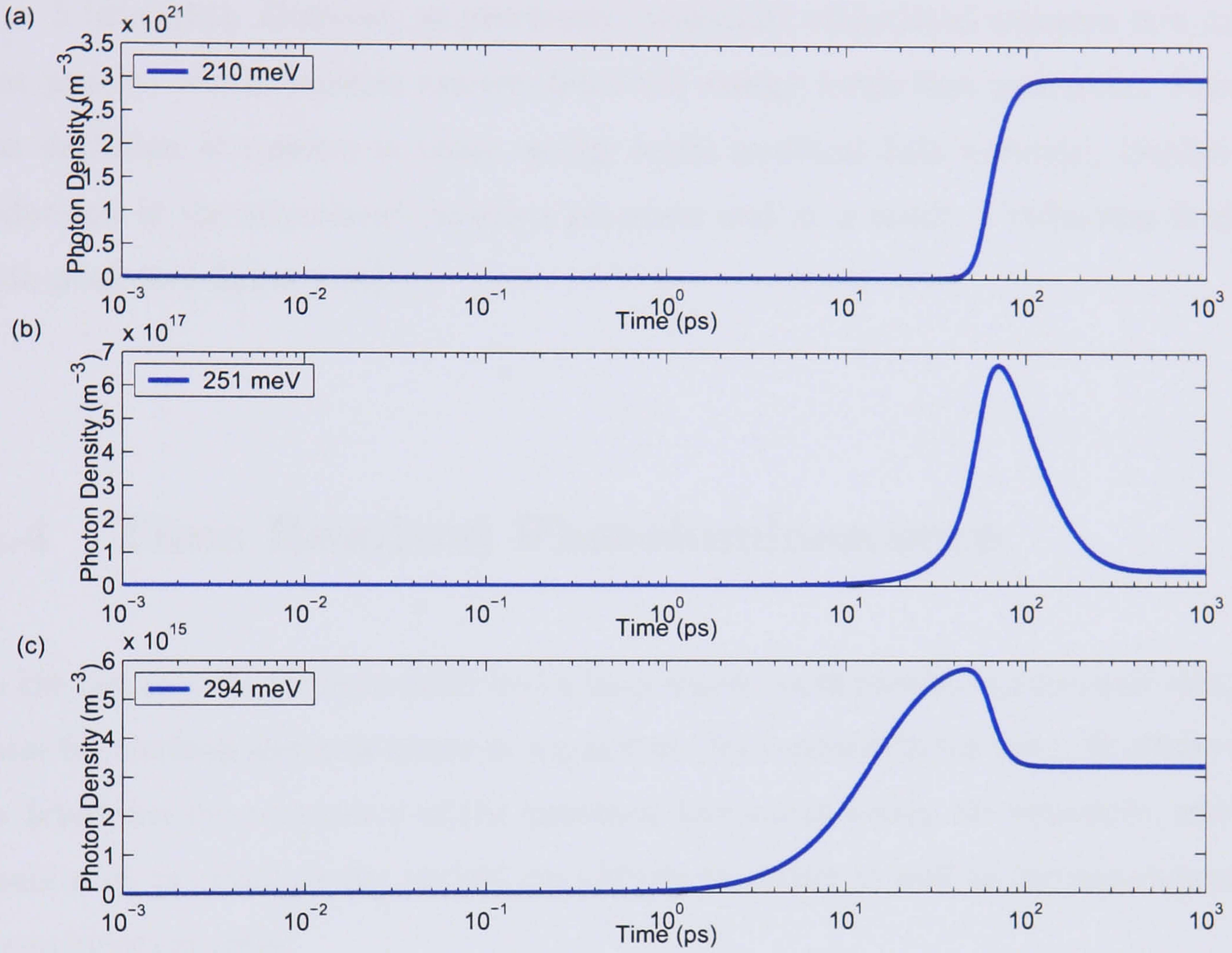

Figure 5.9: (a) Time evolution of the photon mode at the interband transition energy of 212 meV. (b) Time evolution of the photon mode at 251 meV. (c) Time evolution of the photon mode at 294 meV.

value, while figure 5.10(b) shows its evolution until it saturates after spectral hole burning. Initially there is a broad absorption spectra when we turn the injection current on. The dots start populating with carriers and recombination processes start to happen, reaching the gain its maximum value after the first $\sim$ 18 ps (see Fig. 5.10(a),(b)). However, as previously mentioned, stimulated emission is a very fast process which depletes carriers from the energy levels that give gain. Hence the depletion of carriers in those energy levels (spectral hole burning), implies a reduction in the stimulated emission processes and as a result, a reduction in the gain peak (see figure 5.11).

5.4 Time Resolved Photoluminescence

In the last section, we have presented a laser which could predict capture and escape rates for electron and hole states in a quantum dot semiconductor laser. It allows us to determine the occupancy of the quantum dots states within the ensemble, which enables us to calculate the optical gain of the structure as well as the spontaneous recombination rates.

Among the methods for probing radiative recombination of carriers in quantum dot systems, the time resolving photoluminescence (TRPL) method is one of the most popular [2]. In TRPL experiments, the radiative emission from the quantum dots is measured by optically pumping the material. An optical pulse is used to pump carriers into the quantum dots. Therefore, in order to obtain information about the carrier capture, relaxation and emission rates for the energy levels within the quantum dots, time resolved photoluminescence (TRPL) experiments, make use of a spectrometer to spectrally resolve the device luminescence. Our model, can also be used to simulate TRPL experiments.

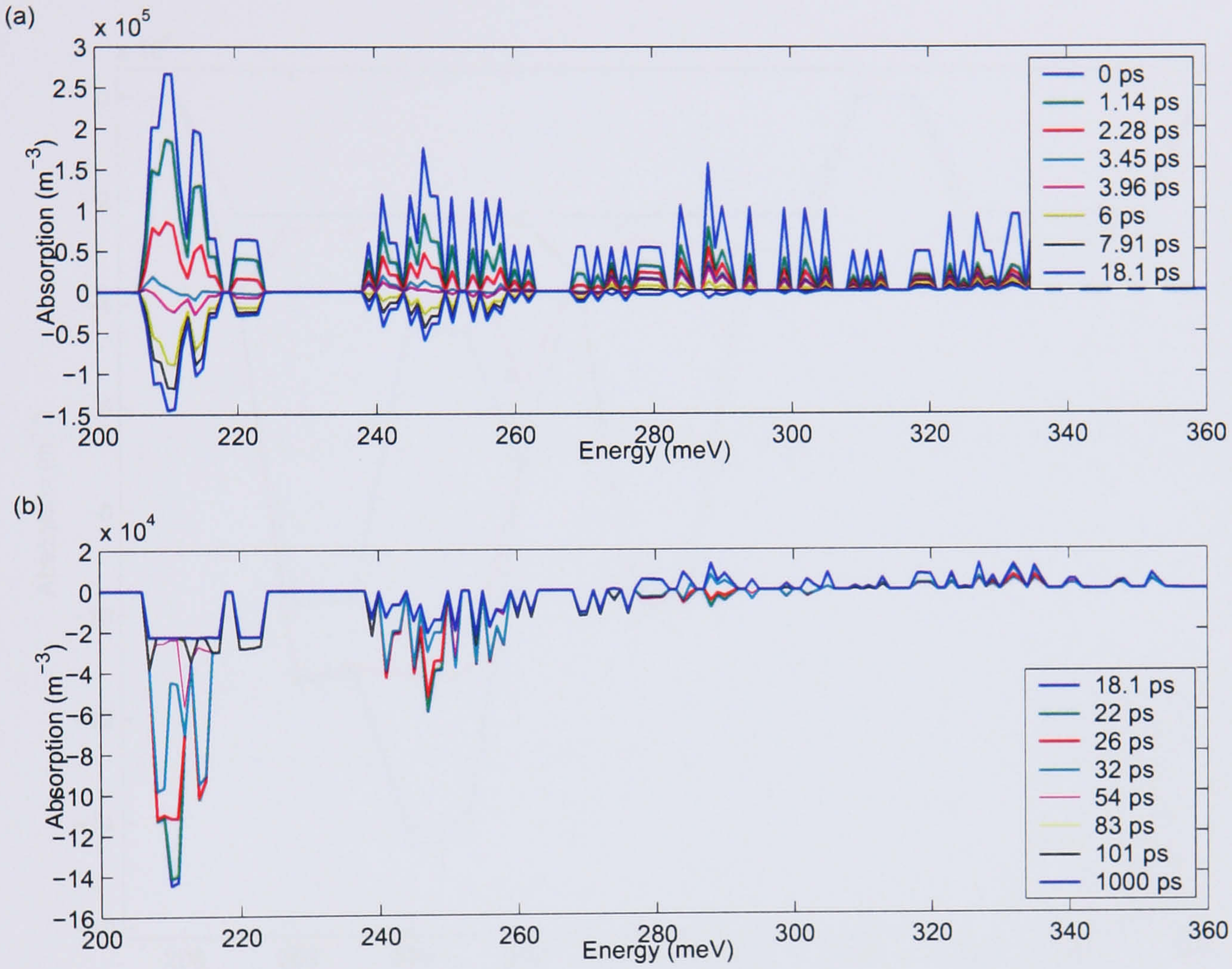

Figure 5.10: (a) Absorption as a function of the interband transition energy plotted for 8 different time values, starting from 0 ps to 18.1 ps, where the gain reaches its maximum value. (b) Last 8 time values.

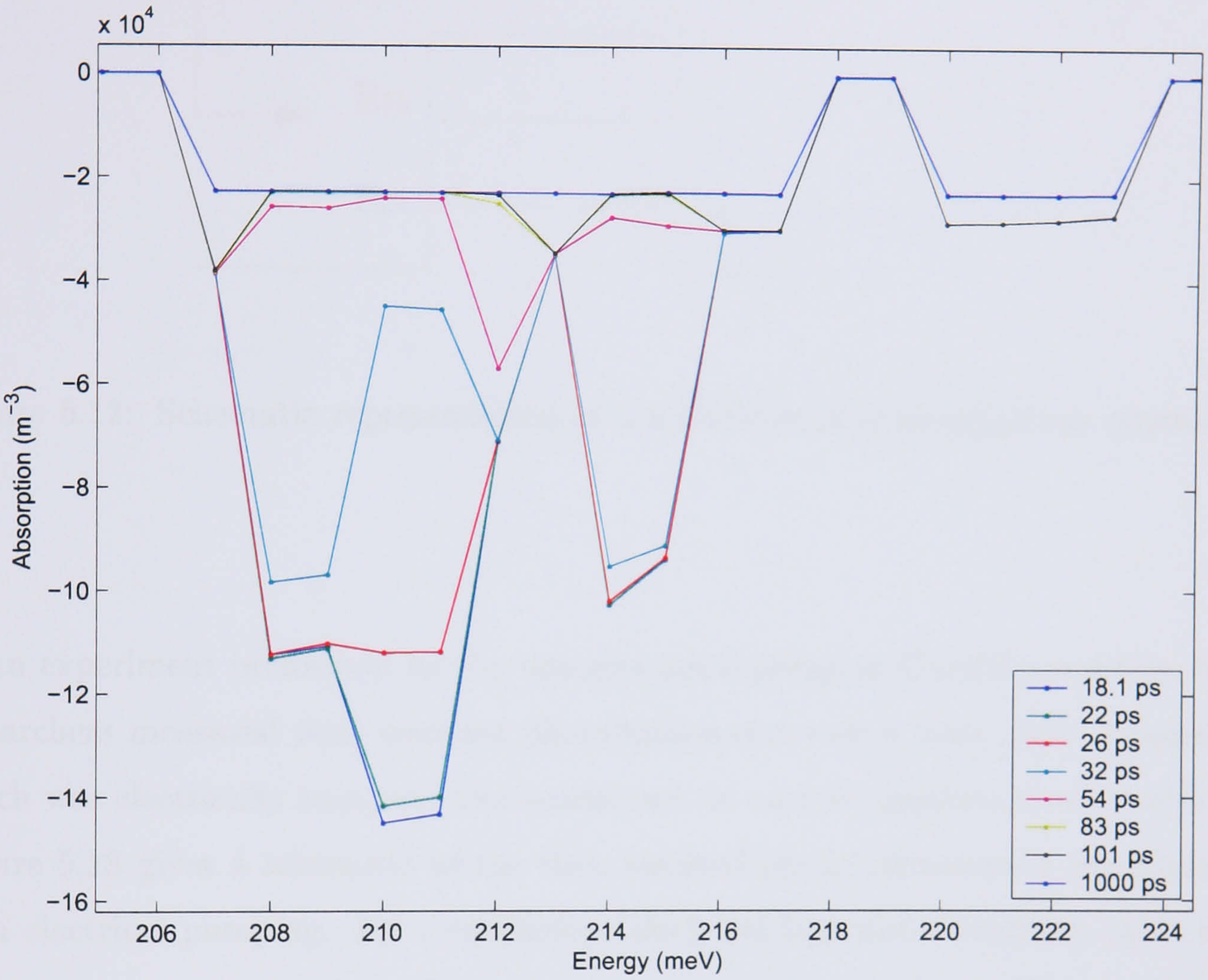

Figure 5.11: (a) Zoom of the lowest transition energy values in figure 5.10(b). The reduce in the peak gain as a consequence of spectral hole burning can be observed.

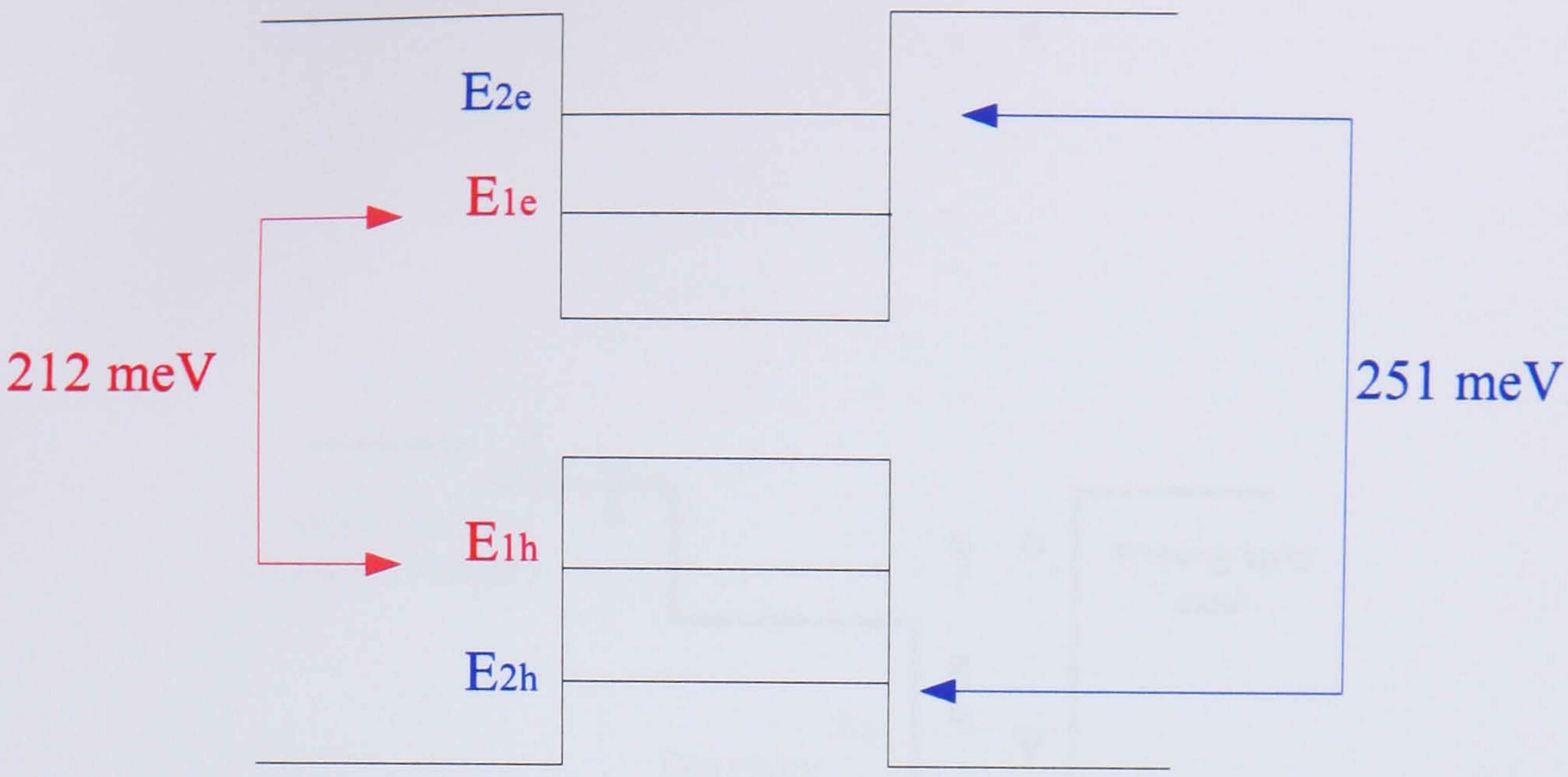

Figure 5.12: Schematic representation of a 2-electron/hole-energy-levels quantum dot.

In an experiment performed by the optoelectronic group at Cardiff university, the researchers measured time resolved photoluminescence on a laser diode structure which was electrically pumped. Our model can be used to simulate these results. Figure 5.13 gives a schematic of the time resolved photoluminescence experiment with electrical pumping. By a continuous electrical injection of carriers (blue arrow), they get captured into the quantum dot energy levels, where they can either relax into a lower energy level or radiative recombine, resulting in a luminescence signal. We have considered an ensemble which consists of 1 dot of 4-energy-levels (2 electron-energy-levels and 2 hole-energy-levels) with transition energies $E_{1e1h} = 212$ meV and $E_{2e2h} = 251$ meV, as pictured in figure 5.12. After running our model to steady state ($\sim$ 200 ps), we introduced a pulse of photons to simulate the laser pumping. Figure 5.14, shows the photon intensity achieved by transitions involving the ground state (red line) and the excited state (blue line). However, a different behavior in decay times appears depending on which state it is being pumped. It

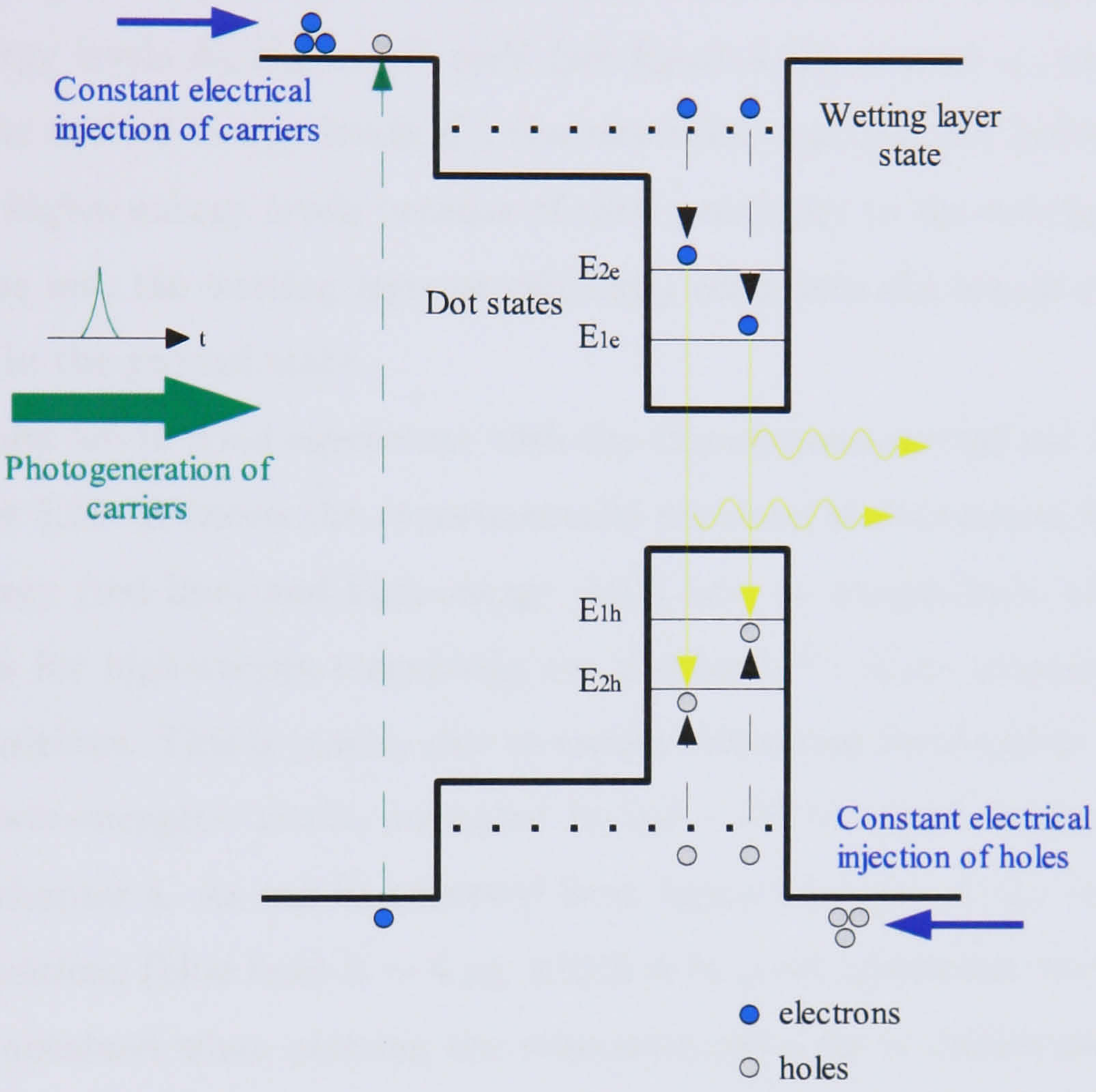

Figure 5.13: Energy band structure of the device showing the electrical and optical generation of carriers.

can be observed that the decay time is longer ($\sim$ 60 ps) than the extremely short duration ($\sim$ 4 ps) obtained when pumping the system with photons of energies equal to transition energies involving the excited state, i.e., $E_{2e2h} = 251$ meV (see figure 5.12), as shown in figure 5.14 (blue line). This is due to the fact that when introducing a pulse of photons of energies equal to the transition energy between the excited energy levels $E_{2e}E_{2h} = 251$ meV (see figure 5.12), carrier occupation probability of the excited energy levels E_{2e} (for electrons) and E_{2h} (for holes) increases. Carriers in higher energy levels because of their proximity to the wetting layer, can easily escape into the wetting layer or efficiently relax into the lowest energy level, than those in the ground state.

These results are in good agreement with the experiments carried out by [7], plotted in figure 5.15. It shows the experimentally obtained luminescence decay curves for low-energy (red line) and high-energy (blue line) at temperature of 50 K. The decay times for high-energy transitions are shorter than those measured for low-energy transitions. This is mainly due to carrier relaxation from higher QD energy levels to lower-energetic levels, mediated by $0D - 2D$ Coulomb scattering, as explained in chapter 4. As can be observed from figure 5.14, this decay time for high energy transitions (blue line) is $\sim$ 4 ps, which is in good agreement with the result previously obtained when plotting the relaxation rates for a similar size quantum dot (see figure 4.20, chapter 4). Under the same initial conditions, i.e., $2D$ carrier densities of $n_w = 1 \times 10^{15}\text{m}^{-2}$, $3D$ carrier densities of $n_w = 1 \times 10^{17}\text{m}^{-3}$ and equal temperatures for the $3D$ and $2D$ carriers of 300 K, we obtained an Auger relaxation lifetime of 3.86 ps (see figure 4.20, chapter 4).

The difference in the decay times in both figures (figure 5.14 and figure 5.15) comes from the fact that both models have been performed under different circumstances. For instance, our model has been run considering a single quantum dot and temperature of 300 K, while figure 5.15 shows the results obtained for a dot density of 2×10^2 cm^{-2} at 50 K. Carriers can be captured and relax more efficiently at higher temperatures, hence, decreasing the duration of the decay time. However a quali-

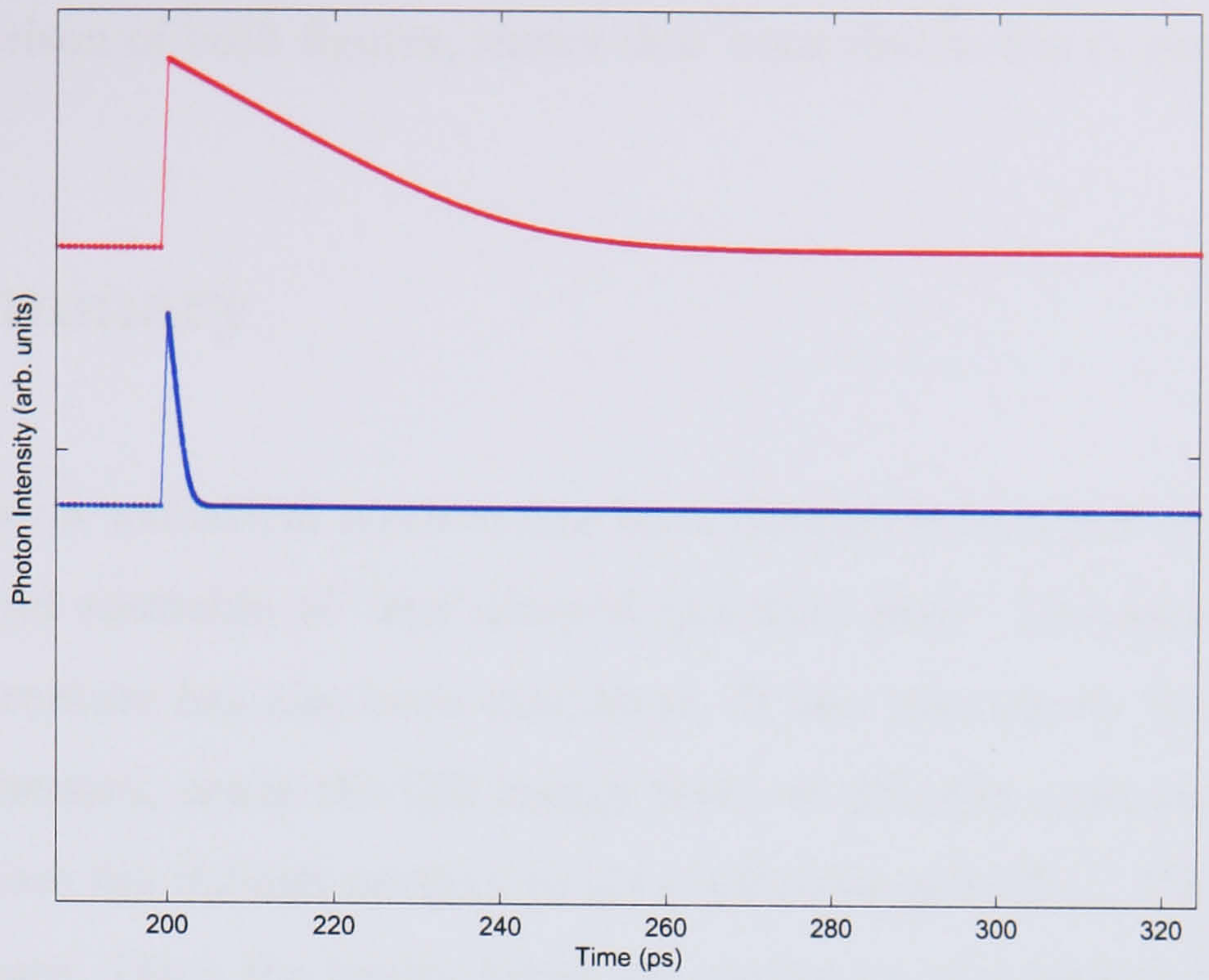

Figure 5.14: Photon intensity at the ground state transition energy, i.e., 212 meV (red line) and at the excited state transition energy, i.e., 251 meV when pumping the structure with more photons after 200 ps.

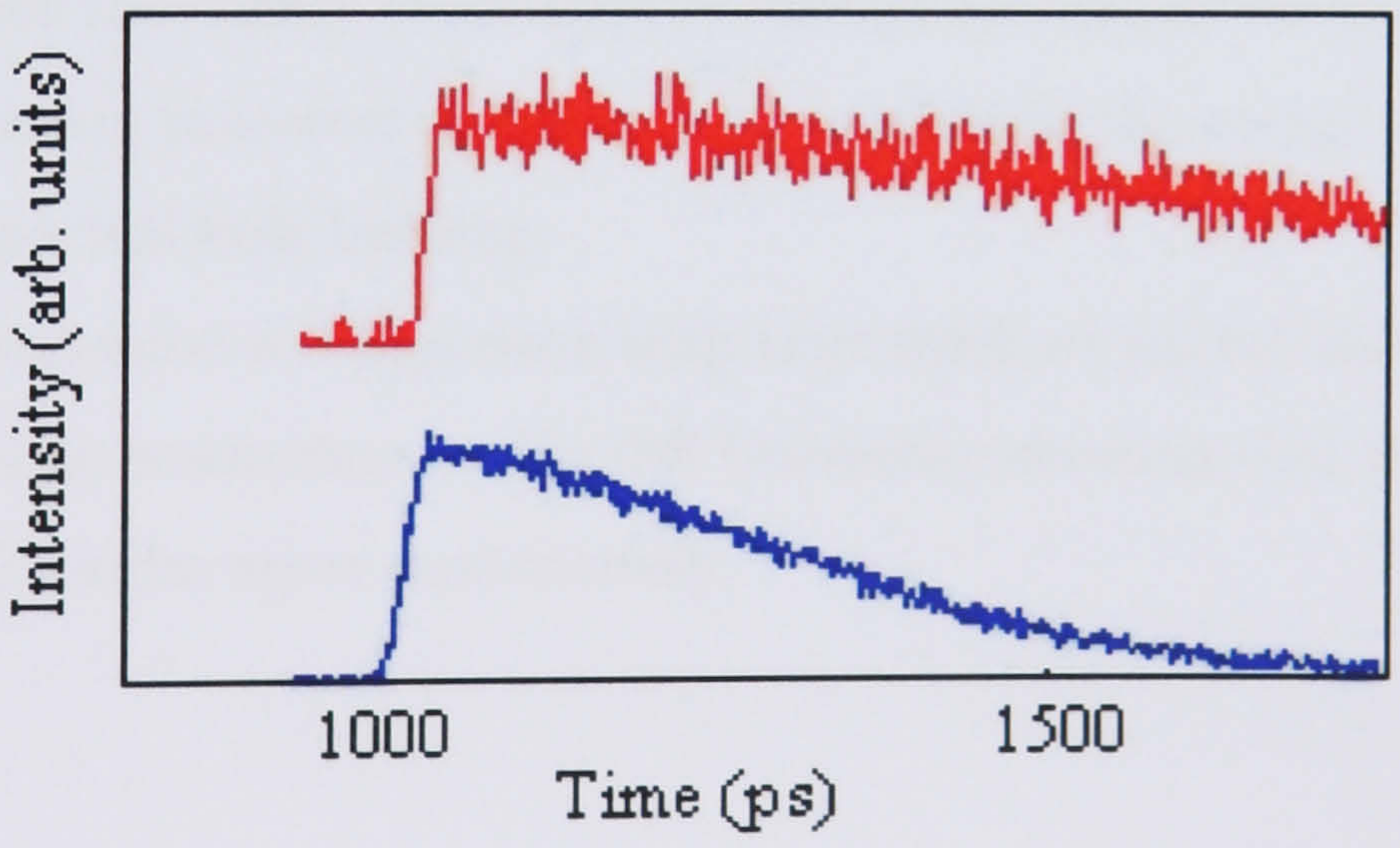

Figure 5.15: Luminescence decay transients, varying injection levels, measured at 50 K, for detection energy E_1 (red line) and E_2 (blue line). [7]

tative comparison of both figures, shows that both results are in good agreement.

5.5 Summary

In this chapter a numerical method has been developed in order to determine the dynamics of an ensemble of 'lens' shaped quantum dots. The optical gain of the considered structure has also been calculated. It has been shown that the very fast scattering processes, cause the QD energy levels to fill with electron and holes. At this point, there are enough carriers to give sufficient gain (Fig. 5.10) to overcome the cavity losses. Once the cavity losses are overcome, the optical output is dominated by stimulated emission, as seen in figure 5.9(a). On the onset of stimulated emission, carriers are depleted from the quantum dots, which gives the maximum gain.

This model simplifies the problem of studying the occupation of different quantum dot types for a considered ensemble of dots. Furthermore, as no Fermi-Dirac distribution functions (see chapter 2 equations 2.22 and 2.23) are included, we may deal with situations of non-thermal equilibrium. As can be observed from figures 5.8 and 5.9, once the energy levels acquire enough occupancy for gain, the very fast stimulated emission processes depletes these carriers in the energy levels leading to the so-called spectral hole burning.

We have also presented a comparison with time resolved photoluminescence experiments obtained by researchers at Cardiff University showing that the experimental and theoretical results agree qualitatively.

Bibliography

[1] Larry A. Coldren and Scott W. Corzine. *Diode Lasers And Photonic Integrated Circuits.* Wiley-Interscience, 1995.

[2] S. Grosse and J. H. H. Sandmann et al. *Physical Review B*, vol. 55:4473–4476, 1997.

[3] M. Grundmann and D. Bimberg. *Physical Review B*, vol. 55:pp. 9740–9745, 1997.

[4] S. Guha, A. Madukar, and K. C. Rajkumar. *Appl. Phys. Lett.*, Lett. 57:pp. 2110, 1990.

[5] H. Huang and D. G. Deppe. Rate equation model for nonequilibrium operating conditions in a self-organized quantum-dot laser. *IEEE Journal of Quantum Electronics*, vol. 37:pp. 691–698, 2001.

[6] I. Jacak, P. Hawrylak, and A. Wojs. *Quantum Dots.* Springer, 1997.

[7] Dan Mathews. PhD thesis, Cardiff University, 2003.

[8] Javier Domínguez. *A theoretical study of coupling and dephasing in semiconductor quantum dots.* PhD thesis, School of Informatics, Bangor, 2004.

[9] A. Sakamoto and M. Sugawara. Theoretical calculation of lasing spectra of quantum-dot lasers: Effect of homogeneous broadenning of optical gain. *IEEE photonics technology letters*, vol. 12(2), 2000.

[10] I. N. Stranski and L. von Krastanov. *Akd. Wiss. Lit. Mainz Abh. Math. Naturwiss. Kl.*, vol. 146:pp. 797, 1939.

Chapter 6

Conclusions

The aim of this work was to calculate capture/escape and relaxation rates of carriers in self-assembled quantum dot structures. Making use of these calculations, it was possible to determine the carrier occupancy of the quantum dot states within the ensemble, which allowed us to calculate the optical gain and spontaneous emission rate.

In chapter 3, we carried out a semi-analytical calculation of the Auger capture/escape and relaxation rates of carriers in a quantum dot embedded in a two dimensional wetting layer. We find there is a strong temperature dependence of the scattering rates, which is due to the screening effect of the bulk carriers on the interaction between carriers in the wetting layer and in the quantum dots. This screening effect becomes less significant at higher temperatures leading to much higher scattering rates as shown in figure 3.4. We note a major limitation of the semi-analytical approach is the assumption of a Boltzmann distribution for carriers in the wetting layer, arising from the assumption of low carrier densities.

In chapter 4 we derive more rigorous expressions for the capture and relaxation rates.

Instead of making use of a Boltzman distribution (as used for the semi-analytical calculations) in order to describe the carriers in the quantum well wetting layer, Fermi-Dirac statistics are utilized. Under these circumstances, more realistic relaxation lifetimes of $\sim$ 4 ps and type II capture lifetimes of $\sim$ 20 ps were obtained for $2D$ carrier densities of $1.0 \times 10^{15}\,\mathrm{m}^{-2}$.

Once the capture and escape rates for electrons and holes in a quantum dot semiconductor structure have been determined, we present in chapter 5 a model which describes the carrier occupancy of the quantum dot states within an ensemble of 30 different quantum dots. Knowing the carrier occupancy allows us to calculate the optical gain and spontaneous emission of the quantum dot structure. Under electrical injection the carriers are initially captured into the highest energy levels (as a consequence of the small energy difference between the highest confined energy state and the wetting layer), and subsequently relax to lower energy levels. Once the occupancy of the lowest energy levels provides enough gain to overcome the cavity losses, the optical output is governed by stimulated emission. Stimulated emission is a relatively fast process compared to the carrier capture rate and this leads to a depletion of carriers in the energy levels which take part in the stimulated emission event. This depletion of carriers leads to reduction of the peak gain known as spectral hole burning.

A simulation of a time resolved photoluminescence experiments on a quantum dot structure is also described in chapter 5. A qualitative comparison was made with experimental results obtained by researchers at Cardiff University. The experimental and theoretical results agree qualitatively. The decay times appear to be longer when pumping the lower energy levels than the higher levels. This is due to photogenerated carriers in the higher energy levels escaping to the wetting layer faster than those in the ground state. As a result, when the excited state is pumped with carriers, it gets depleted faster than when pumping the ground state. This can be explained by the energy difference between the confined quantum dot states and the two dimensional wetting layer. Electrons in the higher energy levels can escape quicker because the energy difference between the confined state and the wetting layer sub-band is smaller.

During the course of this research we derived an expression for the Auger type I capture process. However, given the computer resources we were unable to implement this calculation and this is left for future work. Other future work could include increasing the number of different dot sizes considered in the ensemble to give a more realistic representation of the optical spectra. Also when considering the photon dynamics we neglected the effect of the wavelength selection of the cavity and again this would make an interesting addition to this research.

Appendix A

LO-phonon-carrier capture processes

Carriers within the wetting layer may be captured into the quantum dots by scattering with bulk LO-phonons (see figure A.1). The probability of carrier capture from any possible state in the quantum well (wetting layer) into the quantum dot

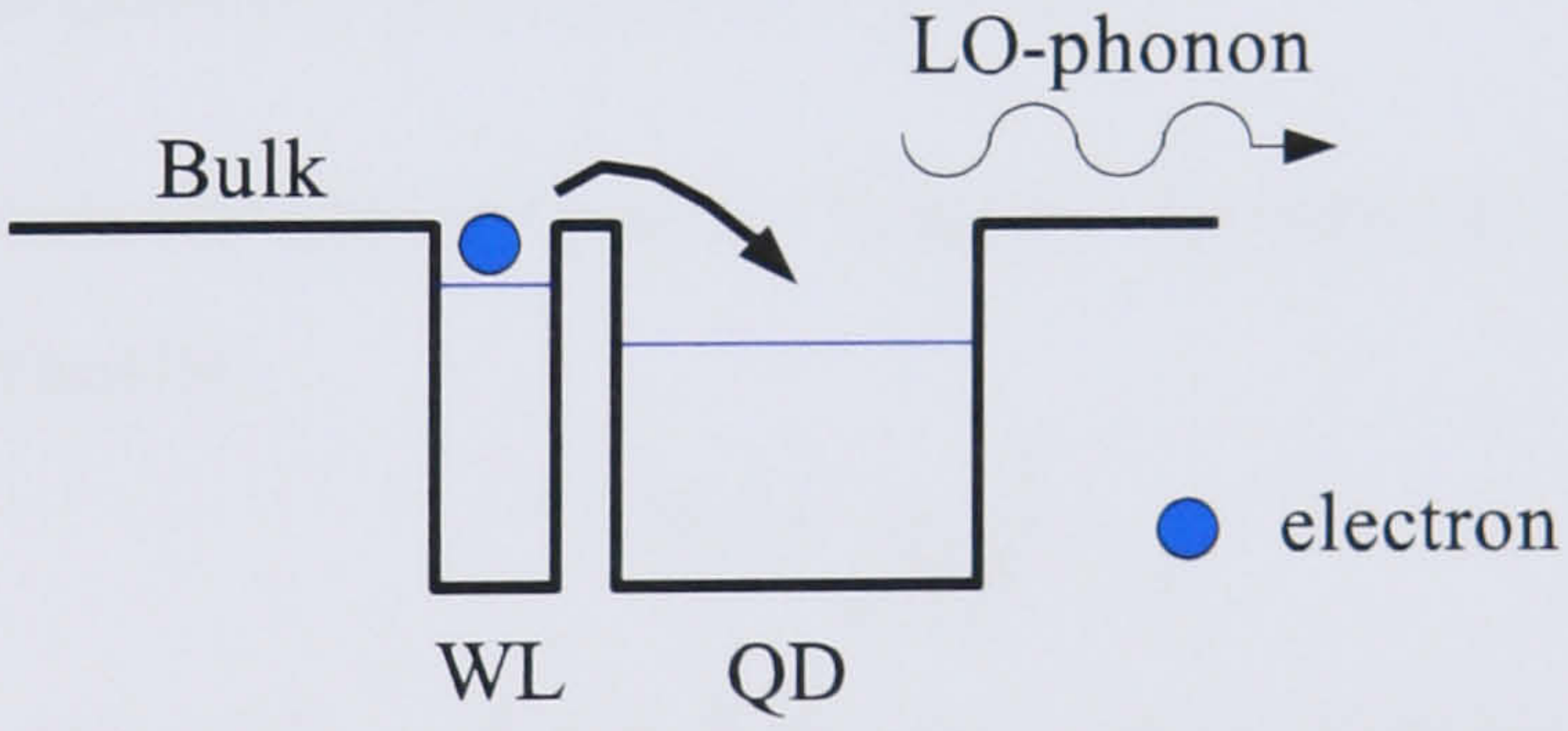

Figure A.1: Carrier-phonon scattering.

by emitting or absorbing a bulk LO-phonon, is given by Fermi's Golden Rule [1]:

$$\frac{1}{\tau} = \frac{2\pi}{\hbar} \sum_{|i>} \left| < f|\tilde{H}|i > \right|^2 \delta(E_f - E_i) \tag{A.1}$$

where

$|i>$ is the carrier initial state

$|f>$ is the carrier final state

$\tilde{H}$ is the interaction between an electron and a LO-phonon [1]

$$\tilde{H} = e \sum_{\vec{q}} \left[\frac{\hbar\omega_{LO} P}{2q^2} \right]^{1/2} \frac{e^{-i\vec{q}\vec{r}}}{V^{1/2}} \tag{A.2}$$

$\vec{q}$ is the phonon wave vector

P is a factor

$$P = \left(\frac{1}{\epsilon_\infty} - \frac{1}{\epsilon_0} \right) (N_0 + 1/2 \mp 1/2)$$

the upper sign of the $\mp$ refers to the absorption of a phonon while the lower sign instead, represents emission of a phonon.

N_0 is the phonon density within the crystal. As bosons, phonons follow Bose-Einstein distribution

$$N_0 = \frac{1}{e^{\frac{\hbar\omega_{LO}}{KT}} - 1}$$

ϵ_∞ and ϵ_0 are the high- and low-frequency permittivities of the material.

Following J. Domínguez mathematical approach [2], the final expression for the probability of carrier capture into the quantum dot by LO-phonon scattering is given by

$$\frac{1}{\tau} = \Gamma \int_{-\infty}^{\infty} \frac{\mathrm{dq}}{q^2} \int_{-\pi}^{\pi} \mathrm{d}\theta_{xy}^{W} |G(\alpha\cos(\theta_{xy}^{W}) + q_x, \alpha\sin(\theta_{xy}^{W}) + q_y, q_z)|^2 \tag{A.3}$$

where

$\Gamma = \frac{me^2\omega_{LO}Pf_D}{2\hbar^2(2\pi)^4}$

$f_D = f_D\left(\frac{\hbar^2\alpha^2}{2m}\right)$ is the $2D$ Fermi-Dirac distribution, where for E^D and E_n^W the carrier energies in the QD and in the QW sub-band respectively, $\alpha = k_{xy}^W = \sqrt{2m\Delta/\hbar^2}$ and $\Delta = E^D \pm \hbar\omega_{LO} - E_n^W$.

$\mathbf{k}_{xy}^W$ is the carrier wave vector within the QW

$\mathbf{q}$ is the phonon wave vector

$G(\mathbf{k}_{xy}^W + \mathbf{q}, q_z) = G_z(q_z)G_{xy}(\mathbf{k}_{xy}^W + \mathbf{q}_{xy})$ where $G_z(q_z) = \int_{-\infty}^{\infty} \psi_z^{\mathrm{D}*}\psi_z^{\mathrm{W}}e^{-iq_z z}\mathrm{d}z$ and $G_{xy}(\mathbf{k}_{xy}^W + \mathbf{q}_{xy}) = \iint_{-\infty}^{\infty} \psi_{xy}^{\mathrm{D}\,*}e^{-i(\mathbf{k}_{xy}^W+\mathbf{q}_{xy})}\mathbf{r}_{xy}\mathrm{d}\mathbf{r}_{xy}$

ψ_{xy}^{D} and ψ_z^{D} are the $x - y$ and z components respectively of the carrier wavefunction within the QD given by equation 4.29 in chapter 4.

ψ_z^{W} is the z component of the carrier wavefunction within the wetting layer given by equation 4.30 chapter 4.

Bibliography

[1] P. Harrison. *Quantum Dots.* Wiley, 1997.

[2] Javier Domínguez. *A theoretical study of coupling and dephasing in semiconductor quantum dots.* PhD thesis, School of Informatics, Bangor, 2004.

Appendix B

Fermi Level

Considering a quantum well structure, the Bloch wavefunction for an electron in a crystal given by equation 2.2 in chapter 2, the slowly varying plane-wave envelope $F(\mathbf{r})$ describing the motion perpendicular to the well (z-direction), can be replaced by a quantized wave $\varphi_n(z)$ as follows:

$$\psi(\mathbf{r}) = \varphi_n(z)\frac{e^{\mathbf{k}_{xy}\mathbf{r}_{xy}}}{\sqrt{A}}u(\mathbf{r}) \tag{B.1}$$

where A the area of normalization of the $2D$ gas and $n = 1, 2, ...$ is the quantum number. The free translational motion is described by a 2-dimensional $\mathbf{k}_{xy}$ wave vector. Making use of the notation $\mathbf{k}$ to denote the wave vector, then the sum over this wave vector can be written as an integral as follows [1]

$$\sum_{\mathbf{k}} = \sum_{\mathbf{k}} \frac{\Delta k_x \Delta k_y}{\Delta k_x \Delta k_y} = \left[\frac{L}{2\pi}\right]^2 \int \mathrm{d}\mathbf{k} \tag{B.2}$$

Rewriting the integral above in polar coordinates then

$$\sum_{\mathbf{k}} = \left[\frac{L}{2\pi}\right]^2 \int_0^{2\pi} \mathrm{d}\theta \int_0^{\infty} k\mathrm{d}k = \left[\frac{L}{2\pi}\right]^2 (2\pi) \int_0^{\infty} k\mathrm{d}k \tag{B.3}$$

Taking into account that $E = \frac{\hbar^2 k^2}{2m}$ (see equation 2.4, chapter 2), equation B.3 may be transformed into an energy integral, hence:

$$\sum_{\mathbf{k}} = \left[\frac{L}{2\pi}\right]^2 (2\pi) \int_0^\infty \frac{\sqrt{2mE}}{\hbar} \frac{2m}{2\hbar^2\left(\sqrt{2mE}/\hbar\right)} \mathrm{d}E = \frac{L^2 m}{\pi\hbar^2} \int_0^\infty \mathrm{d}E \quad \text{(B.4)}$$

Including the occupation probability for all those available states, we will get the total number of carriers (N_2) injected into the energy E, we get

$$N_2 = \sum_{\mathbf{k}} = \frac{L^2 m}{\pi\hbar^2} \int_0^\infty f_c(E)\mathrm{d}E \quad \text{(B.5)}$$

where $f_c(E)$ is the Fermi-Dirac distribution given by equation 2.22 (for holes) or 2.23 (for electrons) described in chapter 2.

Denoting as $n_2 = N_2/L^2$, equation B.5 can be rewritten as follows:

$$n_2 = \sum_{\mathbf{k}} = \frac{m}{\pi\hbar^2} \int_0^\infty \frac{1}{1 + e^{\frac{E-E_F}{k_B T}}} \mathrm{d}E \quad \text{(B.6)}$$

Denoting $z = \frac{E-E_F}{k_B T}$, the integral above can be solved in order to determine the Fermi level E_F, hence:

$$n_2 = \frac{m}{\pi\hbar^2} k_B T \ln\left(\frac{1 + e^{-E_F/k_B T}}{e^{-E_F/k_B T}}\right) \quad \text{(B.7)}$$

so the Fermi level E_F can be determined from:

$$e^{E_F/k_B T} = e^{n_2 \pi\hbar^2/m k_B T} - 1 \quad \text{(B.8)}$$

Bibliography

[1] H. Haug and S. W. Koch. *Quantum theory of the optical and electronic properties of semiconductors.* World Scientific, Third edition, 1990.